
Diploma Thesis

written by
Christoph Ganglbauer

Characterization of wear coatings

Hardfacing of plug screws

GRAZ UNIVERSITY OF TECHNOLOGY

Institute for Materials Science and Welding

Univ.-Prof. Dipl.-Ing. Dr.techn. Priv.-Doz. Christof Sommitsch

Advisor:

Ass.Prof. Dipl.-Ing. Dr.techn. Norbert Enzinger

Dipl.-Ing. Dragan Djuric

Graz, 15.10.2010

Statutory Declaration

I hereby certify that all work presented in this diploma thesis is my own, no other than the sources and aids referred to were used and that all parts which have been adopted either literally or in a general manner from other sources have been indicated accordingly.

Therefore I sign to insure that this work was done independently and on my own.

Acknowledgements

First of all I would like to thank **Univ.-Prof. Dipl.-Ing. Dr.techn. Priv.-Doz. Christof Sommitsch** from the Institute for Material Science and Welding where my thesis was carried out.

I thank in particular my tutor **Ass.Prof. Dipl.-Ing. Dr.techn. Norbert Enzinger** for his guiding, suggestions, useful comments and discussions. As well for his will to help me and for all references.

I would also like to thank **Mr. Yassar Ghanimi, Mr. Ernst Hauck** and **Ms. Margit Hölbling** of Andritz AG for making a thesis at Andritz AG possible.

Furthermore, I would like to thank **Dipl.-Ing. Dragan Djuric** for his support during my thesis and **M.Sc. Matthew Galler** who helped me as a native speaker with translations.

I want to thank the **scientific staff**, the **laboratory group** and the **secretaries** from the **Institute for Material Science and Welding** for their kind help all the time and giving me hints and advices.

Any project depends on the efforts of many different people and this project is no exception. I would like to thank the institute and all members in general for their help and support during the last few months.

I would like to say also thanks to musicians like Paul Kalkbrenner, Parov Stelar, muse, coldplay and many more for producing excellent and motivating music. Not to forget Rudi Vallant's coffee, which always picked me up after lack of sleep. Thank you, because without it, this work would not have been possible.

Finally yet importantly, I thank to my parents for their support, help and patience. Without their encouragement, my studies and this thesis may not have been possible.

Abstract

In the course of this diploma thesis the topic ‘Hardfacing of plug screws’ is investigated. These components are subjected to abrasion and corrosion. To withstand this very harsh environment, the screws are protected by coatings and thus increase their durability. There exist several methods to apply these protective layers and constantly new alloys are developed to meet increasing demands and extend their service life.

A literature study concerning the subject ‘wear protective coatings’ was carried out in order to incorporate possible new results into the work. Some new coating types have been welded on samples and have been studied later on. For the analysis metallographic specimen were prepared and investigated using the light optical microscope and scanning electron microscope. Furthermore, hardness mappings were made by certain samples and additional macro- and micro-hardness measurements were taken.

Based on these investigations, statements should be made about the possible suitability for remanufacture and refurbishment of worn plug screws to enhance the life cycle. The recommendations of these new welding consumables are noted in an application table which should lead to uniformity in the group, as well recording experience with the particular welding consumables in the future.

Zusammenfassung

Im Zuge dieser Diplomarbeit soll das Thema „Panzen von Stopfschnecken“ untersucht werden. Diese Bauteile unterliegen einer sehr starken Beanspruchung durch abrasiven Verschleiß kombiniert mit Korrosion. Um dieser Belastung stand zu halten, werden diese Bauteile mit verschleißfesten Schichten geschützt und dadurch die Lebensdauer erhöht. Es gibt verschiedene Verfahren um diese Schutzschichten aufzutragen und es werden auch immer wieder neue Legierungen entwickelt um den steigenden Anforderungen gerecht zu werden und die Lebensdauer noch weiter zu erhöhen.

Eine Literaturstudie zu dem Thema „Verschleißschutzschichten“ wurde durchgeführt, um mögliche, neue Erkenntnisse in die Arbeit einfließen zu lassen. Neue Zusatzwerkstoffe wurden auf Proben aufgeschweißt und sind charakterisiert worden. Für die einzelnen Untersuchungen wurden Schliffbilder angefertigt und mithilfe des Lichtmikroskops und Elektronenmikroskops betrachtet. Des Weiteren wurden Härtefelder von bestimmten Proben angefertigt und weitere Makro- und Mikrohärtmessungen durchgeführt.

Aufgrund dieser Erkenntnisse sollen Aussagen über eine mögliche Eignung zur Neufertigung und die Sanierung von verschlissenen Schnecken getroffen werden, um die Lebensdauer zu erhöhen. Diese Empfehlung über die neuen Verschleißschutzschichten und verschiedenen Schweißzusätze, ist in einer Anwendungstabelle festgehalten. Für die Zukunft soll dies zu einer Vereinheitlichung bei der Anwendung im Konzern, sowie zum Festhalten von Erfahrungen mit dem jeweiligen Schweißzusatz führen.

Table of contents

STATUTORY DECLARATION	II
ACKNOWLEDGEMENTS	III
ABSTRACT	IV
ZUSAMMENFASSUNG	V
TABLE OF CONTENTS.....	VI
ABBREVIATIONS	IX
1 INTRODUCTION	1
1.1 MOTIVATION	1
1.2 OBJECTIVE OF THESIS	1
2 PULP AND PAPER INDUSTRY	3
2.1 PRODUCTION PROCESS	4
2.2 REQUIREMENTS FOR WEAR RESISTANT COMPONENTS	7
2.3 COATINGS DEVELOPMENT AT ANDRITZ	8
3 LITERATURE REVIEW	10
3.1 INTRODUCTION	10
3.2 FRICTION AND WEAR.....	11
3.2.1 <i>Definition of friction</i>	11
3.2.2 <i>Definition of wear</i>	11
3.3 TYPES OF WEAR	13
3.4 WEAR AND TEAR.....	14
3.4.1 <i>Adhesive Wear</i>	15
3.4.2 <i>Abrasive Wear</i>	15
3.4.3 <i>Tribochemical Reaction</i>	15
3.4.4 <i>Material Fatigue</i>	15
3.5 WEAR RATE	17
3.6 TRIBOLOGY	18
3.6.1 <i>Tribological system</i>	18
3.6.2 <i>Influence of tribological system on wear</i>	19
3.7 WEAR TESTING	20
3.7.1 <i>Pin-on-disc test (ASTM G99)</i>	21
3.7.2 <i>Dry-sand-rubber-wheel test (ASTM G65)</i>	21
3.7.3 <i>Impeller-tumbler apparatus</i>	22
3.8 DILUTION	24
3.9 HEAT AFFECTED ZONE (HAZ).....	25
3.9.1 <i>Weld metal</i>	26
3.9.2 <i>Soft martensitic steels</i>	27
3.9.3 <i>Effect of heat input on soft martensitic stainless steel</i>	27
3.10 DIFFUSION	28

3.10.1	<i>Fick's Laws</i>	28
3.11	CHARACTERIZATION OF COATINGS.....	30
3.11.1	<i>Structure and composition of protective layers</i>	30
3.11.2	<i>Hard particles</i>	40
3.11.3	<i>Interface of matrix and hard particles</i>	44
3.11.4	<i>Hardness</i>	45
3.11.5	<i>Types of damage</i>	47
3.11.6	<i>Process parameters</i>	53
3.12	COATING PROCESSES	56
3.12.1	<i>Thermal Spraying</i>	56
3.12.2	<i>Oxyacetylene welding</i>	60
3.12.3	<i>Eutalloy process (Brazing)</i>	60
3.12.4	<i>Shielded metal-arc welding</i>	63
3.12.5	<i>Flux-core arc welding</i>	65
3.12.6	<i>Plasma Transfer Arc (PTA) Welding</i>	66
3.12.7	<i>Composite coating - Polymer surfacing</i>	69
3.13	COMPARISON OF COATING PROCESSES.....	70
4	INVESTIGATION METHODS	71
4.1	LIGHT OPTICAL MICROSCOPY.....	71
4.2	SCANNING ELECTRON MICROSCOPY (SEM)	72
4.2.1	<i>Principle of SEM</i>	73
4.2.2	<i>Energy Dispersive X-ray spectroscopy (EDX)</i>	73
4.2.3	<i>Wavelength Dispersive X-Ray Analysis (WDX)</i>	74
4.3	HARDNESS TESTING	75
4.3.1	<i>Principle of hardness testing</i>	75
4.3.2	<i>Microhardness testing (HV 0,02)</i>	75
4.3.3	<i>Macro hardness testing (HV 10)</i>	76
4.3.4	<i>Hardness mapping (HV 1)</i>	77
5	INVESTIGATION	81
5.1	SUBSTRATE	81
5.2	WELDING CONSUMABLES.....	83
5.3	SAMPLE OVERVIEW	84
5.4	SAMPLE I.....	85
5.4.1	<i>Sample I – Eutalloy (Refurbishment)</i>	86
5.4.2	<i>Sample I – 1302 A</i>	90
5.4.3	<i>EDX and WDX analysis of PTA powder 1302 A</i>	93
5.5	SAMPLE II	97
5.6	SAMPLE III.....	101
5.6.1	<i>Sample III – PG 6503</i>	102
5.6.2	<i>Sample III - AbraTec 6088 (Refurbishment)</i>	104
5.7	SAMPLE IV.....	109
5.7.1	<i>Trailing torch</i>	110
5.7.2	<i>Leading torch</i>	113
5.8	SAMPLE V.....	116

5.9	SAMPLE VI.....	121
5.9.1	<i>'Hammer fall test'</i>	122
5.9.2	<i>Sample VI - AbraTec 6088</i>	123
5.9.3	<i>Sample VI – DO 390N</i>	126
5.9.4	<i>Sample VI – DO 321</i>	130
5.10	SAMPLE VII.....	133
5.10.1	<i>Penetration Testing</i>	134
5.10.2	<i>Sample VII – Stellite 6</i>	135
5.10.3	<i>Sample VII – Keraloy</i>	138
5.10.4	<i>Sample VII - Deloro 56</i>	142
6	RESULTS.....	146
6.1	CRACKS	147
6.2	POROSITY	148
6.3	BINDING, CHIPPING & DILUTION.....	150
7	DISCUSSION	151
7.1	WELDING CONSUMABLES.....	151
7.2	WELDING TECHNIQUE	153
7.3	RECOMMENDATION & OUTLOOK.....	155
8	CONCLUSION	156
9	BIBLIOGRAPHY.....	158
10	LIST OF FIGURES.....	166
11	LIST OF EQUATIONS	170
12	LIST OF TABLES	171
13	APPENDIX	172
13.1	DILUTION.....	172
13.2	COMPARISON SHARP EDGE – BEVELED EDGE	173

Abbreviations

A.....	surface.....	[m ²]
ASTM.....	American Society for Testing and Materials	
BSE.....	Back-Scattered Electrons	
CMT.....	Cold Metal Transfer	
CRT.....	Cathode-Ray tube	
d.....	Diameter of pores.....	[mm]
D.....	Diffusion coefficient.....	[m ² /s]
D ₀	Material-dependent size.....	[m ² /s]
E.....	Activation energy.....	[J/mol]
$e^{-\frac{E}{k \cdot T}}$	Boltzmann factor	
EBIC.....	Electron-Beam-Induced Current	
EDX.....	Energy Dispersive X-Ray analysis	
F.....	Force.....	[N]
fcc.....	Face-Centered Cubic crystal structure	
FCAW.....	Flux-Core Arc Welding	
F _F	Friction Force.....	[N]
F _N	Normal Force.....	[N]
GMA.....	Gas Metal Arc welding	
HAZ.....	Heat Affected Zone	
HVOF.....	High Velocity Oxy-Fuel thermal spray process	
IWS.....	Institute for Materials Science and Welding	
J.....	[mol/m ² s]
k.....	Factor for probability to generate a wear particle	
k.....	Boltzmann constant.....	[J/K]
K.....	Wear factor	
L.....	Load.....	[N]

LOF	Lack Of Fusion	
MMC	Metal Matrix Composites	
OAW.....	Oxy Acetylene Welding	
Osc. width	Oscillation width (of PTA torch)	
PT	Penetration Testing	
PTA.....	Plasma Transferred Arc	
PU.....	Polyurethane	
PWHT	Post Weld Heat Treatment	
s.....	Path	[m]
SC	Specimen Current	
SE	Secondary Electrons	
SEM	Scanning Electron Microscope	
SMAW	Shielded Metal Arc Welding	
t.....	time	[s]
T	Absolute temperature.....	[K]
v	Velocity.....	[m/s]
VC.....	Vanadium Carbide	
vol%.....	volume %	
V_{osc}	Oscillation speed (of PTA torch)	
VPS	Vacuum Plasma Spraying	
V_{weld}	Weld speed (for all welding processes)	
W.....	Wear volume.....	[m ³]
WC.....	Tungsten Carbide (Wolfram Carbide)	
WDX	Wavelength Dispersive X-Ray analysis	
W_s	Wear rate	
wt%	weight %	
$\partial n/\partial t$	Number of particles which diffuse per time.....	[mol/s]
$\partial c/\partial x$	Concentration gradient.....	[mol/m ⁴]

1 Introduction

1.1 Motivation

The phenomenon wear is of major concern to industry, causing down time, loss of production, low efficiency, maintenance costs and the need for replacement parts.

Wear is defined according to DIN 50320 as *'the damage to a solid surface as a result of relative motion between it and another surface or substance. That involves in progressive loss of material and is due to relative motion between that surface and a contacting substance or substances.'* [1]

However, in engineering the concern with wear is usually associated with dimensional or appearance changes which may affect performance. It has important technological and economic significance because any worn tool or part will influence the product quality and the operating process. Moreover, the profitability of the manufacturing operation is affected as well.

Therefore many techniques have been developed to enhance the wear resistance of components, apart from using better materials. In principle there exist two different methods to protect parts and components. On one hand surface treatments like case hardening, nitriding and so on can be applied and on the other hand cladding with protective layers like hardfacing and thermal spraying extend also the lifetime.

Despite the successful application of protective layers, wear still occurs as a result of high work load, high relative speed between the contact areas or the abrasive nature of the counter body. It is not surprising that a lot of work has been carried out to study the wear resistance of engineering materials all over the world. To give just an impression on the economic scale, in Germany alone, wear and corrosion of technical systems destroy annually €35 billion, the equivalent of about 4.5% of the GNP. [2] [3] [4]

1.2 Objective of thesis

In the course of this diploma thesis hardfacing is investigated. The ANDRITZ AG has already a lot of experience concerning the manufacturing and refurbishment of plug screws but a huge potential is still assumed. The welding samples for the analysis have been provided and manufactured by ANDRITZ AG. Only some specific layers had been manufactured by Castolin Eutectic GmbH.

Different welding techniques as well as different filler materials should be examined. In particular, manual techniques which can be used directly on site and without dismounting the machine. Metallographic specimens of the welding samples have to be investigated using light and electron microscopy and measurement of hardness.

The following list contains the main issues of the thesis:

- A **literature survey** regarding state of the art of coating methods for plug screws using welding, thermal spraying and ceramic-synthetic resin composites is one important issue
- The **requirements** for wear resistant components in the Pulp and Paper industry should be discussed
- A **standard procedure** for the fabrication of screws and the refurbishment at the plant but also on the customer's site should be worked out.
- The **definition of grades** with respect to the quality of the layer is another point which is of additional interest

In summary, the goal is a recommendation for the fabrication and the refurbishment of worn plug screws based on the investigations and the theoretical knowledge.

2 Pulp and Paper Industry

The parts in the pulp and paper business area are affected by several influences during the operation. Two factors that are destroying the components are wear due to the impurities of the raw material, and corrosion because of the chemical treatment of the material.

The plug screw feeder is the subassembly which has to be assayed in this thesis. In Figure 1 a worn plug screw before the refurbishment at ANDRITZ is shown.



Figure 1: Worn plug screw [ANDRITZ]

Especially at the compression zone, where wood chips and other wood waste are processed, the pressure is very high. This area suffers extremely from wear and sometimes after a longer time of usage, the screw flights even cannot be seen anymore due to the high abrasion.

Some rust can be also seen in the Figure 1, which is a result of corrosion. Corrosion of this part is normally only a problem if the production gets stopped for a longer period. Considering the costs of stopping the production in the pulp and paper business, corrosion is definitely not so influencing but abrasion is the issue of concern.

2.1 Production process

For the production of panelboards, paper and pulp the plug screw feeder plays an important role. The purpose of the plug screw feeder is to dewater the chips by compression. In the following Figure 2, a detail of the production process can be seen in a very rough way and only the processes before and after the plug screw feeder are described a little more detailed.

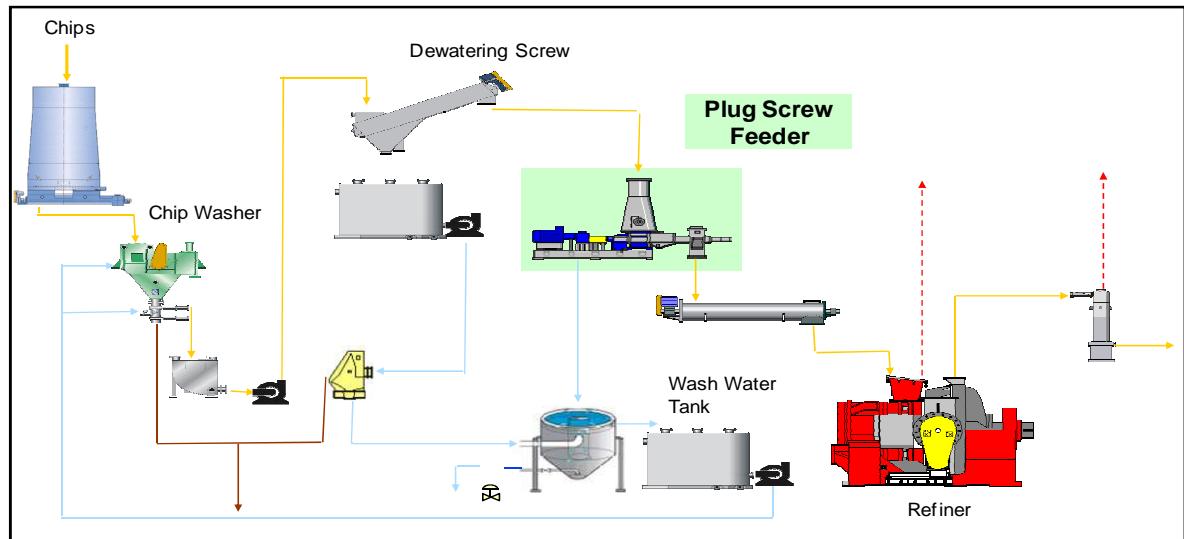


Figure 2: Plug Screw Feeder installation in production process [ANDRITZ]

Wood is the main raw material for the pulp and paper production but also waste wood, sawdust and wood shavings are used very often. Therefore a lot of impurities like concrete, metal screws, nails and a lot more are in the raw material if wood is processed, which was used for example at construction sites. In this case the machinery suffers extremely from wear. Hence the screening, washing and cleaning is very important because the result should be clean raw material for the refining process.

The pressurized refining systems of ANDRITZ are designed according to specific needs. Increasing raw material costs can be compensated by using inexpensive sawdust as a raw material. The systems allow that either chips or sawdust as well can be treated. The sawdust and the chips can be mixed at specific ratios and fed to the refining process.

The refining system starts with the 'ANDRITZ presteamer bin'. It is used as a device where the raw material is treated by fresh steam. The presteamed chips are discharged out of the bin by a vibrating discharger that feeds the chips directly into the plug screw feeder which is located underneath the bin (cf. Figure 3).

The purpose of the plug screw feeder is to dewater the chips by compression and also to convey them into the steaming unit at a certain steam pressure. The plug screw feeder also creates a continuous seal against atmosphere. As a safety device, a blow back valve takes care that in case of full or partial loss of this continuous seal, no steam will disappear against the conveying direction of the plug screw feeder.

In the following two figures the general assembly of the plug screw feeder is shown. In Figure 3, the drive unit with all feeding and discharging devices is illustrated.

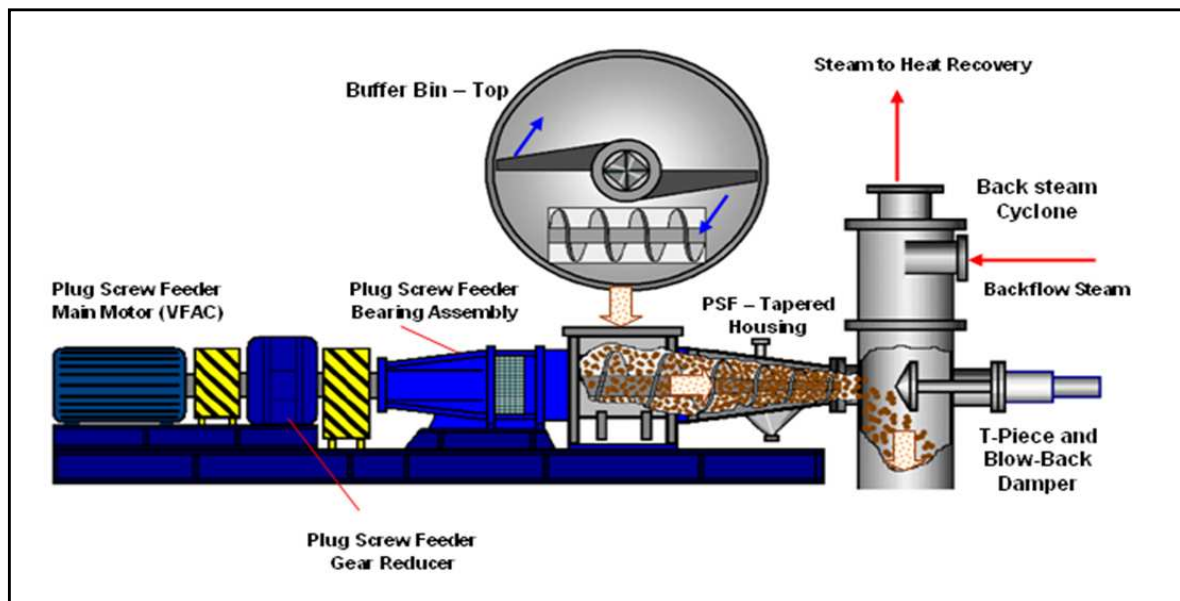


Figure 3: Plug Screw Feeder – General Assembly [ANDRITZ]

In Figure 4 the cross section of the plug screw feeder is illustrated to gain insight into the construction. The image shows the plug screw, the compression housing and the inlet housing where the pre-steamed wood chips come in. The retained water in the chips, is squeezed out and flows out through the holes in the plug feeder housing in the compression area.

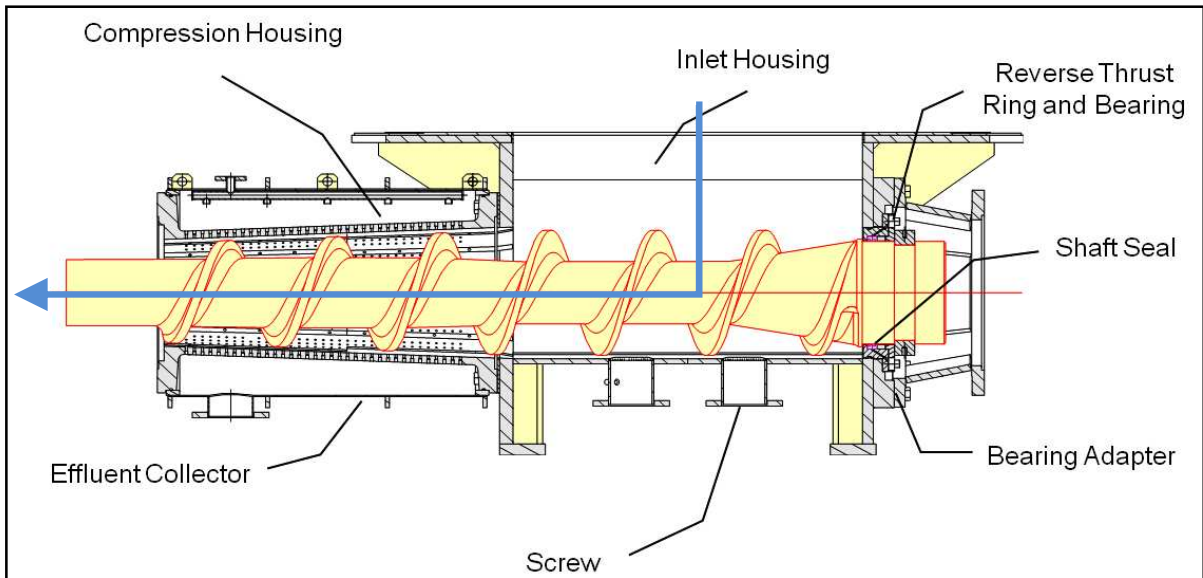


Figure 4: Screw Feeder – cross Section [ANDRITZ]

In the following picture, Figure 5, the open compression housing at ANDRITZ Graz is shown before the refurbishment process.



Figure 5: Worn compression housing before refurbishment [ANDRITZ]

After compression, the plug screw feeder conveys the raw material into the vertical digester. Depending on the material and the required end product, the retention time in the vertical digester usually ranges from three to five minutes. [5] [6]

2.2 Requirements for wear resistant components

The components in the pulp and paper industry and the plug screw in particular must fulfill specific requirements, most relevant being resistant to abrasion. The raw material and its impurities particularly, wear the surface and especially the edges. A stable screw edge or leading flank is necessary to ensure a stable production process with constant product quality. Moreover, an overload of the drive must be avoided. If the edge is disappearing and a radius is formed out, it acts like a hopper and the material is pinched between the outer diameter and the plug screw housing.

Beside abrasion irregularities in the flow of material cause impacts during production and erode the coating. Another point is the corrosion resistance of the plug screw. In this application it is not of major concern because during production abrasion and not corrosion damages the part. Corrosion, like already mentioned before, is more relevant at downtimes.

Following numeration summarizes again the requirements according to its importance under operating conditions: [7]

1. Abrasion resistance
2. Stability of leading flanks
3. Impact resistance
4. Corrosion resistance

Crack-free coatings are also an important requirement. Lamellar fractures inside the coating may cause a break-out of small pieces of the coating which may damage subsequent machinery. [8]

To be able to guarantee perfect production conditions, the geometry of the plug screw has to be according to the drawing. Hence, the grinding of the hardfaced parts is a precondition. Under ideal conditions grinding of the coating is not anymore needed. Welding techniques like Plasma transferred arc (PTA) allow a near net shape surface. Only the outer diameter of the conical screw section is ground in order to reach the required fit precision to the conical compression housing. [7] [8]

Summarizing two other important facts considering refurbishment:

- ‘Crack-free’ coating
- Enabling of machining after coating process

2.3 Coatings development at ANDRITZ

The coatings for plug screws at ANDRITZ evolve from own experience, expert knowledge and expertise of suppliers and consultants, which are specialized in wear and tear coatings. The first plug screws did not have any protective layers but due to the high loads and demands, a development and extension of protective layers was necessary to protect the screws from wear and corrosion. The process of claddings took several steps and the actual screws are completely coated. These steps of development are briefly described and illustrated in the following paragraphs.

1. The first plug screws were made of stainless steel with the material number 1.4410 (forged iron) and 1.4408 (cast iron) without any coating
2. The first coating layer was **Stellite 6**, which was used to cover only the outer diameter in the transition zone from the cylindrical area to the conical part of the screw. 75 mm before the buckle and 75 mm after it; in total 150 mm have been coated. The figure below illustrates the coating layer Stellite 6 (blue)

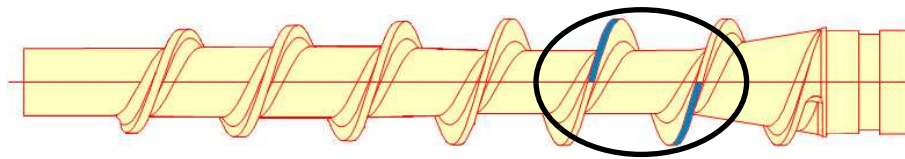


Figure 6: Plug screw with Stellite 6 at outer diameter

3. In the next step the **Stellite 6** coating was extended to the conical zone. The whole area from the outer diameter to the screw base of the front side of the screw flights was coated

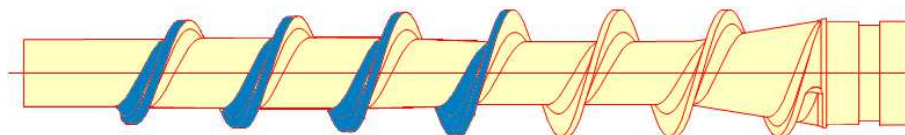


Figure 7: Plug Screw with Stellite 6 at outer diameter and leading side of flight

4. Later on, the base material was changed to 1.4317 (cast iron) but the coating was the same like described in point 3, **Stellite 6**. The material 1.4317 is similar to 1.4313, which is forged and was also used for the samples in this thesis

5. Afterwards Stellite 6 in the conical area was substituted by **Deloro 56** and **Deloro 60** at the outer diameter and the front side of the threads

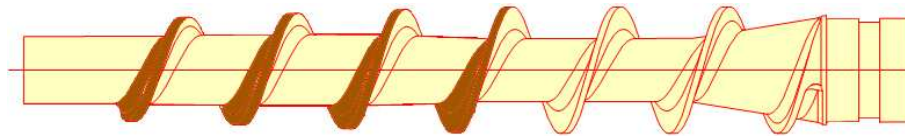


Figure 8: Plug screw with Deloro 56 / 60 coating

6. The outer diameter of screws was covered with **Stellite 6** due to its lower hardness compared to **Deloro 56** (orange). This fact guarantees that the sharp edge of the screw threads sustain. Deloro 56 was used for the edge and the screw base. Deloro 60 on the other hand was too brittle to pursue

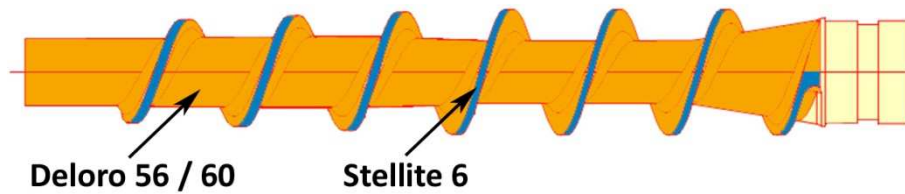


Figure 9: Plug screw with Stellite 6 at outer diameter and Deloro 56 at the remaining surfaces

7. The actual coating standard is **Stellite 6** at the outer diameter and ANDRITZ's welding consumable **Keraloy** at the threads and screw base

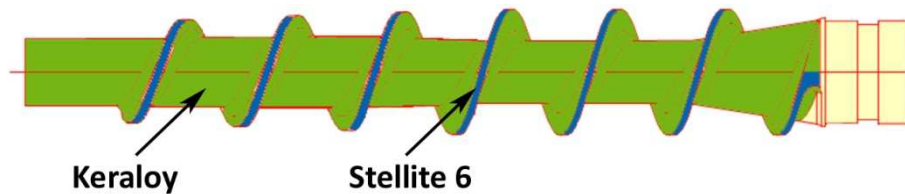


Figure 10: Plug screw with actual coating standard (2009/2010)

3 Literature review

Frequently, the costs to strip down or to remove a failed part are higher than the costs of the part itself. Therefore, it is more cost effective to repair the part in-situ. Moreover, coated components are more robust against wear, so they will last longer.

There exist different concepts and ways to protect machine parts and component surfaces from wear. Especially for applications exposed to aggressive wear and mild corrosion hardfacing plays a major role. The utilization of coating technologies and appropriate consumables satisfy the requirements and simultaneously offer an effective barrier against the harsh environment. [3]

3.1 Introduction

Wear is influenced by several parameters and it is necessary to know the effects of the different variables. The following list contains the most important factors: [9]

- Temperature
- Mechanical load
- Relative velocity
- Contact area
- Shape
- Sliding distance
- Atmosphere
- Material properties
- Types of lubrication
- Surface finish
- Vibration
- Type of motion

3.2 Friction and wear

Friction and wear occur where two surfaces undergo sliding or rolling under load. Friction is a serious cause of energy dissipation and wear is the main cause of material loss. Suitable materials are selected if two bodies are in contact with each other and solid or liquid lubricants are used to reduce friction. Lubrication reduces the wear rate at which the mating surface degrades. In order to make the best choice of material combination for certain conditions, a deeper understanding of these two processes is necessary. [10]

3.2.1 Definition of friction

Friction, according to Coulomb model, is the resistance to relative motion of two bodies which are in contact. The degree of friction is expressed by the coefficient of friction μ . The coefficient μ is expressed as the ratio of frictional force (F_F) [N] required initiating or sustaining relative motion, to the normal force (F_N) [N] that presses the two bodies together.

$$\mu = \frac{F_F}{F_N}$$

Equation 3-1: Coefficient of friction [10]

Two different kinds of friction are distinguished. Sliding friction is due to the combined effects of adhesion between flat surfaces, wear particles and asperities are ploughing the surface and asperity deformation. Rolling friction is a more complex phenomenon. The reason is its dependence on so many factors, including inconsistent sliding during rolling (slipping), and energy losses due to elastic and plastic deformations. [10]

3.2.2 Definition of wear

Wear is a phenomenon which can be observed everywhere in our life but to understand its reason is quite a demanding challenge. If two surfaces get in touch and they are in relative motion to each other, reversible and irreversible changes in both surfaces occurs. These modifications can either appear in the upper level of the surface or in the lower levels of the material as well. Very often the irreversible changes cause loss of material in one or both surfaces and can be seen as wear. [11]

'Wear is a process of removal of material from one or both of two solid surfaces in solid state contact, occurring when two solid surfaces are in sliding or rolling motion together and under load.' [2] [10]

Another definition was already mentioned above and according to DIN 50320 wear is *'the damage to a solid surface as a result of relative motion between it and another surface or*

substance. That involves in general in the progressive loss of material and is due to relative motion between that surface and a contacting substance or substances.’ [1]

The following Figure 11 shows the five main categories of wear and the specific wear mechanisms which occur in each type of wear process.

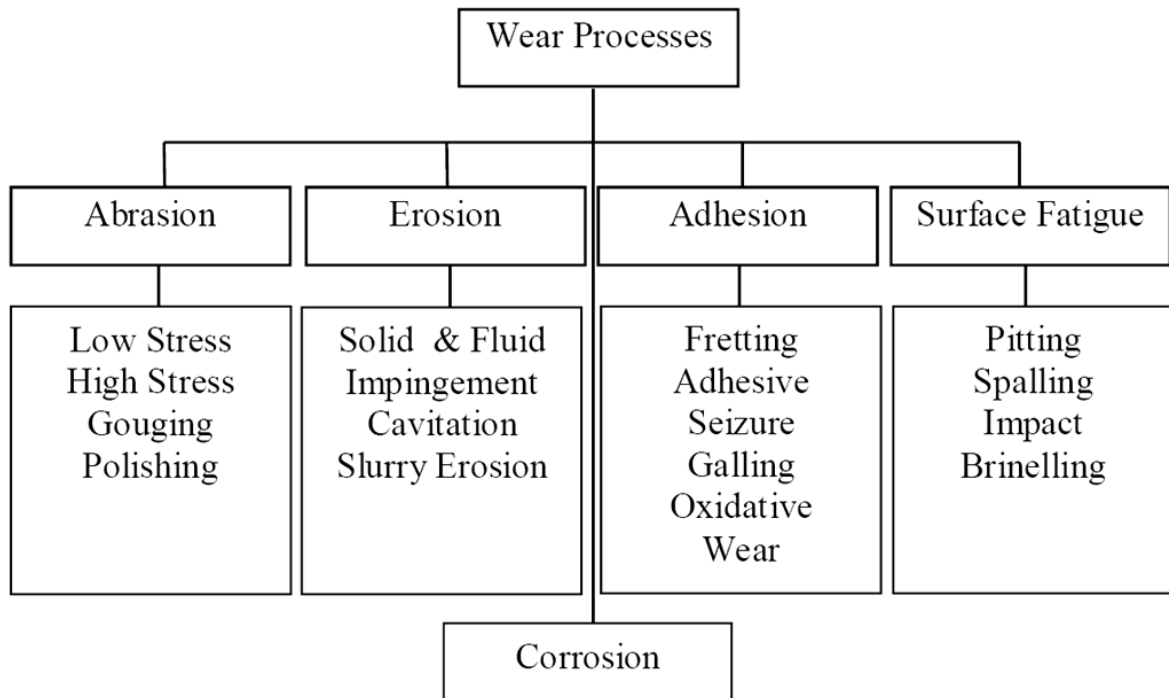


Figure 11: Classification of various wear mechanisms [10]

The definition above is maybe too restricted. It should include the possibility that wear can occur through the combined effects of chemical reaction with the ambient fluid and mechanical interaction as well. It also should be distinguished between the deliberate removals of one surface, for example, the workpiece and the unwanted wear of the other surface like the cutting tool.

Even for two specimen A and B of identical bulk composition and hardness, where one might expect equal wear on either face, it is found that differences in the rate of surface removal may occur, especially if there exist differences in nominal surface configurations. Different surface configurations will lead to different surface temperatures which, in turn, lead to differences in oxidation states, differences in substrate hardness and differences in the type and amount of interaction between the lubricant and the oxide film on the two surfaces.

Hence, the consideration of specimen geometry, specimen hardness and precise knowledge of the ambient conditions under which the system is wearing is necessary. [2]

3.3 Types of wear

Wear can be classified according to several criteria like the action between the two surfaces or the amount of bodies which participate at the wear process. The common classification of abrasive wear into 'two-body abrasion' and 'three-body abrasion' is seriously insufficient.

For these terms no definitions have been agreed upon and the implications are mutually inconsistent. The two different concepts can be described whether the abrasive particles are constrained on one side, then we talk of the two body concept, or the particles are free to move, the three body concept.

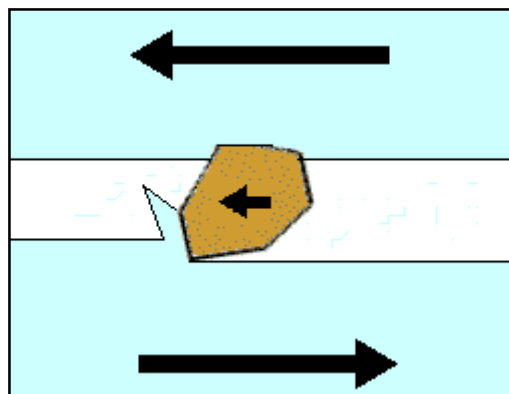


Figure 12: Two body abrasion [12]

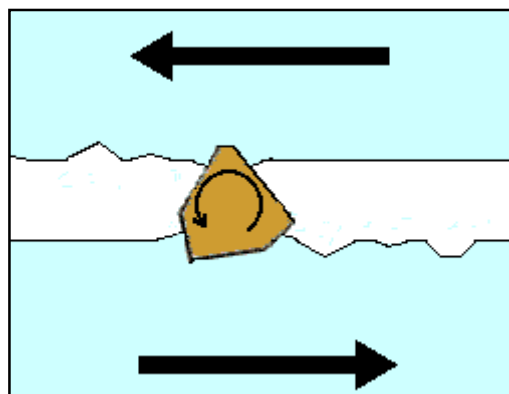


Figure 13: Three body abrasion [12]

Hence two-body abrasion is generally much more present and severe than three-body abrasion. Another alternative interpretation emphasizes the presence, three-body concept or absence, two-body concept, of a rigid counterface backing the abrasive. From this point of view, three-body abrasion is similar to high-stress abrasion and is generally more severe than two-body, low-stress abrasion. To avoid misunderstandings and confusion, these two terms should be replaced by an alternative classification scheme. [13]

Another possibility is the differentiation concerning the transaction type that leads to the following **types of wear**:

- Sliding wear
- Rolling wear
- Oscillating wear
- Impact wear
- Erosive wear

Another approach for a classification is the **type of load**:

- Mechanical wear
- Chemical wear
- Thermal wear

Mechanical wear concerns mainly deformations in ductile material and cracking and fractures of brittle materials. Chemical wear takes place if thin surface films are formed due to the reaction of the surface with a corrosive environment. Thermal wear occurs as a result of great amount of heat which causes surface softening. [11]

3.4 Wear and tear

Wear and tear can be classified to the underlying wear mechanism as well. Based on the following categorization of Koji Kato [14] who specified seven different wear mechanisms only the first four are well established: [11]

1. Adhesive wear
2. Abrasive wear
3. Tribochemical reaction
4. Surface fatigue

and the others still have to be investigated:

- Flow wear (erosion)
- Melting wear
- Diffusion wear

The four mentioned wear mechanisms which are well established are described a little bit more in detail in the following paragraphs.

3.4.1 Adhesive Wear

Adhesive wear occurs when adhesive junctions that are newly formed lock together and two surfaces slide across each other under pressure. Local breaks through the oxide layers result in cold welding and material particles are torn off the surface.

When normal pressure is applied, local pressure at the asperities becomes extremely high. In this case, the yield stress of these areas is exceeded and the asperities deform plastically until the contact area increases sufficiently to carry the full load.

3.4.2 Abrasive Wear

Abrasive wear happens when the particular material is being removed from one surface, by another harder material. The hard particles of the debris between the two surfaces are formed and the harder material scratches the softer material.

3.4.3 Tribochemical Reaction

An accelerated chemical reaction of contact surfaces under load or elevated temperature with lubricants, additives or other media. The reactions lead to thin films or particles which get removed.

3.4.4 Material Fatigue

Progressive and localized structural damage occurs if a material is subjected to cyclic loading. The maximum stress values are less than the ultimate tensile stress limit and are also below the yield stress limit of the material. Due to long term elasto-plastic deformation of the contact surface, material achieves the fatigue limit. This leads to morphological changes and microscopic cracks will begin to form at the surface or in a certain distance below it. That depends on the contact situation and the microstructure of the contacting materials. If a crack reaches a critical size, the structure will suddenly fracture and cracks are formed below the surface. [3] [10] [15] [16]

In the following Figure 14 the four phenomena of wear are illustrated.

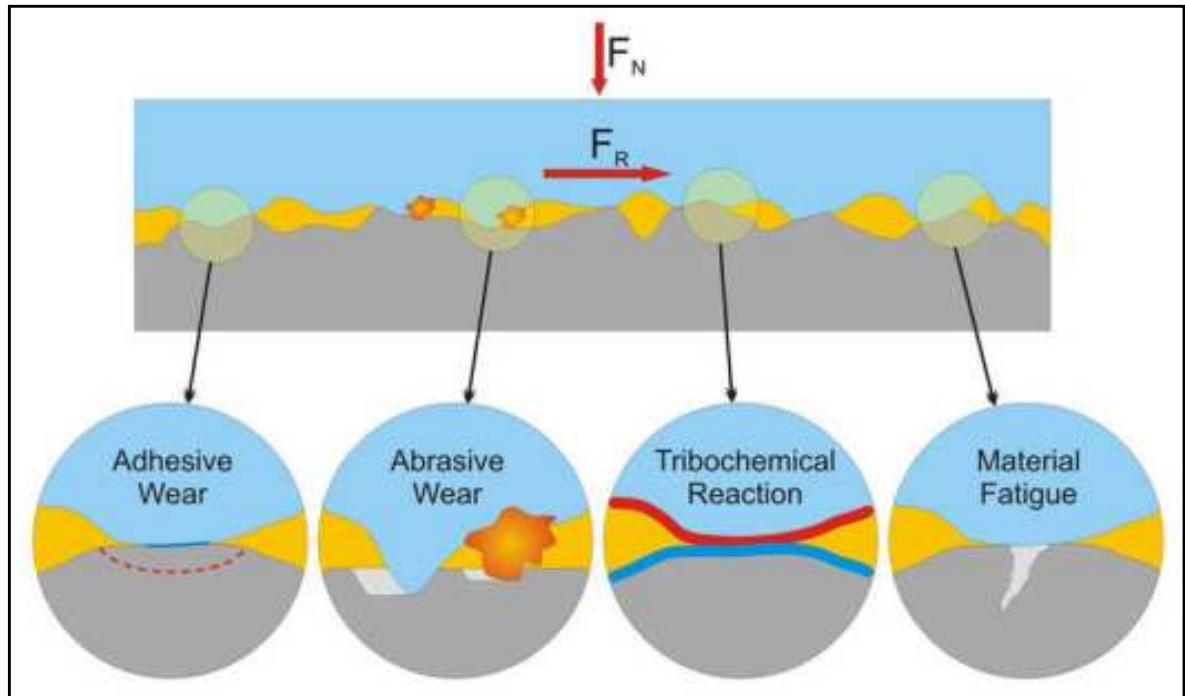


Figure 14: Four types of wear [15]

3.5 Wear rate

There exist several approaches to describe the wear rate which is the material removal or dimensional change due to wear. [17]

The wear rate is mostly influenced by: [18]

- The ratio of material hardness to abrasive hardness
- The worn-out material
- The size of the hard particles

Wear rate is often defined as volumetric loss of material over a unit of time and several mechanisms operate simultaneously to remove material from the wear interface. In Figure 15, the effect of hardness of the abrasive media and the worn material is shown.

As the hardness of the abrasive exceeds that of the wear material, abrasive wear becomes worse. It is able to penetrate the surface and remove material. [4]

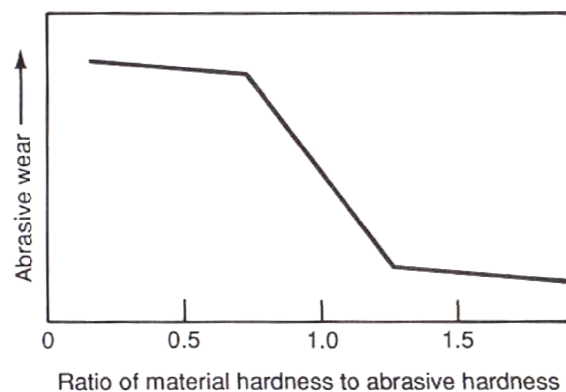


Figure 15: Effect of abrasive hardness, relative to material hardness, on abrasive wear [4]

A common used and simple equation to calculate the wear rate was found by **Arachand**. This model assumes that surface asperities are in contact and build adhesive bindings. Therefore wear occurs due to adhesive mechanism at peaks of roughness. [16]

$$W_s = k * L * s$$

Equation 3-2: Wear rate Arachand [16]

W_s , the wear rate result in the path s [m], and the applied load L [N] and the factor k , which describes the probability to generate a wear particle during the path and contains all constants and variables of a tribological system. [16] [19]

Another possibility to compare wear is the wear factor **K**. In the chapter 3.7 methods for wear testing are introduced and for it the wear of an unlubricated surface in sliding is quite important. The testing principle of standard tests such as 'Pin-on-disc test', are based on the wear of an unlubricated surface in sliding. This kind of wear is proportional to the load multiplied by the distance traveled. Therefore, a factor of proportionality, the wear factor **K**, can be introduced and determined as follows: [4]

$$K = \frac{W}{F * v * t}$$

Equation 3-3: Wear factor **K** of unlubricated surface in sliding wear [4]

The other appearing parameters that affect sliding wear are wear volume **W** [mm³], the normal force **F** [N], the velocity **v** [m/s] and the time **t** [s]. [4]

3.6 Tribology

Tribology is a multidisciplinary science dealing with friction, wear and lubrication of surfaces in relative motion. This multidisciplinary field based on fluid and machine dynamics, metallurgy, heat transfer, stresses, physical and surface chemistry is quite difficult to understand due to its complexity. [20]

3.6.1 Tribological system

A tribological system consists of two surfaces of components which are in moving contact with one another and their surroundings. Several issues influence the type, progress and extent of wear determined by the materials of the components, any intermediate materials, surrounding influences and operating conditions. [21]

A tribological system transforms input work into output and has four main elements which are: [22]

- body
- counter body
- interfacial medium
- surrounding medium

Figure 16 shows the principle of a tribological system with its four main elements.

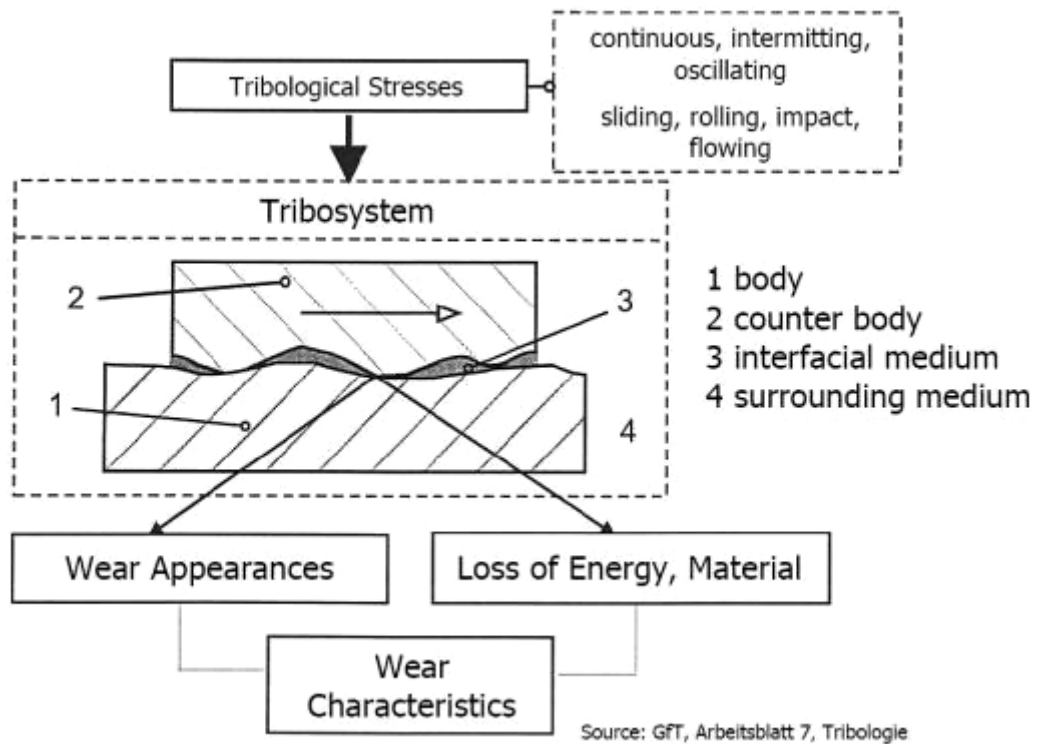


Figure 16: Tribological System [22]

3.6.2 Influence of tribological system on wear

The solution of wear problems starts with a detailed examination of the tribological system. All influencing factors like body, intermediate substrate, counter body, load, type of motion, environment and the temperature that are involved, have to be taken into account.

Under real conditions, always more than one of these effects are active at any given time or they occur consecutively during the wearing process. However, usually one effect plays the predominant role in failure due to wear. Experience and research show that every tribological system can be optimized by the surface properties. [20] [21]

3.7 Wear testing

Tests for tribology and wear can deliver important information concerning investigations on friction, wear and lubrication. The purpose is to determine wear and friction characteristics of materials under defined conditions. There are many types of wear test methods both because there are many types of wear and on the other hand there are many different situations in which wear causes problems.

Wear test methods fall into any of several categories. Some wear test methods are aimed at a specific type of material, some are aimed at evaluating a material's response to a specific type of wear and other wear tests are designed to simulate a particular field of application in order to screen materials. [23]

ASTM, the American Society for Testing and Materials, developed a standard for wear testing methods to help solving important industrial problems involving sliding wear, abrasive wear etc. The principal advantages of using standard wear test methods are: [23]

- The test methods are evaluated and the procedures documented
- The repeatability and reproducibility tends to be better documented and understood than for specialized wear testing machines
- In many cases, a lot of previous data exists which can be used for comparison with new results

Like mentioned above, allow these standardized tests a comparison of different materials but the problem is the transfer to real applications. Very often components endure a combination of several interactions like abrasion, impact and corrosion. In such cases it is difficult to make useful and significant statements based on tests. Only tendencies can be seen and there is often no getting around of real applications or special designed testing equipment. [23]

The following list provides some wear test methods used for the screening of wear coatings and the most common are described later on in detail.

- Pin-on-disk test
- Dry-sand-rubber-wheel abrasion test
- Block-on-ring test
- Ball-on-ring test
- Ball cratering test
- Single impact test
- Impeller-tumbler apparatus
- Miller test

3.7.1 Pin-on-disc test (ASTM G99)

This relatively simple ASTM test provides a fast answer on the abrasion wear resistance of materials. Therefore, a pin rotates on abrasive paper. The mass loss after the test is measured and converted into a wear coefficient. Applications are friction and wear investigations on pin-on-disc principle. [18] [24]

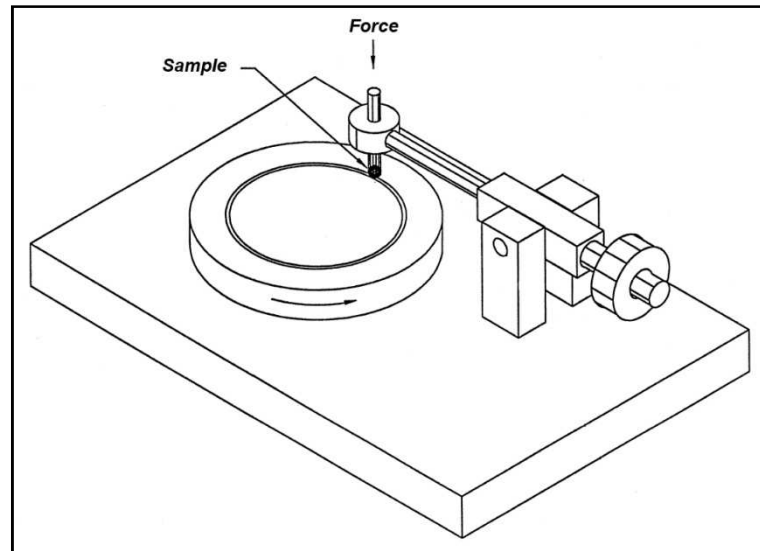


Figure 17: Schematic of pin-on-disc testing machine (ASTM G99) [23]

3.7.2 Dry-sand-rubber-wheel test (ASTM G65)

This test method covers laboratory procedures for determining the resistance of metallic materials to scratching by sand between a specimen and a rubber wheel (three-body abrasion). The intent of this test method is to rank materials in their resistance to scratching abrasion. Sand flows through the special nozzle, in the shape of thin layer between the test piece and a rotating hard rubber wheel. The applied force presses the sample against the wheel which wears the surface. Afterwards the tested specimen is weighed. Abrasion test results are reported as volume loss and materials of higher abrasion resistance will have a lower volume loss. [25]

The following Figure 18 shows the schematic of the dry-sand-rubber-wheel tester.

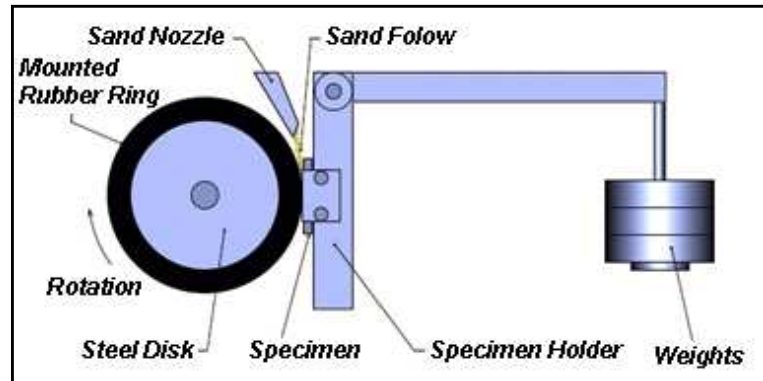


Figure 18: Schematic of ASTM G65 dry-sand rubber-wheel tester [26]

The comparison will provide a general indication of the quality of the unknown materials if abrasion is the predominant factor causing deterioration of the material. [18] [27]

3.7.3 Impeller-tumbler apparatus

The impeller-tumbler testing device is not a standardized method according to ASTM but allows a combination of abrasion and impact. This apparatus consists of a slowly rotating outer tumbler and a fast rotating inner impeller where the testing specimens are mounted on. The tumbler is filled with a defined amount of abrasive and controls the flow of abrasive particles hitting the fast moving testing specimens. [27] [28]

The following Figure 19 illustrates the impeller-tumbler apparatus at the *AC²T research GmbH* in Wiener Neustadt.



Figure 19: Impeller-tumbler apparatus [25]

Figure 20 illustrates the schema of the Impeller – tumbler testing device.

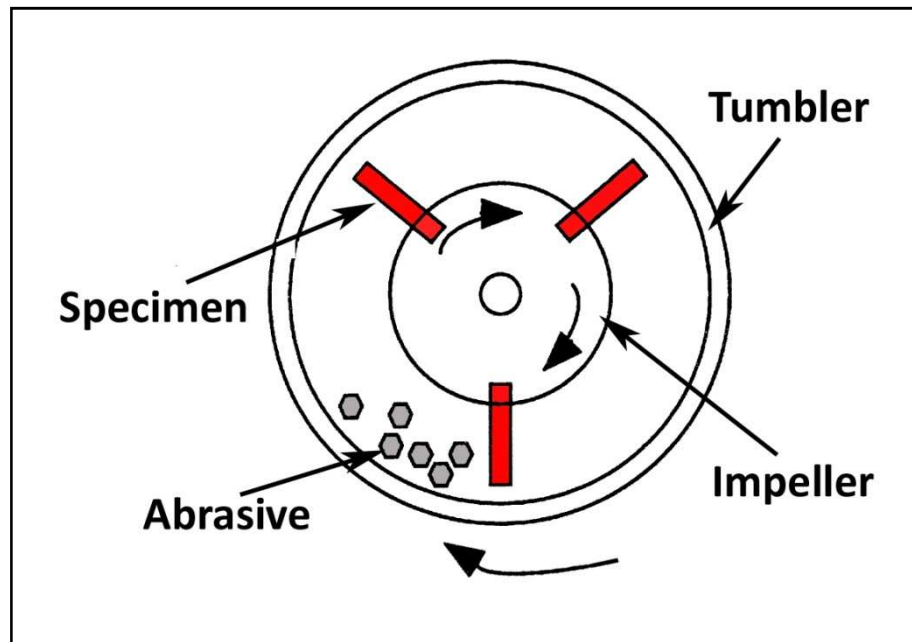


Figure 20: Impeller-tumbler schema [25]

3.8 Dilution

Dilution is used to express the amount of ‘alloying’ that occurs between the coating and the substrate. It is determined experimentally by optical microscopy of the cross-section and is defined by the following relationship.

$$Dilution = \frac{A_1}{A_1 + A_2} * 100$$

Equation 3-4: Dilution [29]

A_1 [m²] stands for the cross-section area of the penetration zone of the parent metal and A_2 [m²] is the cross-sectional area of the deposit (above the original surface).

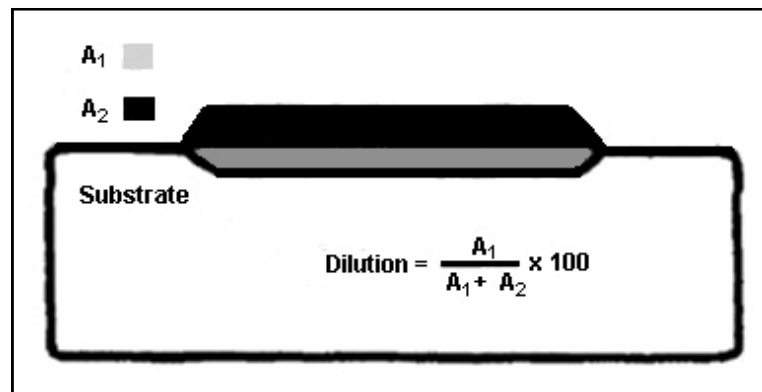


Figure 21: Schematic diagram illustrating the cross-sectional areas for calculation of dilution content [30]

Dilution has a significant effect on the chemical composition and properties of the deposited metal. On one hand a high value is associated with a large heat affected zone (HAZ) and a reduction in the hardness of the coating. On the other hand a low value is often indicative for lack of fusion but it also depends in a very strong way on the welding technique. [29]

The most significant factors that influence overlay dilution are:

- plasma gas flow-rate
- voltage & current
- filler metal feed rate

For given filler metal feed-rate and deposition speed an increase in arc current results in higher dilution content. With increased filler metal feed-rate and all other parameters are hold constant, this would reduce the dilution. A high plasma gas flow-rate increases the penetration and therefore, the dilution is increased as well. Preheating increases the solidification time and encourages dilution too. [30]

3.9 Heat affected zone (HAZ)

The HAZ can be defined as followed: *'The portion of the base metal that has not been melted, but whose mechanical properties or microstructure have been altered by the heat of welding, brazing, soldering or cutting'*. [31]

During a welding process the metal undergoes various changes according to peak temperature and cooling rate experienced at each location. The heat input affects the peak temperature, the time at peak temperature and the temperature gradient as well. [32]

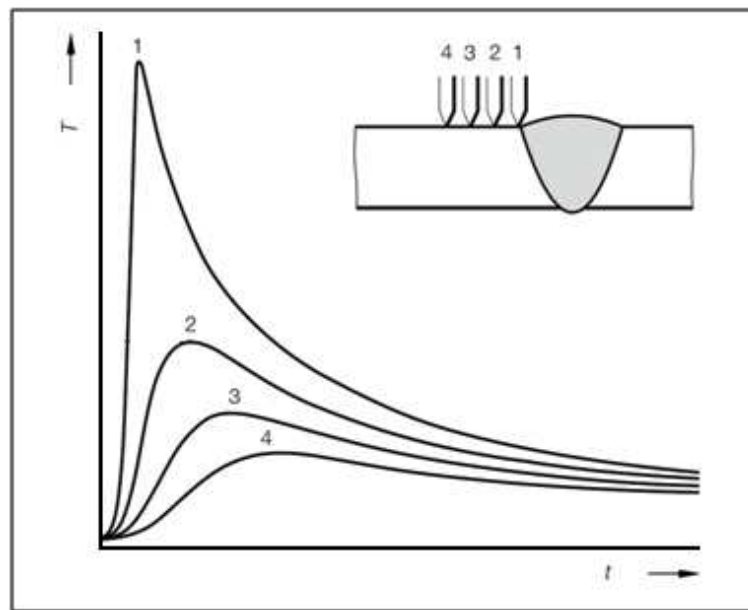


Figure 22: Temperature-time cycle depending on the distance to weld pool [29]

In the fusion area the temperature will be high enough to cause complete transformation to austenite. A zone with coarse grain beside the fusion zone can be noticed. Other modifications like lattice structure, precipitates and mechanical properties occur as well. An increase of hardness which mainly depends on the carbon content is the consequence. Moving away from the fusion boundary the peak temperature is insufficient to cause any microstructural changes although other effects such as aging may occur. [32] [33]

Studies of brittle fractures in welds show the site of initiation of the fracture is often the HAZ. It is very often at a point of stress concentration, is subjected to high residual stresses and may contain defects. If in addition the HAZ toughness is low it becomes a prime candidate for starting a brittle fracture. To avoid the presence of hard and brittle martensitic structures in the HAZ, welding energy input and preheating can ensure an adequate slow cooling rate. [32]

3.9.1 Weld metal

Weld metal, molten base metal and filler metal, is heated up very quick during the welding process and starts off as a small casting, cools rapidly down and it is not surprising that the properties of weld metal can be quite different from those of the base metal and the HAZ. The microstructure of the weld metal is influenced first by the solidification structure which occurs after the metal freezes. Normally long austenite grains extend from the fusion boundary towards the centre of the weld. This typical cast structure (columnar grains) has anisotropic characteristics and unfavorable mechanical properties. The final composition of the weld metal is determined by three factors: [32] [33]

- Filler metal composition
- Dilution from base metal
- Chemical reactions

The following Figure 23 illustrates the various zones adjacent to the weld metal in a low alloy steel.

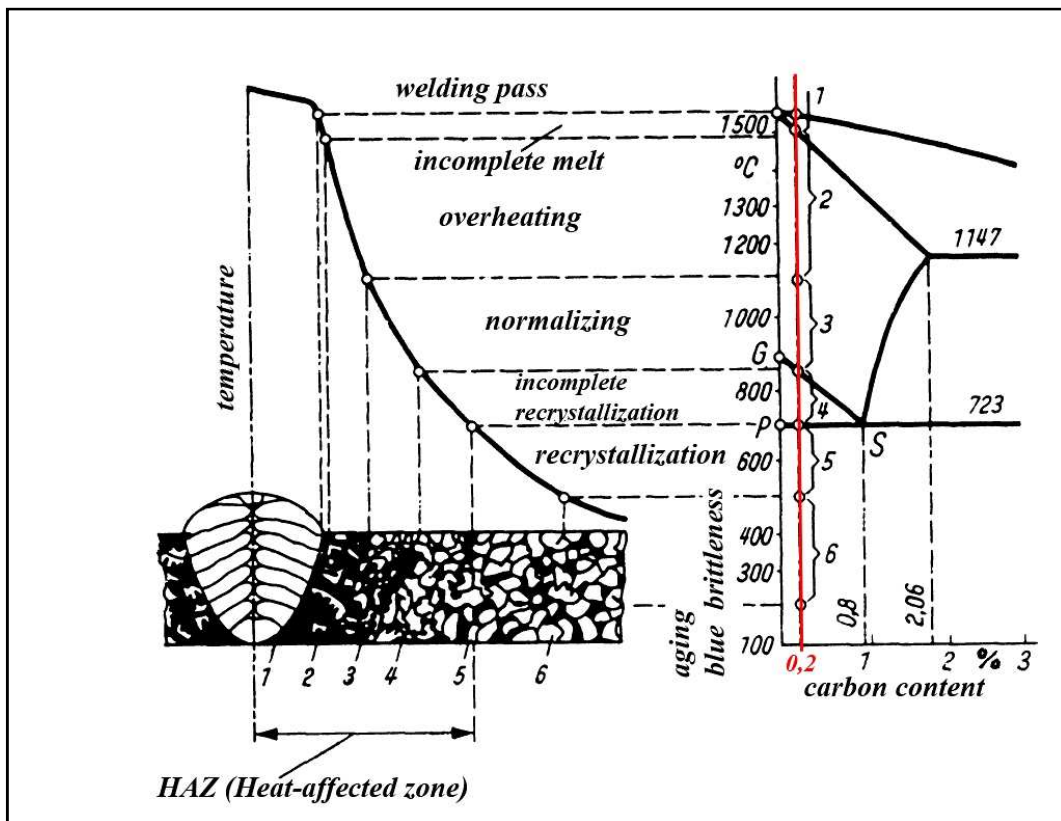


Figure 23: Microstructures in HAZ of low-alloyed steels [34]

3.9.2 Soft martensitic steels

The aim of developing soft martensitic steel was to improve weldability and toughness. Furthermore, the reduction of the crack susceptibility while maintaining high strength levels was an issue.

The lower carbon content improves weldability but makes the addition of Ni necessary. The addition of 3.5-6 % Ni, a powerful austenite former, is required to avoid delta ferrite, which is deleterious to impact toughness. The increasing of Ni depresses the Ac1 temperature to about 600 °C as opposed to 720 °C for a conventional martensitic stainless steel without nickel. Hence, this slows down the tempering reactions. For enhanced corrosion, temper embrittlement and tempering resistance, 0.5 % to 2 % Mo is added, depending on the intended use. [35] [36]

3.9.3 Effect of heat input on soft martensitic stainless steel

Postweld heat treatments (PWHT) are necessary to satisfy the service mechanical property requirements. In order to achieve maximum strength and toughness, the steel must be dominantly martensitic after cooling, with limited delta ferrite. To obtain beside good hardness also ductility and stress corrosion resistance, the martensite must be tempered; solution annealing plus tempering or double tempering are necessary.

The aim of solution annealing is the homogenization of the microstructure by dissolution of delta ferrite. An initial high-temperature heat treatment at 670 °C (hypercritical, well above Ac1) causes softening of martensite. At the same time, it results also in partial retransformation to unstable austenite. When it is cooled, this austenite reverts to fresh martensite, producing a mixed structure of tempered and untempered martensite.

During the second tempering at a lower temperature (intercritical, 600 °C), fresh stable austenite precipitate through new interfaces and the fresh martensite is transformed into tempered martensite.

In the as-welded condition, the microstructure consists of low-carbon martensite, some presence of delta ferrite, and retained austenite depending on the steel composition. Hence, as a result of this complete post weld heat treatment, an increase of the number of austenite after double tempering is produced with a more uniform distribution. This secondary austenite improves the toughness, is extremely stable, and does not transform even at very low temperatures (-200°C). [35] [36] [37] [38] [39]

3.10 Diffusion

Diffusion is the mass transport without convection in fluids, gases and solids. In solid state, the direct exchange and the ring exchange do not play a major role in diffusion due to the high packing density of metals. Two other diffusion mechanisms, the vacancy diffusion and interstitial diffusion are more relevant. [40] [41]

Diffusion within the crystal lattice occurs due to interstitial or substitutional mechanisms. In interstitial lattice diffusion, a diffusant element like carbon in an iron alloy, diffuses in between the lattice structure of a crystalline element. In substitutional lattice diffusion, the atoms move by changing place with another atom. Substitutional lattice diffusion occurs frequently because of point vacancies throughout the crystal lattice. [40] [41]

3.10.1 Fick's Laws

Adolf Fick enunciated first two assumptions in 1855. They describe an atomic process in a quantitative way without specifying the process itself. This means that the assumptions are still valid if other processes are underlying. [40]

Fick's First law

This equation describes the rate of movement of a substance by diffusion from a higher to a lower concentration. [41]

According to the first law of Fick, the number of atoms ∂n , which diffuse in a certain time ∂t through a surface A [m²], which stands perpendicular to the diffusion current, is proportional to the local concentration gradient $\partial c/\partial x$ [mol/m⁴]. [40] [41]

The number of particles ∂n , which diffuse in a certain time ∂t through a perpendicular standing area A , can be expressed by the diffusive flux J [mol/m²s].

$$J = \frac{1}{A} * \frac{\partial n}{\partial t}$$

For space, stationary, isotropic and isothermal diffusion:

$$J = -D * \frac{\partial c}{\partial x}$$

Equation 3-5: Fick's First law [42]

Diffusion coefficient:

D is the diffusion coefficient and describes the speed of the diffusion process. It has the unit [m²/s].

$$D = D_0 * e^{-\frac{E}{k*T}}$$

Equation 3-6: Diffusion coefficient [41]

D_0 [m²/s] is a material-dependent size. $e^{-\frac{E}{k*T}}$ is the Boltzmann factor and describes the probability for a particle to perform in excess of an activation energy E [J/mol] a migration. T [K] is the absolute temperature and k [J/K] is the Boltzmann constant.

Fick's Second law

The second law of Fick describes the unsteady state or in other words the concentration change in one point depending on time. [40] [41]

It is:

$$\frac{\partial c}{\partial t} = \frac{\partial}{\partial x} * \left(D \frac{\partial c}{\partial x} \right)$$

Equation 3-7: Fick's Second law [42]

3.11 Characterization of coatings

Wear causes different types of damage and destroy the coatings. For each wear mechanism a specific concept fits better. Protective layers can be described by several aspects. Their structure and composition strongly influence and determine the characteristics. For high abrasive wear so called '*pseudo alloys*' are widespread in industrial applications. These pseudo alloys are mixtures of hard alloy powder and hard particles.

After the welding process a relative ductile matrix with tight embedded hard particles is formed. If applied correctly the hard particles are an effective protection against wear. Process parameters have also a huge effect on the quality of the coating and must be taken into account. [43]

Requirements for a functional layer:[43] [44] [45] [46] [47]

- The bonding with the substrate must be strong
- The hard particles should be dispersed homogeneously in the matrix
- The particles must be also embedded tightly in the matrix so they cannot be pulled out easily
- The hard particles should not be dissolved to avoid a loss of wear resistance and a decrease of the matrix ductility

3.11.1 Structure and composition of protective layers

Coatings often consist of hard phases, which are embedded in a softer matrix to enhance the wear resistance.

Matrix

The matrix is a homogenous material into which the reinforcement is embedded. Very often the matrix is a lighter material compared to the hard particles and provides a compliant support for the reinforcement. A further requirement is the shock-absorbing function of the matrix. It is also responsible for a strong bonding with the substrate and should allow a homogenous dispersion of the tightly embedded hard particles to avoid pulling out. [43] [45] [46]

Reinforcement:

The reinforcement material is embedded into the matrix and has a structural task; reinforcing the compound. In the application of wear it is used to change physical properties such as wear resistance and friction coefficient. The hard particles should not be dissolved to avoid a loss of wear resistance and a decrease of the matrix ductility. [43] [45] [48]

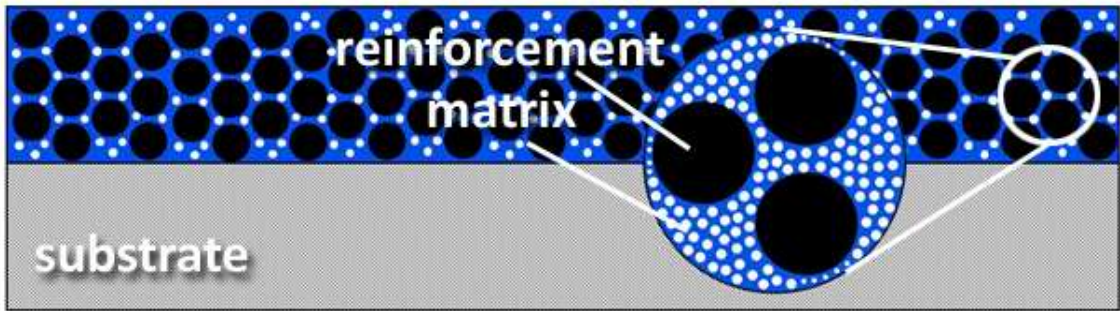


Figure 24: Schematic of structure and composition of coating [49]

In Figure 25 the structure of the coating type *Keraloy* can be seen. In the NiBSi-matrix tungsten carbides are embedded.



Figure 25: Ni-based matrix with embedded tungsten carbides - specimen_29 (Keraloy)

The chemical composition of the matrix has significant influence on wear and corrosion resistance of the coating. Therefore, the welding consumables must be adapted to the kind of expected wear like abrasion, corrosion, erosion, and cavitation and so on.

A distinction between coatings with premixed synthetic hard particles like tungsten carbide, 'pseudo alloys' and coatings which gain their wear resistance due to precipitations must be done. [50]

Multi-phase coating materials like iron-based FeCrC-alloys, nickel-based self-fluxing NiBSi-respectively NiCrBSi-alloys and cobalt-based Stellite alloys according to DIN 14700 are the most commonly used.

Each type can be modified by multiple alloying elements to achieve specific properties of the matrix adapted to the wear mechanism. It is very difficult to predict or estimate the influence of specific alloying elements on existing compositions. Especially the variety of concepts is huge and metallurgical effects are very complex.

Ni- and Co-based alloys have gained high acceptance and are widespread in many industrial applications for wear protection of components. Based on rising costs of nickel and cobalt, intentions arise for new alternatives. Newly developed iron-based alloys can reach the same wear resistance as Ni-based alloys with fused tungsten carbides at the same level of corrosion resistance but lower costs. [45]

3.11.1.1 Co-based

Cobalt is the preferred binder due to its outstanding wetting and adhesion characteristics. The crystal structure of cobalt is face-centered cubic (fcc) above 422 °C and hexagonal close packed below 422 °C. [4]

Cobalt alloys used for wear applications can be applied by any known fusion welding process or spraying process. Their unique combination of wear resistance, heat and corrosion resistance make them adaptable to many harsh environments.

A lot of properties of these alloys arise from the crystallographic nature of cobalt, the solid solution strengthening effects of chromium, tungsten and molybdenum, the formation of metal carbides and the corrosion resistance imparted by chromium. Cobalt has a hexagonal crystal structure which promotes a low adhesion and thus it is very resistant in metal-to-metal wear. [48] [51]

There are two types of commercially available cobalt-base hardfacing alloys:

- Carbide containing alloys
- Alloys containing Laves phase

The Laves phase alloys are not so common because it is quite difficult to attain crack-free overlays. Moreover, it has disadvantageous effects on the mechanical properties like ductility and impact strength but it is very resistant in metal-to-metal wear and responsible for outstanding abrasion resistance.

The carbide-containing alloys like Co-Cr-W-C alloys (*Stellite*) are more widespread and extremely versatile. They contain generous amounts of carbide-forming elements like

chromium, tungsten and molybdenum. The microstructures generally consist of chromium-rich M_7C_3 carbides and with a higher amount of tungsten, the tungsten rich M_6C type of carbide is precipitated. The matrix of cobalt-based alloys such as Stellite 6 is austenitic. In general, alloys with more than about 1.3 % C are already very brittle and only can be made by casting. [52] [53]

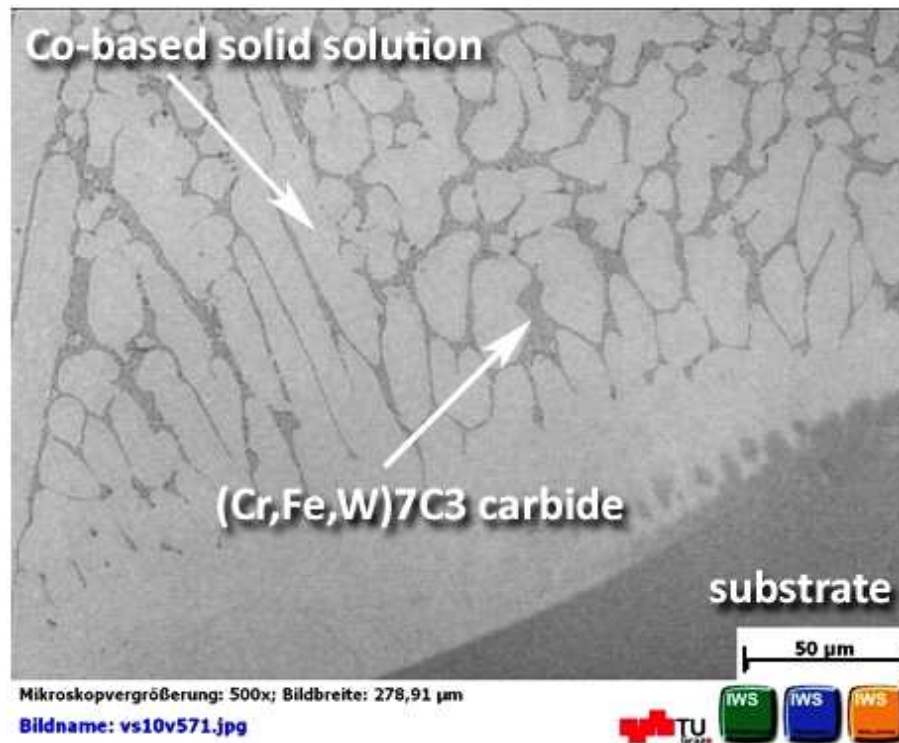


Figure 26: Co-based Stellite 6 coating on 1.4313 stainless steel – specimen_27

Co-based alloys are particularly effective when high-temperature or corrosive conditions are combined with abrasive, erosive or other wear conditions. These materials retain their hardness at elevated temperatures and therefore they are excellent in applications in which lubrication cannot be used. [31] [48] [54] [55]

3.11.1.2 Ni-based

Nickel-based alloys are resistant to wear and corrosion and possess good high temperature properties. For applications in which extreme wear is combined with high temperatures and corrosive media they are very suitable for use in adhesive wear situations. [56] [57] [58]

Nickel-based hardfacing alloys can be divided into three different groups:

- Boride containing alloys
- Carbide containing alloys
- Laves phase containing alloys

Nickel has a face-centered cubic crystal structure (fcc) which is responsible for its excellent ductility and toughness. Due to the extensive solid solubility of nickel for many alloying elements, the microstructure of nickel alloys consist of the fcc solid-solution austenite in which particles precipitate and disperse. [52]

Among the hardfacing alloys, nickel-base/boride type alloys are the most complex considering the microstructure. Chromium, boron and carbon are the determining elements for the level and type of hard phases within the structure. Iron content varies and is largely incidental to allow the use of ferro compounds during manufacturing.

Boron is the primary hard-phase forming element for which nickel and chromium are competing. Appearing hard phases are Ni_3B and chromium boride like CrB , Cr_2B and Cr_3B_2 . Additional types like M_{23}C_6 and M_7C_{23} are also present. An addition of boron lowers also the melting point and viscosity of the melt.

Carbon is the secondary hard phase forming element. Amounts of silicon are also added to provide together with boron self-fluxing characteristics. This means that the addition of a flux in order to wet the substrate is not necessary because of self-deoxidization and self-slag formation when melting. Moreover, silicon promotes intermetallic precipitates and strongly influences the wear properties of alloys.

Due to the boride and carbide dispersions within their microstructure, the nickel-base/boride-type alloys exhibit excellent resistance to abrasion. Nickel-base/boride type alloys offer the least corrosion resistance among nonferrous materials. This is attributed to the lack of chromium in the matrix which follows boride and carbide formation. [4]

Carbide-containing nickel alloys are gaining popularity as low-cost alternatives to cobalt-base alloys. Depending on their precise composition, they contain M_7C_3 or M_6C -type carbides similar to the cobalt-base alloys. [4]

Laves phase containing nickel-base alloys can be readily applied by oxyacetylene process or PTA process. These alloys have excellent metal-to-metal wear resistance but moderate abrasive wear resistance and poor impact resistance. Very often the high hardness demanded for wear resistance makes a crack-free deposition nearly impossible. [4] [48]

Some applied welding consumables have a nickel-base matrix (NiCrBSi- or NiBSi-system) and added tungsten carbides (pseudo alloys) to enhance wear resistance. Nickel also reduces the dissolution of the synthetic tungsten carbides during the welding process. [48]

The investigated consumables like **Deloro 56** can be classified to boride containing nickel-base alloys. Deloro 56 consists of an austenitic matrix on nickel basis with embedded chromium borides and offers a good protection against corrosion.

Also other welding consumables based on a NiCrBSi-system like **TeroCote 7888T** and **TungTec 10122** might be classified to this group as well, although synthetic produced tungsten carbides are admixed.

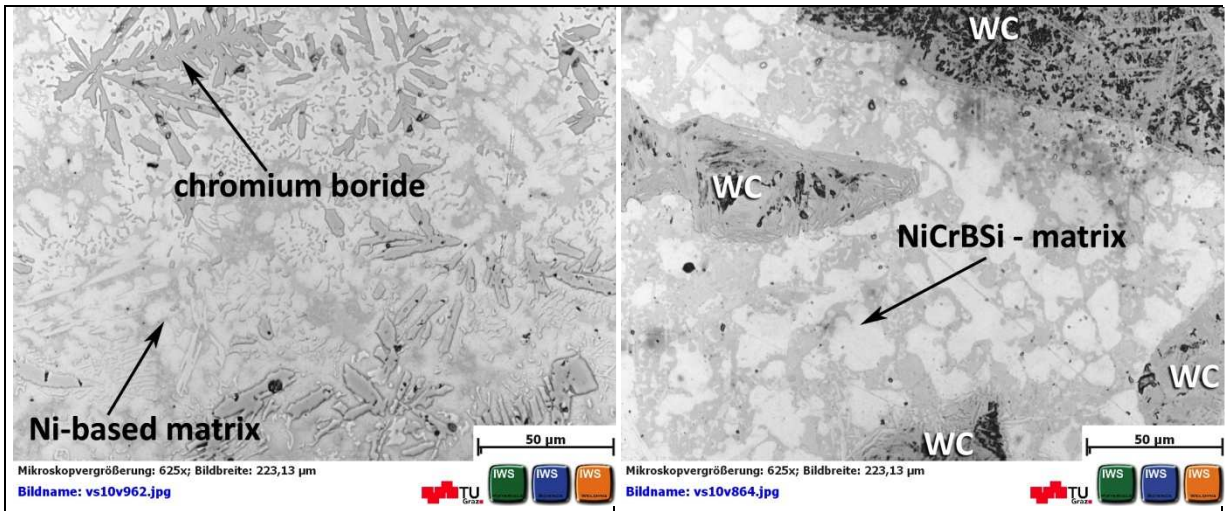


Figure 27: Left: Deloro 56; Right: TeroCote 7888T & TungTec 10122

All the other cladded nickel-based alloys (**AbraTec 6088**, **PG 6503**, **DO 321** & **Keraloy**) belong to the NiBSi-system. Their classification is not so easy due to the lack of the very influencing element chromium. They mostly fit to boride-containing nickel base alloys.

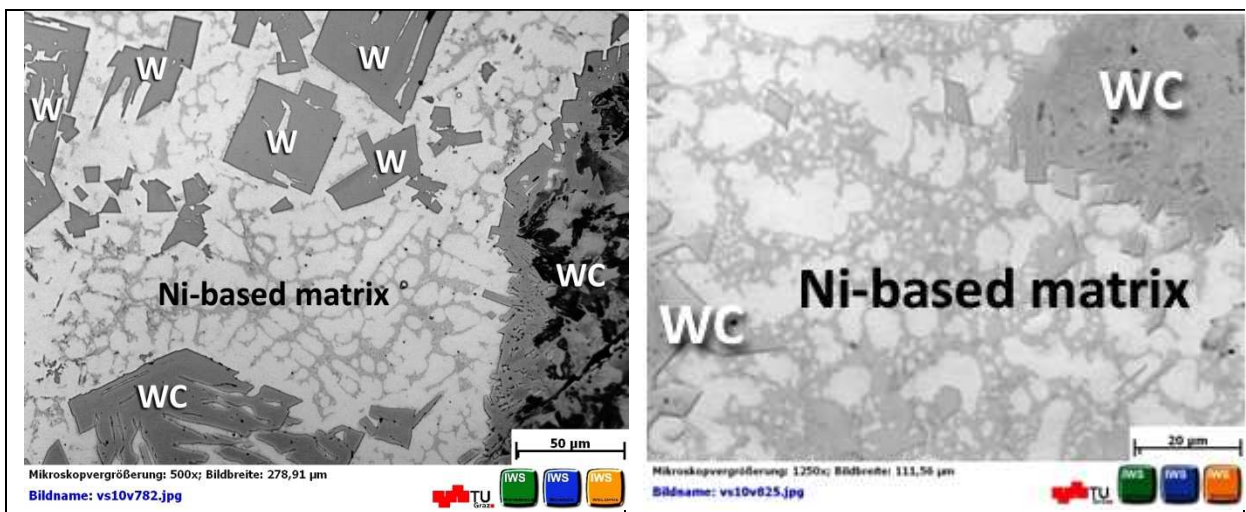


Figure 28: Left: AbraTec 6088, Right: PG 6503

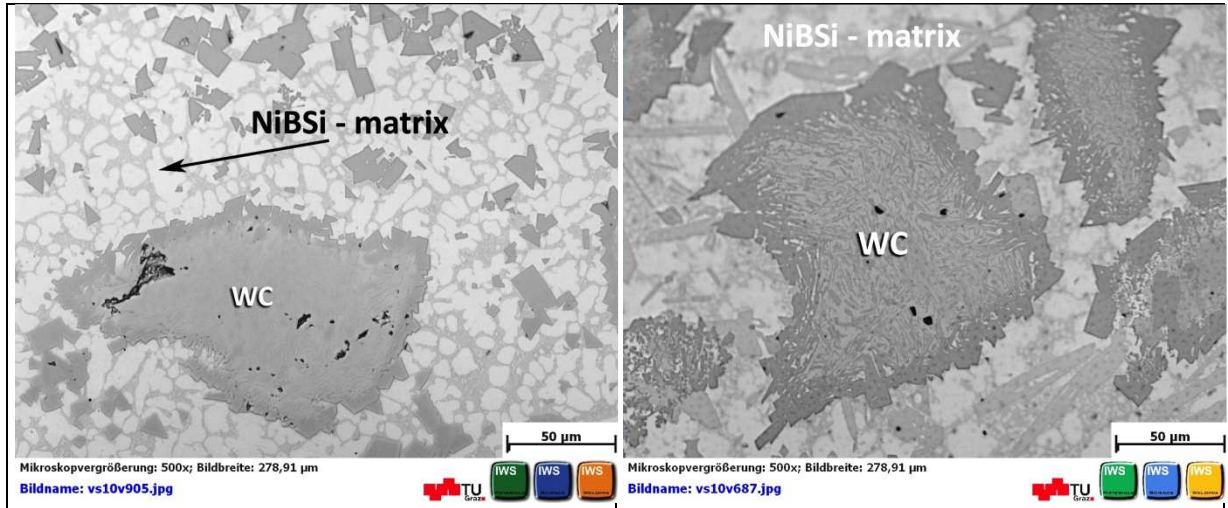


Figure 29: Left: DO 321; Right: Keraloy

Beside Terocote 7888T exist also a similar welding consumable. Terocote 7888 LT (LT stands for Low Temperature) combines the wear resistance of 7888 T with a new low temperature nickel alloy. TeroCote 7888 LT utilizes the newest advancement in low temperature nickel alloys and has a fusion temperature of about 940°C, which is about 100°C below that of existing products on the market today. These lower temperatures mean less heating, less structural change of the substrate and carbides. Further advantages are less thermal stress, less embrittlement of the matrix and faster application. [59]

An interesting comparison of different welding consumables was done in the paper 'Erosion and abrasion wear resistance of GMA wire surfaced nanostructural deposits'. The following three consumables have been investigated: DO 390N, which was also applied on Sample IV, Sample V and Sample VI. The two other ones are also of Castolin Eutectic; DO 33 and DO 48. The welding consumable DO 48 outperforms all the others in erosion and abrasion tests although it shows the most cracks in the macrostructure and slightly lower hardness like DO 390N. Therefore, DO 48 could be an interesting alternative. [60]

3.11.1.3 Fe-based

Iron-based alloys are relatively new in the area of wear coatings but they are a cost-effective alternative. The demand is rapidly rising and the range of compositions is getting bigger and bigger. Therefore, iron-base hardfacing alloys can be better classified by their matrix microstructure than by the chemical composition. [4]

The following four groups are established:

- Pearlitic steels
- Austenitic steels
- Martensitic steels
- High-alloy irons

Two similar iron-based welding consumables have been applied with two different welding techniques for this investigation. **1302 A** was deposited by PTA and **DO 390N** by MAG process. Based on their composition, they can be assigned somewhere between to the groups of martensitic steels and high-alloy irons.

Martensitic steels typically form martensite on normal air cooling of weld deposit and thus they are also called 'self-hardening' or 'air-hardening'. The carbon content of the martensitic steels ranges up to 0.7 %. Other elements like molybdenum, tungsten, nickel, silicon and chromium are added to increase hardenability, strength and martensite formation. In addition manganese and boron are added to enhance weldability. Compared to austenitic and pearlitic alloys the impact resistance is inferior but on the other side martensitic alloys offer increased hardness and excellent resistance to abrasive wear. [4]

In corrosive environments, a higher chromium amount is beneficial to enhance the corrosion resistance. Carbon content is a good indicator of abrasion resistance for this class of materials. The most important microstructural characteristic of high amount of chromium in iron-based alloys is the M_7C_3 carbide. This carbide contains chromium, iron and in the actual case also molybdenum. [4]

High-alloy iron encompasses a wide range of compositions in which chromium may vary between 6 and 35 wt% and a variation range of carbon within 2 to 6 wt%. Additional alloying elements are molybdenum, manganese, silicon, boron, tungsten, niobium and so on. The most important microstructural feature in high-alloy irons considering wear resistance, are M_7C_3 carbides similar to martensitic steels. These carbides form in abundance during solidification and contain chromium, iron and molybdenum if present. [31]

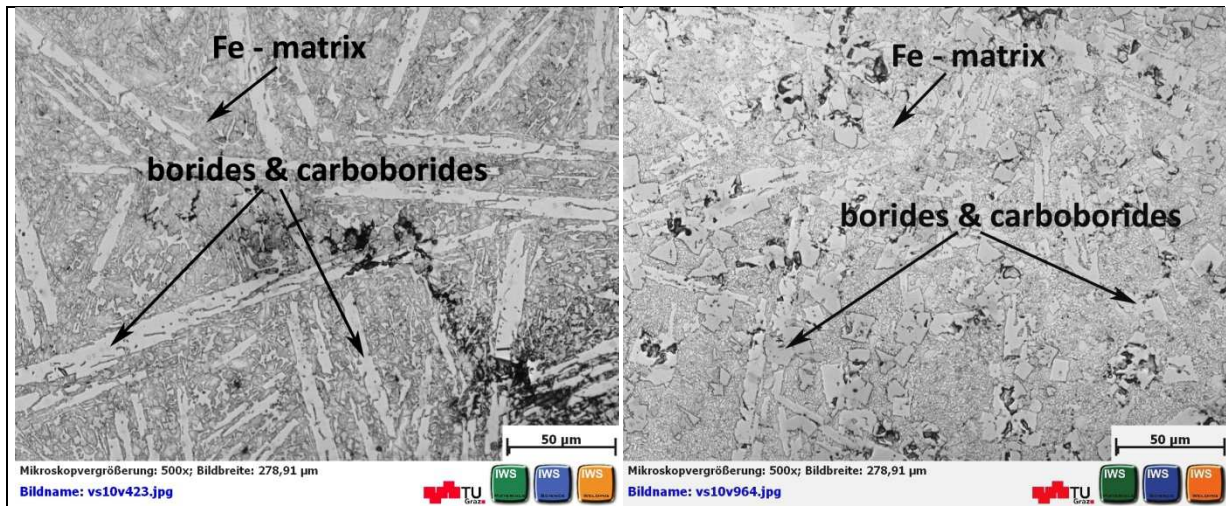


Figure 30: Left: DO 390N; Right: 1302A

A new hardfacing alloy (D2PTA) based on a FeCrVCoCB alloy system by RWTH Aachen University was tested and compared to a Co-based Stellite 6 and an alloy with a NiCrBSi matrix with 60 % fused tungsten carbides. Good metallurgical bonding with the base material at low dilution and good weldbead appearance can be noticed. A smooth surface free of defects and cracks and exceptional multi-pass weldability make this alloy very interesting for thicker coatings or repair welding. [45]

The microstructure of the FeCrVCoCB-based coating (D2PTA) is complex and result of particular solidification of the multi-component composition. Chromium and vanadium-rich carboborides as well uniformly distributed hard phases are embedded in the iron matrix. [45]

The wear resistance of this newly developed iron-based hardfacing alloy is on the same level as standard NiCrBSi alloys with fused tungsten proved by pin on disk testing and dry sand rubber wheel test. Concerning corrosion, the D2PTA coating shows better resistance. [45]

Fe-hard alloys offer already high hardness of about 60HRC welded in one layer. The addition of vanadium promotes the formation of relatively small chromium carbides. These coatings feature good protection against abrasion and also adequate sliding properties. One problem which occurs is the crack formation due to carbide networks. FeCrMoV-alloys with 12 to 18 % V gain more and more importance because cladding which are free of cracks can be produced. Fine-grained and fine dispersed vanadium carbides with a hardness of about 2900HV are formed. Depending on the amount of vanadium, a free of crack hardfacing with 61HRC (10 % V) to 65HRC (18 % V) is possible. [50]

Iron-based matrices are not so suitable for 'pseudo alloys'. The added hard particles such as tungsten carbide tend to dissolve and to embrittle the matrix. [48]

3.11.1.4 Synthetic resin composites & polymer surfacing

A state of the art theoretical elaboration of coating methods for screws using ceramic-synthetic resin composites is also a part of this thesis. Polymeric materials contain different fillers and reinforcements and they are frequently used for applications in which friction and wear are critical issues. In literature, a lot of research is reported in the area of polymers. Considering the high demands in the case of plug screws, no really comparable application or wear tests have been found. Moreover, several inquiries at suppliers and interviews with experts have not been very promising.

Mr. Kirchgassner of **Castolin Eutectic** said that *'protective layer of synthetic resin composites at the moment are not very promising considering the same coating quality. The problem is not really the wear resistance but the bond quality of a hardfacing process can not be reached. Otherwise polymer surfacing would be a good alternative due to its simplicity.'* [48]

Two more interviewed persons are Karl Heinz Pichler from **Sonnek Engineering GmbH** and Wolfgang Kavelius, ARC Manager at **Chesterton International** said: *'The success of the composite coating is strongly regulated by the specific basic conditions and the application. The actual coating systems do not show very good shock-absorbing performance after hardening but polyurethane-based materials (PU) should perform much better.'*

*'Excellent results can be reached against corrosion, abrasion and chemical attack with the composite **MX1** which can be used for the type of wear appearing at plug screws. Experience shows that **ARC 890** is much better in handling and even the durability is higher at lower costs.'*

*'**ARC 890** should be applied at a thickness of 6 mm and the average hardness is about 62HRC but this layer is not really fitting for impacts. **ARC 890** can withstand higher temperatures; 205°C in dry but also only 95° in wet conditions.'* [61] [62]

These maximum temperatures are too low to be resistant for plug screws applications. Another problem could be chipping of the layer due to recommended coat thickness of 6 or 10 mm; especially at the edges of the screw flights.

In accordance with the two suppliers, **ARC Chesterton & Castolin Eutectic**, and a literature study, the actual materials would not withstand the high demands of wear in the specific application. Polymer surfacing provides good wear properties but the impact resistance might be too low. The most critical issue is the bonding to the substrate which is not sufficient like mentioned above. [48] [63] [64] [65]

3.11.2 Hard particles

The overall wear performance is a combination of the volume fraction and the microhardness of the matrix and the hard particles. An adequate amount of hard phases in the matrix and their regular distribution impede the removal of material and thus improve the wear resistance of the component. The degree of wear resistance of the coating or alloy with respect to the hard particles mainly depends on: [18] [43] [45]

- Types of hard phases / particles
- Size of hard particles
- Amount of hard particles
- Distribution of hard particles
- Bonding between matrix and hard phase
- Matrix properties adapted to hard particles

Some alloys are already mixed with hard phases before the coating process, '*pseudo-alloys*' and others precipitate hard phases while solidifying. Alloys which are already mixed with hard particles are often nickel-based alloys but also iron- or cobalt- based ones. The amount of primary hard phases in alloys is limited and therefore different types of hard materials are mixed to improve the wear properties. [4]

Recently, however carbides of elements, such as titanium, molybdenum, tantalum, vanadium, chromium and so on, have proved useful in many hardfacing applications. [52]

Carbides, nitrides, borides and silicides of elements like Cr, W, V and so on are conventionally used as metallic hard materials in particle reinforced coatings. For desired and defined coating properties melting metallurgical reactions between the carbides and the matrix have to be taken into account. [43] [44] [50]

3.11.2.1 Type of hard particles

Several types of hard particles are used in the field of wear resistance to increase the durability of components. The most common are briefly described on the following pages.

Tungsten carbide (WC)

Historically, tungsten carbides were used exclusively for hardfacing applications in many industrial sectors. Fused tungsten carbide reinforced alloys extend the service life of machine parts which are exposed to wear. The experience over the years has shown that fused tungsten carbides, an eutectic mixture of tungsten monocarbide (WC) and di-tungsten carbide (W_2C), which are the most suitable reinforcing conventional hard alloys. Its melting point is about 2870°C. [31] [43] [50] [66]

They combine high hardness and high resistance against heavy abrasion. Welding consumables are available in several types like rods, electrodes, metal-cored wires and blended powders. [43]

Tungsten carbide has compared to titanium and vanadium carbide low strength at room temperature and a high tendency to dissolve especially in Fe-matrix. At higher temperatures tungsten carbide gain high hardness and has good wettability. A disadvantage of tungsten carbides can be the ambition of carbon depletion. This enrichment of W and C in the matrix increases the hardness. The layers are less ductile and show more cracks. Therefore, tungsten carbides should only be processed in self fluxing matrix materials with coarse grain. Because of its high density it tends to segregation based on gravity. [43] [50] [67]

Due to its popularity it is relatively cheap and readily available compared to other types of hard particles. [48]

Vanadium carbide (VC)

In recent years, investigations were made to use vanadium carbide as a reinforcing particle in coating processes as well. Great success was achieved with new alloys with additionally embedded vanadium carbides concerning durability. [50]

Vanadium carbide is an extremely hard refractory ceramic material which is chemically stable and has excellent high-temperature properties. Another advantage of Vanadium carbide is the tendency to precipitate as Vanadium carbide again after it gets molten. In addition vanadium can bond carbon of the dissolved tungsten carbides. Thus the matrix gets additionally reinforced and hardness of about 1200HV can be reached. [50]

The use of vanadium carbide prevents undesirable reactions because it has no solution tendency in Fe- and Ni-matrix. The addition of vanadium carbide to iron-based or nickel-based materials improves the resistance against abrasive wear compared to cobalt-based Stellite materials. On the other hand the price for vanadium carbide is higher and so it should only be used for highest requirements. Its impact and abrasion resistance is also higher compared to tungsten carbide. Another advantage is the possibility to produce crack-free coatings. [44] [48] [67]

Chromium carbide (Cr₃C₂)

It often appears in corrosion-resistant and wear-resistant materials. Chromium carbides show good hardness, toughness and chemical stability. Due to its properties it is used as protective coatings in corrosive environments and thought to be a possible replacement for conventional coatings, such as hard chrome. Chromium carbide is an extremely hard

refractory ceramic material and it often appears in Cr_{23}C_6 and Cr_7C_3 composition. The thermal expansion coefficient of chromium carbide is almost equal to that of steel which reduces the mechanical stresses at the layer boundaries. [51] [53]

On the other hand chromium carbide has the lowest melting point (1895 °C) among the described carbide types. [44]

3.11.2.2 Summary of hard particle properties

Carbide Type	+	-	Hardness [HV]	Melting Point [°C]	Density [kg/dm ³]
Tungsten	<ul style="list-style-type: none"> • Cheap • Availability • Hot hardness 	<ul style="list-style-type: none"> • High density leads to segregation • Dissolve in Fe- & Ni-matrix 	~ 2300	2870	15,65
Vanadium	<ul style="list-style-type: none"> • Forming of precipitations • Hot hardness • No tendency solution • High hardness • Impact resistance 	<ul style="list-style-type: none"> • Price • Availability • Not established 	~ 3200	2810	5,77
Chromium	<ul style="list-style-type: none"> • Chemical stability • Toughness • Widespread 	<ul style="list-style-type: none"> • Lower hardness • Low melting point 	~ 1500	1895	6,68

Table 1: Comparison of carbide types [4] [44]

3.11.2.3 *Size of hard particles*

The grain size of hard particles plays an important factor and must be adapted to the type of wear and application. Very often empiric tests or operating experience are necessary to make statements and decisions about the adequate choice because it is nearly impossible to predict the right size for a specific use.

Experience shows, if the abrading particles are large in comparison to the microstructural particles, then, the softer matrix at the surface is worn down and the abrading particles ride over the hard microstructural outcrops. On the other hand, if the abrading particles are small in comparison to the particles in the coating, it is believed that the opportunity exists for wear of the matrix around the hard particles. The softer matrix could not be effectively protected by the reinforcing particles and may be easily removed by the abrasive and drop out. [4] [18]

A greater surface to volume ratio of porous and nanostructured carbides result in a higher dissolution of the carbides and therefore small carbides show a greater extent of dissolution than bigger ones. [24] [50]

3.11.2.4 *Morphology of hard particles*

Hard materials can be distinguished as either angular or spherical particles and due to the production process they differ in their properties. An investigation on different types of tungsten carbide, which are the mainly used hard particles in abrasive wear resistance, shows the following results.

Angular tungsten monocarbide (WC) particles have high thermal stability and show the best resistance in two different abrasive wear tests (Dry-sand-rubber-wheel test and Miller test) compared to angular fused tungsten carbide (WC/W₂C).

A combination of angular and spherical fused tungsten carbides (WC/W₂C) show considerable lower thermal stability. The occurrence of carbon depletion can be noticed and thus the formation of a brittle phase as well. The hardness of the outer edges of the carbide decreases and the marred edges of the particle lead to abrasion. A refinement of the microstructure of angular tungsten carbide increases abrasion resistance. [66]

Compared to angular carbides, spherical ones achieve higher hardness of about 3000HV. Additionally they show better wear and slide behavior than irregular crushed carbides. Moreover, spherical hard particles have also advantages in conveying as the welding consumable is used as powder. A denser carbide distribution within the coating layer is also possible and improved carbide bonding into the matrix. [43] [68] [69]

3.11.2.5 Amount of hard particles

Nearly all powder mixtures are weldable with contents of hard particles up to 60% which is equal to about 68 vol.%. With rising contents of reinforcing particles, the weldability degrades and especially the welding bead is getting worse and welding defects occur. Therefore, values of 50% - 60% hard particles can be a good reference value for practical applications. A higher amount does not really show any better wear resistance and would also lead to an undesired higher dilution. Moreover, the costs will also increase. [44] [70]

3.11.2.6 Distribution of hard particles

Hard particles and matrix alloys often have different densities and due to those density differences, segregation based on gravitational force occurs. Especially tungsten carbides are prone to segregation due to their very high density. [46]

In iron-, cobalt- and nickel-based matrices hard particle contents of 40 - 60 vol.% are necessary to induce some kind of 'support-effect'. The reinforcing particles rest on the others and avoid segregation or sinking down. This leads to a random distribution of hard particles in the protective layer. [46]

A reduced energy contribution of the welding process can also help to achieve a homogenous distribution of hard particles. The reduction minimizes the descent as well. [46]

3.11.3 Interface of matrix and hard particles

The properties of hard particle-containing alloys are strongly affected by the interaction between the particles and the matrix material. The microstructure of protective layers with premixed hard particles shows a relatively ductile matrix containing tightly embedded hard material particles. During the coating process reactions between the matrix and the hard particles take place. A reaction zone, the interface is formed. The interface has a significant influence on the mechanical properties of the metal matrix composite (MMC) due to the fact that it embeds the carbides into the matrix. [43] [47]

The formation of the interface itself is affected by a lot of factors during the deposition process. Metallurgical reactions and diffusion occur and result in an interface layer which is formed by melting of the outer parts of the hard particles and a diffusion of the melted grains into the liquid alloy. [47]

Further research on three different hardfacing materials with tungsten carbide embedded in iron-based matrices show that alloying elements like Fe, W, Cr and Mo lead to a greater reaction zone. Molybdenum seems to be the strongest influencing element. [47]

3.11.4 Hardness

If two surfaces are in relative motion and under load, deformation occurs. The amount of deformation depends mainly on the strength of materials in contact, the surface roughness and load. The surface asperities are in contact and deformation takes place. The result is work hardening and thus a consequent loss of ductility can be noticed and the asperities become brittle and break off. [9]

Generally speaking, the wear resistance increases as the hardness of the coating layer increases and the other influencing factors remain constant. The hardness ratio between the abrasive media and the worn-out material plays the most important role considering wear rate, followed by the size of the hard particles. [18]

A correlation of abrasive wear and hardness can be seen in the following Figure 31. A better performance against three body abrasion can be obtained by increasing material hardness. [71]



Figure 31: Abrasive wear behavior and hardness for different Alloys A – F in dry sand rubber wheel test [71]

The abrasive wear behavior was tested by dry-sand rubber-wheel testing. The influence of coarse primary precipitations on abrasive wear resistance can be seen for alloys C and D. Very good wear resistance can be obtained for alloy F which is a Fe-based ‘pseudo alloy’ with tungsten carbides. Alloy E, shows highest hardness and performed best in the dry-sand rubber-wheel testing. [71]

The impeller-tumbler wear rates obtained for the six different Fe-based hardfacing alloys tested under low impact loading are given in the Figure 32. The softest material, alloy A, has the highest wear rate. The better performance of alloy C compared to alloy A can be explained by its higher hardness. Best wear resistance can be seen for alloys D and E, which is in good agreement with their high hardness. [71]

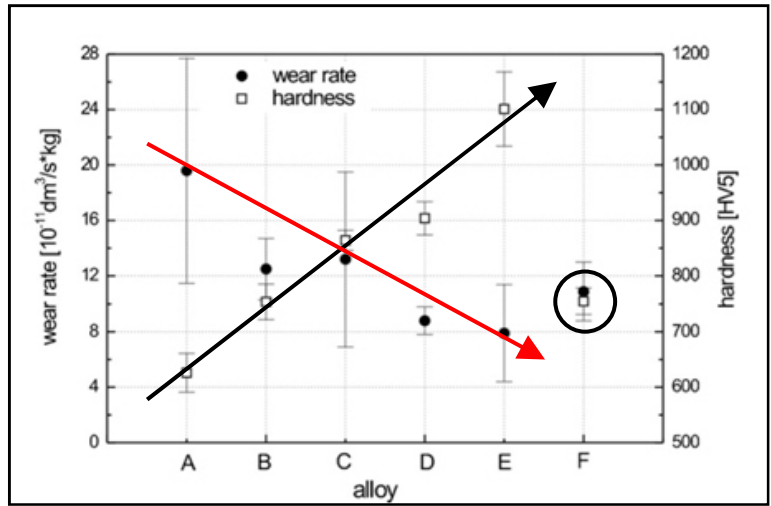


Figure 32: Wear rate at low level impact test for different alloys A – F tested by Impeller-tumbler apparatus [71]

The impeller-tumbler wear rates obtained for high impact loading are given in Figure 33. Very good correlation of wear rate and material hardness can be seen. Higher hardness reduces the ductility and consequently offers a lower impact resistance. For alloy F, the synthetic multiphase alloy, a high wear level can be seen.

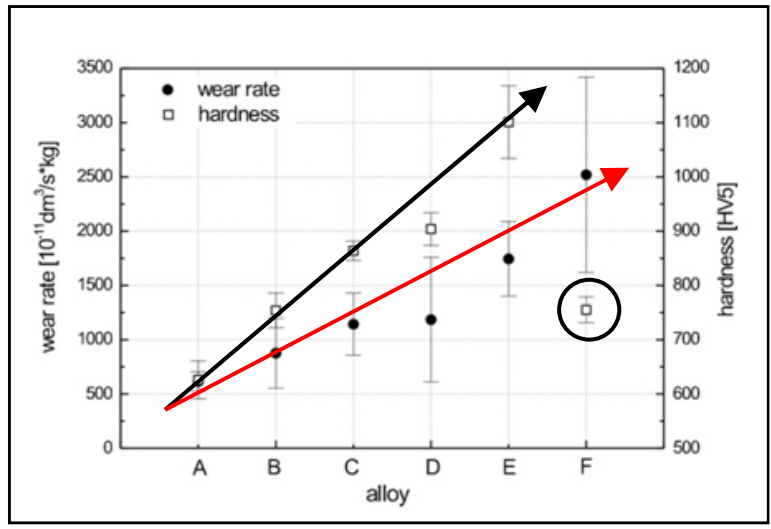


Figure 33: Wear rate at upper impact level for different alloys A – F tested by Impeller-tumbler apparatus [71]

3.11.5 Types of damage

Protective layers show very often imperfections and welding defects. Cracks are running through nearly all coatings and pores appear as well. These two main defects are described in the following paragraphs.

3.11.5.1 Cracks

A general problem of hardfacing is the occurrence of cracks inside the matrix of the coating. The cracks are caused by stresses which originate of different coefficients of thermal expansion of the coating and substrate material. Additionally, the high brittleness due to the high hardness of the coating enforces this problem. The risk for the occurrence of these cracks increases, the harder the coating and the bigger the outside diameter of the screws are. [3] [7]

The cracks which can be found in the coating are so called 'Entspannungsrisse' [48] [72] or after VDI guidelines 3822-part 4 'Härterisse' ('hardening cracks') [1]. According to standard EN ISO 6520-1 the term 'Aufhärtungsrisse' is used ('age hardening cracks') and they can be classified to cold cracks. [73]

Cold cracks occur in the solid state of the material and are the direct or delayed influence of stresses and strains. An excess of ductility of the material leads to a damage or fracture of the welded joint or substrate. [74]

Moreover, the heterogeneous composition of welding powders for hardfacing application enforces this problem. With increasing amount of carbides such as tungsten carbide, the layer embrittles additionally. Only a compromise between hardness and cracks is possible. On one hand the content of hard particles should be high enough to be resistant against wear and on the other hand a higher content of hard particles facilitates the brittleness of the coating. [75] [76]

Many hardfacing layers and especially high-alloy coating materials show age hardening cracks. For the wear resistance of coatings, these cracks are not so problematic. Neither crumble nor chipping of the layer occurs normally, if the crack propagates perpendicular to the fusion line. Otherwise, if the cracks run parallel to the fusion line and the coating are under impact load, chipping is a lot more critical. A buffer layer can help to reduce this problem. The tendency for corrosion is also emphasized due to the cracks.

On the other hand cracks reduce the residual stresses in the protective layer and avoid warping of big surfaces. [48]

Cracks occur more frequently at low welding currents and high welding speeds due to the rapid cooling sequence. Specific preheating, interpass temperatures and PWHT conditions for each welding consumable and substrate can help to reduce or even to avoid cracks. [48] [75] [72]

Hard particles

Basically there are two types of failure concerning the hard particles and the interface of protective layers:

- Particle cracking
- Decohesion from the matrix

It can be assumed that metal matrix composites containing carbides, show significant differences concerning mechanical properties in consideration of the reaction zone. Carbides which only have a thin reaction zone are not bonded to the matrix so well and show a tendency to decohesion but act more ductile. [47]

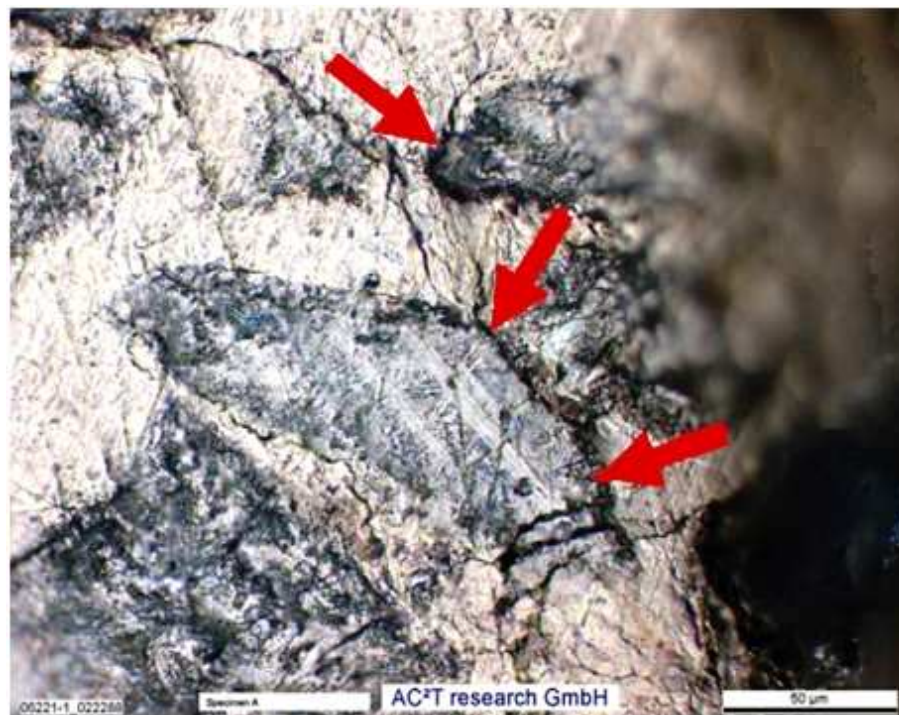


Figure 34: Decohesion of carbides after impact test [47]

Otherwise carbide cracking, a transcrystalline crack formation, indicates a good bonding between carbides and the matrix because of thicker interface, which makes the coating more brittle. [47]

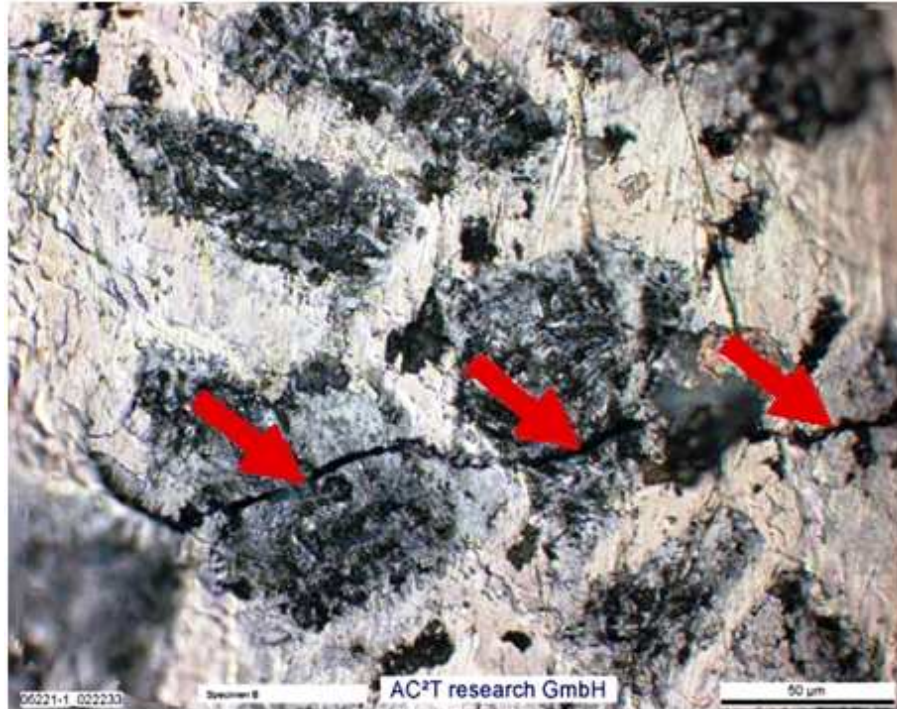


Figure 35: Carbide cracking after impact test [47]

3.11.5.2 Pores

Pores are gas filled cavities (globular) in the welding material, which are formed during the weld pool solidification, as the material cools. Porosity in welds can be caused by gas entrapment in molten metal, by too much moisture on the base or filler metal, or by improper cleaning of the joint before weld preparation. In arc welding porosity can additionally be found after inadequate shielding of the arc and weld pool. [77] [78]

The morphology of pores depends on: [78]

- Formation mechanism
- Cooling rate
- Solidification velocity
- Precipitation velocity
- Kind of substrate
- Welding consumable

According to the formation mechanism in the weld metal, pores can be classified by metallurgical pores and mechanical pores.

Metallurgical pores arise from the different solubility of gases in solid and liquid phase. Molten metal can bind notable concentrations of nitrogen, hydrogen and oxygen. An essential distinction of metallurgical pore formation is made between:

- Metallurgical reactions with gas formation (mainly CO)
- Decrease of solubility of gases (mainly H₂, N₂) which depends on the temperature. The solubility decreases at lower temperatures
 - If the solidification is slow enough the different gases rise up and leave the weld pool by help of diffusion and pin holes.
 - Otherwise, if the solidification is too fast, pores can be uniformly distributed throughout the weld or isolated in small groups; they can also be concentrated at the root or toe of weld.

Mechanical pores arise from expanding gases due to welding heat and the pores get entrapped by rapid solidification of the weld pool. Moreover, turbulences and the injector effect are also reasons for mechanical pore formation if a shielding gas is used. [34]

Because of a too big inclination angle of the welding torch the shielding gas causes suction and air is blown into the weld pool. A correct flow and quantity of shielding and torch angle can avoid them. [34] [78]

The following Figure 36 summarizes the reasons for metallurgical and mechanical pore formation for a welding process with shielding gas.

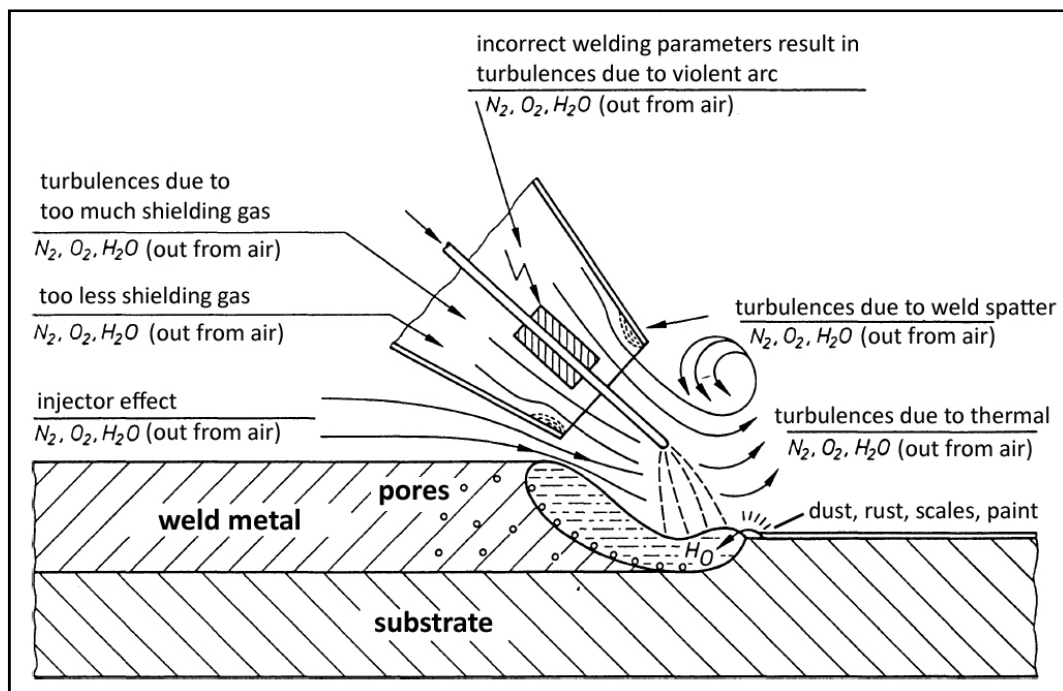


Figure 36: Metallurgical and mechanical pore formation for MAG process [34]

The pores occur according to standard **EN ISO 6520-1** as:

- gas pores
- uniformly distributed porosity
- clustered porosity
- linear porosity
- elongated cavity
- worm-holes
- surface pore

and can be assessed according to standard **EN ISO 5817: 2003 (D)**.

The detected pores on the investigated welding samples can be categorized to both groups – metallurgical and mechanical ones. It can be assumed that especially very big pores with a diameter of about 200 μm or even bigger, can be assigned to mechanical pores. Furthermore, uniformly distributed porosity fits best for the detected pore formation.

The next picture, Figure 37, shows different types of porosity which are commonly found in weld metal: [78] [79]

- a) Uniformly scattered porosity
- b) Cluster porosity
- c) Linear porosity
- d) Elongated porosity

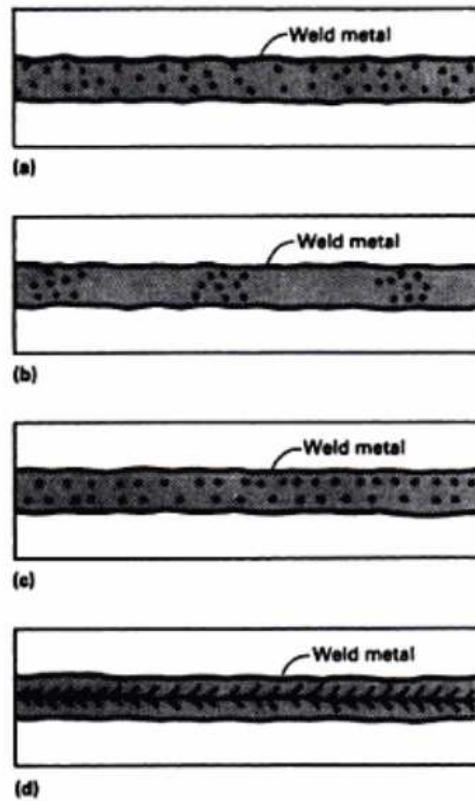
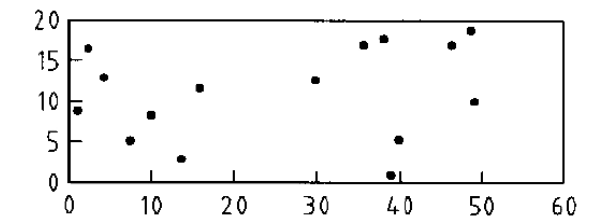


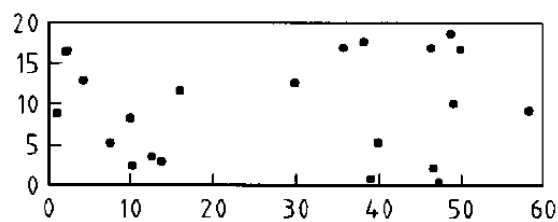
Figure 37: Different types of gas porosity [79]

The standard **EN ISO 5817: 2003 (D)** gives a recommendation for an objective quantification of pores. The diameter (d) of pores according to the standard is 1 mm. In this thesis the pore detection was based on the standard but the criteria considering the pore diameter was changed. A random area at a defined magnification was chosen to count the detected pores.

Figure 38 shows some examples of pore quantities.



1 % surface proportion, 15 pores, d= 1mm



1,5 % surface proportion, 23 pores, d= 1mm

Figure 38: Examples for the determination of irregularities according to EN ISO 5817 [80]

3.11.6 Process parameters

The parameters of the coating process have significant influence on the quality and appearance of the coating. A reduced energy contribution during the welding process helps to avoid the dissolution and fusion of hard particles. This lower energy input results in a faster cooling of the coating and this could explain a higher microhardness of the matrix. A higher welding current generates a higher dilution and a deeper weld penetration but results in an increase of microhardness of the matrix. [46] [47]

It is important to limit the heat input of the welding process in order to prevent melting of premixed hard particles in ‘pseudo alloys’. If they melt, they mix with the matrix and consequently the matrix tends to embrittle. [4]

Depending on the process parameters, two types of interface formation can be noticed in '*pseudo alloys*':

- Melting of outer part of the carbide and subsequent diffusion into the liquid alloy
- Pure diffusion without melting of the carbide on the other hand

Usually the diffusion coefficient of carbon in the matrix material like Ni, Co or Fe is higher than the diffusion coefficient of the carbide-forming metal. This leads to diffusion of carbon out of the carbide-forming metal into the matrix. Various factors exist which influences the speed as well as the extent of the reaction between matrix and carbide. The most obvious influence is the incorporated temperature and the time of its activation. A lower welding speed implicates a longer activation of heat and thus a greater extent of carbides dissolve. [47] [81]

The most widespread hard particles used in industrial applications are fused tungsten carbides. In iron-based matrices the tungsten carbides tend to be more dissolved because of the higher welding temperatures compared to Ni-based alloys. These higher temperatures are necessary due to the higher melting point of the Fe-based alloy. This leads to a more significant diffusion of carbon in iron and thus fewer hard particles remain in the matrix. The fused tungsten carbide is transformed into monocarbide WC and result in an enrichment of W and C which increases the hardness of the matrix. Hence, these layers are less ductile and show more cracks in the coating and consequently the resistance against wear decreases as well. [43] [50]

Nickel-base alloys have a lower melting point like mentioned above. Moreover, they have a very good wetting ability. These facts make them easier to weld and the lower thermal impact reduces the dissolution of the carbides. New nickel-base alloys with additives of silicon and boron enable the use of welding consumables at relative low welding current. Hence, the high content of fused tungsten carbides a very high wear resistance can be achieved. Long duration of particles in the arc may cause partial or complete solution in the base alloy. [43]

In Figure 39 the dispersion of the hard particles, fused tungsten carbides is shown.

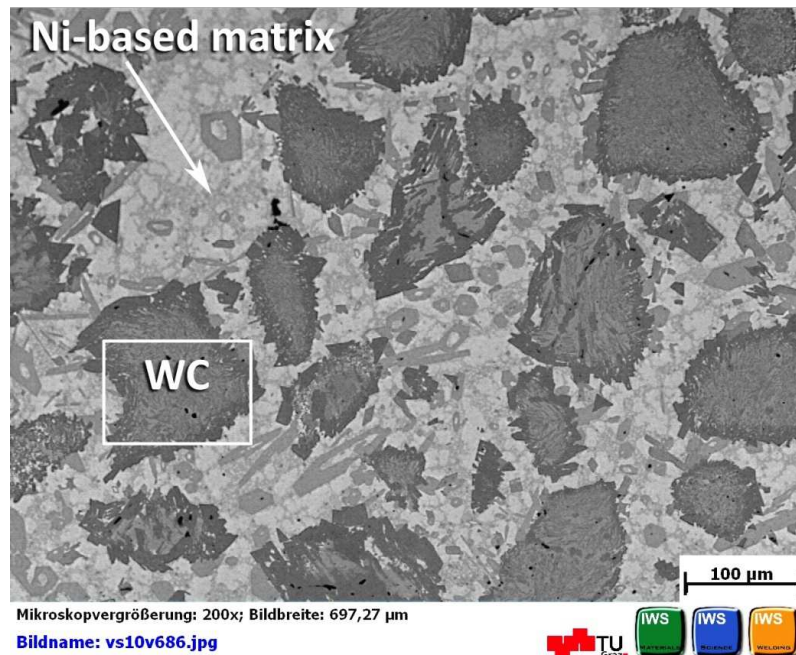


Figure 39: Dispersion and microstructure of fused tungsten carbides in nickel-base alloy; “Keraloy” - Specimen 29

The magnification of a single embedded tungsten carbide (Figure 39) is shown in Figure 40. A ring of solution of about 15 μm thickness can be seen around the carbide because of interactions between fused tungsten carbides and the surrounding matrix which result in a fringed edge. The carbide is tightly embedded in NiBSi-matrix.

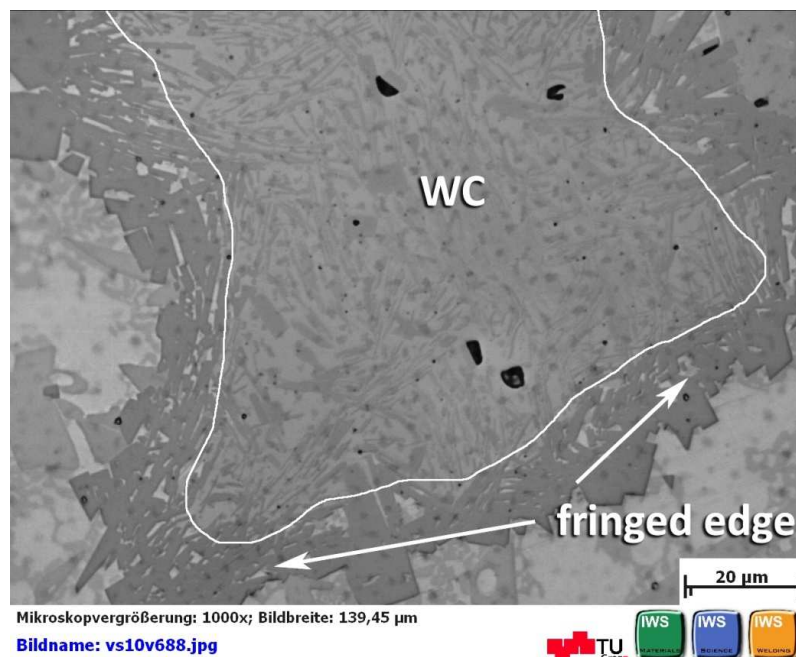


Figure 40: Embedded fused tungsten carbide with ring of solution; fringed diffusion edge - Specimen 29

3.12 Coating processes

The properties of coatings are influenced by several factors. Hence, it is very important to understand the coating process itself and the specific characteristics of the welding consumable.

In practice often problems appear such as the desired welding machine is not available, the welding process is not efficient enough, the welding process needs a specific welding position, the geometric dimensions of the part or the accessibility do not allow the designated welding process and a lot more.

The most appropriate conditions must be selected for each case of application. Careful considerations of material and process parameters are necessary to obtain excellent wear resistance. Depending on availability and manufacturing conditions, coatings can be applied by different processes. There are several welding techniques such as oxyacetylene welding, shielded metal-arc welding, gas metal-arc welding and plasma transfer arc welding which are used in industry. On the other hand thermal spraying offers also an interesting and huge field of application. All these processes can be applied manually or nearly fully automated. [43]

The specimens investigated in this thesis were made by ANDRITZ AG and Castolin Eutectic in Graz. The following techniques were used for the coating process investigated in this work and they are described in this chapter. The PTA welding and the thermal spraying are the most outstanding among them and thus described a little bit more detailed.

3.12.1 Thermal Spraying

'Thermal spraying is a generic term for a group of processes which apply a consumable in form of a spray of finely divided molten or semi-molten droplets to produce a coating.' [52]

3.12.1.1 Classification

There are a number of processes, which have been developed and adapted to specific applications. Commonly known are techniques like plasma spraying, high velocity oxy-fuel (HVOF) thermal spraying, vacuum plasma spraying (VPS), arc spraying, flame spraying and cold gas spraying. The relatively low heat transfer from the sprayed particles to the substrate causes no significant deformation, change of structure or damage to the coated part. [4] [29] [82] [83]

Thermal-spray equipment can be classified according to the energy source needed to heat and accelerate the particles. In the following figure a typical overview of thermal-spray processes is shown according to the European standards EN 657. [84]

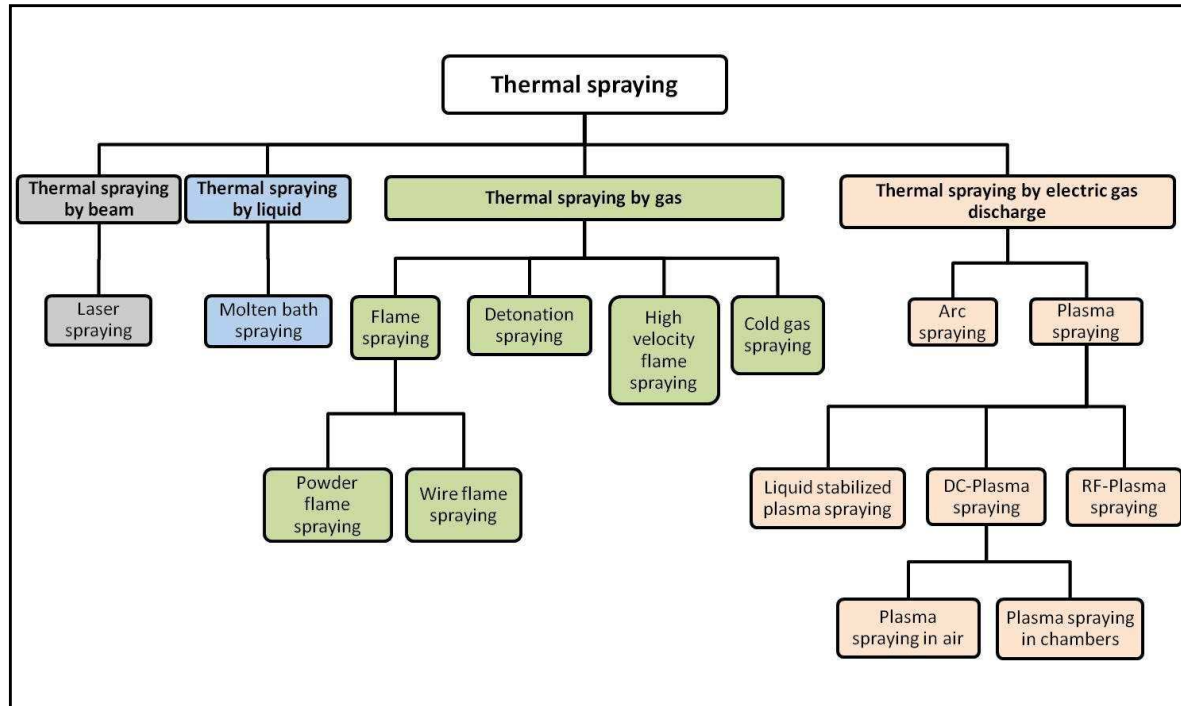


Figure 41: Overview of different thermal-spray processes in analogy to EN 657 [84]

3.12.1.2 Differences of thermal sprayed to welded coatings

The differences are: [4] [52] [85]

- Substrate adhesion is dependent on the materials and their properties and it is characterized as a mechanical bond between the coating and the substrate unlike the metallurgical bond found in weld-overlay coatings
- Spray deposits can be applied in thinner layers than welded coating
- Almost all material compositions can be deposited, including metals, cermets, ceramics and plastics
- Thermal spray processes are usually used on cold substrates, reducing distortion, dilution or metallurgical degradation of the substrate

The 'Eutalloy process' which was applied on sample I, is a specific process developed by and a brand of Castolin Eutectic. It is a combination of powder flame spraying and oxyacetylene welding. Therefore these two different techniques are separately described and later on the Eutalloy process itself is characterized in detail.

3.12.1.3 Powder flame spraying

In powder flame spraying, the consumable is a powder which is melted or fused in an oxyacetylene flame and propelled onto the substrate with the aid of expanding combustion

gases. The range of spray powders available is enormous and they are classified as self-fluxing and self-adhering.

Self-fluxing powders normally require additional thermal post-treatment. In most cases, this ‘fusing’ step is carried out using oxy-acetylene torches, which are well-suited for this task. The adhesion of the spray coating to the base material is greatly enhanced by this heat treatment. [4] [86]

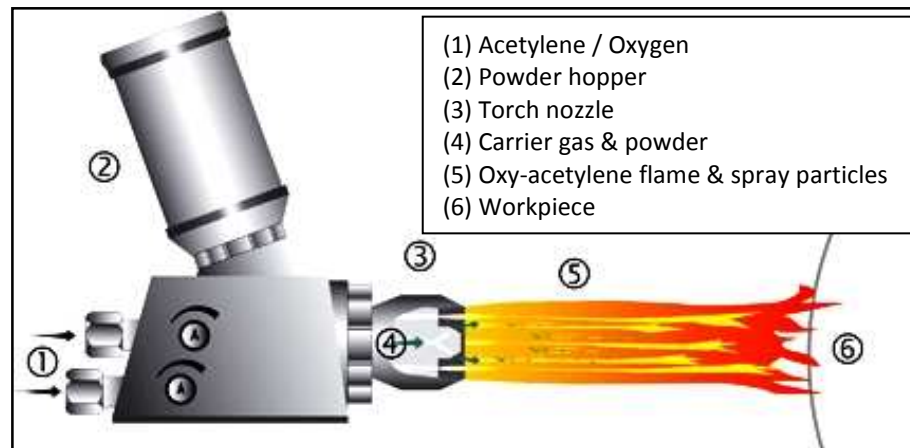


Figure 42: Thermal spraying with powder [87]

3.12.1.4 High-velocity oxyfuel thermal spray process (HVOF process)

The HVOF process has been developed to produce extremely high spray velocity and operates with oxygen–fuel mixture consisting of oxygen and either acetylene, propylene, propane or hydrogen fuel gas depending on coating requirements. There are a number of HVOF guns which use different methods to achieve these high velocities. The HVOF process allows significantly greater thickness due to the low residual stresses while providing low porosity, lower oxide content and higher coating adhesion. Among thermal spray processes, the coatings applied by HVOF offer the best resistance to abrasion and erosion. [4]

In Figure 43 the principle of HVOF thermal spraying is explained. The fuel gas flows through the siphon system, where it is mixed with oxygen. The mixed gases are ignited and expand inside a special designed combustion nozzle. Much of this energy is converted into mechanical force which accelerates the powder particles through the flame very quickly. The powder moves so quickly through the flame that the particles in many applications do not fully melt. Combustion temperatures approach about 2700°C and form a circular flame configuration. The energy out of the collision of the particles on the substrate supplies the final heat needed to complete the melting process of the powder. [4]

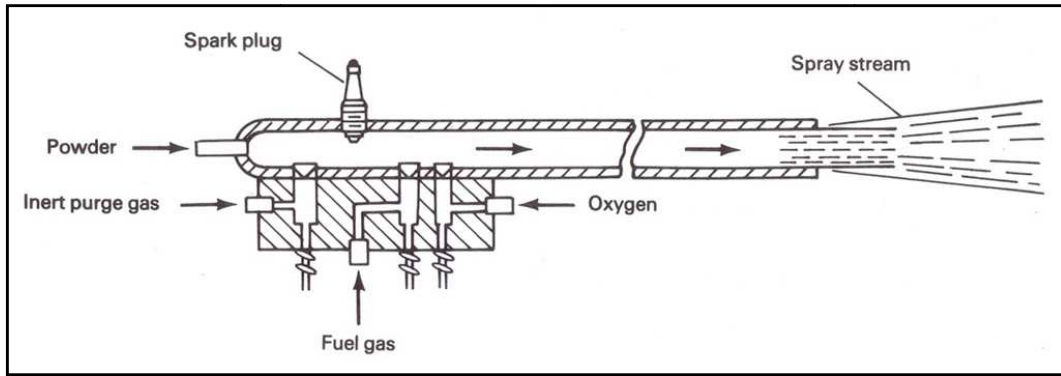


Figure 43: Schematic of an HVOF powder spray device [4]

3.12.1.5 Application of thermal spraying for plug screw coatings

A theoretical elaboration of coating methods for screws using thermal spraying was not very promising. According to literature [2] [4] [10] [82] and the expertise of several interviewed engineers [48] [56] thermal sprayed coatings are for thinner coating layers with the average thickness of about 0,3mm.

To verify the application of the HVOF process, one screw was coated. The result after a couple of few weeks in use can be seen in Figure 44. The following picture was provided by Mr. Ernst Hauck (ANDRITZ Vienna) which illustrates the chipping of the protective layer.

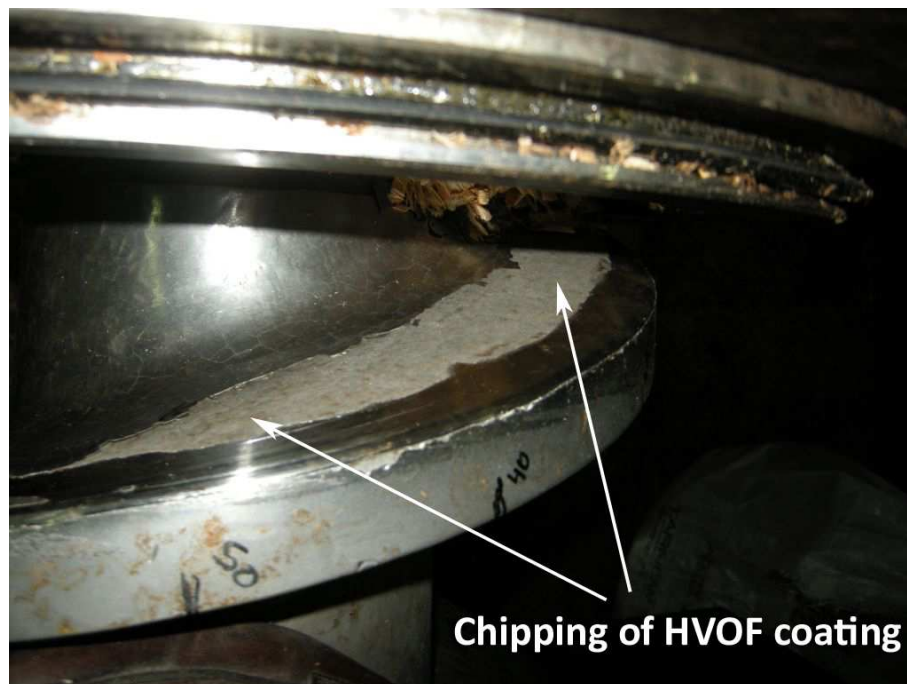


Figure 44: Chipping of HVOF coated screw [ANDRITZ]

3.12.2 Oxyacetylene welding

Gas welding is a welding process that melts and joins metals by heating them with a flame caused by the reaction between a fuel gas and oxygen.

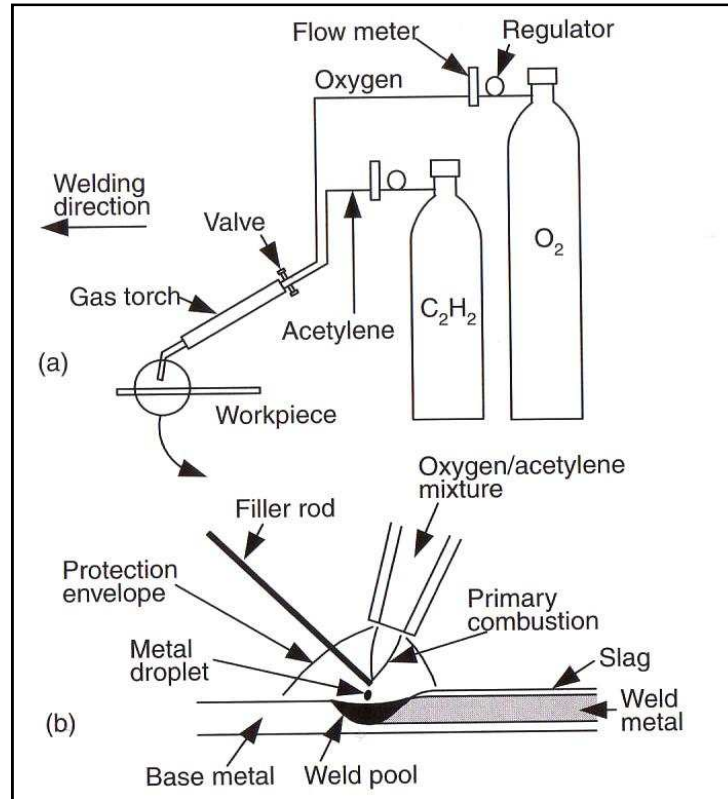


Figure 45: Oxyacetylene welding (a) overall process; (b) welding area [88]

Oxyacetylene welding (OAW) is simple in concept and therefore mainly used at construction sites for piping. Two pieces of metal are brought together and the touching edges are melted by the flame with or without the addition of filler rod. The oxyacetylene flame burns at 3200°C. A flux may be used to clean and deoxidizes the weld metal. The flux melts, solidifies and forms a slag skin on the resultant weld metal. One distinguishes between three different types of flames regarding the combustion of oxygen and acetylene; neutral, reducing and oxidizing. [33] [88]

3.12.3 Eutalloy process (Brazing)

The Eutalloy technique was developed by Castolin Eutectic and applied to one sample for the refurbishment simulation of a plug screw. The Eutalloy process is a method of thermal spraying with melting-in and is designed to produce wear protective coatings. Layer thickness typically ranges from 0.5 to 3 mm and can be deposited in only one pass. The Eutalloy technique is used for coatings of new parts and for refurbishment of worn ones. The Eutalloy self-fluxing welding consumables are based on NiCrBSi, NiBSi and CoBSi and

conveyed by means of an oxyacetylene delivery system. The melting characteristics of these powders allow surface alloying to take place below the melting point of the base metal. The powders are flame sprayed on to the work piece surface to bond by diffusion with the base metal. Powder application and melting takes place simultaneously and a fully dense metallurgical bonded overlay coating can be applied, quickly and easily. [86] [89]

3.12.3.1 Operating principle of SuperJet torch

The SuperJet Eutalloy torch operates on the oxy acetylene gas principle which means that each gas is manually regulated via the torch valves. The acetylene flows in a separate circuit and through a filter unit which avoids a flashback if any error occurs. The oxygen flows through the injector which also draws the powder into the system by aspiration. In the mixer unit (C) both gases and the powder are mixed and carrying the powder through the system until it reaches the tip and the flame. The powders are supplied in special plastic containers to be mounted directly on the burner and the feed rate is controlled by means of a lever (G) on the burner handle. [86] [90]

The following picture, Figure 46 the SuperJet torch is illustrated.

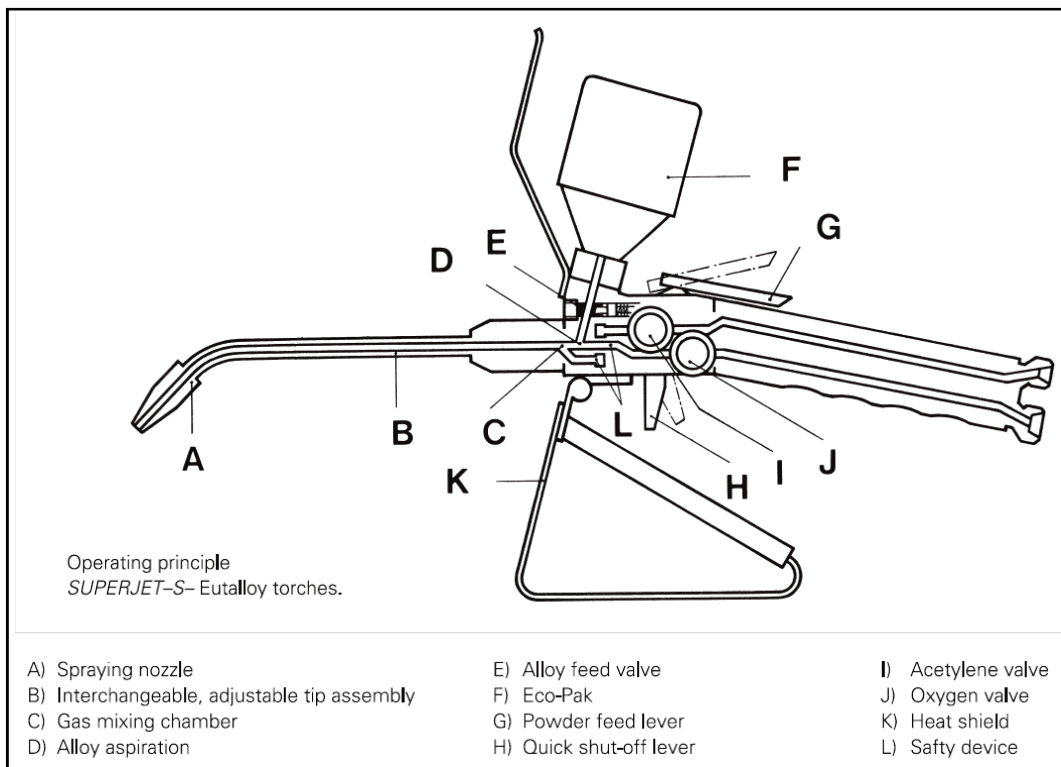


Figure 46: Cross section of SuperJet-Eutalloy torch [86]

3.12.3.2 Application of the Eutalloy process

Several details have to be taken into account if the Eutalloy process is applied. In all cases, the surfaces to be coated must be carefully prepared and all traces of grease, oxides, paint, etc. must be removed. Depending on the welding consumable and base metal a preheating is necessary but only to a maximum of 300°C. A very thin layer with an alloy such as TungTec 10112 (like on sample I) is sprayed on the area to avoid oxidation. After preheating, the real coating process can be applied. A distinction between two different techniques can be done.

One-step technique

In this case, only one welding consumable like flexible cord wires or powder consumables are used. The powder must be sprayed and fused simultaneously. The speed of deposition depends on the powder feed and on the temperature of the base material because accumulation of unfused alloy must be avoided. The SuperJet torch can also be used to produce coating layers with products in rod form such as TeroCote 7888. The brazing temperatures of these self fluxing filler metals are in the range of 850 – 1050 °C.

In the next picture, Figure 47, the principle of the 'one-step technique' and the use of welding rod is shown.

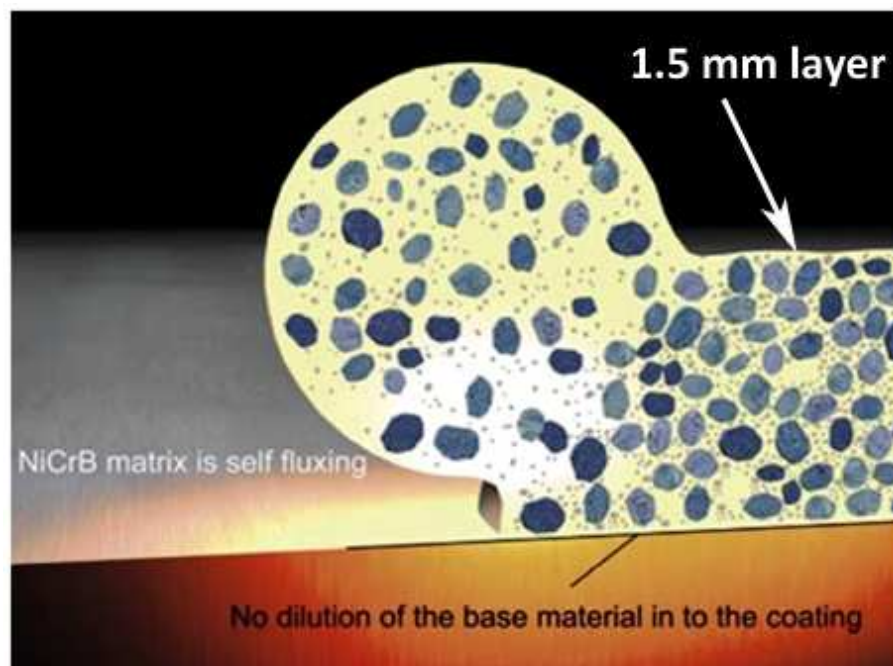


Figure 47: Principle of 'one-step technique' with self fluxing cord [90]

Two-step technique

This technique is also known as the spray-fuse technique. The coating process is slowly progressed; spraying and wetting is done simultaneously. This technique combines two welding consumables, the powder and the wire in one pass, what was done in the case of sample I. Both filler metals were used and melted at temperatures at about 1000°C. [86] [89]

In the following Figure 48 the SuperJet–S Eutalloy process is illustrated. The torch is used to preheat and spray the powder on the substrate. In the next step the powder is fused and the rod melted to provide additional wear resistance.



Figure 48: Coating process with Castolin SuperJet-S Eutalloy [89]

3.12.4 Shielded metal-arc welding

Shielded metal arc welding (SMAW) is a process that melts and joins metals by heating them with an arc established between a covered electrode and the base metal. Due to the electrode's shape of a stick, it is often called stick welding. The electrode holder is connected via a cable to the power source (-) and the workpiece is connected through another cable to the other pole (+) of the power source. The core of the covered electrode conducts the electric current to the arc and provides filler metal for the joint. The heat of the arc causes

both, the core wire and the flux covering at the electrode tip to melt off as droplets. The molten metal collects in the weld pool and solidifies into the weld metal. The molten flux is lighter and floats on the pool surface and solidifies into a slag layer at the top of the weld metal.

The cover of the electrode contains various chemicals and even metal powder to ensure one or more of the functions described below. [88]

- **Protection** by a gaseous shield to protect the molten metal from air
- **Oxidation** of the weld metal has to be avoided. The solid slag also protects the already solidified but still hot weld metal
- **Arc stabilization** is also important to maintain a stable arc. The arc is an ionic gas (plasma) and arc stabilizers increase the electrical conductivity and help the arc to conduct the electric current more smoothly
- **Metal Addition** facilitate the control of the composition of the weld metal and to increase the deposition rate

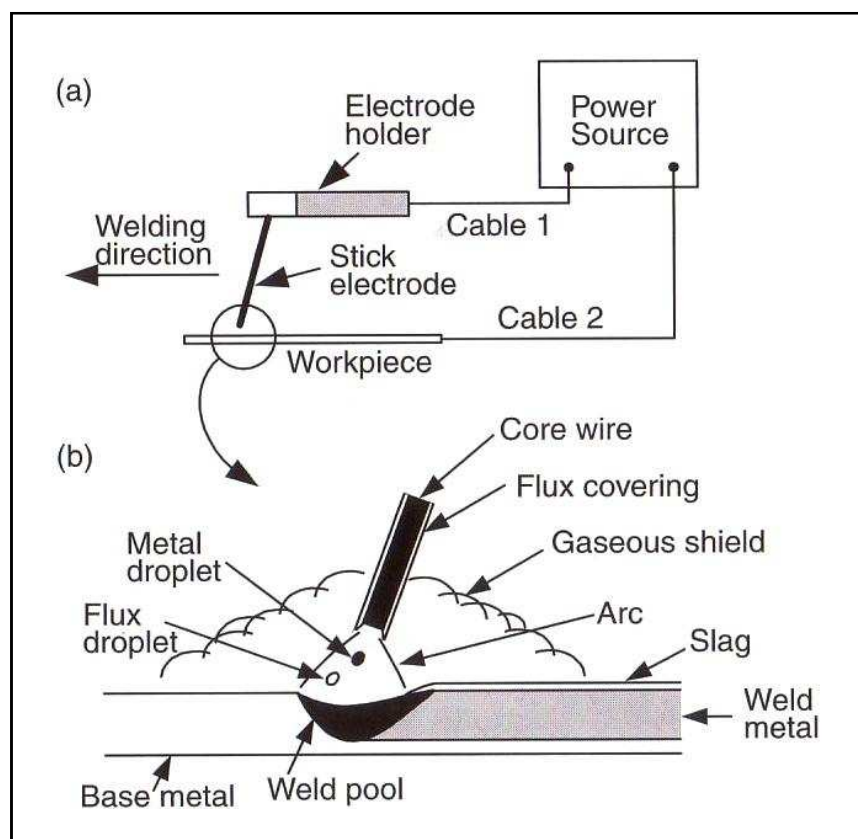


Figure 49: Shielded metal arc welding (a) overall process; (b) welding area [88]

The electric arc should be as short as possible so that particles remain only for a short time in the arc to prevent dissolution of the carbides. [43]

3.12.5 Flux-core arc welding

Flux-core arc welding (FCAW) is a process that melts and joins metals by heating them with an arc established between a continuously fed filler wire electrode and the metals. The arc and the molten weld pool are shielded by using inert gases like argon and helium or non inert gases such as CO₂. Due to the different shielding gases and their mixtures the arc energy and thermal conductivity can be varied and consequently the penetration is diverse. [88]

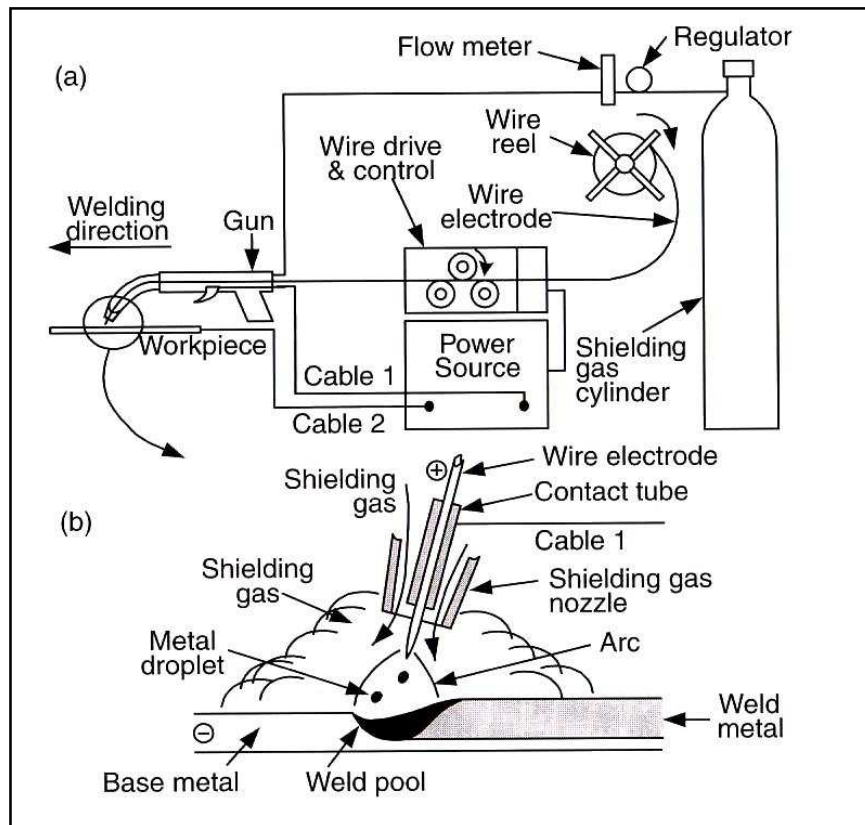


Figure 50: Flux-core arc welding (a) overall process; (b) welding area [88]

Different modes of metal transfer are also possible and to enhance the field of application.

- **Globular transfer** is often considered the most undesirable of the different variations because of its tendency to produce high heat, a poor weld surface and spatter
- **Spray transfer** enables the metal transfer in small discrete metal drops due to the electromagnetic force at much higher frequency and speed than in globular mode. Metal transfer is much more stable and spatter free and result in a high-quality weld finish
- **Short-circuiting transfer** form molten droplets on the tip of the electrode which touch into the weld pool surface and a short circuit occurs. This type of metal

transfer provides better weld quality and fewer spatters than the globular transfer and allows welding in all positions. Furthermore, the heat input for the short-arc variation is considerably reduced

- **Modified short-circuiting transfer** reduces some of the problems which occur with short-circuiting such as spatter and a turbulent weld pool. These systems sense the progression of the short circuit as it happens and modulate the current to limit the amount of force behind spatter and turbulence-producing events. Fronius has a technique called Cold Metal Transfer (CMT) which withdraws the electrode from the welding pool at a certain rate and pattern [33] [88]

3.12.6 Plasma Transfer Arc (PTA) Welding

PTA surfacing was developed as a modification of the plasma arc welding method in the 1960s. Compared to other processes such as oxyfuel gas welding, gas tungsten arc process, manual metal arc welding, gas metal arc welding and submerged arc welding, PTA surfacing provides a higher deposition rate except in the case of submerged arc welding and a relatively low dilution. [30]

Protective layers of high quality and very low dilution of about 5 % can be produced. Moreover, coat thicknesses of two to three millimeter can be achieved in one layer. The deposition rate is also quite high and so it is a quite efficient welding process. PTA surface welding has primarily been applied as mechanized or automated process but also equipment for manual PTA welding is available; a manual PTA torch is shown in Figure 51. [43] [50]



Figure 51: Manual PTA torch [50]

The PTA surfacing technique allows the deposition of a wider compositional spectrum of metallic and composite coatings because the coating consumables used mainly are in powder form but also wire and rod form are possible. It has gained more importance during the last years due to increasing automation and the introduction of quality assurance. In summary, PTA surfacing deposits high quality coatings consisting of a wide compositional range, at a moderate deposition rate and at lower production costs. [30] [91]

3.12.6.1 PTA principle

A high frequency initiated non-transferred pilot arc is generated between a tungsten cathode (negative pole) and a water-cooled copper anode. Argon gas passes through an inner annulus between the cathode and anode and a constricted plasma arc column is formed. This ionized gas provides a current path for a transferred arc. [29] [30]

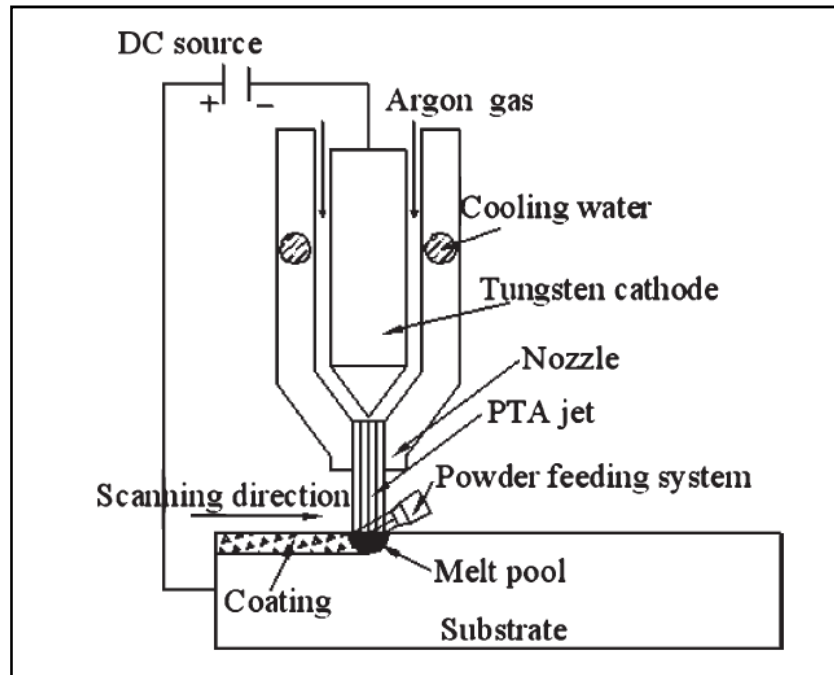


Figure 52: Schematic diagram of the PTA weld-surfacing system [92]

A powder consumable is transported internally through the torch via a carrier gas and exits at orifices on the anode face which intersects the plasma column. The powder is introduced into a weld pool that forms on the substrate the coating surface. The weld pool is protected from oxidation by a shielding gas that flows from an outer annulus in the torch. A metallurgical bond between coating and substrate is formed. [29] [30] [50]

3.12.6.2 Process parameters and influencing factors

In general, the parameters which control the welding quality are:

- Powder feed-rate
- Deposition rate
- Flow-rates of the process gas
- Arc current
- Torch stand-off distance

However, the powder size range utilized by PTA is restricted to 45 - 200 μm and the powder particle morphology influences the process as well. Spherical particles are preferred over particles of irregular shape because there might be problems with the feeding. However, the production costs of spherical particles are higher. [29] [30] [83]

The efficient deposition of powders in the PTA process depends upon the optimum use of flow-rates for the shield gas, pilot gas and carrier gas. The carrier gas flow-rate has to be adapted for each powder. Generally, the carrier gas consists of argon or an argon/hydrogen mixture. [30]

The plasma column generated in the PTA process consists of ionized argon and the plasma gas flow-rate affects heat generation within the plasma arc. A too high flow-rate creates turbulence within the plasma arc. Furthermore, a high plasma gas flow-rate promotes the formation of porosity and oxides within the deposit. [30]

The plasma arc column formed is also influenced by powder feed-rate. An increase in feed-rate restricts and cools the arc column.

An optimum arc current exists that represents the maximum powder utilization efficiency. At a lower than optimum value, there is insufficient heat generated to melt the powder or the substrate's surface and the injected powder is not incorporated within the weld pool. When the arc current levels above the optimum value, smaller powder particles are vaporized in the plasma arc and powder efficiency is reduced and leads to matrix embrittlement.

The stand-off distance is the distance between the PTA torch and the surface of the substrate which also influences the coating quality. For efficient deposition, the stand-off distance has an upper limit of 10-15 mm due to above this range shielding gas efficiency is reduced significantly. [30]

But there are not only advantages using PTA welding technique for wear coatings. These overlays are sometimes associated with higher dilution contents within the range of 5-20 %. Coating properties, such as hardness, matrix composition and reinforcement content are all influenced by this unwanted 'alloying effect'. Finally, the high arc currents that are reported to minimize coating porosity and encourage high quality overlays also promote carbide melting or dissolution. A high fraction of carbide melting has been associated with poor abrasive wear resistance in composite coating studies. [29] [30] [45] [46] [66] [83]

3.12.7 Composite coating - Polymer surfacing

An alternative coating process is polymer surfacing with products like **MeCaTeC** of Castolin Eutectic. It is a synthetic, thermosetting polymer with a three dimensionally cross linked network structure. Composite compounds conduce as reinforcement material. These compositions rapidly solidify and polymerize completely after mixing the bulk polymer and hardening reagent ingredients. [48]

In the Figure 53 the described polymer surfacing product **MeCaTec** is deposited on a screw.

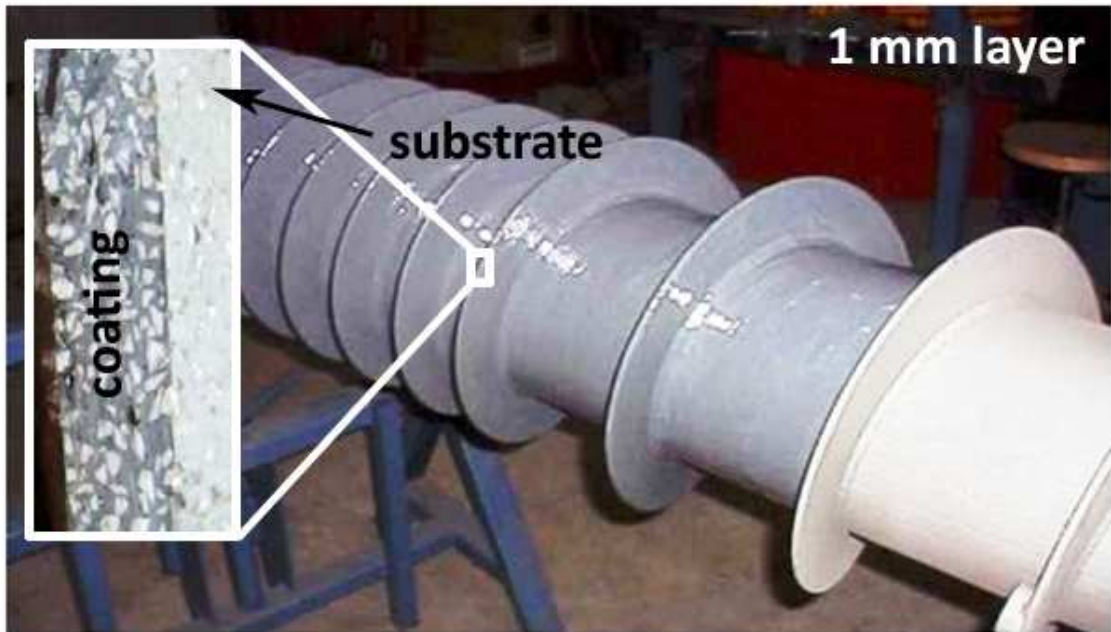


Figure 53: Thin 1mm layer of surfacing polymer (MeCaTec - Castolin) on screw [49]

According to literature and the interviews with experts, which are already mentioned above, polymer surfacing is not really an alternative for hardfacing applications.

3.13 Comparison of coating processes

Process	+	-	Layer Thickness (in one pass)	Dilution
PTA	<ul style="list-style-type: none"> • Precise surface • Homogeneous layer • Low dilution rate • High repeatability • Automatable • Great surfaces • Manual operation possible 	<ul style="list-style-type: none"> • Dismantling of screw if automated • Surface preparation • Equipment 	<ul style="list-style-type: none"> • 0.5 – 5 mm 	<ul style="list-style-type: none"> • ~5%
MAG	<ul style="list-style-type: none"> • Automatable • Repeatability • Refurbishment 	<ul style="list-style-type: none"> • Surface quality • Inhomogeneities 	<ul style="list-style-type: none"> • 1 – 3 mm 	<ul style="list-style-type: none"> • ~15-30%
EUTALLOY (Braze)	<ul style="list-style-type: none"> • Low heat input • ‘No’ dilution • Manually operated • Refurbishment 	<ul style="list-style-type: none"> • Slower • Surface quality • Poor bonding if applied without melting-in 	<ul style="list-style-type: none"> • 0.5 – 3 mm 	<ul style="list-style-type: none"> • ~0%
SMAW	<ul style="list-style-type: none"> • Manually operated 	<ul style="list-style-type: none"> • High dilution • Surface quality • Heat input 	<ul style="list-style-type: none"> • 1.5 – 3 mm 	<ul style="list-style-type: none"> • 20-30%
Polymer surfacing	<ul style="list-style-type: none"> • No heat input • No dilution • Easy to apply • Refurbishment 	<ul style="list-style-type: none"> • Bonding • Impact resistance 	<ul style="list-style-type: none"> • 1 – 10 mm 	<ul style="list-style-type: none"> • 0%

Table 2: Comparison of coating processes

4 Investigation methods

For the investigation of the welding samples the following methods have been used:

- Light optical microscopy
- Scanning electron microscopy
- Hardness testing

4.1 Light optical microscopy

Each of the 32 metallographic specimens has been examined by light optical microscopy to get a good overview of the different coatings. Several properties of the coatings can be investigated and examined.

The following list contains the assessment criteria:

- a. Binding to substrate / to the subjacent coating layer (refurbishment)
- b. Porosity of the coating
- c. Cracks inside the coating
- d. Dilution
- e. Characterization of hard particles



Figure 54: Light microscope - Zeiss Observer Z1m

4.2 Scanning electron microscopy (SEM)

The scanning electron microscope (SEM) is an electron microscope which is scanning the sample by a high-energy beam in a raster scan pattern. The electrons impact on the surface of the sample and interact with the atoms. The interaction produces signals such as secondary electrons (SE), back-scattered electrons (BSE), characteristic X-rays, specimen current and transmitted electrons. These signals contain information about the surface topography, composition and other properties such as electrical conductivity.

All SEMs have normally SE detectors. The signal results from interactions of the electron beam with atoms at or near the surface of the sample. In standard detection mode using secondary electron imaging, the SEM is able to deliver very high-resolution images with a magnification up to 1.000.000. In addition, SEM micrographs have due to their very narrow electron beam a relative great depth of field and can deliver images with a good representation of a three-dimensional shape of the sample which is useful for understanding the surface topography of a specimen.

BSE are electrons which are reflected from the sample. They are often used in analytical SEM because the intensity of the BSE signal is strongly related to the atomic number and so they provide information about the distribution of different elements in the sample. Characteristic x-rays are emitted when the electron beam removes an inner shell electron from the sample. A higher energy electron fills the shell and releases energy. Heavy elements (high atomic number) backscatter electrons more strongly than light elements and appear brighter in the image. [93]

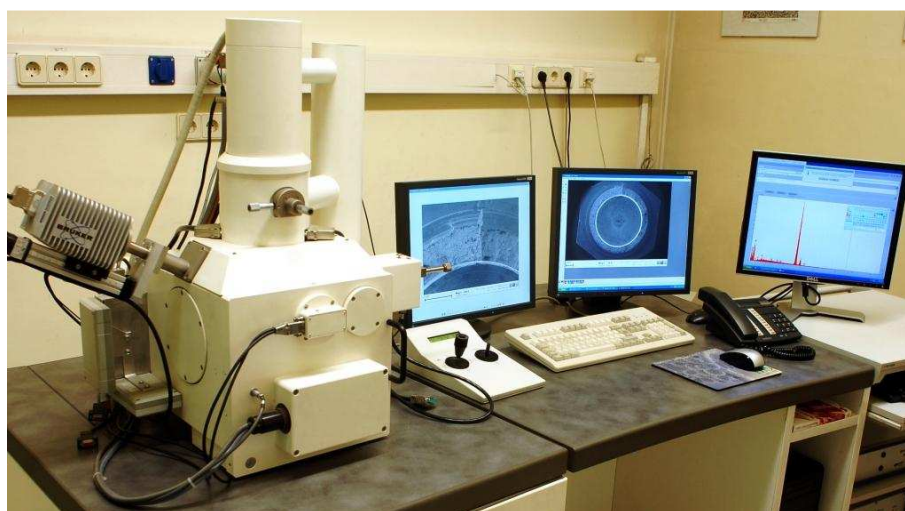


Figure 55: SEM at TU Graz - Leo 1450 VP (Zeiss)

4.2.1 Principle of SEM

In Figure 56 the principle of SEM is illustrated.

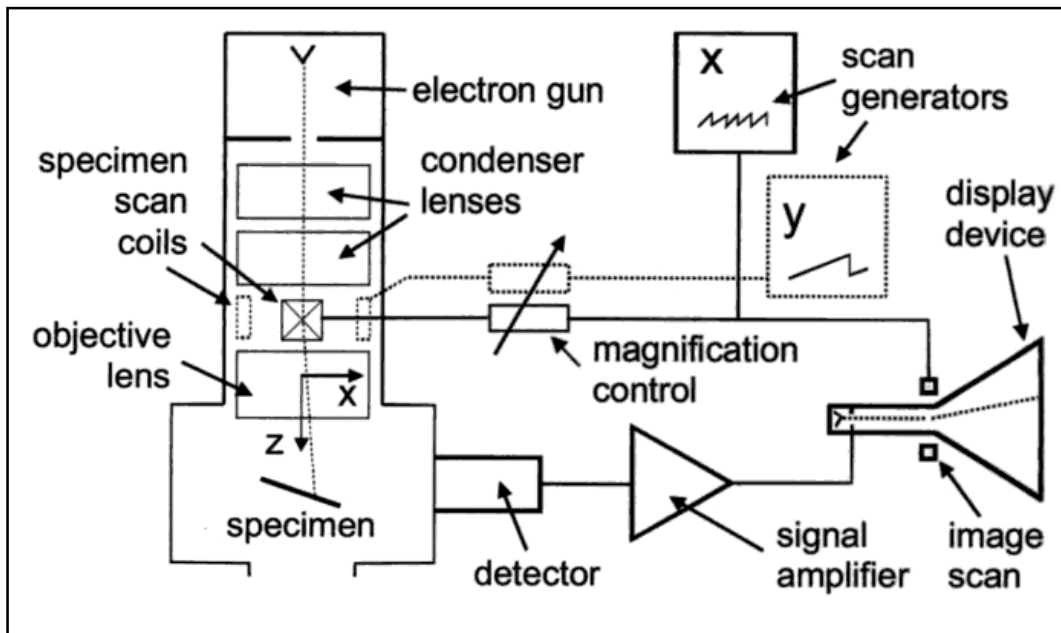


Figure 56: Principle of SEM [94]

Only selected specimens have been investigated with SEM but they cover all different types of coating to preserve a certain overview of all welding consumables.

4.2.2 Energy Dispersive X-ray spectroscopy (EDX)

For the elemental analysis or chemical characterization of a sample the energy dispersive x-ray spectroscopy can be used. The EDX method is based on the detection and energy measurement of individual x-rays. Interactions between electromagnetic radiation and the analyzing material take place. X-rays are emitted by the matter in response to be hit with accelerated electrons. This characteristic radiation relies on the fact that each element has a unique atomic structure and can be identified uniquely from one another.

A high-energy beam of accelerated electrons is focused onto the sample and stimulate the emission of characteristic x-rays from a specimen. The atoms within the probe are at ground state and the incident beam may excite an electron in an inner shell. This results in the ejection of the electron from the shell and a vacancy is created. Another electron from an outer shell which has a higher energy level fills this hole. The energy difference between the higher-energy shell and the lower energy shell may releases an x-ray. The number and energy of the x-rays emitted from a specimen can be measured by an energy dispersive spectrometer. As said before, the energy of the x-rays is characteristic of the energy difference between these two shells and also of the atomic structure of an element.

Therefore, the elemental composition of the specimen can be measured. EDX allows the measurement of nearly the entire x-ray spectrum of a specimen. Except the distinction of light elements like hydrogen (H), helium (He), boron (B) and carbon (C) is not possible. The lighter the elements, the harder they are to identify. [95]

4.2.3 Wavelength Dispersive X-Ray Analysis (WDX)

The wavelength dispersive x-ray spectroscopy uses the diffraction of a crystal to count the numbers of x-rays of a specific wavelength. If the wavelength of the impinging x-ray and the spacing of the crystal lattice are related by Bragg's law, they produce a constructive interference. The x-rays emitted by the sample, irradiate a known single crystal at a precise angle. The crystal is adapted to the energy being analyzed to allow the determination of nearly all elements except the very light ones. All elements, which have an atomic number of at least four, beryllium (Be), boron (B), carbon (C) and so on, can be detected. The single crystal diffracts the photons and they are collected by a detector. It is convenient and sensitive method for determining the chemical constituents and composition of phases.

Unlike the related technique of EDX, WDX counts only the x-rays of a single wavelength. Therefore, it is generally necessary to know the elements which should be found within the specimen to find a crystal capable of diffracting it properly. Hence this technique is often used with EDX to get the entire spectrum of elements of the sample. Compared to EDX, the detection sensitivity is better and the resolution of the x-ray spectrum of WDX is more accurate. [95]

4.3 Hardness testing

Another main issue of this thesis is the hardness measurement of the different coating types due to the rather proportional correlation of hardness and wear resistance.

4.3.1 Principle of hardness testing

Hardness is the measure of the resistance to impinge into solid material depending on various kinds of test specimen.

In our case we used the Vickers hardness test which can be used for all metals and has one of the widest scales among hardness tests.

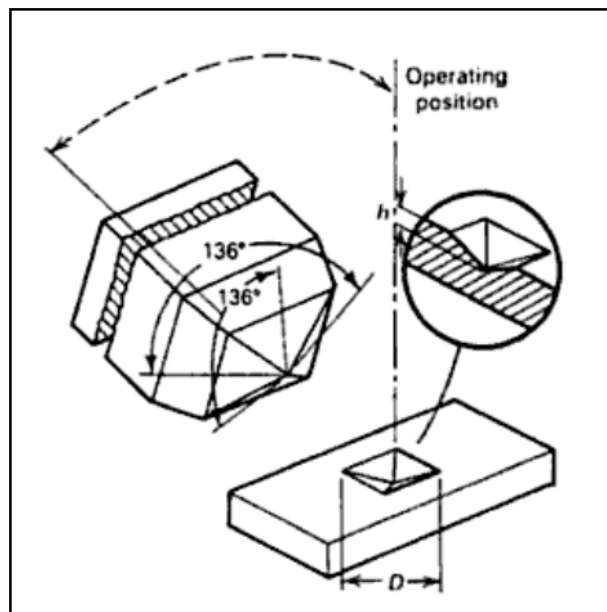


Figure 57: Diamond pyramid indenter for Vickers testing [96]

The unit of hardness given by this test is known as the Vickers Pyramid Number (HV). The hardness number is determined by the load over the surface area of the impression and therefore it is not a pressure. [96]

4.3.2 Microhardness testing (HV 0,02)

To measure and investigate the hardness more locally, microhardness testing is necessary. To verify the transition area of the coating and the substrate, a load of 0,02 kilopond (HV 0,02) has been chosen for the measurement. The maximum magnification of the device is 1880x.

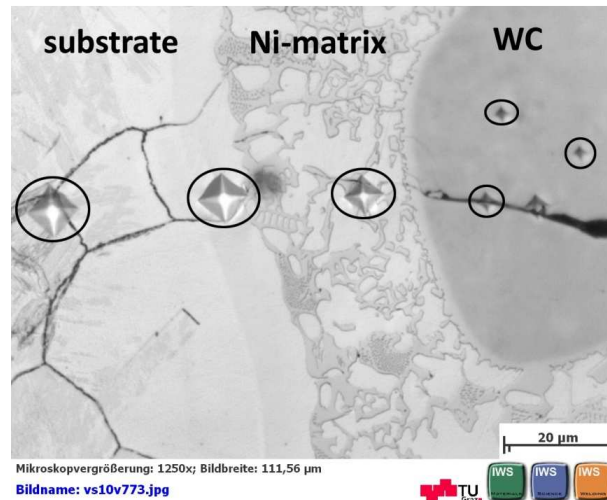


Figure 58: Microhardness testing specimen_29 – Keraloy

4.3.3 Macro hardness testing (HV 10)

All 14 specimens which have been applied to hardness mapping have also been tested by a macro hardness test to verify the results in each coating layer by three random marks. The substrate in contrast was tested at different positions. One position quite far away from the coating layers to avoid the HAZ and the two other ones in the vicinity of the coatings.

The following picture, Figure 59, show the macro hardness tester 'Emco Test M4C'.



Figure 59: Macro Hardness test - Emco Test M4C

4.3.4 Hardness mapping (HV 1)

Hardness mappings give a good overview concerning the hardness distribution in the layer. Moreover, they also show the influence of heat on the substrate during the welding process which involves a heat affected zone as well.

All coating types and combinations have been investigated by this method, altogether 14 different specimen. For each mapping about 400 to 600 measurement points were necessary to create such an image. The load for the measurement was one kilopond (HV 1).

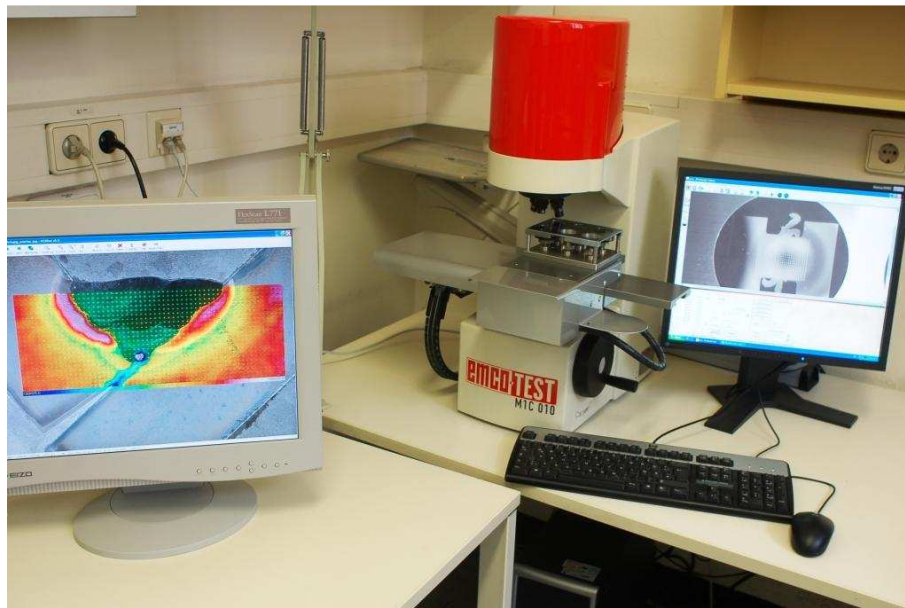


Figure 60: Hardness tester - Emco Test M1C

In the following two figures, the difference between the image with and without interpolation is illustrated. In the first image, each square stands for one hardness measurement point. In the second image in contrast, an image processing with interpolation between each value has been carried out and a homogenous transition can be recognized.

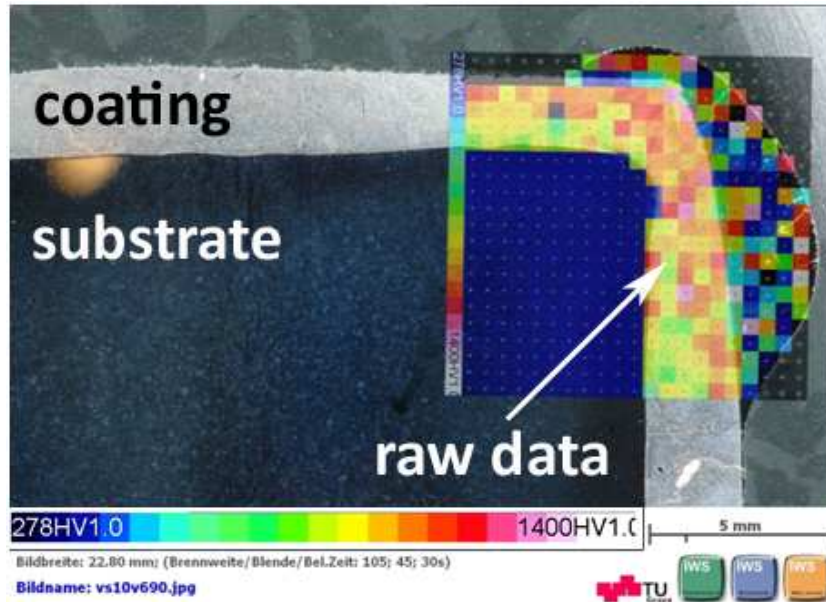


Figure 61: Specimen 1 – hardness mapping without interpolation

The colour gradient, like mentioned above, is only an interpolation between two values. This area between two measurement points can be verified by microhardness testing to get the real hardness value of a specific position.

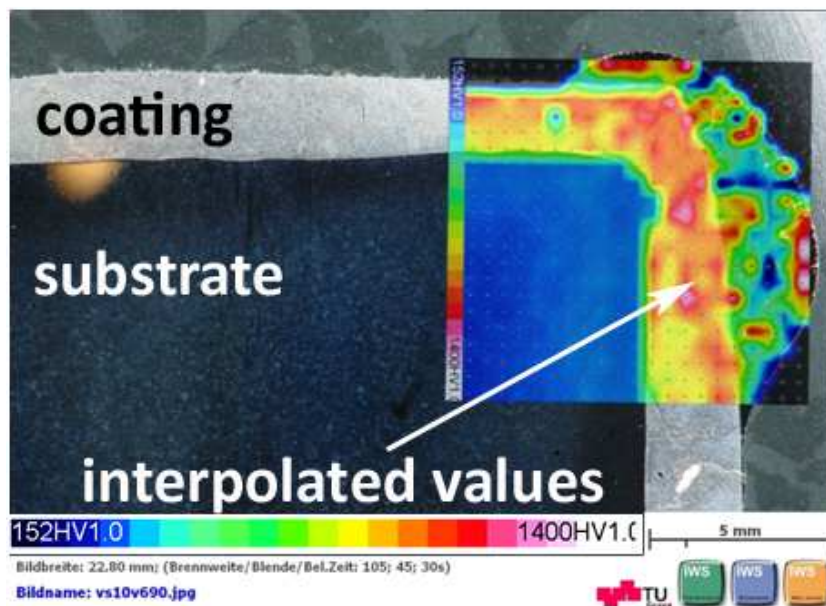


Figure 62: Specimen 1 – hardness mapping with interpolation

One more thing has to be mentioned concerning the scaling of the hardness tests. Due to the wide range of values (relative soft substrate and very hard particles) the maximum hardness has been limited to a maximum of 1400 HV. Hence, all hardness values over 1400 HV such as measuring points of tungsten carbides with for example 2400 HV, are also illustrated with white color like they would have the hardness value of 1400 HV. This scaling was necessary to be able to distinguish better between softer and harder areas.

In the following figure a comparison is shown of a hardness mapping without (left) and with (right) scaling. The range of the hardness values in the left picture is quite big and thus a differentiation of the hardness values inside the coating is impossible; all is light green. In the right picture, a differentiation of hardness values inside the protective layer is possible because of the different colours.

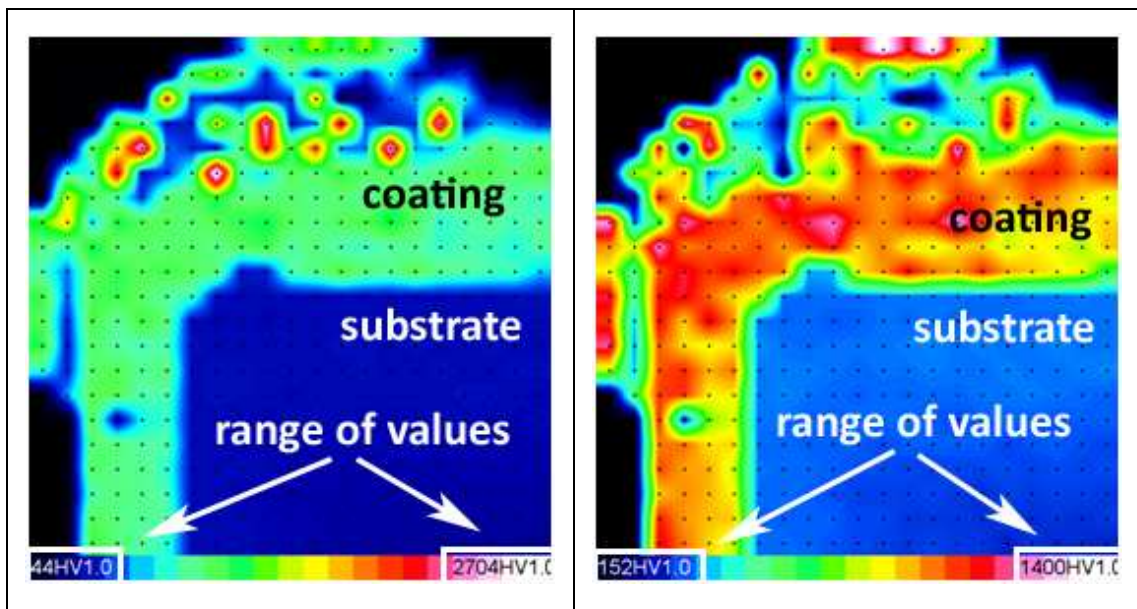


Figure 63: Unscaled hardness mapping / Scaled hardness mapping

Exceptions of this standard scaling up to 1400 HV are the hardness mappings of the coatings Stellite 6 and Deloro 56 (specimen_27 & Specimen_31). Hence, we have a smaller range of hardness values, an individual scaling was necessary to enable a distinction.

Another point which can also be found out due to the hardness mapping is the influence of the deposition process on the substrate. The different heat input of each welding technique or parameters changes the properties of the substrate.

For the first mapping a large testing area was selected to get an idea of the HAZ. In this case two different welding consumables were applied on specimen 19 by MAG process. The coating on the left, DO 390N was coated with nearly the double of current like the other layer, DO 321. The HAZ is also nearly twice as wide like the other one.

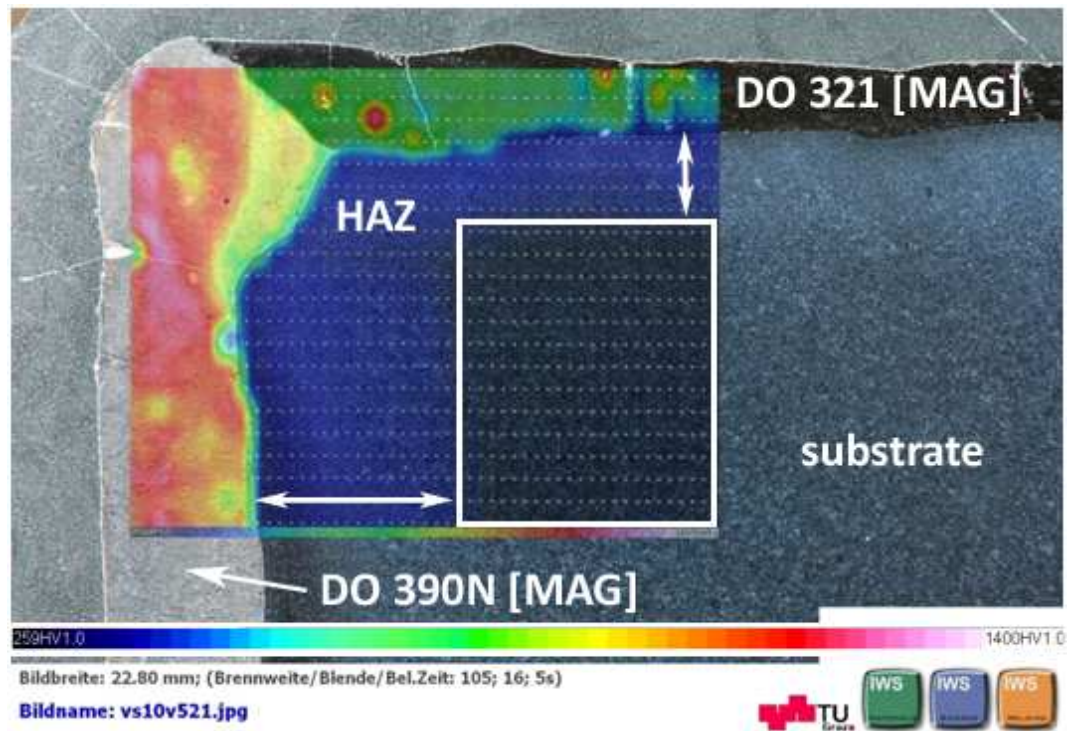


Figure 64: Specimen 19 – hardness mapping with HAZ

5 Investigation

In the previous chapter, different investigation methods have been illustrated and described. Based on these analyses, which have been carried out for all specimens, results are provided and illustrated in this section.

A coating is a complex system and each factor influences the other and thus an adjustment of them is very important. The following numeration contains the criteria of the coating without any ranking:

- a) Pores
- b) Cracks
- c) Binding to substrate and subjacent layer
- d) Dilution
- e) Chipping
- f) Hardness

5.1 Substrate

The samples (I – VII) have been coated by ANDRITZ and Castolin Eutectic together. The substrate, the soft-martensitic stainless steel X3CrNiMo13-4 with the material number 1.4313 was used for each sample and the table below shows the chemical composition in wt-%.

Substrate: 1.4313 (X3CrNiMo13-4)								
C	Si	Mn	P	S	Cr	Mo	Ni	N
max. 0,05	max. 0,60	max. 1,00	max. 0,035	max. 0,015	12,5 - 14,0	0,40 - 0,70	3,5 - 4,5	min.0,02

Table 3: Composition of 1.4313 martensitic stainless steel [wt%] [97]

The dimensions of the samples are illustrated in Figure 65 only varying in the length. The red color indicates the coated area of the sample.

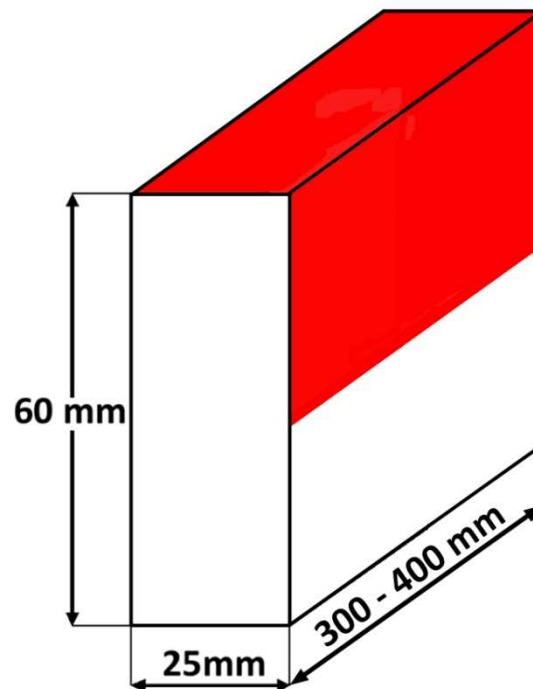


Figure 65: Dimensions of samples and indicated coating

Nearly all samples have sharp edges. Only Sample II has a beveled edge and the difference can be seen in Figure 66. This different prefabrication was tried out to compare the influence of the edge on the coating of 1302 A deposited by PTA.

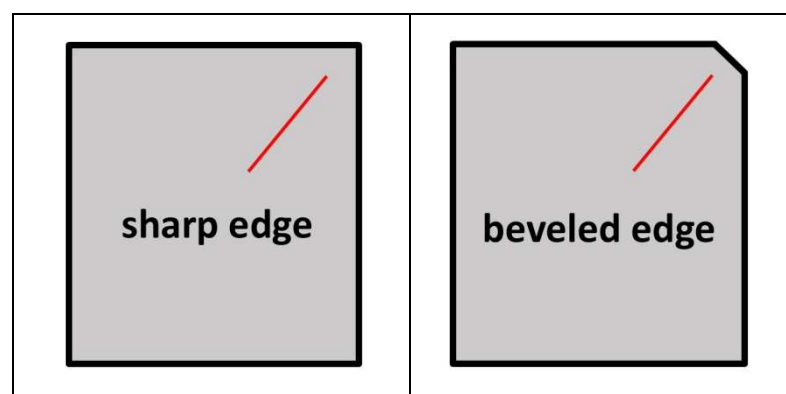


Figure 66: Prefabrication of edges of welding samples

A distinctive feature cannot be recognized and an enlarged view of four different specimens can be found in the appendix, 13.2 - Comparison sharp edge – beveled edge.

5.2 Welding consumables

At each substrate, at least one welding consumable was applied. Some samples also have sections with different coatings or multipass layers have been deposited to simulate a refurbishment. The following table contains the most important information of each of the 10 applied and tested welding consumables. The information about hardness, size of hard particles and the composition derives from the different manufacturer.

Welding Consumable	Welding Technique	Type	Matrix basis	Hard-phase	Hard particle [μm]	Hardness [HRC/HV]	Manufacturer		
1302A	PTA	Powder	Fe	carboborides, borides	-	68-71 HRC	Castolin Eutectic		
DO 390N	MAG	Flux cored wire							
TeroCote 7888T	EUTALLOY (Brazing)	Wire	NiCrBSi	75 % WC	250 – 700	Matrix - 35 HRC			
TungTec 10112		Powder				60 % WC		20 – 125	Matrix - 59 HRC
AbraTec 6088	SMAW	Electrode	NiBSi	55 % WC	500 – 1000	Matrix - 56HRC			
DO 321	MAG	Flux cored wire				60 – 170		Matrix - 55 HRC	
PG 6503	PTA	Powder				60 % WC		63 – 180	Matrix - 49 HRC
Keraloy									80 – 180
						~2400 HV0.02		ANDRITZ	
Deloro 56	PTA	Powder	Ni	Ni ₃ B, CrB, Cr ₂ B, Cr ₃ B ₂ , M ₂₃ C ₆ , M ₇ C ₂₃	-	56 HRC		Deloro Stellite	
Stellite 6	PTA	Powder	Co	(Cr,Fe) ₇ C ₃ - carbide	-	40 HRC			

Table 4: Summary of all 10 deposited welding consumables

5.3 Sample overview

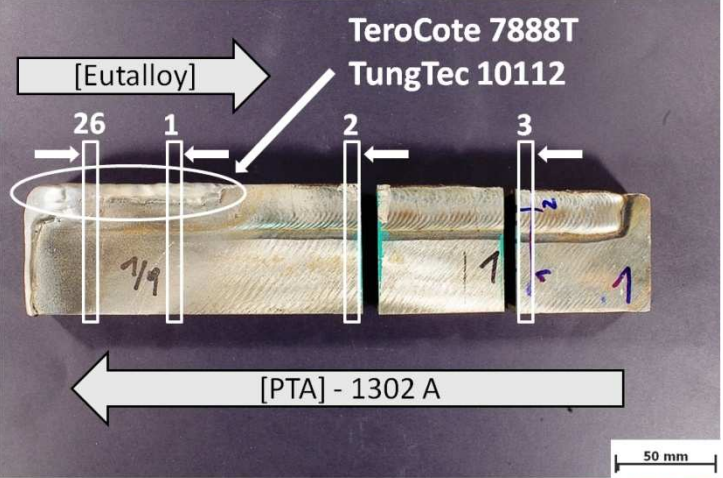
The follow matrix shows the deposited welding consumable for each sample.

Welding Consumable	Sample I	Sample II	Sample III	Sample IV	Sample V	Sample VI	Sample VII
1302A	✓	✓	✓			✓	
DO 390N				✓	✓	✓	
TeroCote 7888T	✓						
TungTec 10112	✓						
AbraTec 6088			✓			✓	
DO 321					✓	✓	
PG 6503			✓				
Keraloy							✓
Deloro 56							✓
Stellite 6							✓

Table 5: Applied welding consumables on each sample

5.4 Sample I

The overview table below shows a picture of sample I with all specimens and the deposited welding consumables. Additionally, the applied welding techniques and the welding direction can be also seen. Below, in Table 6, the known welding parameters for sample I are listed.

Sample I - overview	Welding technique	Welding consumable
 <p>Bildbreite: 362.33 mm; (Brennweite/Blende/Bel.Zeit: 24; 16; 1/2s) Bildname: vs09v001.jpg</p>	PTA	<u>1302 A:</u> <ul style="list-style-type: none"> • Fe-based • Borocarbides
	EUTALLOY	<u>TeroCote 788T:</u> <ul style="list-style-type: none"> • NiCrBSi matrix • 75 % WC
	EUTALLOY	<u>TungTec 10112:</u> <ul style="list-style-type: none"> • NiCrBSi matrix • 60 % WC

Substrate: 1.4313								
Welding parameters								
Weld Pass	Technique	Consumable	I [A]	V_{weld} [mm/min]	V_{osc} [mm/min]	Osc. width [mm]	Feed rate [g/min.]	Gas flow [l/min.]
1	PTA	1302 A	85	200	1200	2	15	1.3 Ar
2			75	200	-	-	15	
3			125	85	1200	15	20	
4								
5	Eutalloy	TeroCote 788T TungTec 10112	Unknown parameters					

Table 6: Welding parameters - Sample I

5.4.1 Sample I - Eutalloy (Refurbishment)

Figure 67 shows specimen 1 with its buildup sequence. Furthermore the used welding consumables 1302 A deposited by PTA technique and subsequently TeroCote 7888T and TungTec 10112 applied by Eutalloy process for refurbishment simulation.

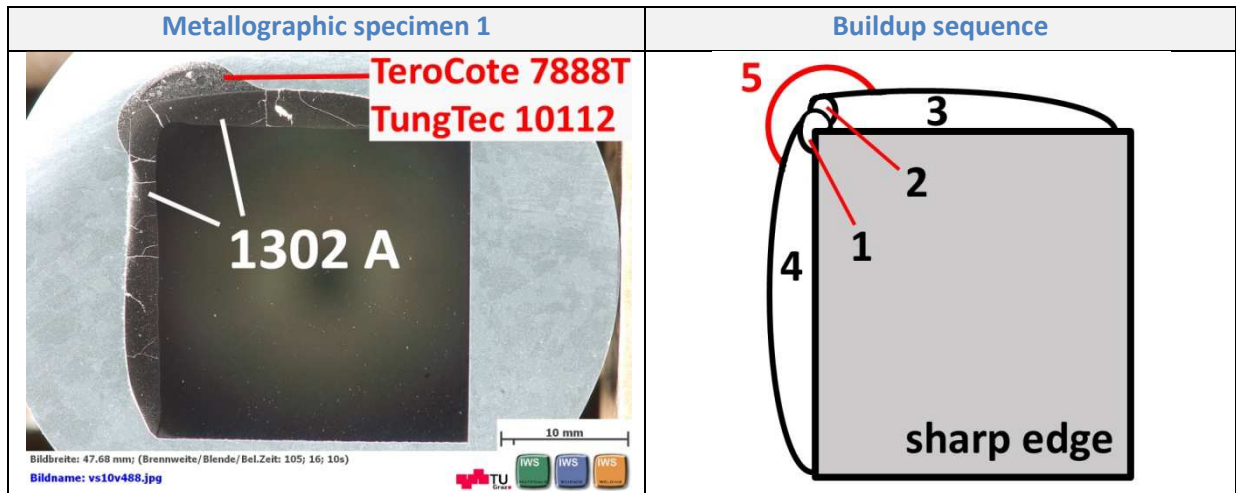


Figure 67: Specimen 1 – buildup sequence

5.4.1.1 Hardness

The hardness mapping of specimen 1 shows a relative homogenous distribution of hardness in layer 1 – 4. The values vary between ~ 850 HV1 and 1200 HV1 except discontinuities like pores and cracks.

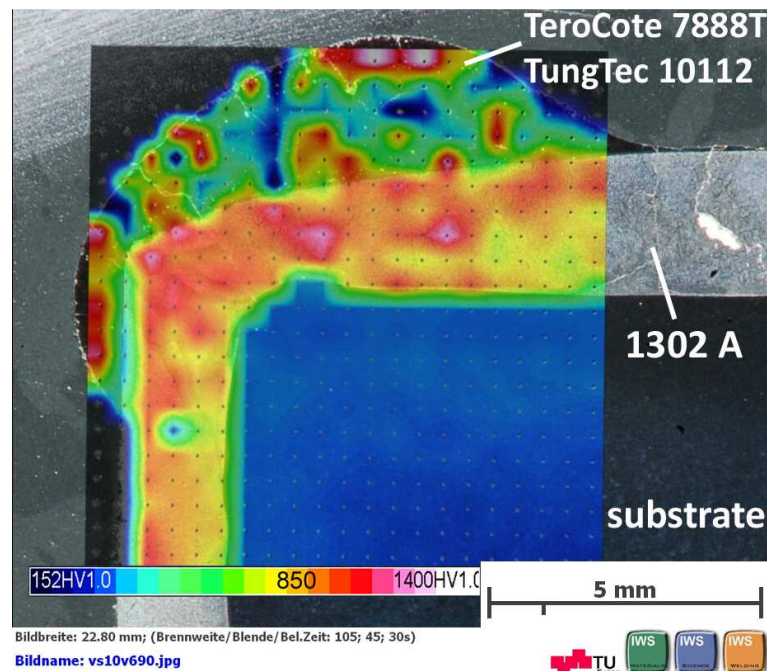


Figure 68: Specimen 1 – hardness mapping

On the 1302 A – layer a refurbishment simulation was done with the two consumables TeroCote 7888T and TungTec 10112 applied by Eutalloy process. In opposite, this combined layer shows extreme inhomogeneities. The matrix is relative soft ranging from ~ 300 HV1 to 550 HV1. Some tungsten carbides are hit or semi-hit during measurement and displayed by the red and white spots inside this layer. The dark blue spots in this layer are mainly areas with missing carbides due to irregular distribution.

5.4.1.2 EDX Eutalloy

The EDX analysis in Figure 69 shows the homogenous carbide distribution of TungTec 10112. In this area, at the edge, mainly TungTec 10112 was deposited. LOF (Lack of fusion), the black stripe and black holes, to the subjacent layer 1302 A can be seen clearly. This bad binding is due to the missing melting-in of the powder consumable TungTec 10112. In the bottom right corner, where TeroCote7888 and TungTec 10112 have been applied together, a better bond because of the melting-in can be seen. This area is illustrated and discussed again in the paragraph ‘binding’ – page 89.

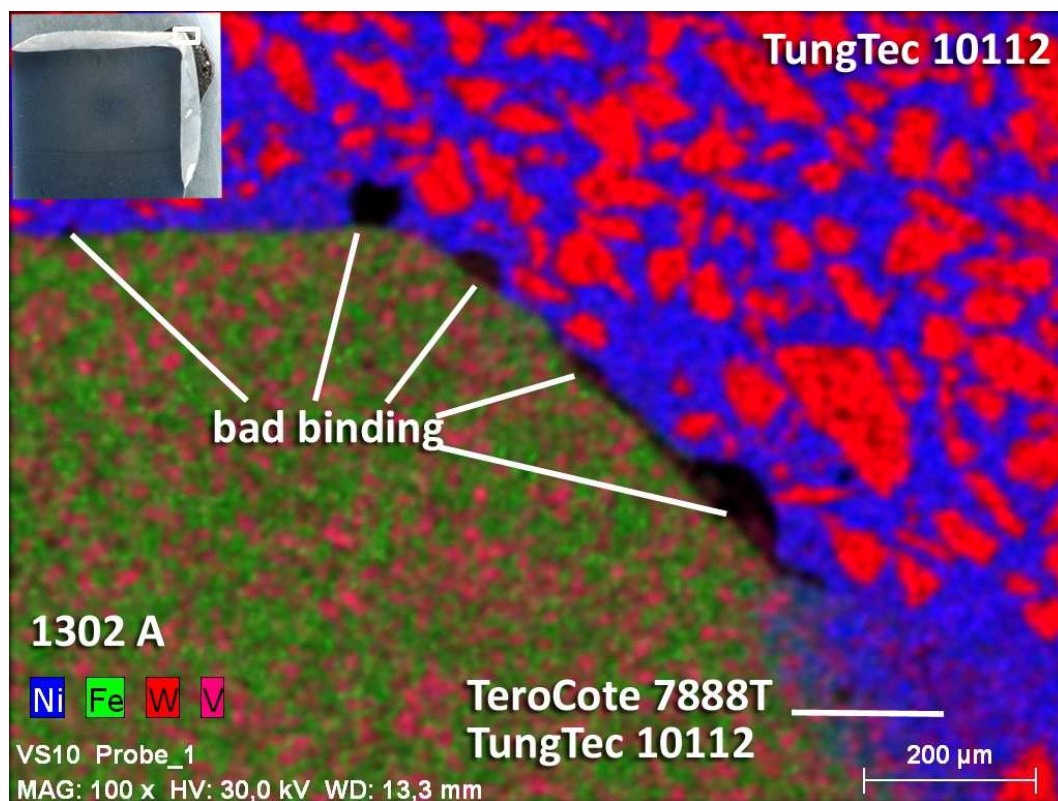


Figure 69: Specimen 1 – EDX scan

5.4.1.3 Pores

In Figure 70 some small pores with an average diameter of 75 μm can be observed. The distribution is quite random. They can be assigned to uniformly scattered porosity. The size of the pores is relative small. In the layer applied by the Eutalloy process the pore size is about 70 μm and in the PTA – layer (1302 A) they are smaller with an average size of about 20 μm .

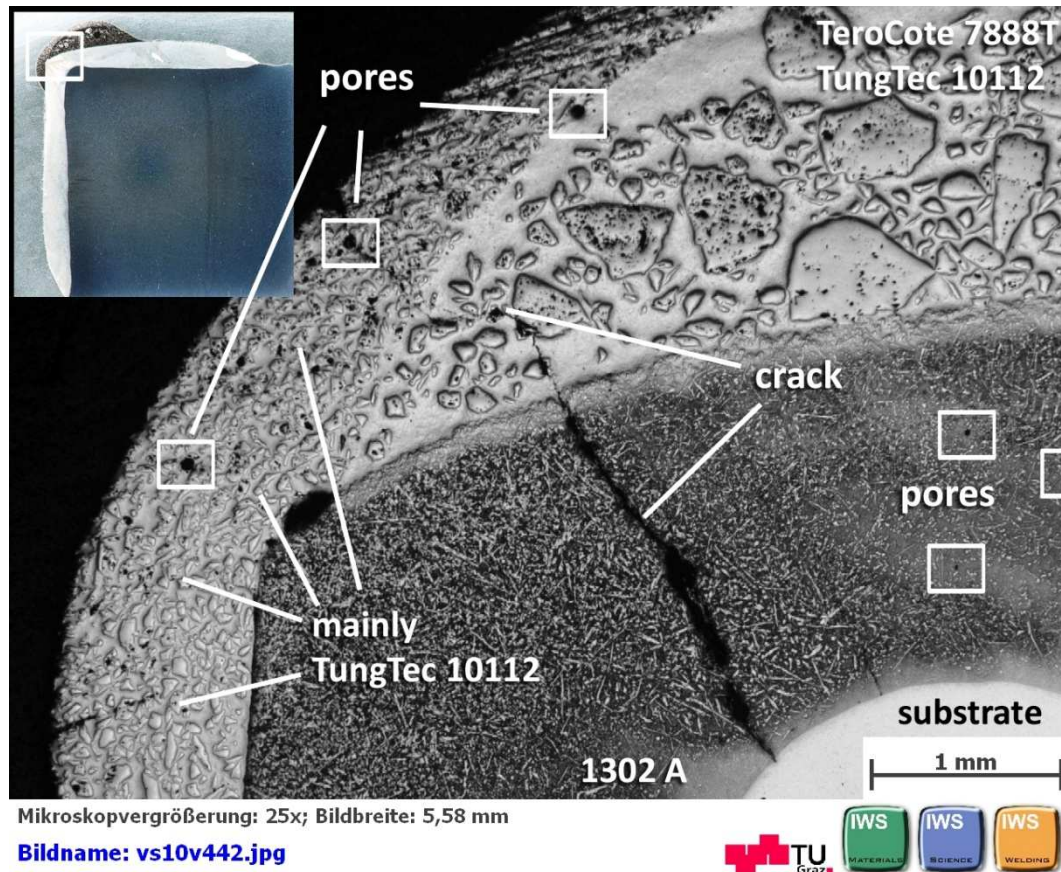


Figure 70: Specimen 1 – pores

5.4.1.4 Cracks

Figure 70 and Figure 71 show cracks which can be found and are typical for all 1302 A layers. In Figure 70, the crack configuration goes through both layers. First the layer 1302 A has been deposited by PTA and afterwards, the other layer has been applied by Eutalloy process. This means that this crack occurs after the Eutalloy process. The additional heat input by the refurbishment simulation could be the reason for this specific crack or the additional crack propagation. The crack propagates perpendicular to the fusion line. It means that the tendency of the coating for chipping is not so critical.

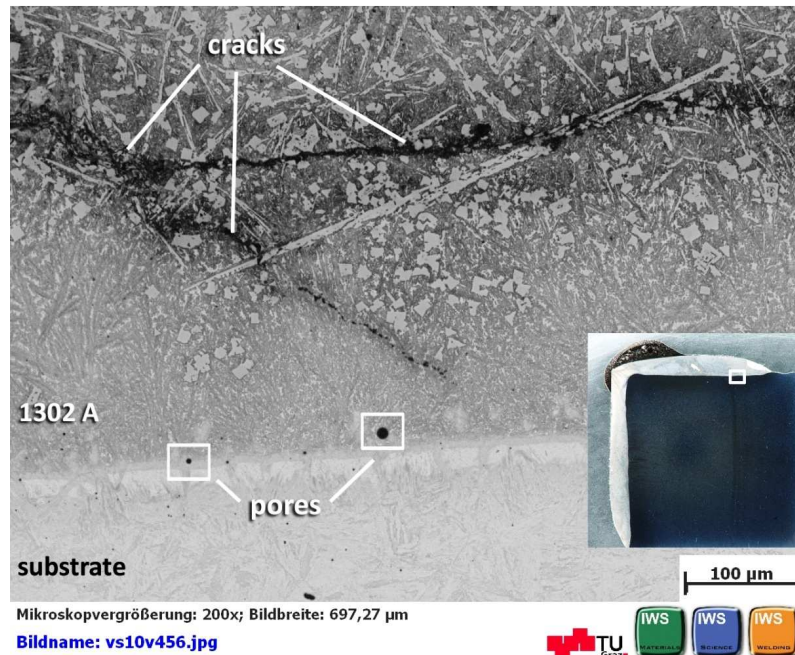


Figure 71: Specimen 1 – cracks in 1302 layer

5.4.1.5 Binding

Discontinuities of the bond are illustrated in Figure 72 again. In the right upper corner of Figure 72, the bonding seems to be okay. In this area the brazing or dilution of the welding consumables happened in opposite to the area with poor bond qualities. Due to the size and distribution of the tungsten carbides in this area, the missing fusing (melting-in) of TungTec 10112 might be the reason for the unsatisfying bonding on the PTA layer 1302 A.

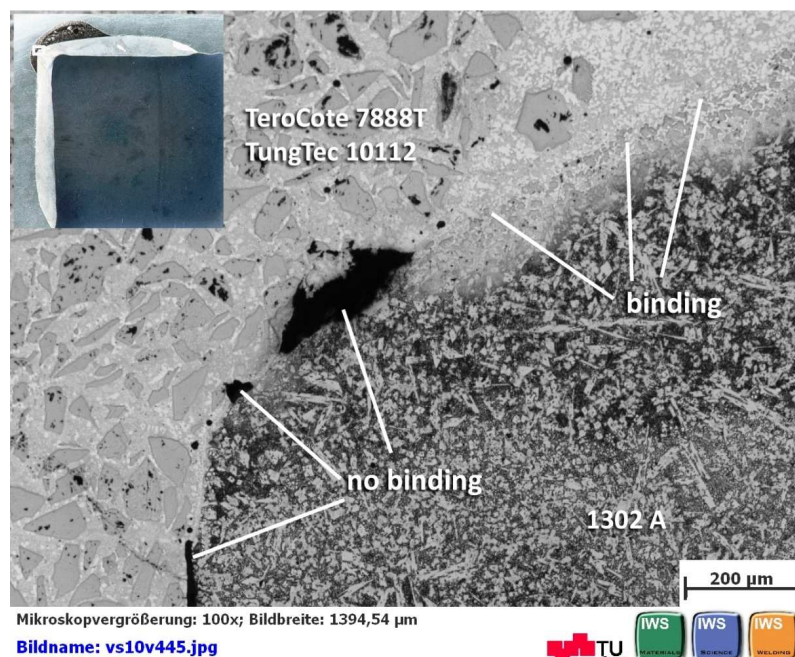


Figure 72: Specimen 1 – binding of Eutalloy coating

5.4.2 Sample I - 1302 A

Figure 73 shows the coating layer 1302 A of specimen 3 deposited by PTA process on and its buildup sequence.

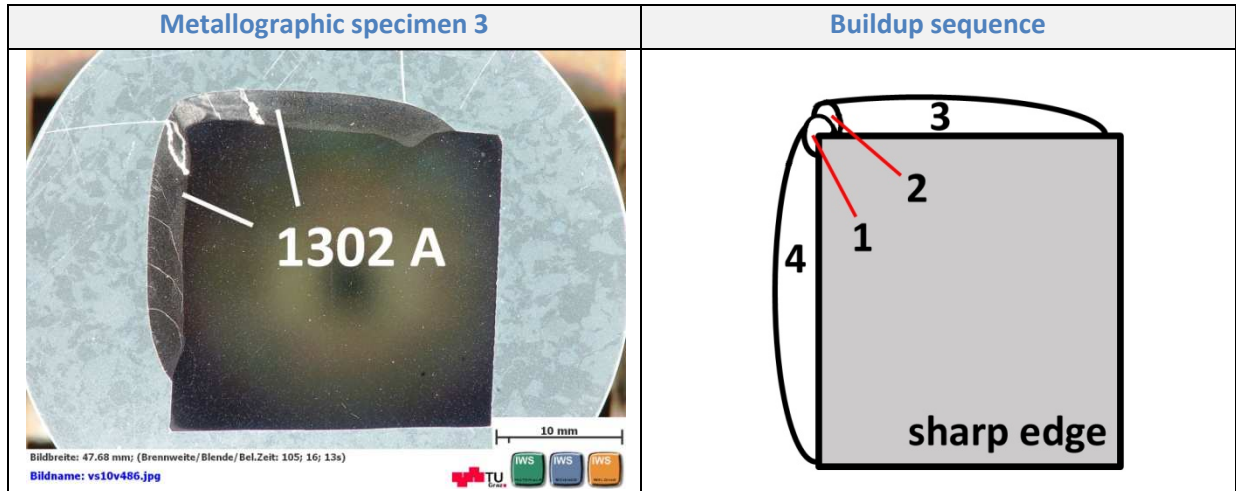


Figure 73: Specimen 3 – buildup sequence

5.4.2.1 Hardness

The hardness mapping of specimen 3 also shows a relative homogenous distribution of hardness. The values are slightly higher compared to specimen 1 and vary between ~ 900 HV1 and 1250 HV1. The higher hardness of specimen 3 may result due to the missing refurbishment simulation with the Eutalloy process applied on specimen 1.

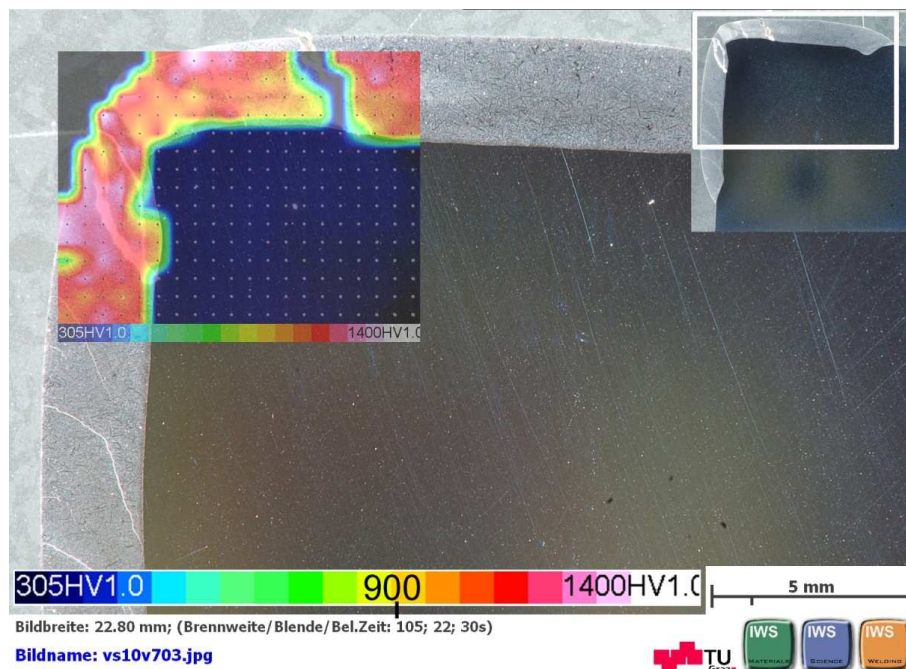


Figure 74: Specimen 3 – hardness mapping

The additional heat input of the refurbishment simulation with the Eutalloy process might have caused annealing effects on specimen 1 and consequently a decrease of hardness.

5.4.2.2 Pores

In Figure 75 some small pores with a diameter in the range of 50 μm can be observed. Only one is outstanding considering the size with a diameter of about 80 μm . The distribution is quite random and they show a globular shape. It can be classified to uniformly scattered porosity.

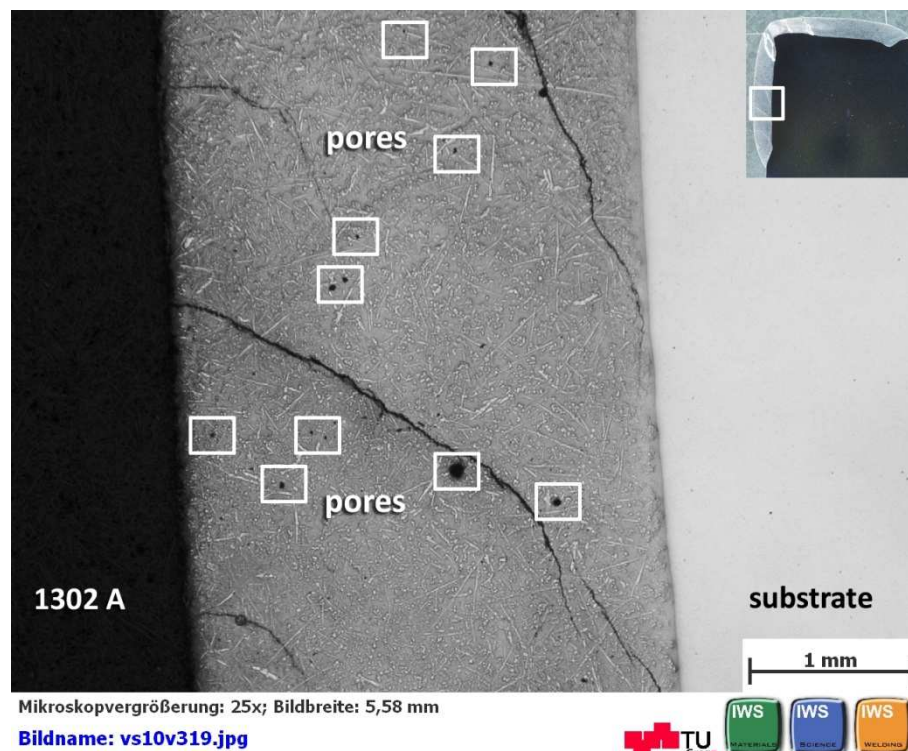


Figure 75: Specimen 3 – pores

5.4.2.3 Cracks

In Figure 75 and Figure 76 cracks inside the coating layer 1302 A occur. In Figure 75 the cracks run parallel to the fusion line and the coating is prone to chipping if the protective layer is under impact load. Unlike to the cracks in Figure 76 where the direction of the cracks is again perpendicular to the fusion line.

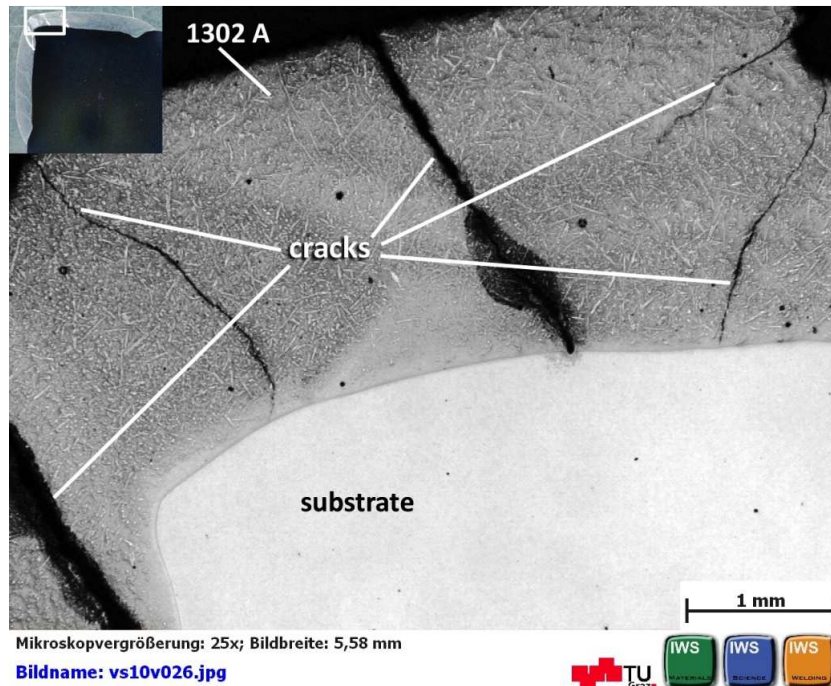


Figure 76: Specimen 3 – cracks in layer 1302 A

5.4.2.4 Binding

Figure 77 illustrates a perfect bonding of the PTA layer 1302 A on the substrate what can be also noticed in Figure 75 and Figure 76. The heat input of the deposition process causes grain coarsening of the substrate in the fusion zone.

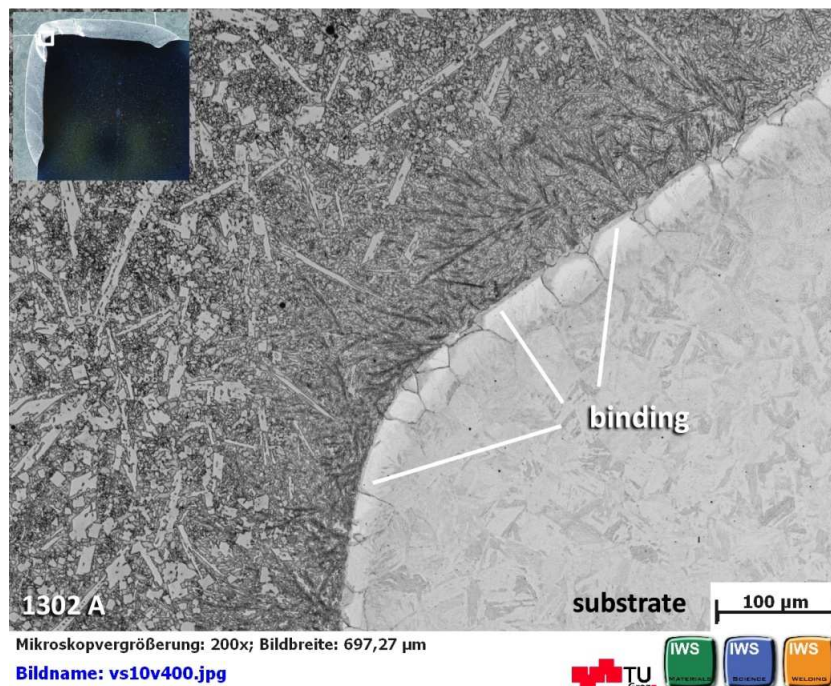


Figure 77: Specimen 3 – binding of PTA layer 1302 A

5.4.3 EDX and WDX analysis of PTA powder 1302 A

The exact composition of the PTA powder 1302 A, identical to the flux cored wire DO 390N, is unknown. Only the composing elements, which are Fe, Cr, W, Nb, Mo, B, Si, and C are published by Castolin Eutectic. The following picture, Figure 78, illustrates the powder 1302 A, which was first investigated by means of EDX.

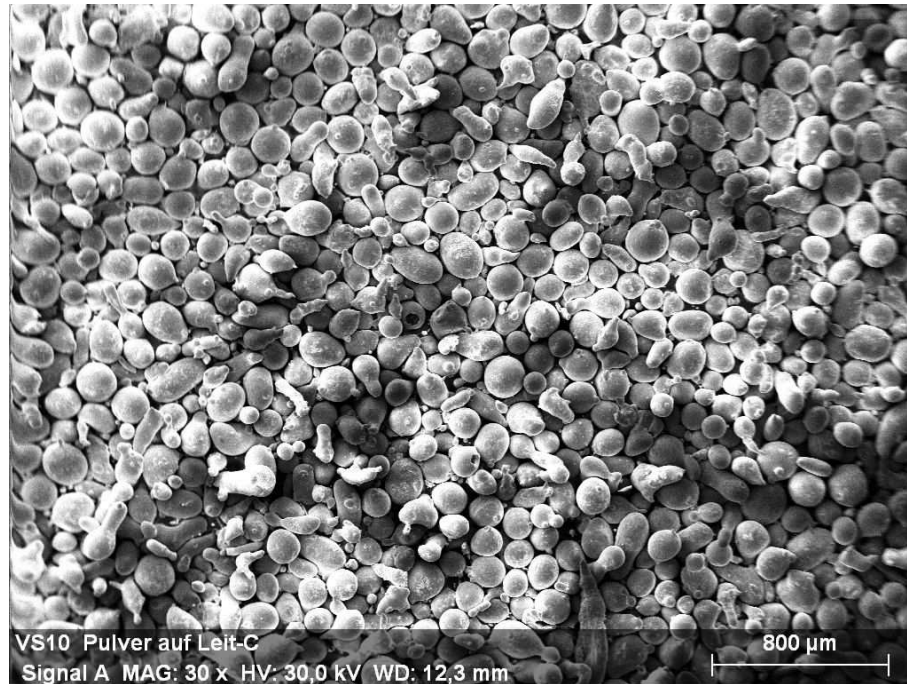


Figure 78: PTA powder 1302 A investigated by EDX

The multiple numbers of elements makes the identification by means of EDX nearly impossible. Especially the lighter elements like boron are difficult or rather impossible to detect and consequently the EDX analysis is not very accurate. Therefore, WDX analysis was used due to its higher resolution of the x-ray spectrum. This analysis was done external at Montanuniversität Leoben.

Figure 79 shows on the left the area of the PTA layer 1302 A which was used for the WDX analysis and on the right the detail which was investigated.

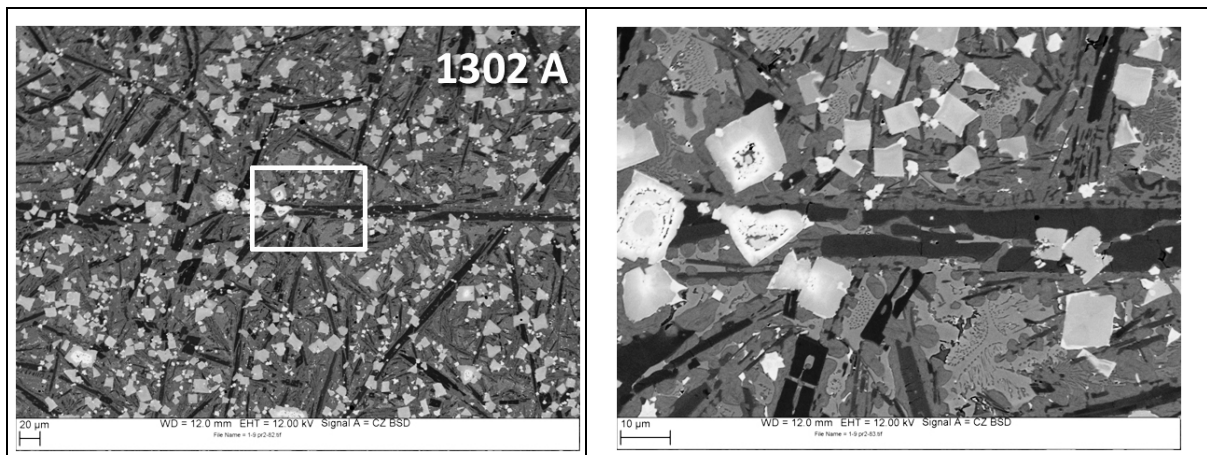


Figure 79: Specimen 1 – SEM - image of PTA layer 1302 A and detail of analysis

Figure 80 illustrates the matrix of 1302 A, which is iron-alloy based and has a microcrystalline martensitic microstructure.

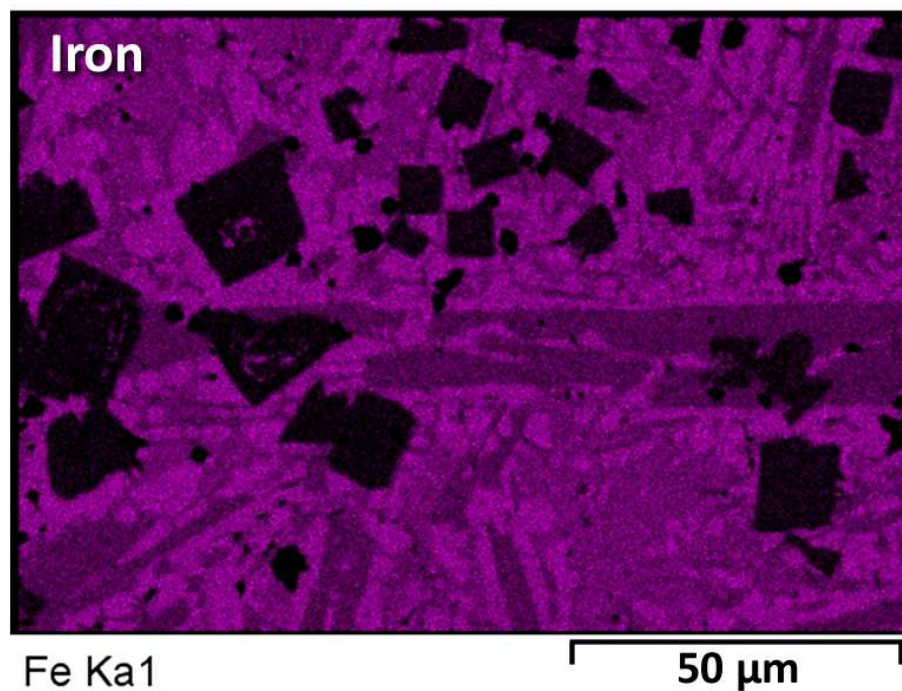


Figure 80: Specimen 1 – Fe-matrix

The following images show the main components, which form the hard phases.

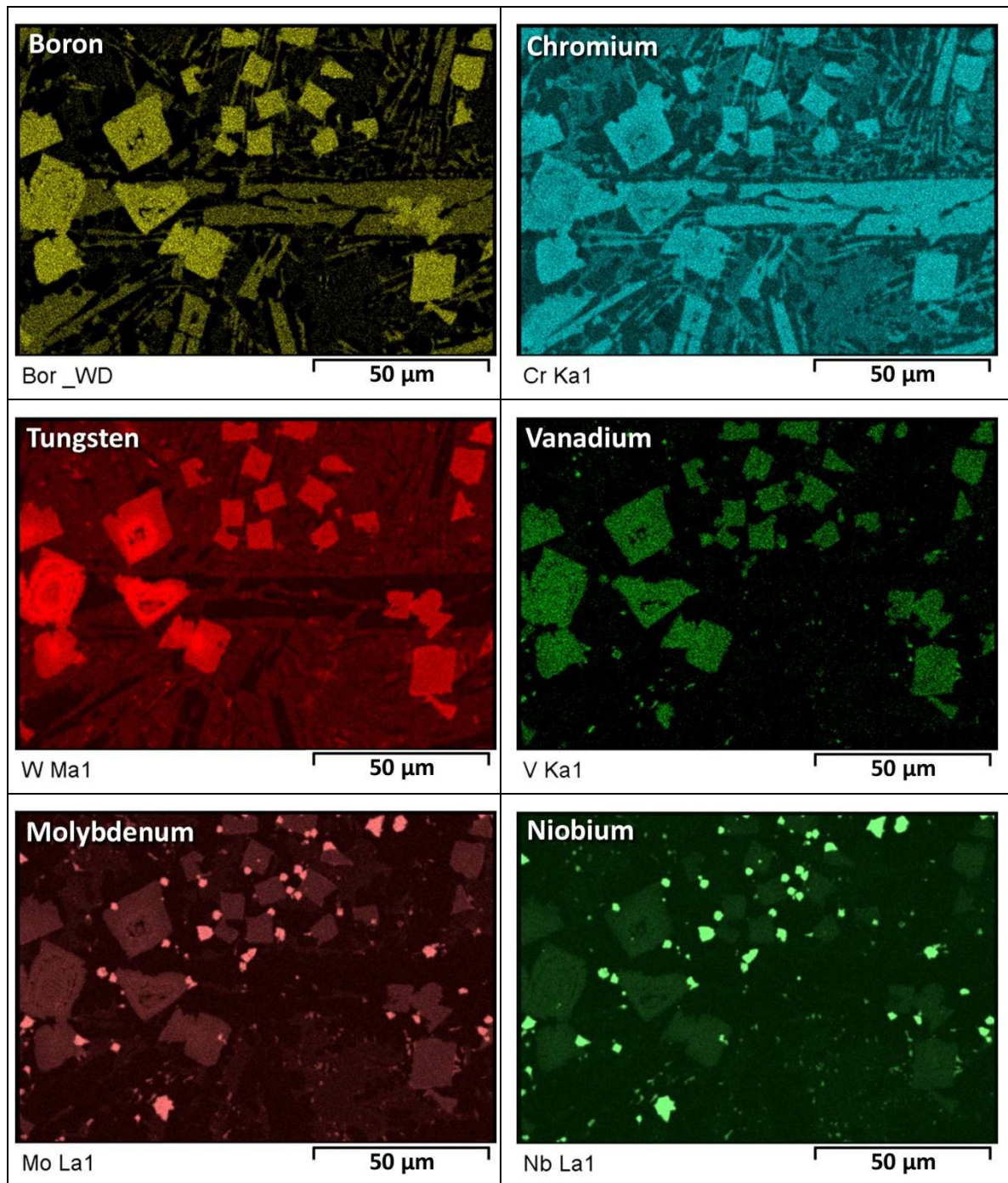


Figure 81: WDX – analysis: B, Cr, W, V, Mo, Nb

Based on the WDX analysis, the complex structure of both welding consumables, 1302 A & DO 390N can be characterized. The hardness and wear resistance is based on precipitations of ultra fine ($\sim 10 \mu\text{m}$) carbides and carboborides distributed in a mesomorphous (mixture of crystalline and amorphous) iron- matrix alloy. [48]

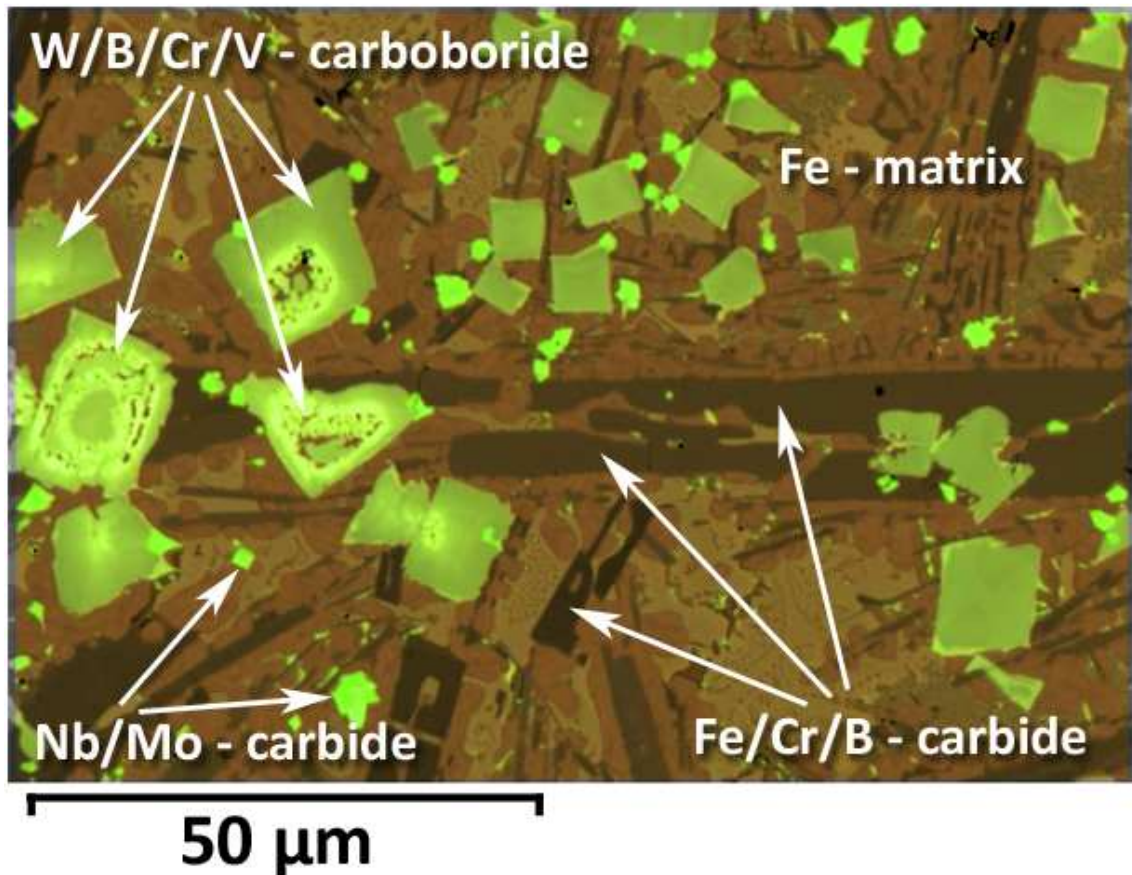
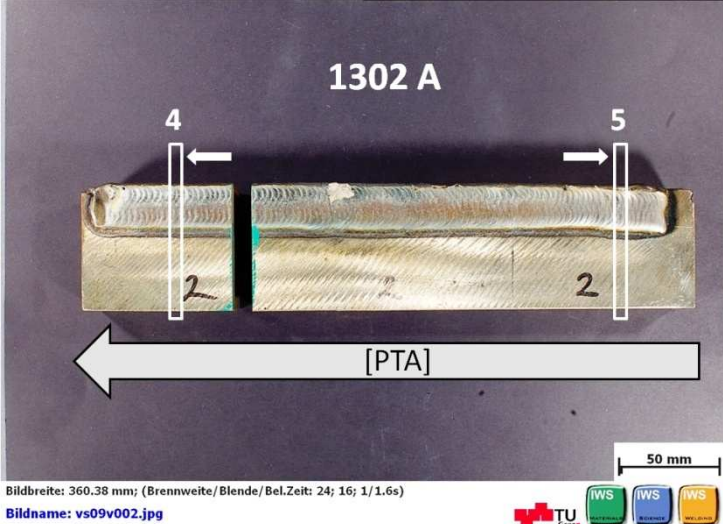


Figure 82: Specimen 1 – WDX analysis of 1302 A

5.5 Sample II

Sample II - overview	Welding technique	Welding consumable
	PTA	<u>1302 A:</u> <ul style="list-style-type: none"> • Fe-based • Borocarbides

Substrate: 1.4313								
Welding parameters								
Weld Pass	Technique	Consumable	I [A]	V_{weld} [mm/min]	V_{osc} [mm/min]	Osc. width [mm]	Feed rate [g/min.]	Gas flow [l/min.]
1	PTA	1302 A	85	200	1200	2	15	1.3 Ar
2			75	200	-	-	15	
3			125	85	1200	15	20	
4								

Table 7: Welding parameters – Sample II

Figure 83 shows specimen 4 and the buildup sequence. The deposited welding consumable is 1302 A by PTA process. In opposite to Sample I, the edge is different.

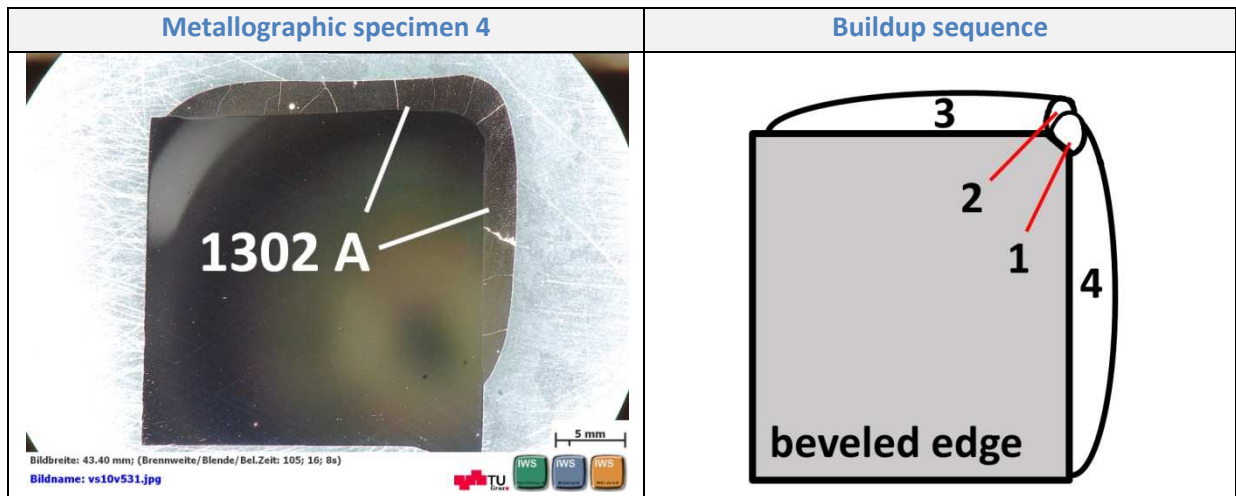


Figure 83: Specimen 4 – buildup sequence

5.5.1.1 Hardness

The hardness mapping of specimen 4 shows a relative homogenous distribution of hardness. The values vary between ~ 850 HV1 and about 1200 HV1 except discontinuities like pores and cracks.

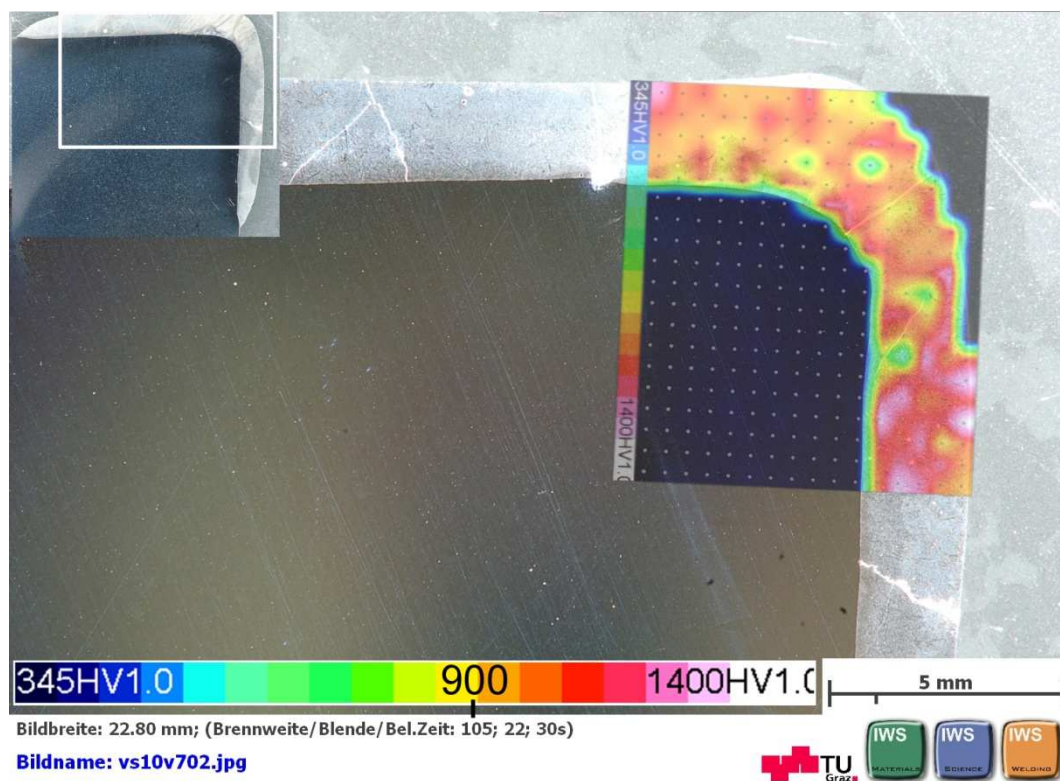


Figure 84: Specimen 4 - hardness mapping

5.5.1.2 Pores

In Figure 85 a lot of small pores can be observed. The distribution is quite random and shows a globular shape and can be assigned to uniformly scattered porosity. One pore has an outstanding size with a diameter of about 250 μm . In the next picture, Figure 86, another huge pore can be noticed with a diameter of about 600 μm . These pores can be probably assigned to mechanical pores due to the exceptional size.

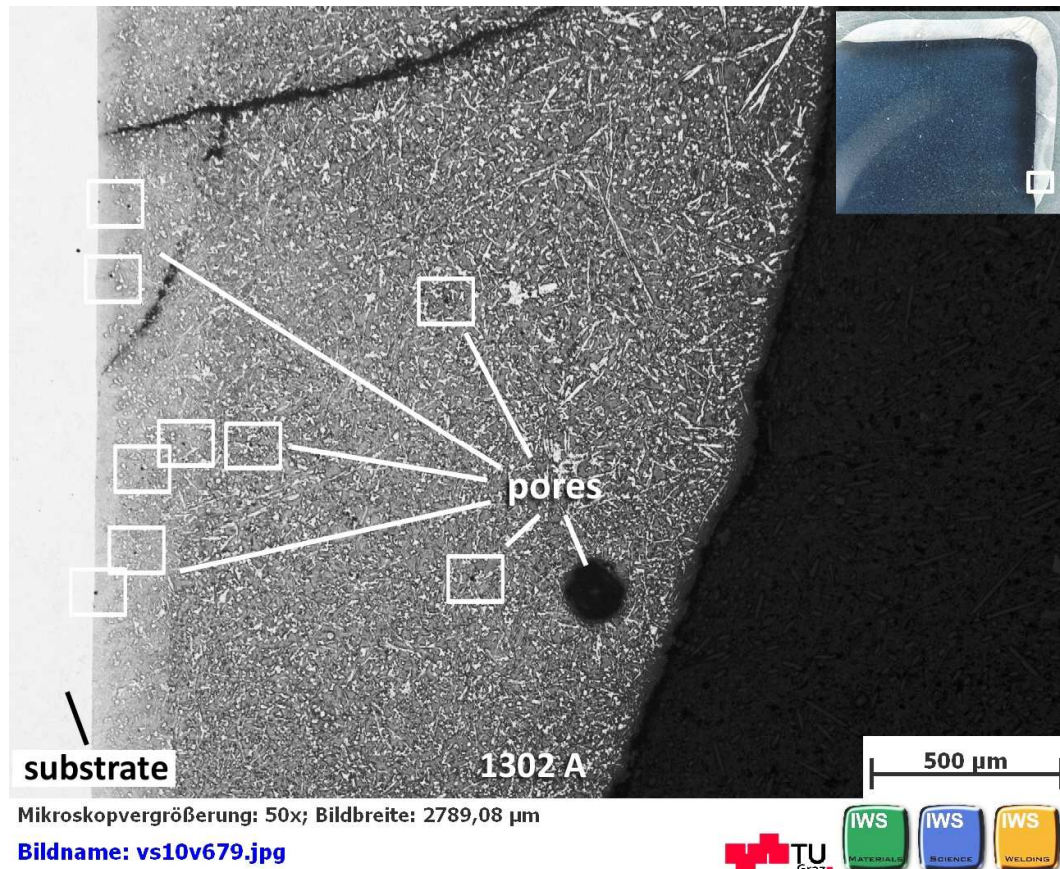


Figure 85: Specimen 4 – pores

5.5.1.3 Cracks

Figure 86 shows cracks which are typical for the coating 1302 A considering the pictures above. The crack propagates perpendicular or at least not parallel to the fusion line, which means that the tendency of the coating for chipping is not so critical in this area.

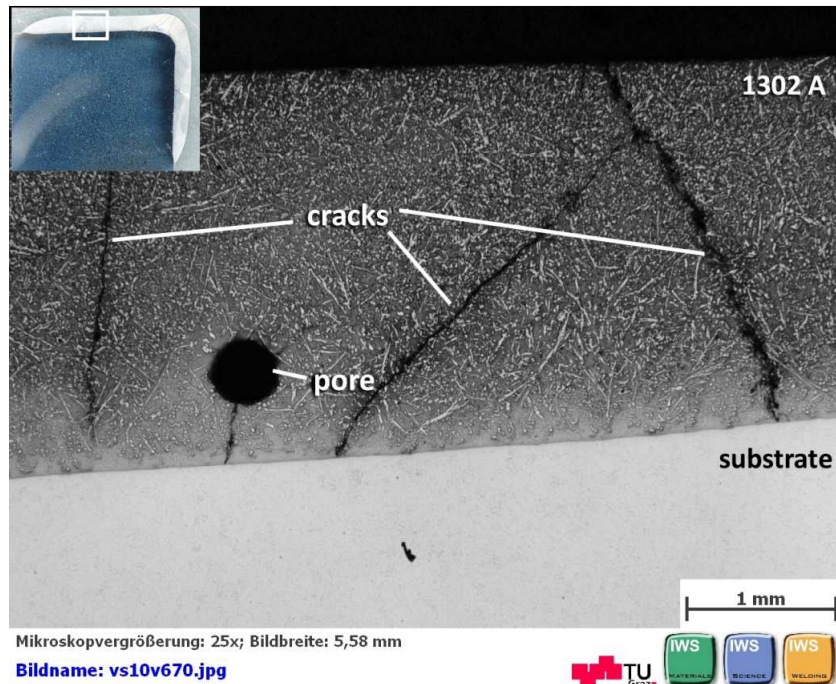


Figure 86: Specimen 4 – cracks

5.5.1.4 Binding

Figure 87 illustrates a perfect bonding of the PTA layer 1302 A on the substrate what can be also noticed in Figure 85 and Figure 86. Cracks run perpendicular to the binding and it can be assumed that chipping is not so critical in this area.

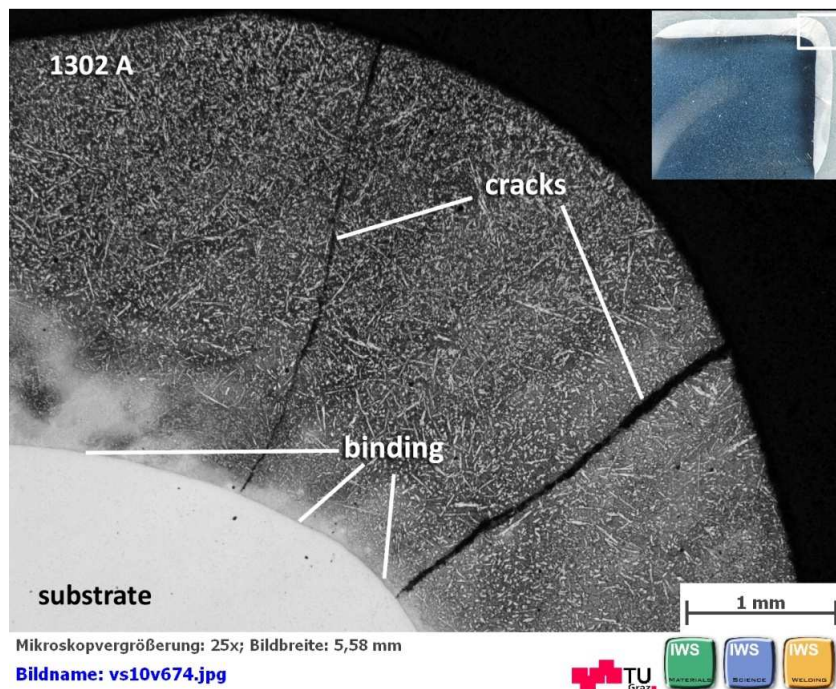


Figure 87: Specimen 4 – binding

5.6 Sample III

Sample III - overview	Welding technique	Welding consumable
	PTA	<u>1302 A:</u> <ul style="list-style-type: none"> • Fe-based • Borocarbides
		<u>PG 6503:</u> <ul style="list-style-type: none"> • NiBSi matrix • 60 % WC
	SMAW	<u>AbraTec 6088:</u> <ul style="list-style-type: none"> • NiBSi matrix • 55 % WC

Substrate: 1.4313								
Welding parameters								
Weld Pass	Technique	Consumable	I [A]	V _{weld} [mm/min]	V _{osc} [mm/min]	Osc. width [mm]	Feed rate [g/min.]	Gas flow [l/min.]
1	PTA	1302 A	85	200	1200	2	15	1.3 Ar
2			75	200	-	-	15	
3			125	85	1200	15	20	
4		PG 6503	90	85	1200	15	25	
5-7	SMAW	AbraTec 6088	Unknown parameters					

Table 8: Welding parameters – Sample III

5.6.1 Sample III - PG 6503

Figure 88 shows the coating layers 1302 A and PG 6503 deposited by PTA and its buildup sequence of specimen 13.

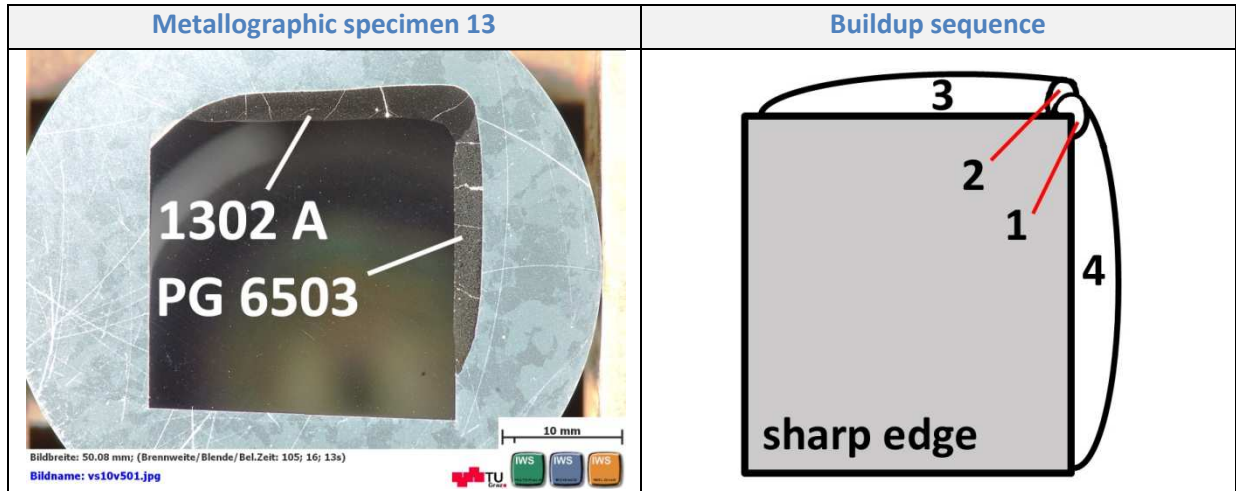


Figure 88: Specimen 13 – buildup sequence

5.6.1.1 Pores

In Figure 89 one pore with a diameter of about 20 μm can be found in the PG 6503 layer. The pore can be probably assigned to a mechanical pore due to the exceptional size.

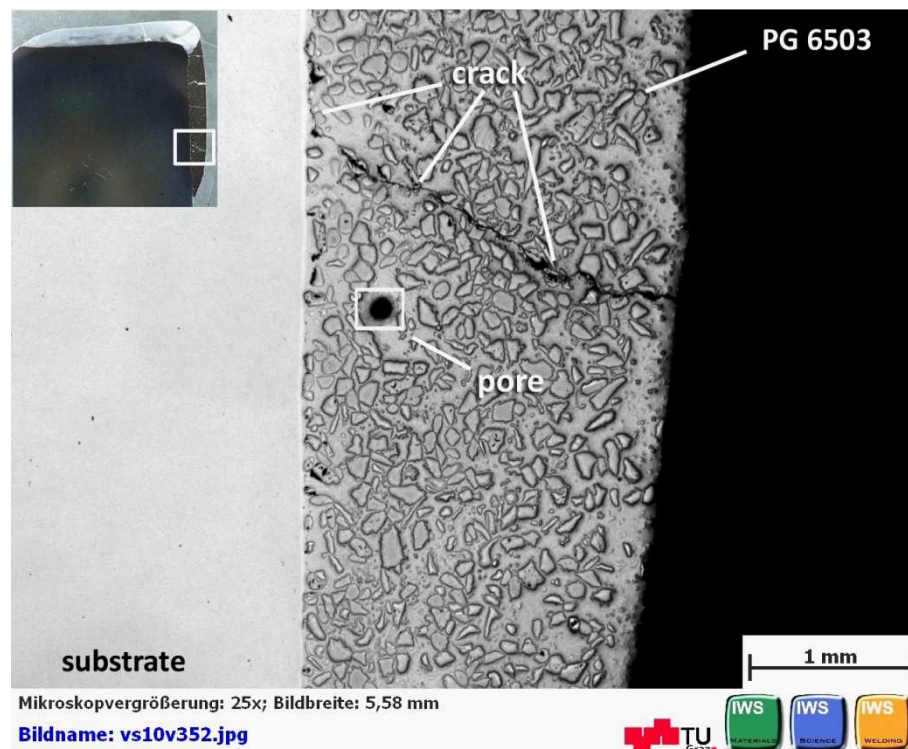


Figure 89: Specimen 13 – pore

5.6.1.2 Cracks

The next picture, Figure 90 illustrates a crack in the transition zone of both PTA layers, the iron-based 1302 A and the nickel-based PG 6503. One crack runs parallel to the fusion line what is critical for chipping.

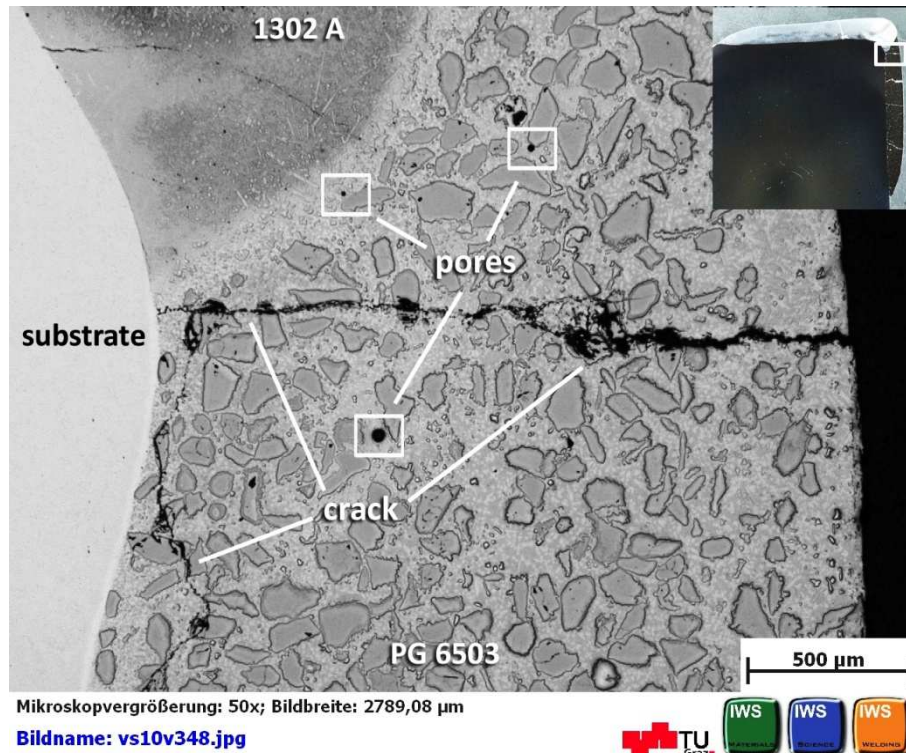


Figure 90: Specimen 13 - crack

5.6.1.3 Binding & Chipping

In Figure 91 the two cracks are perpendicular to the fusion line. The end of the upper crack leads to chipping of the PTA layer. Two areas of LOF can be also noticed. Moreover, a relative big piece of the coating is missing. The reason is the crack in the upper right corner of Figure 91, which leads to chipping of the layer.

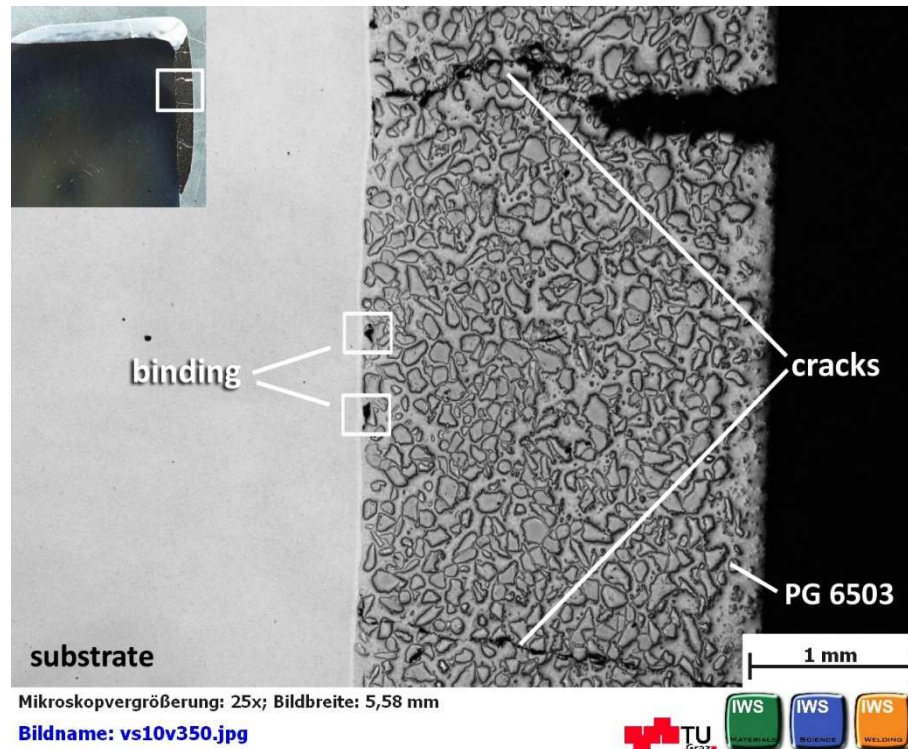


Figure 91: Specimen 13 – binding of PG 6503

5.6.2 Sample III - AbraTec 6088 (Refurbishment)

The next picture, Figure 92 shows specimen 25 and its buildup sequence. Moreover, the deposited welding consumables 1302 A and PG 6503 by PTA are shown with the ensuing refurbishment simulation with AbraTec 6088 on PG 6503 by SMAW process.

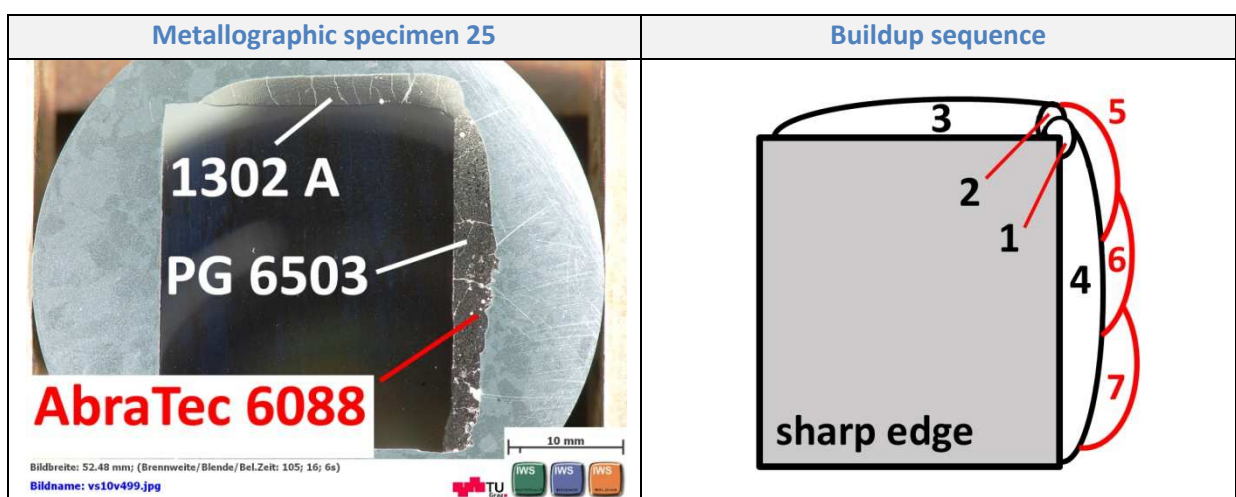


Figure 92: Specimen 25 – buildup sequence

5.6.2.1 Hardness

Figure 93 shows the hardness mapping of three different welding consumables.

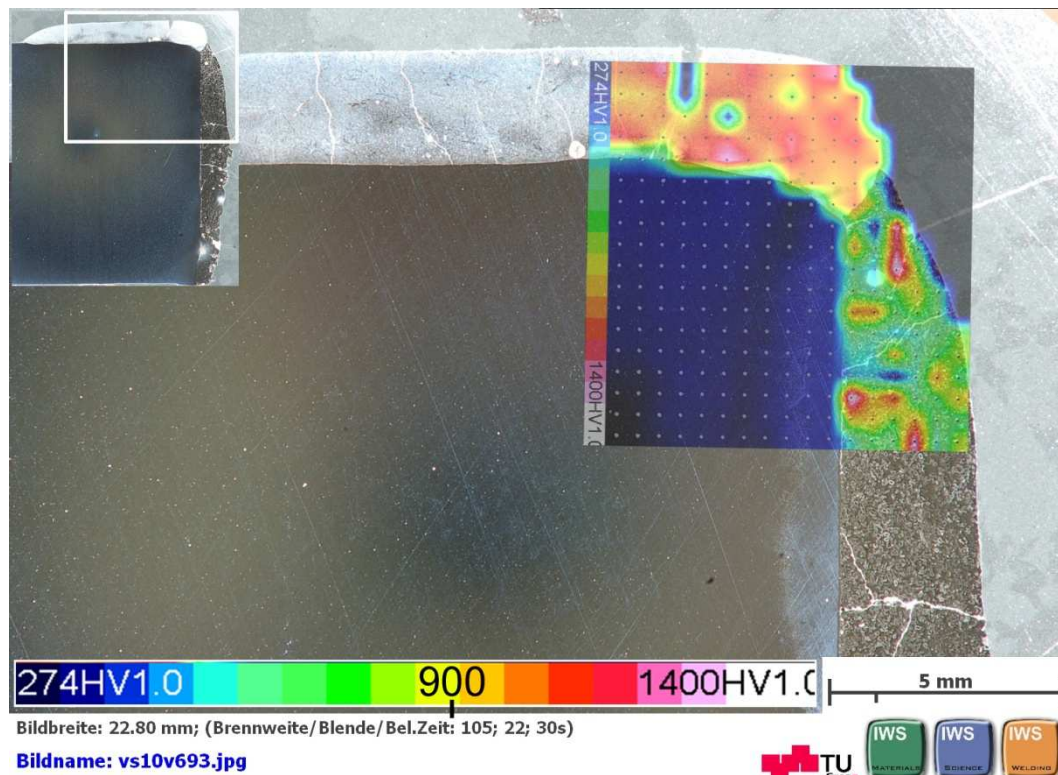


Figure 93: Specimen 25 – hardness mapping

The PTA layer 1302 A shows the same homogenous hardness like in the specimens described above. Hardness values are varying between 850 HV1 and 1200HV 1. The two other applied welding consumables are Ni-based with embedded tungsten carbides and a hardness decrease at the intersection of the coatings can be noticed. The average hardness of the Ni-matrix is about 600 HV1. The tungsten carbides differ completely in hardness compared to the matrix and these hardness spots can be noticed.

On PG 6503 – layer a refurbishment simulation was done with TeroCote 7888T and TungTec 10112 applied by SMAW technique.

5.6.2.2 EDX AbraTec 6088 on PG 6503

Figure 94 shows the area of all three coating layers. The homogenous carbide distribution of both Ni-based consumables, PG 6503 and AbraTec 6088 can be seen as well. In the area around of the huge pore, tungsten carbide is not detected by EDX. In this area the matrix is not protected by the carbides.

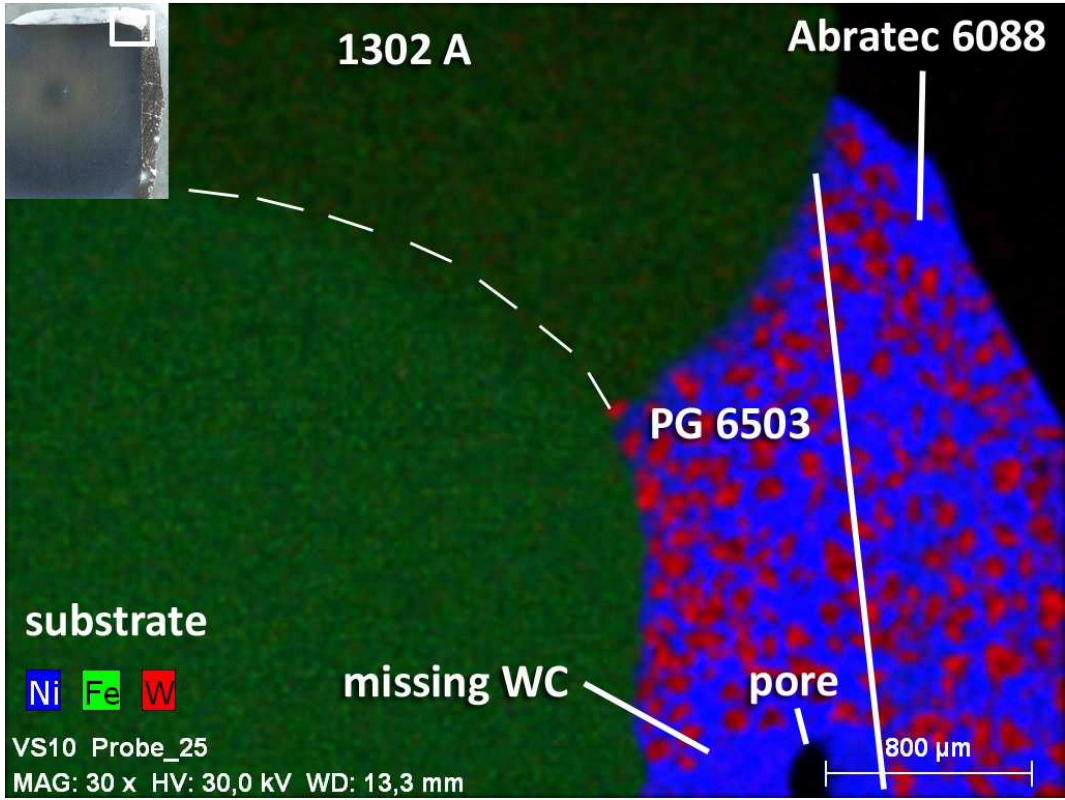


Figure 94: Specimen 25 – EDX scan AbraTec 6088 applied on PG 6503

5.6.2.3 Pores

In Figure 95 one big pore with a diameter of 500 μm can be seen. In the surrounding areas porosity does not occur.

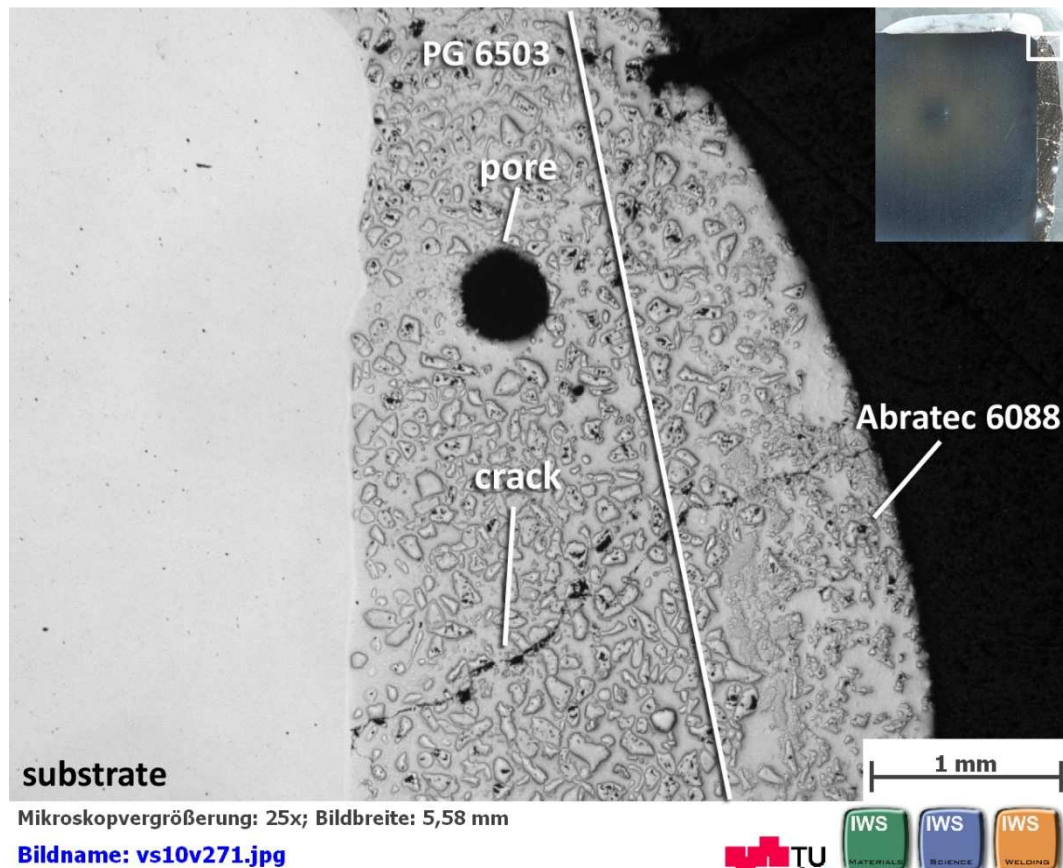


Figure 95: Specimen 25 – pore

5.6.2.4 Cracks

Cracks also appear in both Ni-based layers what can be seen in Figure 95 and Figure 96. Based on the fact that the crack runs through both layers it might indicate that the crack occurred after the refurbishment simulation. In these two figures the good binding of the PTA layer on the substrate and the good bond of the refurbishment can be noticed as well.



Figure 96: Specimen 25 – cracks

5.6.2.5 Binding & Dilution

The next picture, Figure 97 illustrates the good binding of the AbraTec 6088 layer on the PTA layer PG 6503. In this area the dilution is very high due to the huge amount of molten tungsten carbides. This extreme dilution is bad for wear resistance. Big tungsten carbides (WC) of AbraTec 6088 remain their size and shape and can clearly be seen.

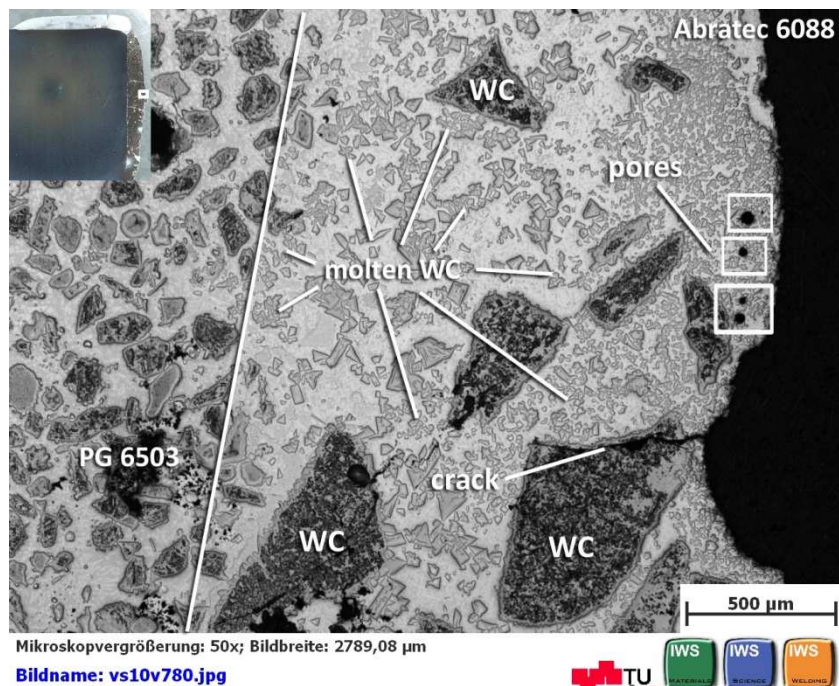



Figure 97: Specimen 25 – binding & dilution

5.7 Sample IV

Sample IV - overview	Welding technique	Welding consumable
	MAG	DO 390N: <ul style="list-style-type: none"> • Fe-based • Borocarbides

Substrate: 1.4313							
Welding parameters							
Weld Pass	Technique	Consumable	I [A]	V _{weld} [m/min]	Arc type	Gas type	Additional
1	MAG	DO 390N	80-90	3.1-3.7	Pulsed arc	Ar 2.5 % CO ₂	<u>Stickout:</u> 20mm
2			190-200	5			

Table 9: Welding parameters – Sample IV

5.7.1 Trailing torch

The next picture, Figure 98 shows specimen 15 and the buildup sequence of the DO 390N layer deposited by MAG process.

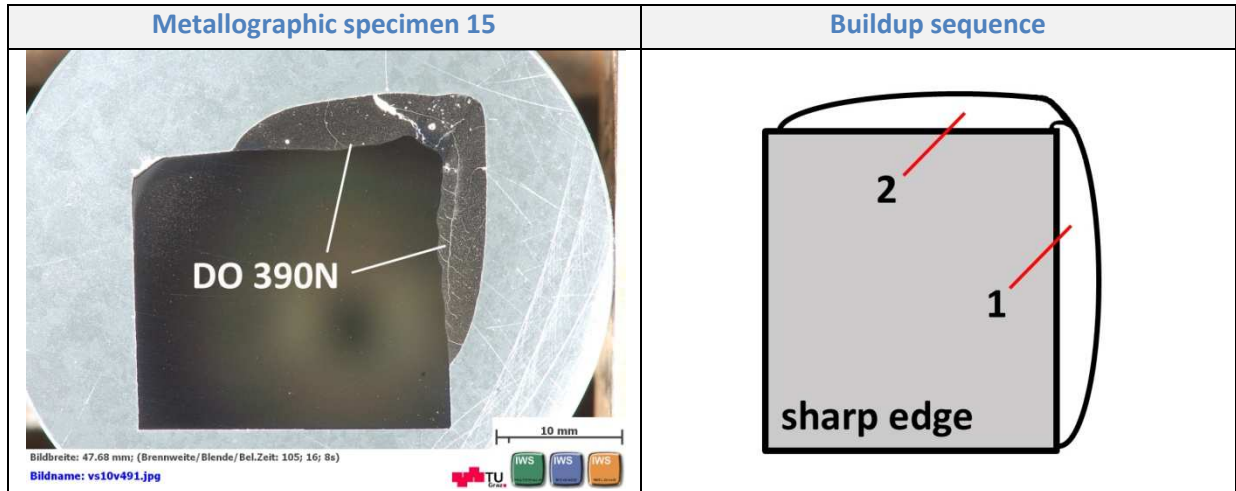


Figure 98: Specimen 15 – buildup sequence

5.7.1.1 Hardness – trailing torch

The hardness values in the range of ~ 750 HV1 and about 1150 HV1 are slightly lower compared to the identical PTA powder 1302 A. This might be due to the different heat input of the MAG process compared to PTA welding process.

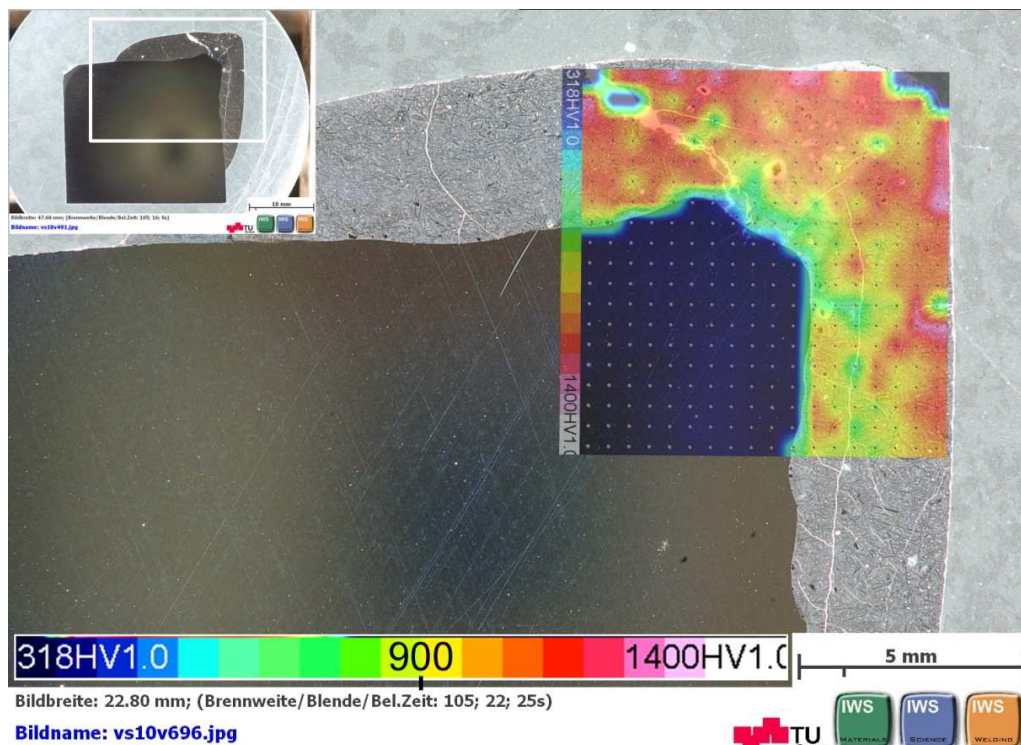


Figure 99: Specimen 15 – hardness mapping

5.7.1.2 Pores

A similar huge pore like in the PTA layer 1302 A with a diameter of about 500 μm can be seen in the following Figure 100 as well. This pore can be classified as mechanical pore. The porosity of the remaining area is rather low and can be categorized under metallurgical pores.

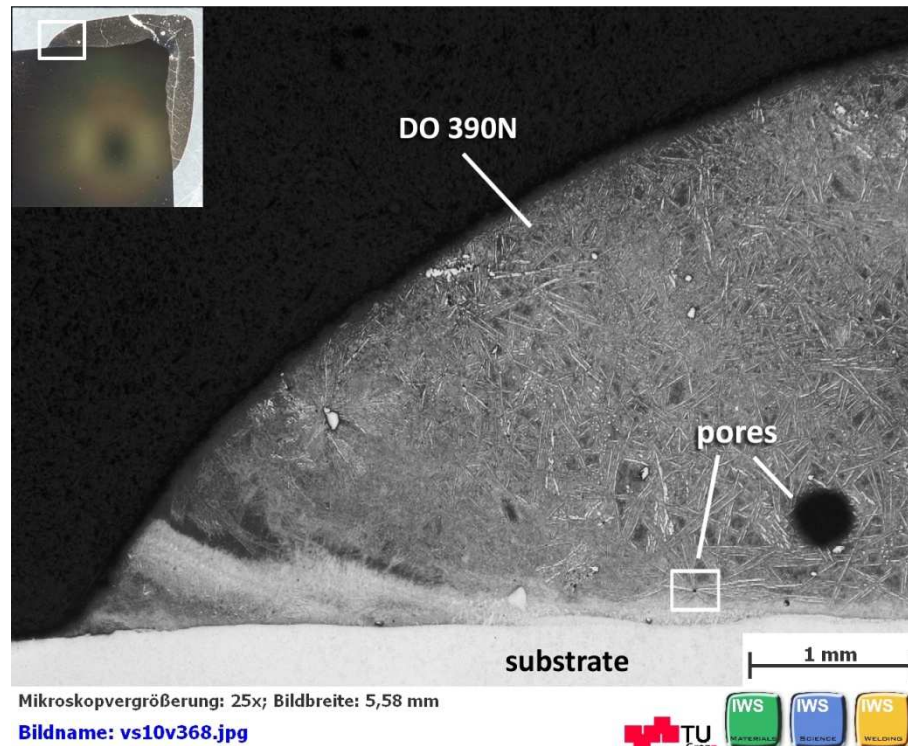


Figure 100: Specimen 15 – pores

5.7.1.3 Cracks

In the area of Figure 101 cracks running through and some big parts are also broken out. If impact load would be applied, the coating would definitely flake off. Another huge pore with a diameter of about 700 μm can be seen as well and it is surrounded by some a lot smaller ones with an average diameter of about 60 μm .

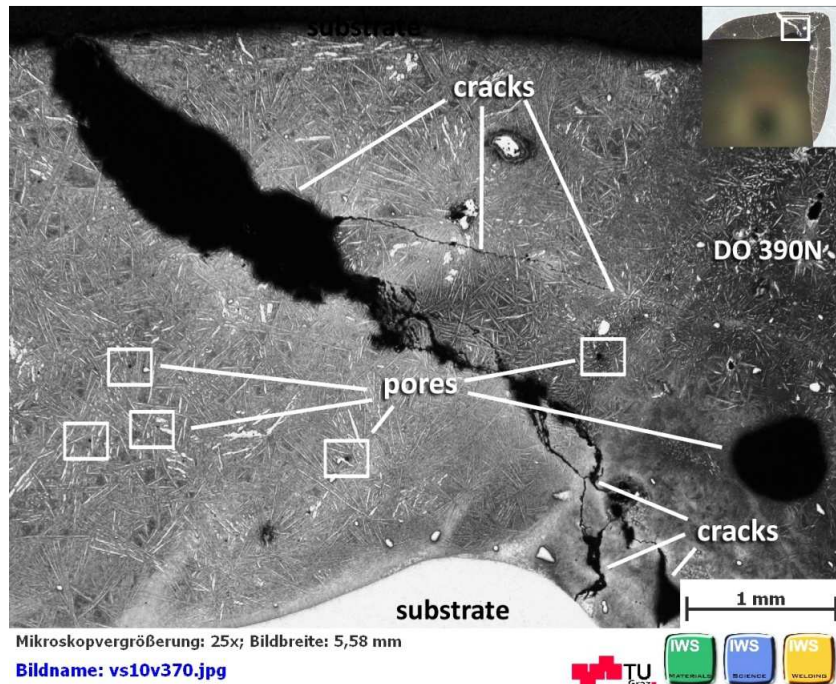


Figure 101: Specimen 15 – cracks

5.7.1.4 Binding

A good bonding of DO 390N on the substrate can be seen in Figure 102. The segregation of tungsten along the fusion line can be also found in the PTA layer 1302 A but not so often like in DO 390N layer. The welding process could be the reason for this phenomenon.

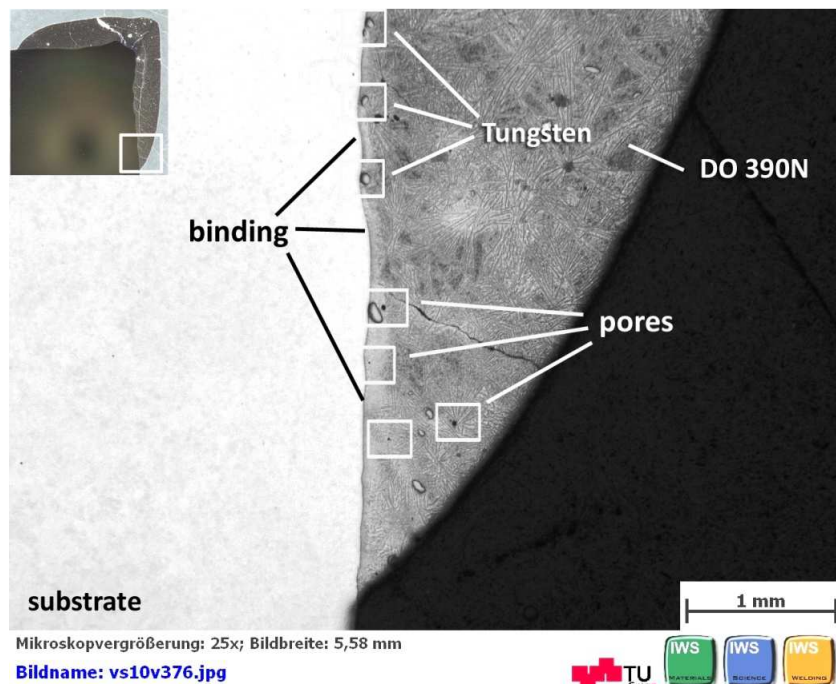


Figure 102: Specimen 15 – bond of DO 390N layer

5.7.2 Leading torch

Figure 103 shows the buildup sequence of specimen 17 and its coating layer DO 390N deposited by MAG.

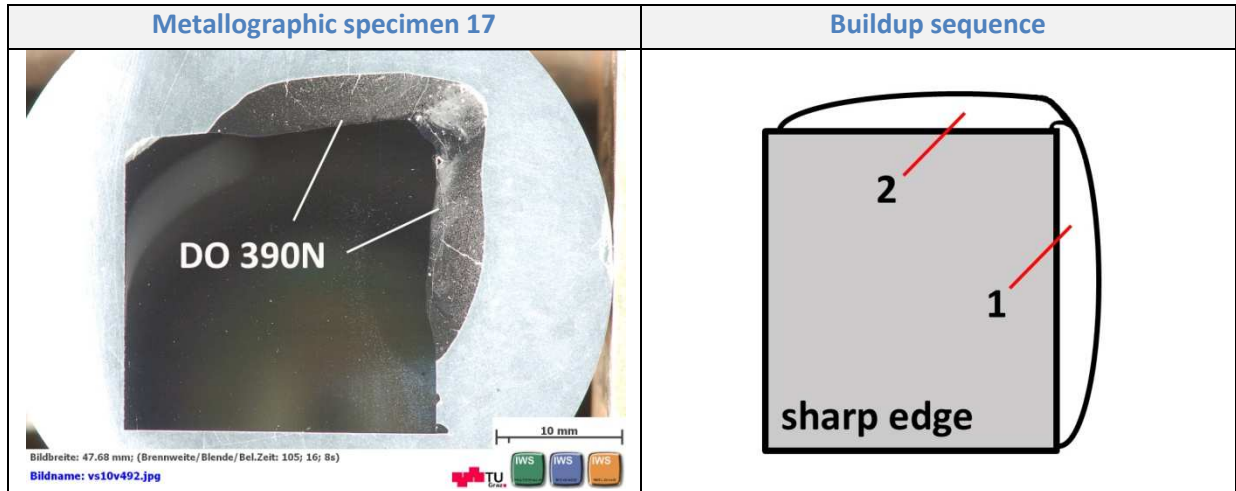


Figure 103: Specimen 17 – buildup sequence

5.7.2.1 Hardness – leading torch

The hardness values are more varying compared to the identical PTA powder 1302 A and are within a range of ~ 750 HV1 and about 1200 HV1. As a result of annealing effects the hardness of layer 1 in the transition area is slightly lower compared to the rest of layer 1.

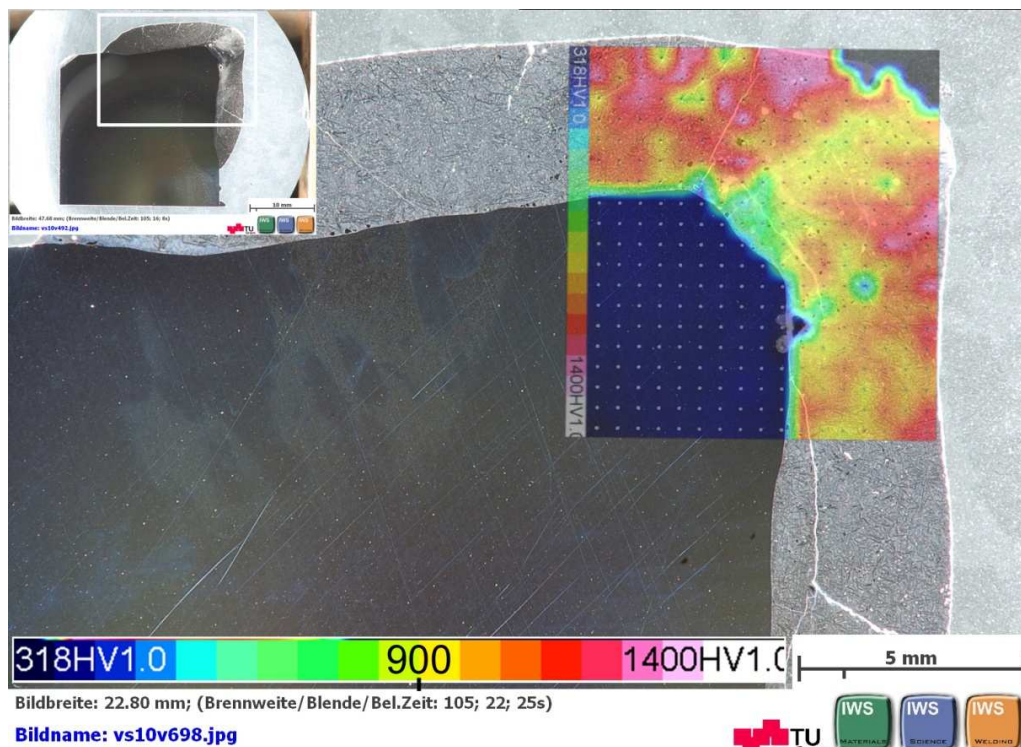


Figure 104: Specimen 17 – hardness mapping

5.7.2.2 Pores

The area in the following Figure 105 shows a relative high porosity compared to the former coating of DO 390N. Two pores with about 500 μm and 200 μm can be also noticed.

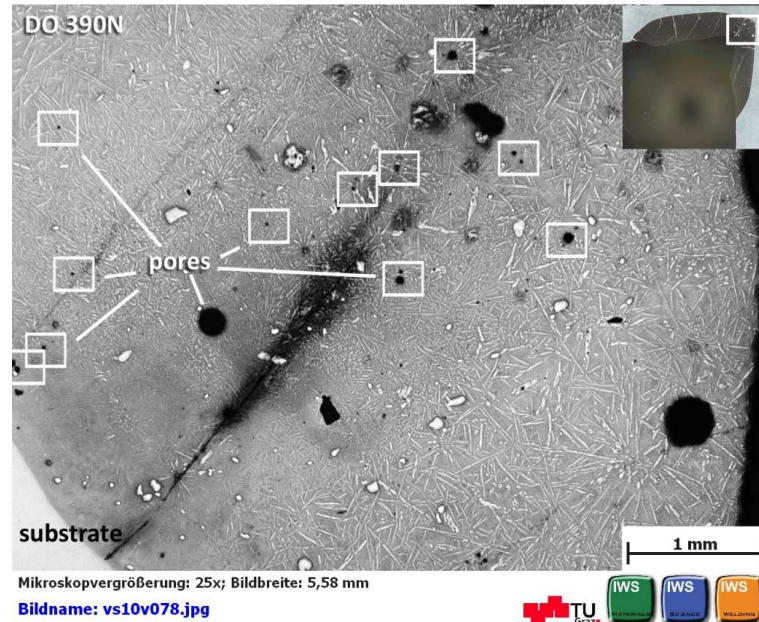


Figure 105: Specimen 16 – pores

5.7.2.3 Cracks

Figure 106 shows several cracks running perpendicular to the fusion line through the coating. Also in the picture above, Figure 105 three cracks are illustrated.

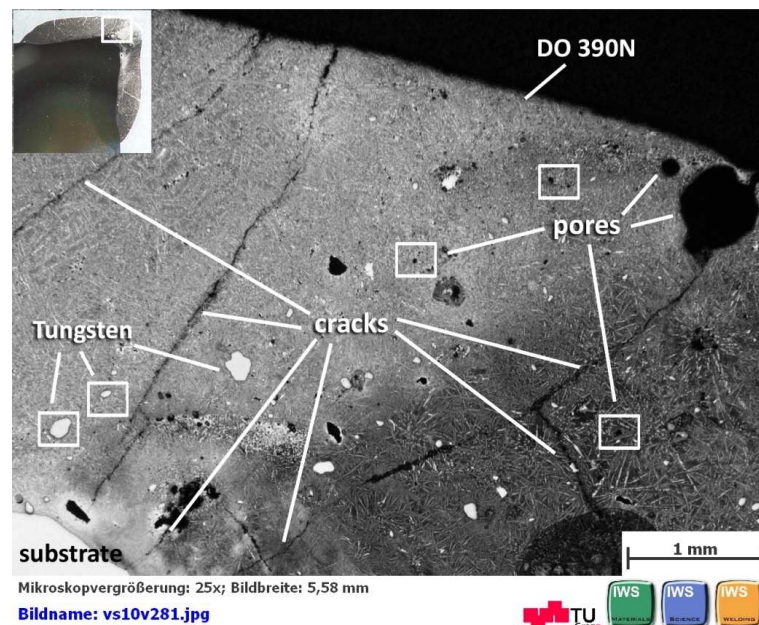


Figure 106: Specimen 17 – cracks

5.7.2.4 Binding & Chipping

The next picture, Figure 107 illustrates a good bonding to the substrate. One crack runs nearly perpendicular to the fusion line which could be critical if impact load occurs and can lead to chipping of the coating.

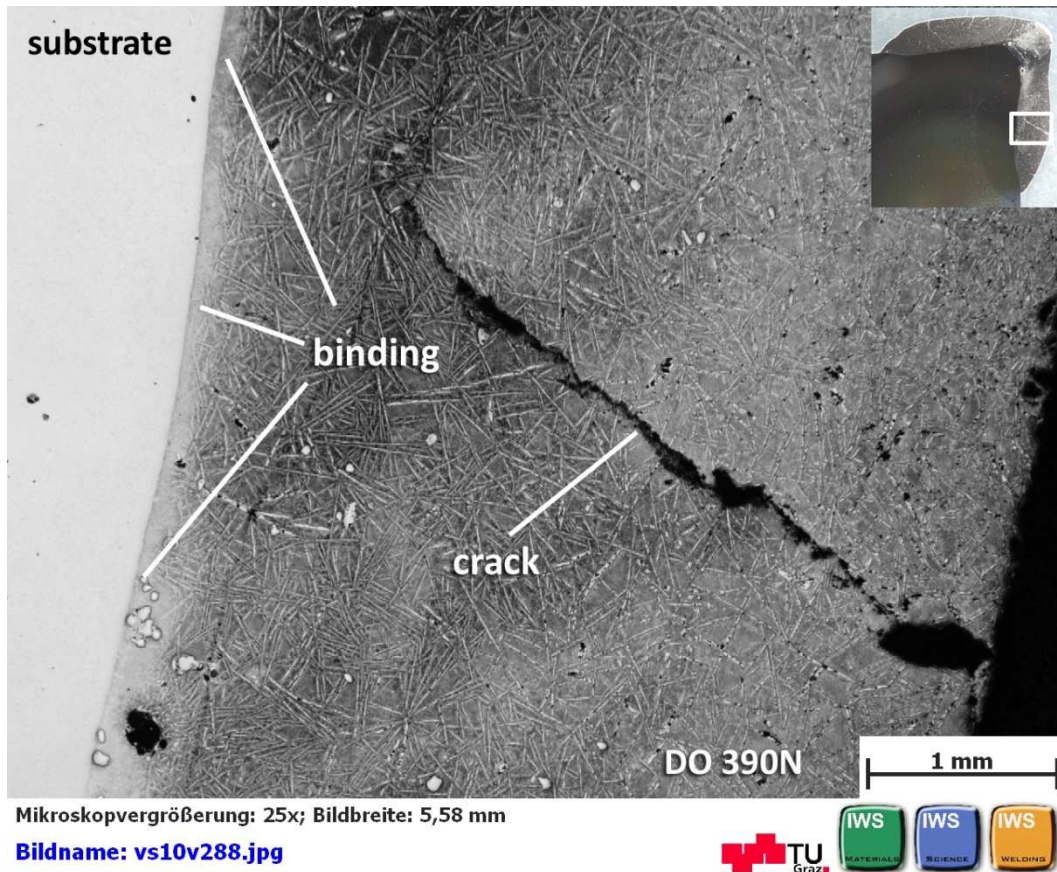
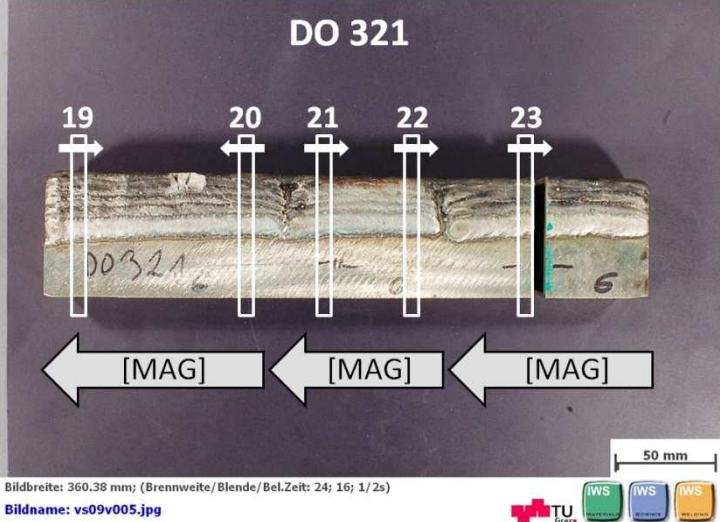


Figure 107: Specimen 17 – bond of DO 390N layer

5.8 Sample V

Sample V - overview	Welding technique	Welding consumable
	MAG	<p><u>DO 390N:</u></p> <ul style="list-style-type: none"> • Fe-based • Borocarbides <p><u>DO 321:</u></p> <ul style="list-style-type: none"> • NiBSi matrix • 60 % WC

Substrate: 1.4313							
Welding parameters							
Weld Pass	Technique	Consumable	I [A]	V _{weld} [m/min]	Arc type	Gas type	Additional
1	MAG	DO 390N	80-90	3.1-3.7	Pulsed arc	Ar 2.5 % CO ₂	<u>Stickout:</u> 20mm
2 - 6		DO 321	100-120	2-2.5			

Table 10: Welding parameters – Sample V

Figure 108 shows specimen 19 and the buildup sequence. The coating consists of DO 390N layer and DO 321 layer deposited by MAG process.

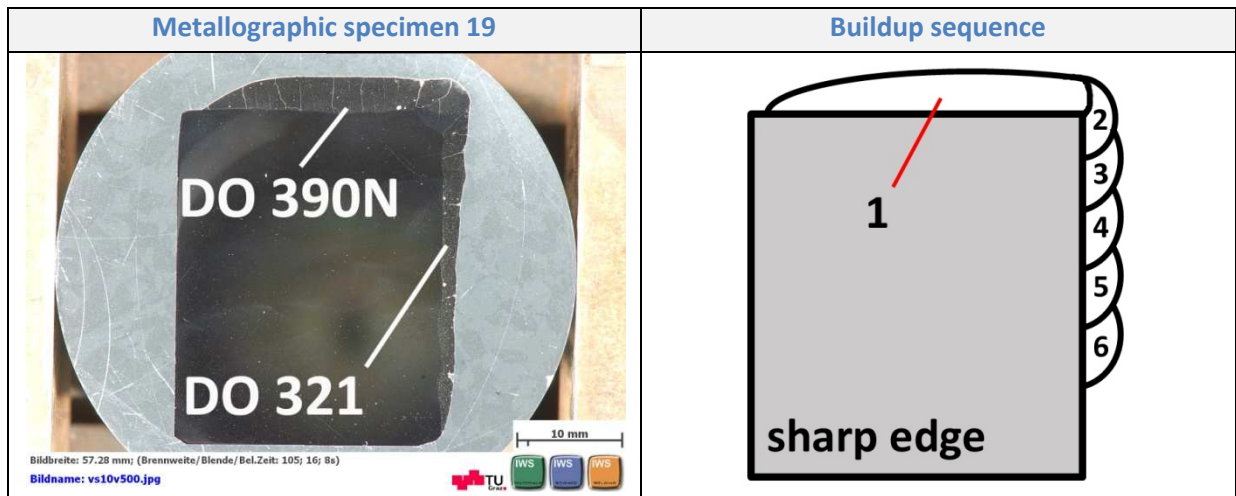


Figure 108: Specimen 19 – buildup sequence

5.8.1.1 Hardness

The hardness mapping in Figure 109 shows a relative homogenous hardness in DO 390N layer within the range of about 1050 HV1 to 1200 HV1. The hardness at the edge is about 100 HV1 lower than the rest of the DO 390N layer. This difference is due to dilution. The iron content in this area is higher than the rest of this layer. The Ni-matrix of DO 321 seems to be very homogenous with an average hardness of about 650HV 1.

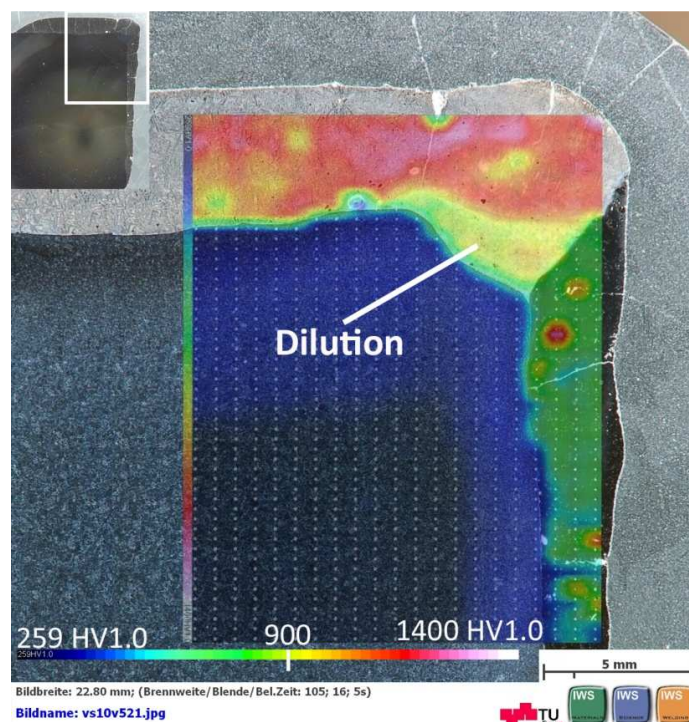


Figure 109: Specimen 19 – hardness mapping

5.8.1.2 EDX DO 390N

The EDX scan in Figure 110 shows tungsten segregations in DO 390N layer, which already have been mentioned at Sample V. Two pores can also be noticed in the coating with a diameter of about 400 μm and about 150 μm . The coating made of DO 390N shows a good binding on the substrate.

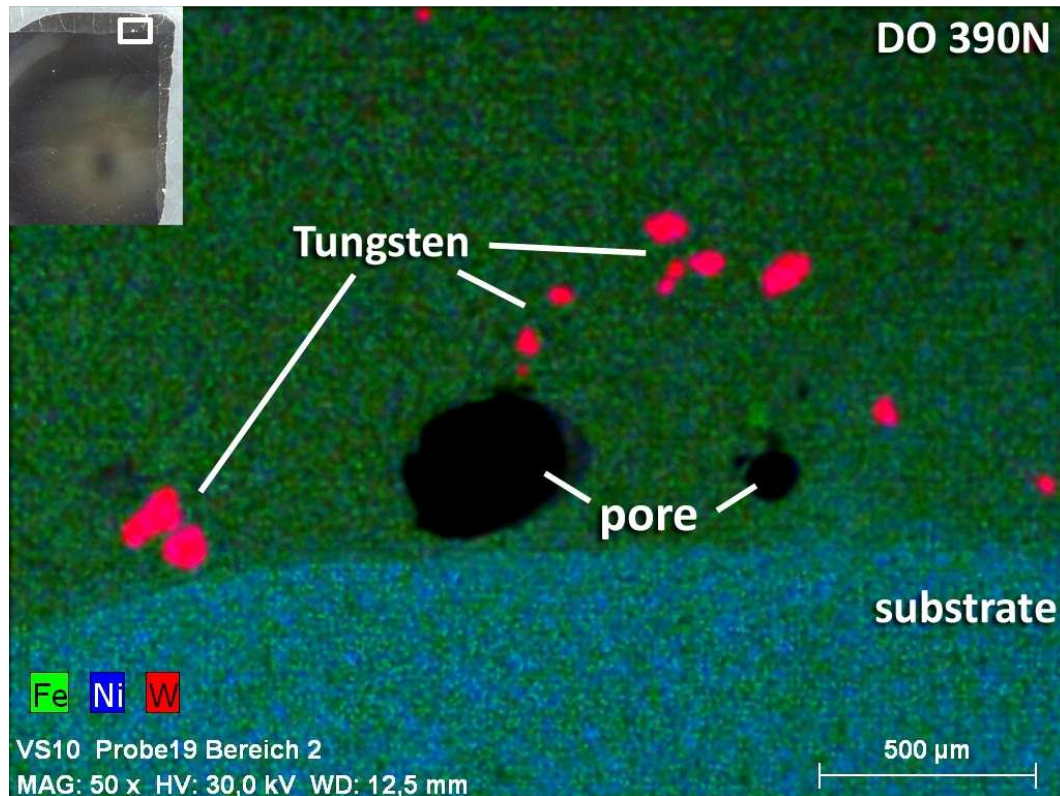


Figure 110: Specimen 19 – EDX scan DO 390N

5.8.1.3 EDX DO 321

The next picture, Figure 111 shows an EDX scan of DO 321. A pore can be noticed with a diameter of about 200 μm and a very homogenous distribution of the tungsten carbides in the layer. Also the diluted tungsten carbides, distributed in the Ni-matrix, can be seen.

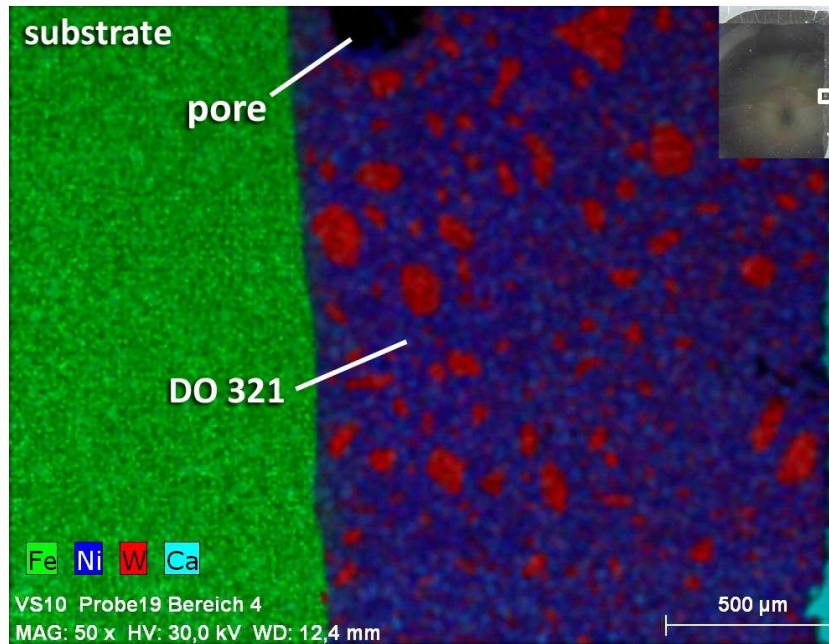


Figure 111: Specimen 19 – EDX scan DO 321

5.8.1.4 Pores

In Figure 111 a pore with a diameter of about 300 μm can be noticed. Moreover, the good binding of DO 321 layer on the substrate. The bigger tungsten carbides are not molten and their distribution is not very homogenous. The smaller carbides are molten and are dispersed in the Ni-matrix.

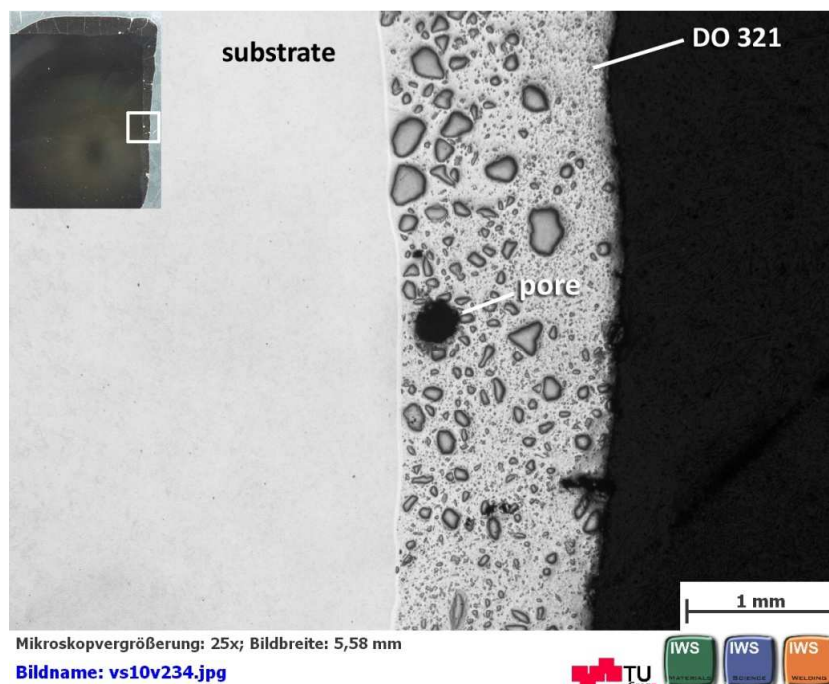


Figure 112: Specimen 19 – pore

5.8.1.5 Cracks

In Figure 113 one crack can be seen. Again, a good binding and a very inhomogeneous carbide distribution and a relative low amount of carbides can be noticed.

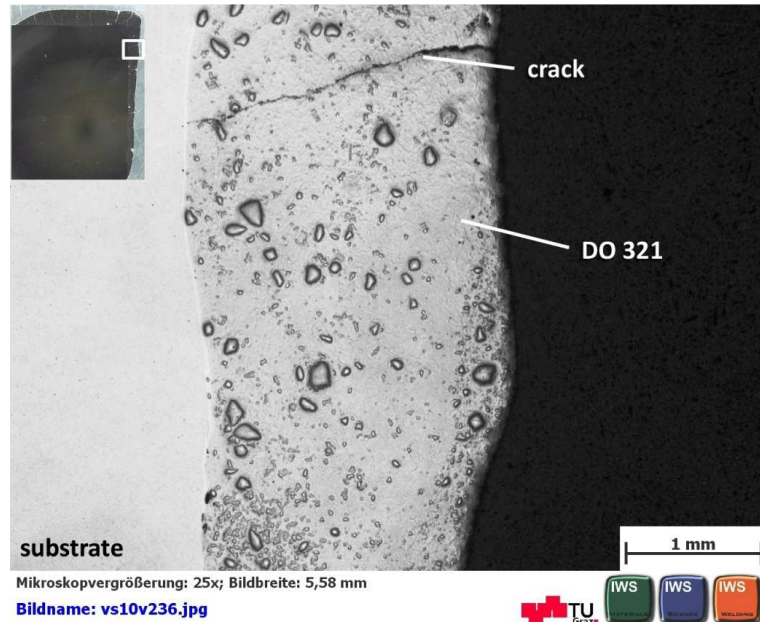


Figure 113: Specimen 19 – crack

5.8.1.6 Binding & Dilution

In Figure 114 a good binding and a very low dilution for the transition zone of DO 390N layer and DO 321 layer can be seen and has been confirmed by EDX analysis.

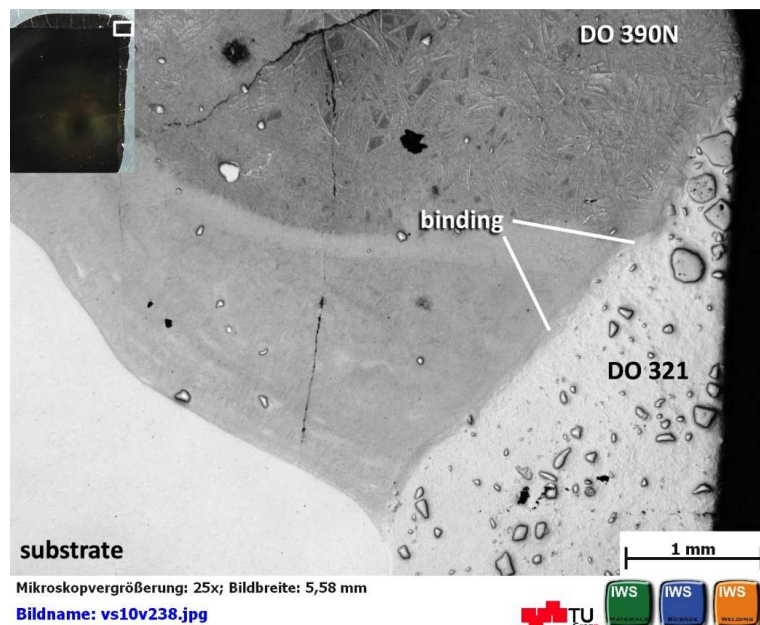


Figure 114: Specimen 19 – binding and dilution of DO 321

5.9 Sample VI

Sample VI - overview	Welding technique	Welding consumable
<p>AbraTec 6088 DO 390 N DO 321</p> <p>6 7 8 24 9 10 11</p> <p>1302 A - [PTA]</p> <p>[SMAW] [MAG] [MAG]</p> <p>50 mm</p> <p>Bildbreite: 360.38 mm; (Brennweite/Blende/Bel.Zeit: 24; 16; 1/2s)</p> <p>Bildname: vs09v006.jpg</p>	PTA	<u>1302 A:</u> <ul style="list-style-type: none"> • Fe-based • Borocarbides
	SMAW	<u>AbraTec 6088:</u> <ul style="list-style-type: none"> • NiBSi matrix • 55 % WC
	MAG	<u>DO 390N:</u> <ul style="list-style-type: none"> • Fe-based • Borocarbides <u>DO 321:</u> <ul style="list-style-type: none"> • NiBSi matrix • 60 % WC

Substrate: 1.4313								
Welding parameters								
Weld Pass	Technique	Consumable	I [A]	V _{weld} [mm/min]	V _{osc} [mm/min]	Osc. width [mm]	Feed rate [g/min.]	Gas flow [l/min.]
1	PTA	1302 A	85	200	1200	2	15	1.3 Ar
2			75	200	-	-	15	
3			125	85	1200	15	20	
4								
5-7	MAG	AbraTec 6088	Unknown parameters					
		DO 390N						
		DO 321						

Table 11: Welding parameters – Sample VI

5.9.1 'Hammer fall test'

Very often, several types of wear occur at the same time like in the case of plug screws. Abrasion dominates but due to production irregularities and polluted wood chips, the coating must also sustain impacts.

For the simulation of impact load some welding samples have been tested by a simple 'hammer fall test'. The deposition area was tested by several strokes of a hammer, till some coating pieces spall off. It is due to their brittleness that no coating layer can withstand the hard impacts of the hammer due to their brittleness. Unfortunately, no documentation or recording of this test is available.¹

Figure 115 shows Sample VI where three different welding consumables were deposited on PTA layer 1302 A for a refurbishment simulation. On the left side, the welding consumable AbraTec 6088 was applied by shielded metal-arc welding. In the middle of sample VI the flux-cored wire DO 390, which has the same composition like 1302 A was deposited. On the right, the tungsten carbide containing flux-cored wire DO 321 was applied.



Figure 115: Sample VI – 'hammer fall test'

¹ Hammer fall test was accomplished by Mr. Ernst HAUCK (ANDRITZ Vienna)

5.9.2 Sample VI - AbraTec 6088

Figure 116 illustrates the buildup sequence of specimen 6 with the layer 1302 A deposited by PTA and the refurbishment simulation with AbraTec 6088 deposited by SMAW.

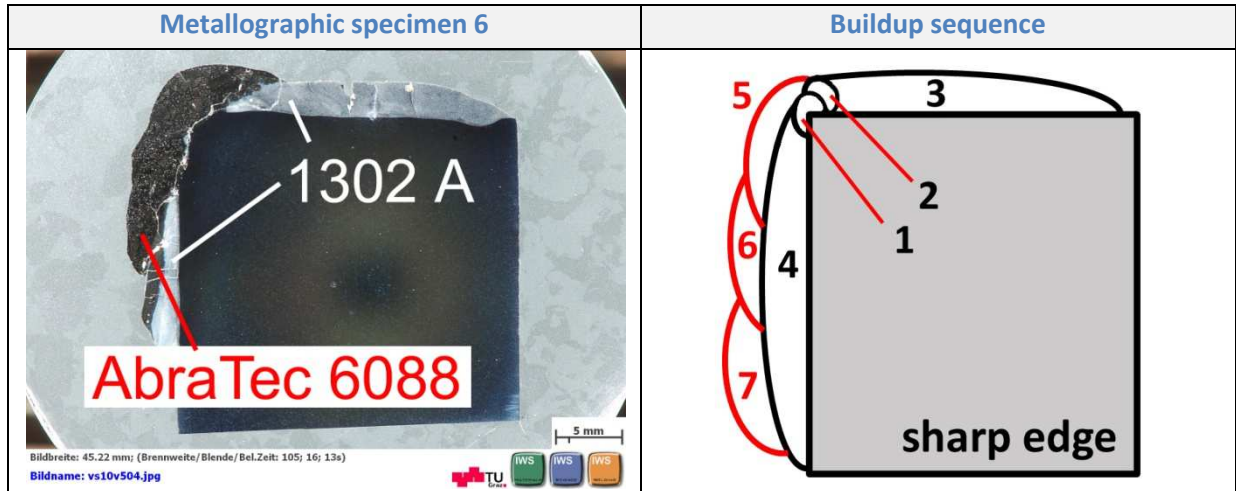


Figure 116: Specimen 6 – buildup sequence

5.9.2.1 Hardness

On the 1302 A – layer a refurbishment simulation was done with the welding consumable AbraTec 6088 applied by SMAW. The matrix of AbraTec 6088 has an average hardness ranging from ~ 500 HV1 to 700 HV1. Some tungsten carbides are hit or semi-hit during measurement and displayed by the red and white spots representing high local hardness inside this layer.

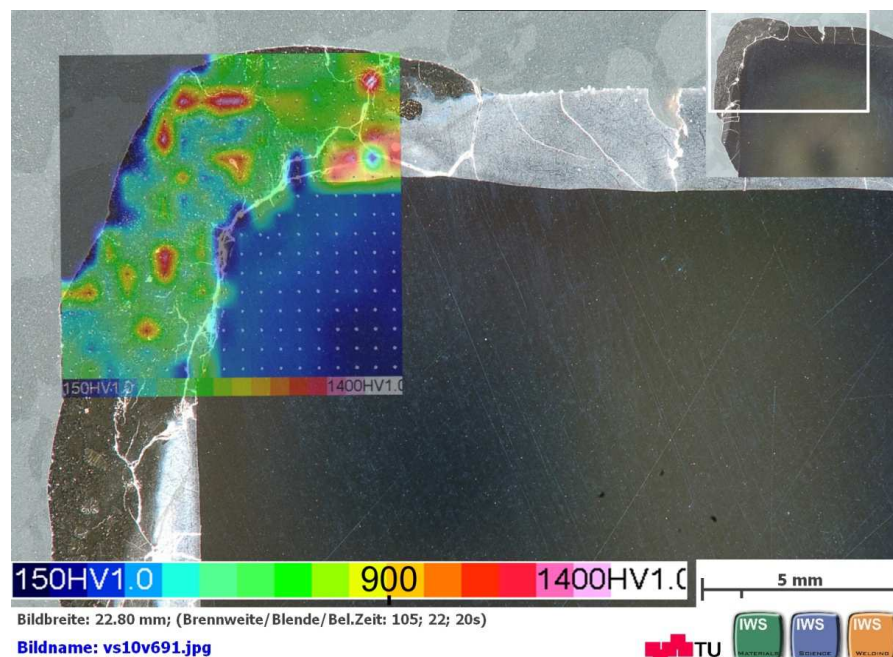


Figure 117: Specimen 6 – hardness mapping

5.9.2.2 Pores

Figure 118 shows one pore with a diameter of about 150 μm . In general, pores are very seldom in AbraTec 6088 layer.

Crack propagation parallel to the fusion line is also illustrated and which is critical for chipping.

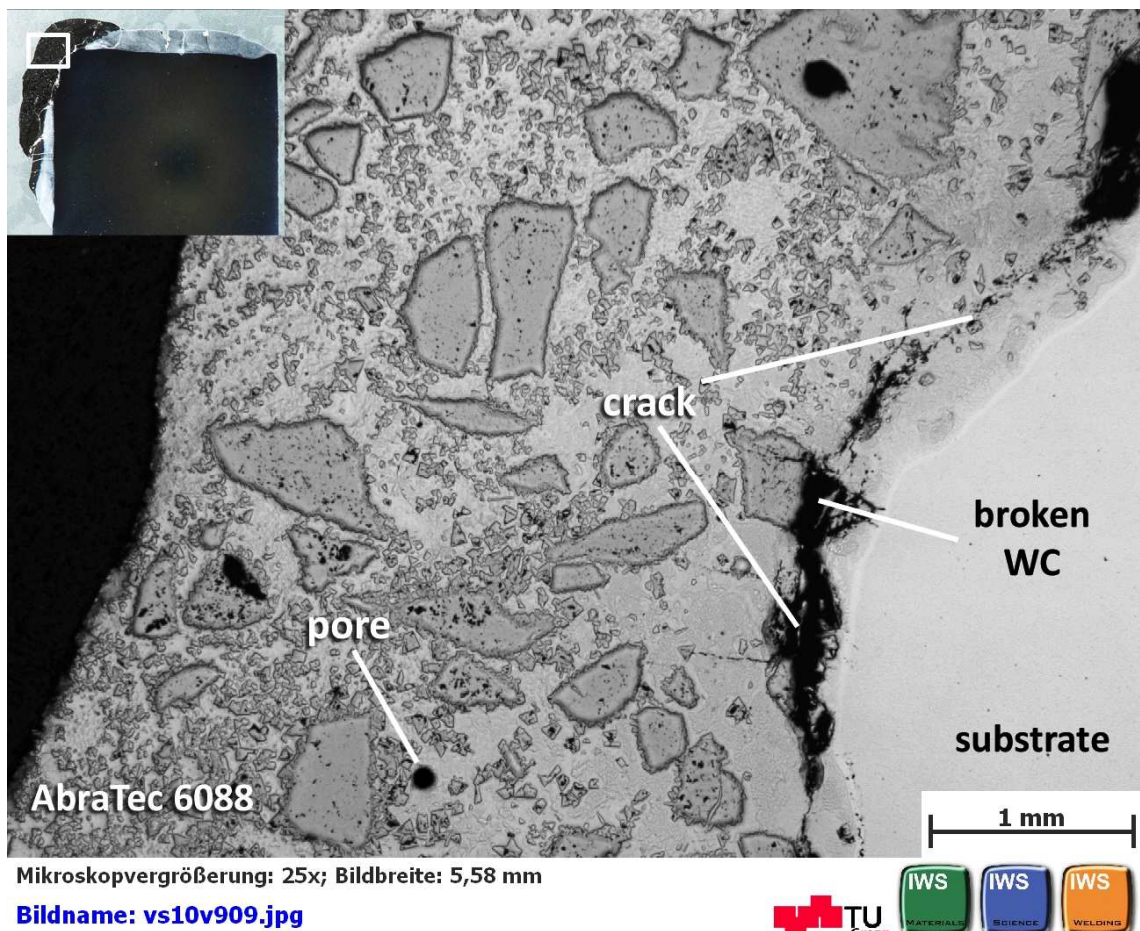


Figure 118: Specimen 6 – pore in AbraTec 6088

5.9.2.3 Cracks

In the next picture, Figure 119, a crack parallel to the fusion line and broken tungsten carbides can be noticed which increase the susceptibility to chipping. Moreover, a lot of molten tungsten carbides are also illustrated which embrittles additionally the Ni-matrix and reduces the wear resistance. Due to the fact that no PTA layer 1302 A can be seen anymore, a high dilution is assumed. Dilution is also indicated by a lot molten the tungsten carbides.

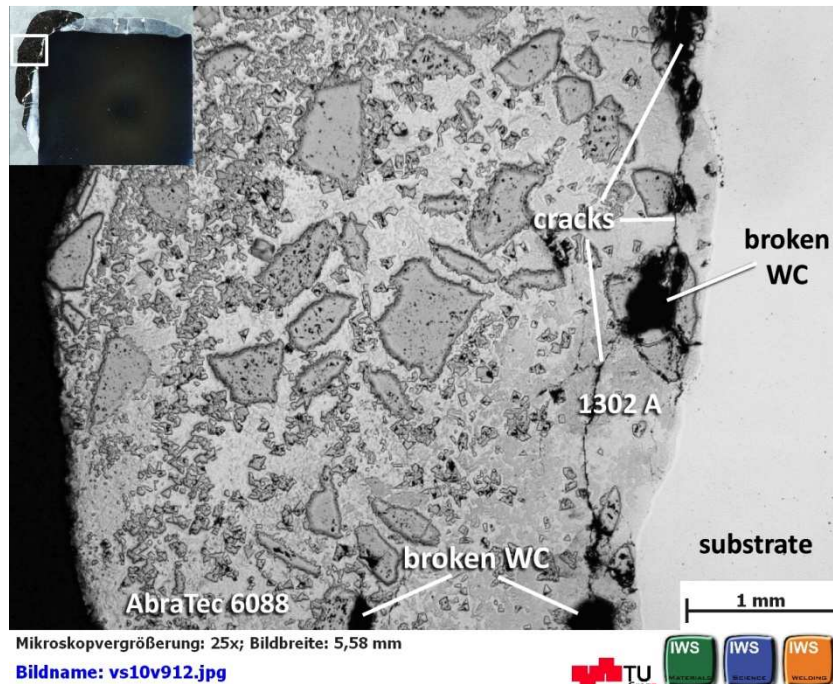


Figure 119: Specimen 6 – no pores in AbraTec 6088

The following Figure 120 shows cracks which run parallel to the fusion zone of AbraTec 6088 and the subjacent layer 1302 A. These cracks enhance the risk of chipping. In opposite to the area of the former picture, Figure 119, remaining parts of the coating layer 1302 A can be seen.

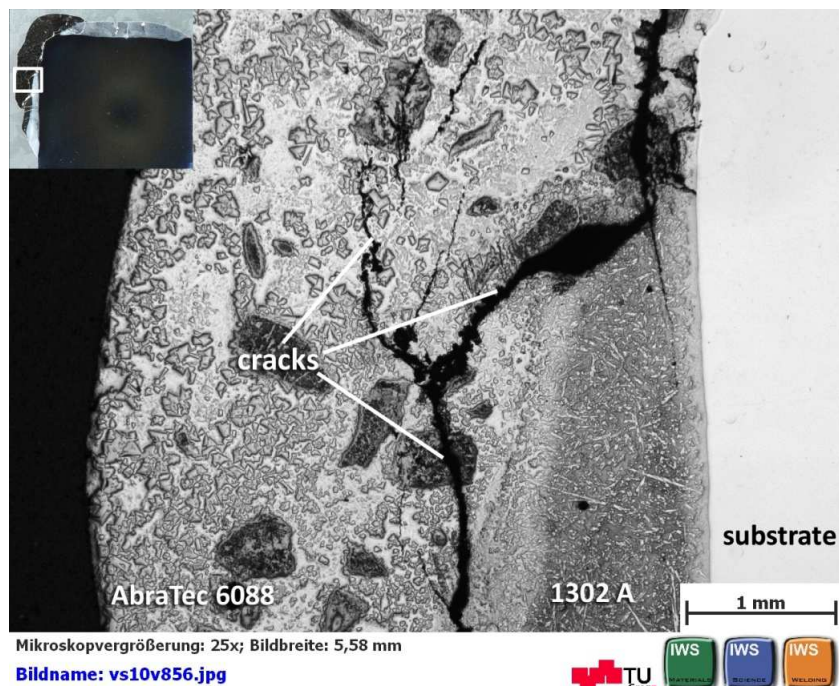


Figure 120: Specimen 6 – cracks inside of AbraTec 6088 layer

5.9.2.4 Binding, Dilution & Chipping

In Figure 121 AbraTec 6088 shows a good binding on PTA layer 1302 A. Nevertheless, the parallel crack along the fusion line of 1302 A and substrate as well as the huge amount of cracks in the PTA layer makes this area of the coating extremely susceptible for chipping.

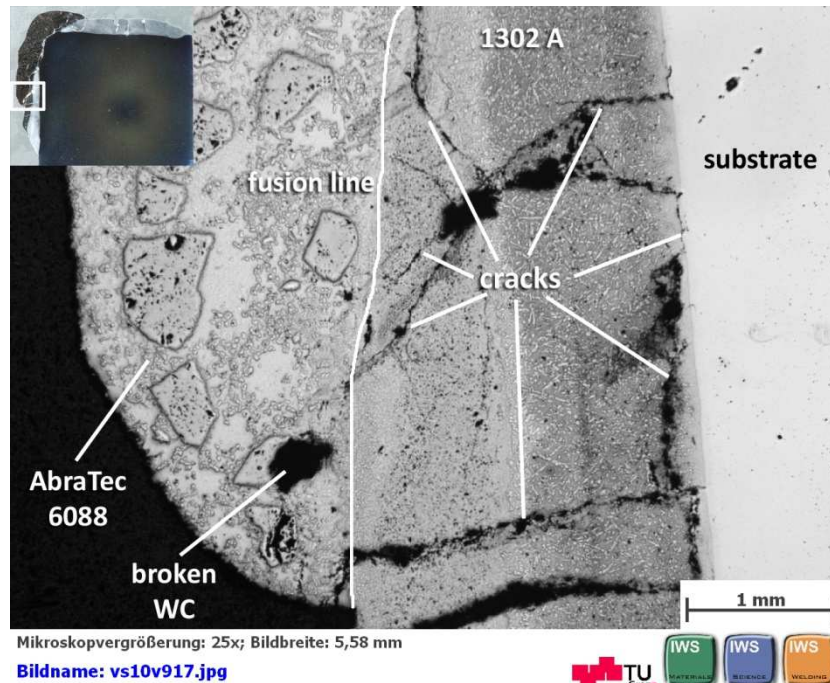


Figure 121: Specimen 6 – binding

5.9.3 Sample VI – DO 390N

Figure 122 illustrates the buildup sequence of specimen 9 with the coating 1302 A deposited by PTA and the refurbishment simulation with DO 390N deposited by MAG process.

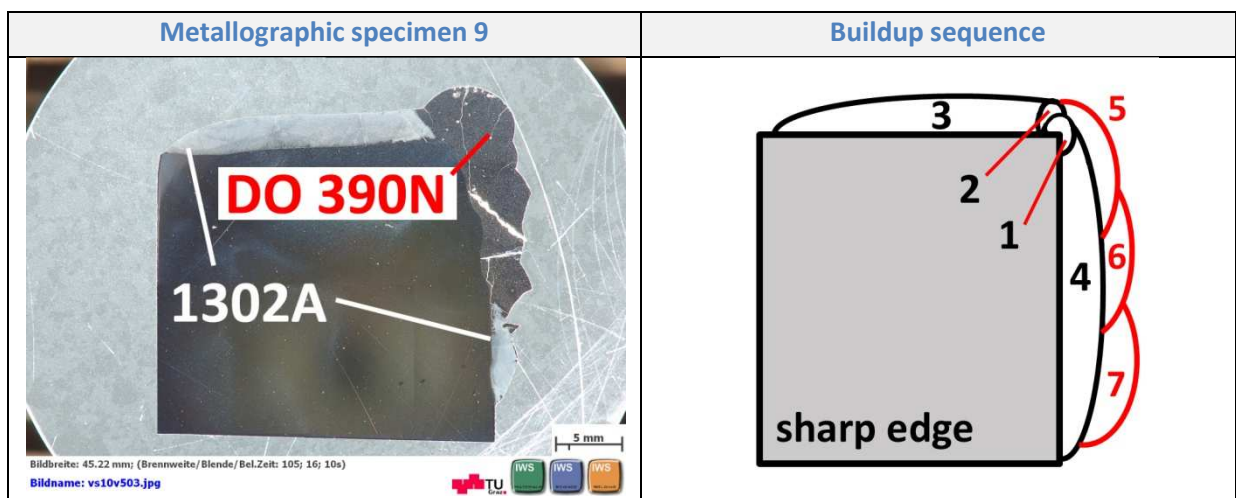


Figure 122: Specimen 9 – buildup sequence

5.9.3.1 Hardness

PTA layer 1302 A shows a homogenous distribution of hardness. The values vary between 900 HV1 and 1050 HV1. At the transition zone of PTA layer 1302 A and MAG layer DO 390N, the hardness of 1302 A decreases and is about 100 HV 1 below the range of DO 390N.

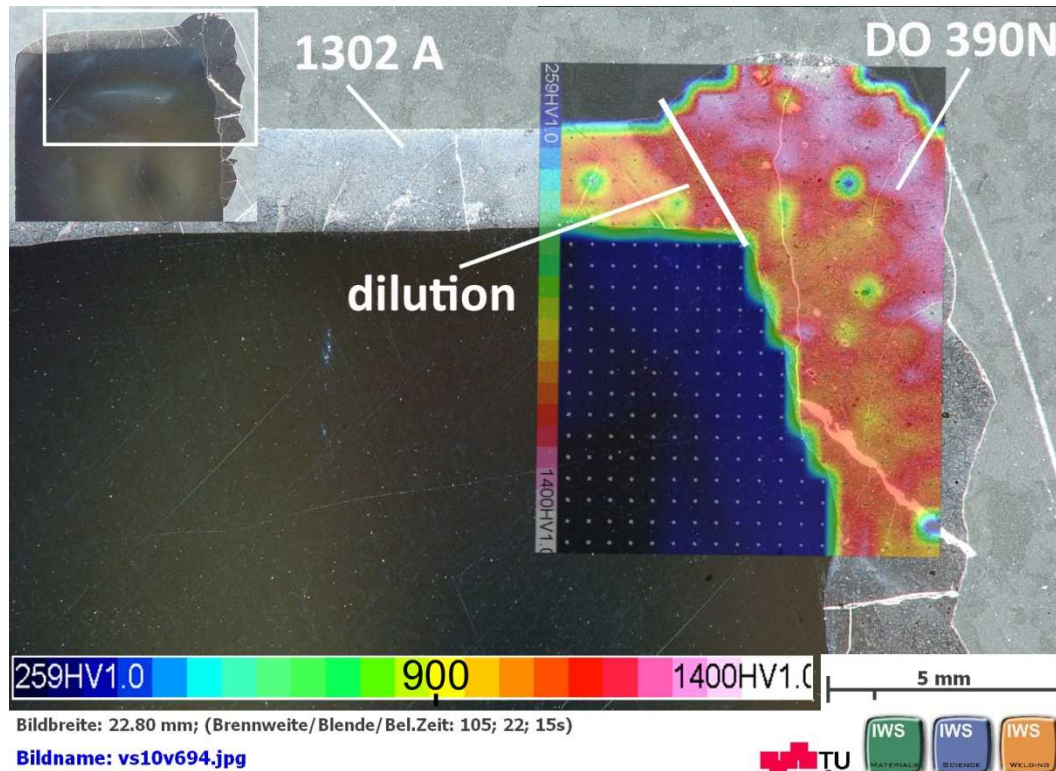
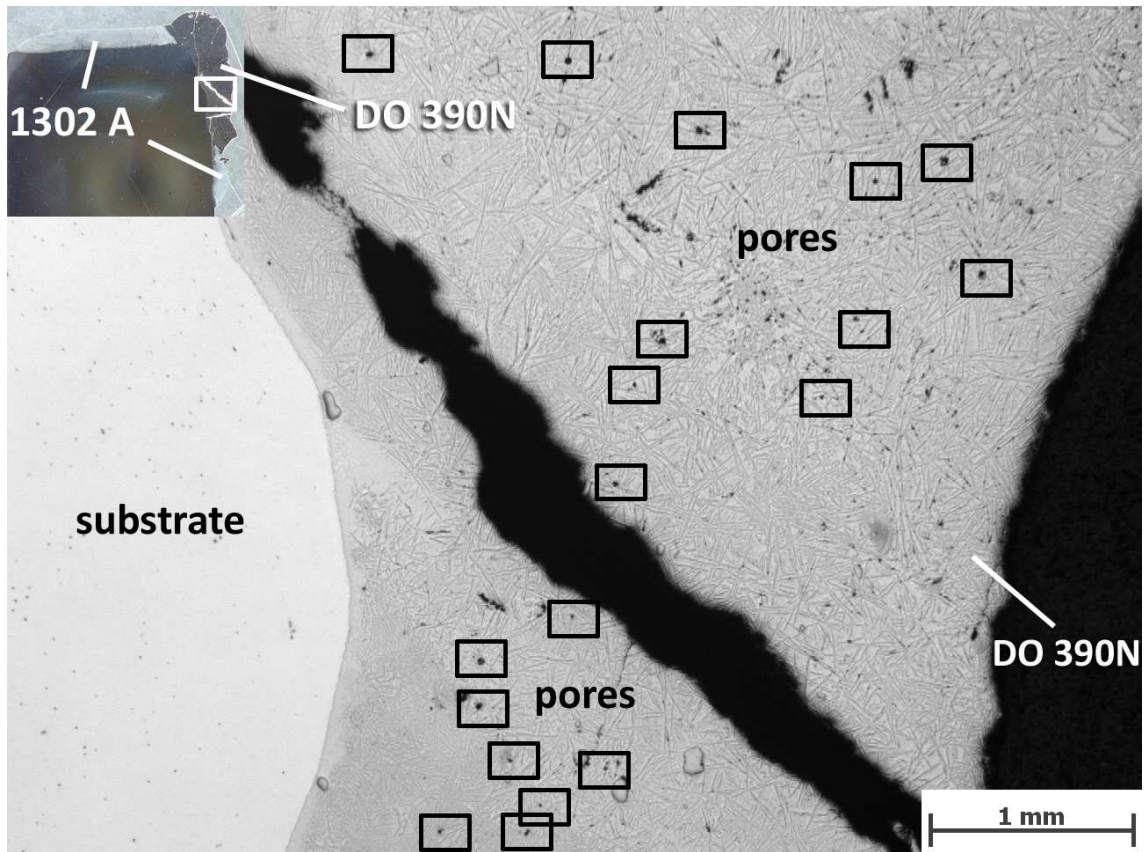


Figure 123: Specimen 9 – hardness mapping

The distribution of hardness in DO 390N layer is also very homogenous but the hardness values are higher within a range of about 1000 HV1 to 1200 HV1. Nearly the whole PTA layer 1302 A is diluted and this effect may lead to the higher hardness in this area. Compared to the hardness of Sample IV (DO 390N applied by trailing/leading torch), also not such a high hardness can be found.

5.9.3.2 Pores

The pores in Figure 124 are very small and can be assigned to uniformly distributed porosity. Inside the DO 390N layer a huge crack can be noticed and pieces of the layer might have been broken out. The subjacent PTA layer 1302 A cannot be seen anymore which indicates a very high or complete dilution of this layer in this area. The layer seems to have a good binding to the substrate like already noticed at Sample IV.



Mikroskopvergrößerung: 25x; Bildbreite: 5,58 mm

Bildname: vs10v879.jpg



Figure 124: Specimen 9 – pores

5.9.3.3 Cracks

In Figure 125 very critical cracks propagate parallel to the fusion line between the substrate and a combination of the molten PTA layer 1302 and DO 390N. The cracks enhance considerably the possibility for chipping. Again the pores are very small and can be assigned to uniformly distributed porosity. In the left bottom corner of Figure 125 a remaining part of the PTA layer 1302 A can be noticed and indicates there a lower dilution.

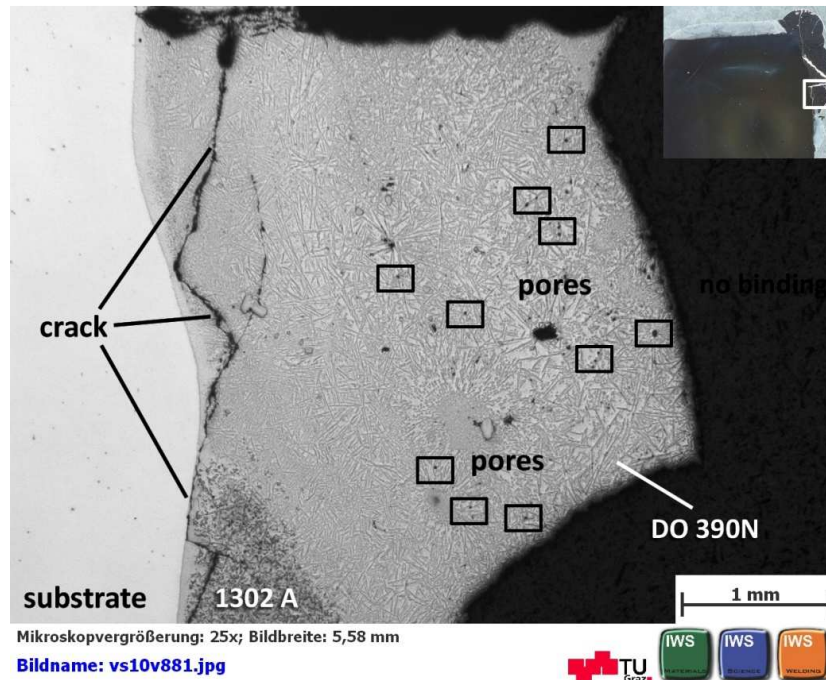


Figure 125: Specimen 9 – cracks

5.9.3.4 Binding & Chipping

The following Figure 126 makes a clear distinction between PTA layer 1302 A and DO 390N possible. The fusion line in this detail shows just three very small imperfections. Chipping occurred during cutting the specimen out of Sample VI and can be seen in Figure 126 but better in Figure 125.

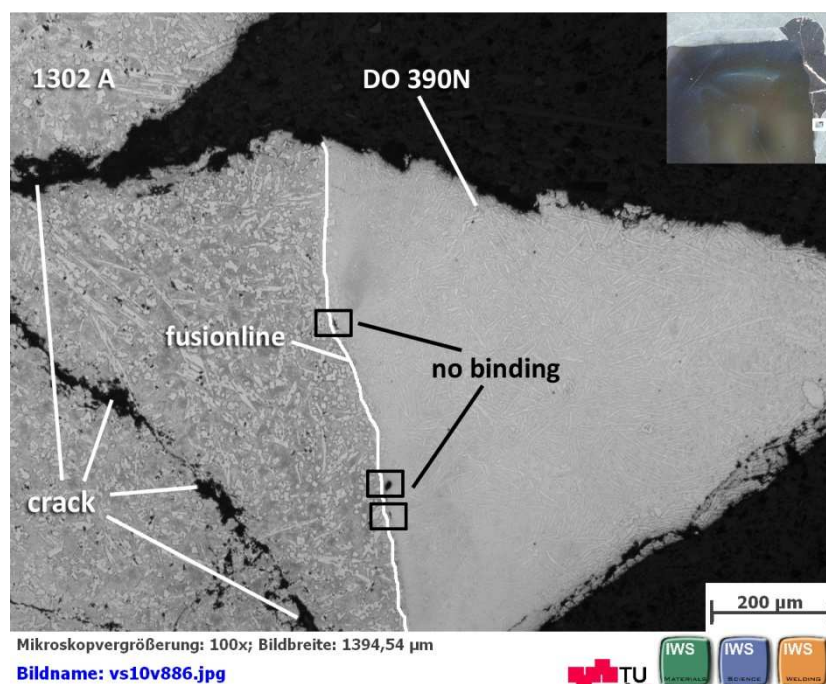


Figure 126: Specimen 9 – binding of DO 390N on PTA layer 1302 A

5.9.4 Sample VI – DO 321

Figure 127 illustrates the buildup sequence of specimen 10 with the layer 1302 A deposited by PTA and the refurbishment simulation with DO 321 applied by MAG.

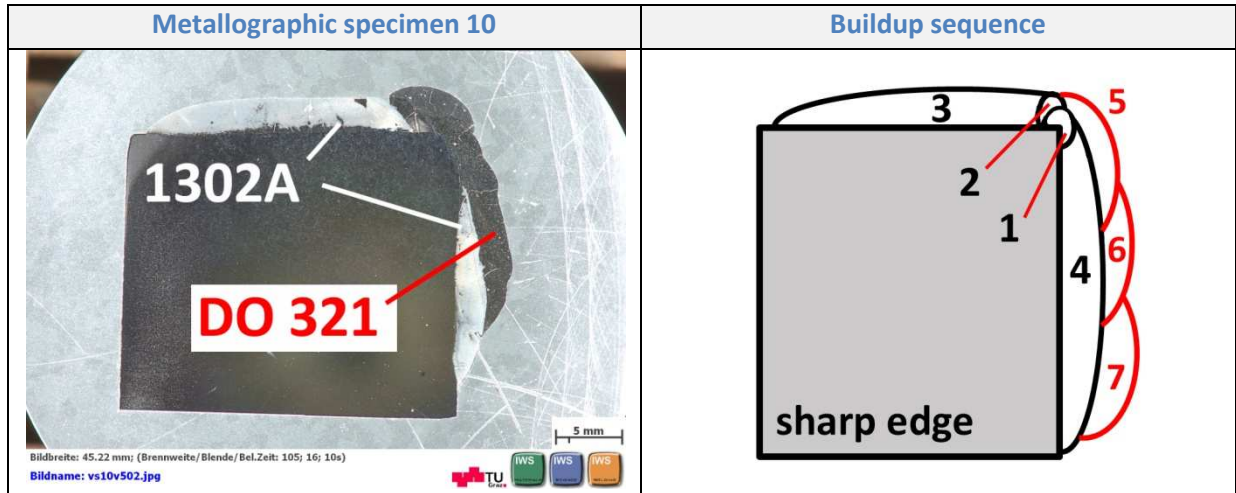


Figure 127: Specimen 10 – buildup sequence

5.9.4.1 Hardness

On the 1302 A – layer a refurbishment simulation was done with DO 321 applied by MAG process. The Ni-matrix of DO 321 has an average hardness ranging from ~ 500 HV1 to 650 HV1.

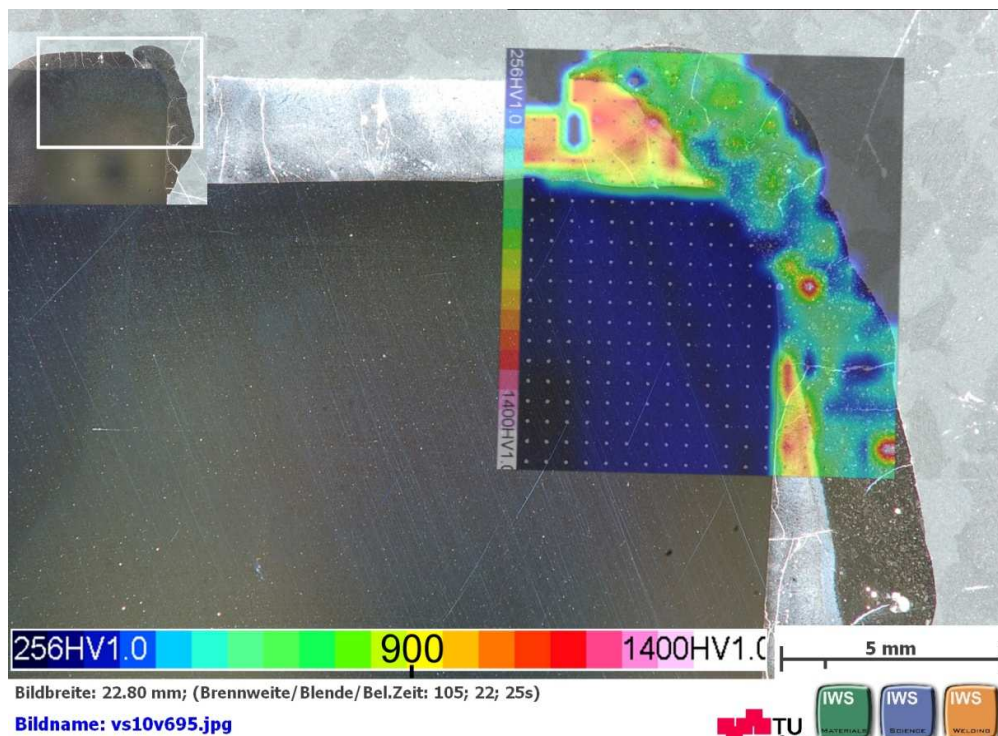


Figure 128: Specimen 10 – hardness mapping

5.9.4.2 Pores

In Figure 129, three significant pores can be noticed. One in the MAG layer DO 321 with a diameter of about 200 μm and two other ones in the subjacent PTA layer 1302 A with a size of about 100 μm and 150 μm .

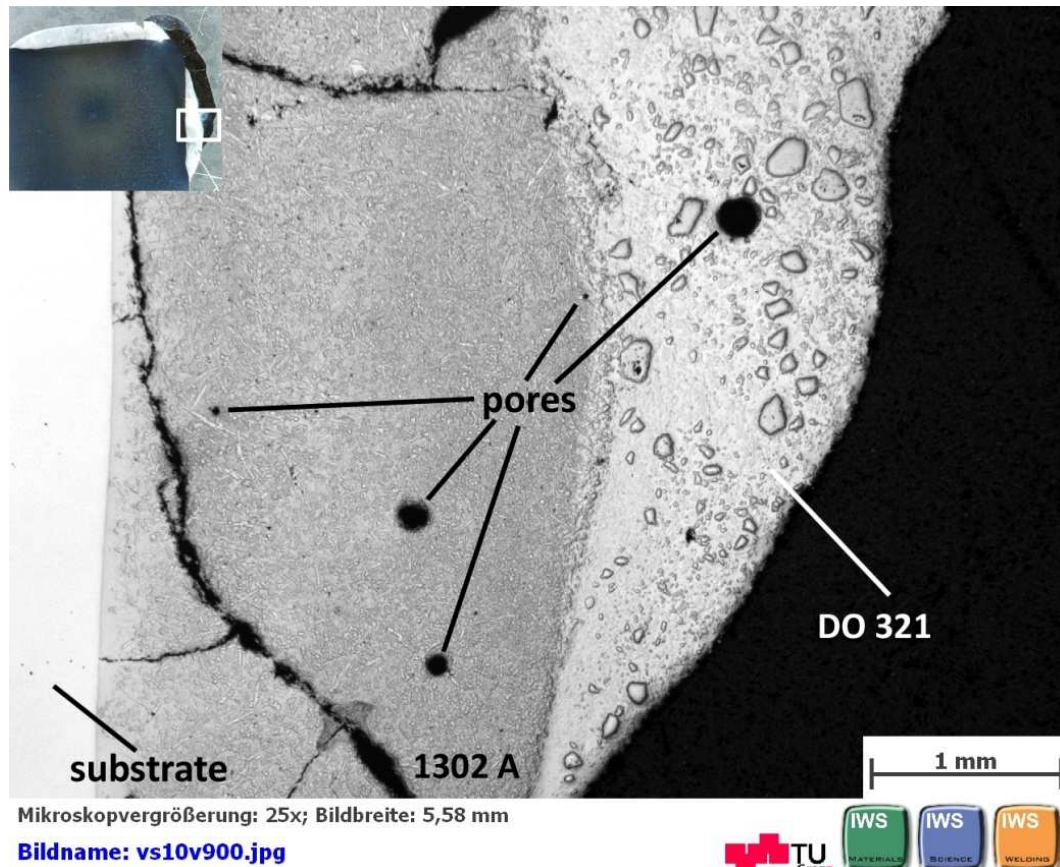


Figure 129: Specimen 10 – pores

5.9.4.3 Cracks

In Figure 129 no cracks can be seen in the coating of DO 321 and the binding of DO 321 on the PTA layer 1302 A looks good as well. In contrast, cracks are running through the coating 1302 A. In this area, some cracks propagate parallel to the fusion line and chipping might occur.

In Figure 130 three cracks can be seen in DO 321 layer. In the subjacent PTA layer 1302 A again cracks propagate parallel to the fusion line what enhance the risk of chipping. The tungsten carbides in DO 321 layer are partly molten and the remaining carbides which can be seen are relative rare. After all the amount of tungsten carbides in DO 321 is 60%. The molten carbides embrittles additionally the Ni-matrix and reduces the wear resistance.

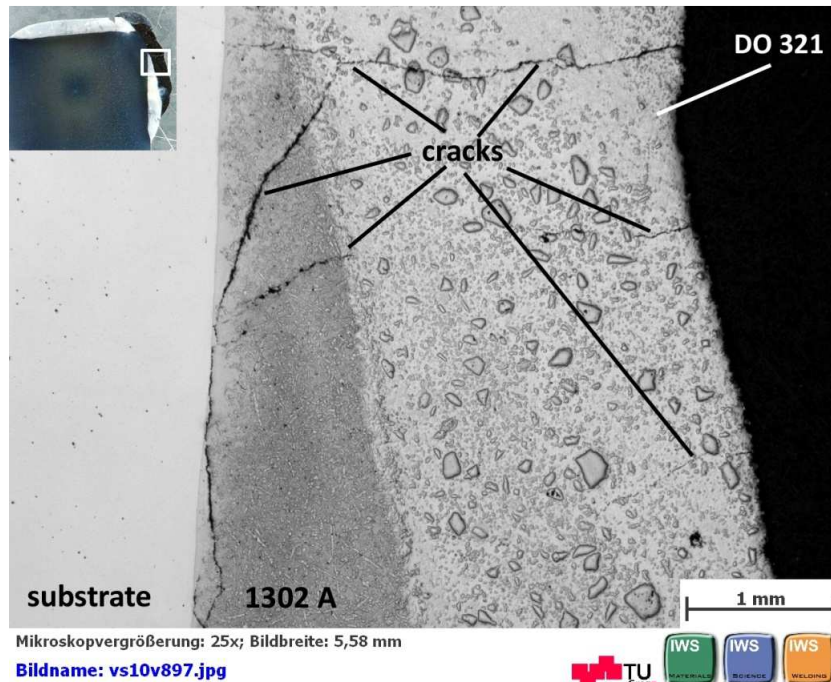


Figure 130: Specimen 10 – cracks in DO 321 layer

5.9.4.4 Binding & Dilution

Due to the high dilution of the PTA layer 1302 A and DO 321, what can be seen in Figure 131, the amount of noticeable carbides seems to be relatively low compared to the other areas of DO 321. The binding of DO 321 on the substrate and the subjacent layer 1302 A looks good.

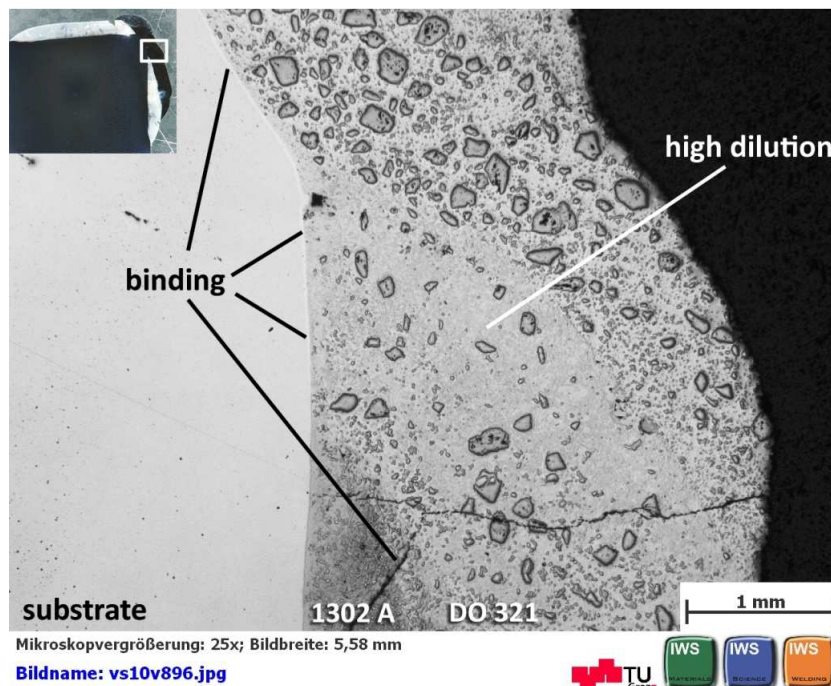
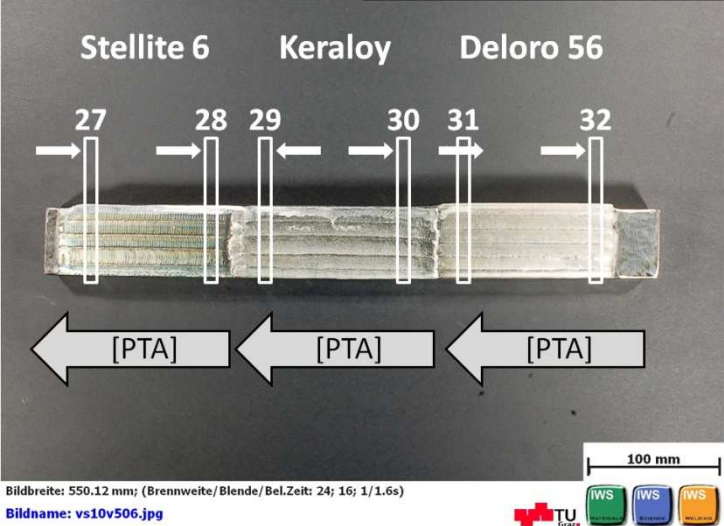


Figure 131: Specimen 10 – binding in DO 321 layer

5.10 Sample VII

Sample VII - overview	Welding technique	Welding consumable
	PTA	<u>Stellite 6:</u> <ul style="list-style-type: none"> • Co-based
		<u>Keraloy:</u> <ul style="list-style-type: none"> • NiBSi matrix • 60 % WC
		<u>Deloro 56:</u> <ul style="list-style-type: none"> • Ni-based

Substrate: 1.4313								
Welding parameters								
Weld Pass	Technique	Consumable	I [A]	V _{weld} [mm/min]	V _{osc} [mm/min]	Osc. width [mm]	Feed rate [g/min.]	Gas flow [l/min.]
1 – 2	PTA	Stellite 6 or / and Deloro 56	70	100	1500	2	9	2.5 Ar
3 – 5			75	45	1200	11	14	12.1 (Ar5%He)
6 – 8		Stellite 6 Keraloy Deloro 56						

Table 12: Welding parameters – Sample VII

5.10.1 Penetration Testing

Sample VII has later been welded than the other samples and before specimen preparation a dye penetration test was done. According to standard *DIN EN ISO 3452-1*, Penetration testing is a non-destructive material testing in which the capillary action of fine surface cracks and pores can be used to make these imperfections visible. A distinction is made between the dye penetration test and the fluorescent penetrant.

Figure 132 shows sample VII with three different coating types after PT.

- **Stellite 6** does not show any purple color except at the end craters. Stellite 6 coating is free of cracks at the surface.
- **Keraloy** layer shows the most surface cracks.
- Also **Deloro 56** coating has cracks but much less than Keraloy.



Figure 132: Sample VII - Penetration testing

5.10.2 Sample VII – Stellite 6

Figure 133 shows specimen 27 and its buildup sequence. The deposited welding consumable is Stellite 6 by PTA.

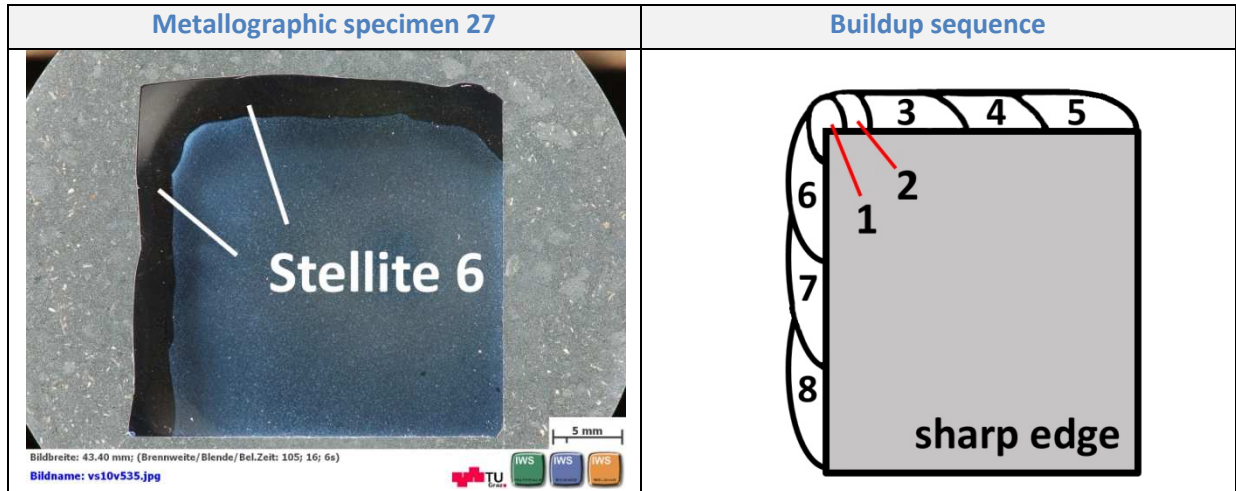


Figure 133: Specimen 27 – buildup sequence

5.10.2.1 Hardness

Figure 134 illustrates the hardness mapping of specimen 27. Stellite 6 is relatively soft compared to the other coatings and shows a homogenous distribution of hardness. The values are slightly varying between about 380 HV1 and about 460 HV1.

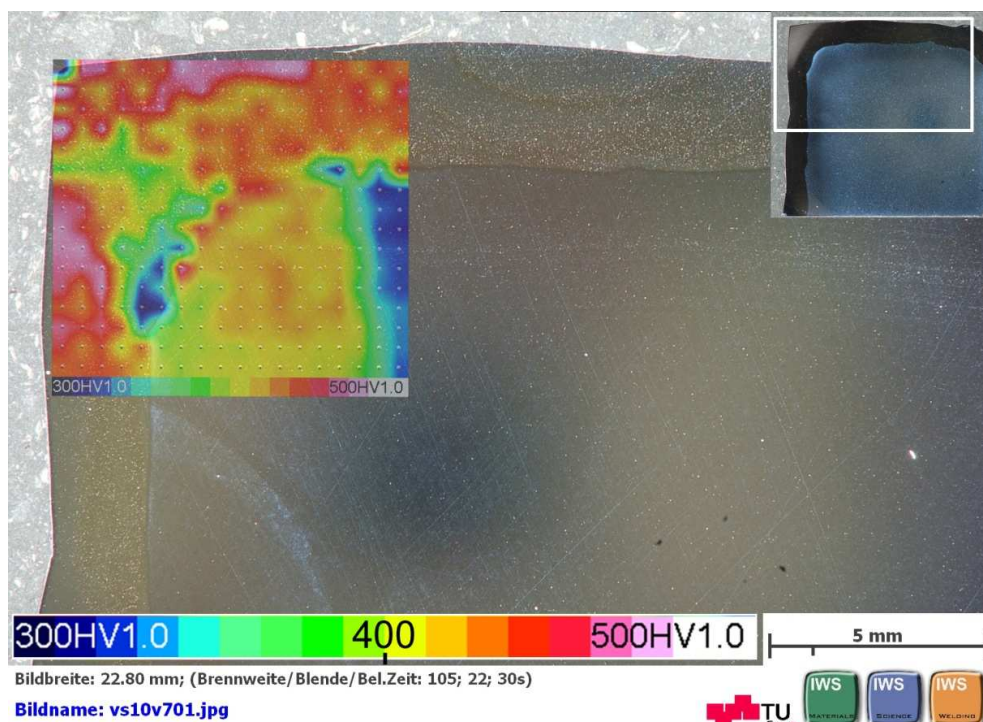


Figure 134: Specimen 27 – hardness mapping

5.10.2.2 Pores

The coatings of Stellite 6 are 'free' of porosity. Figure 135 shows the the only pore which was found with a diameter of about 100 μm .

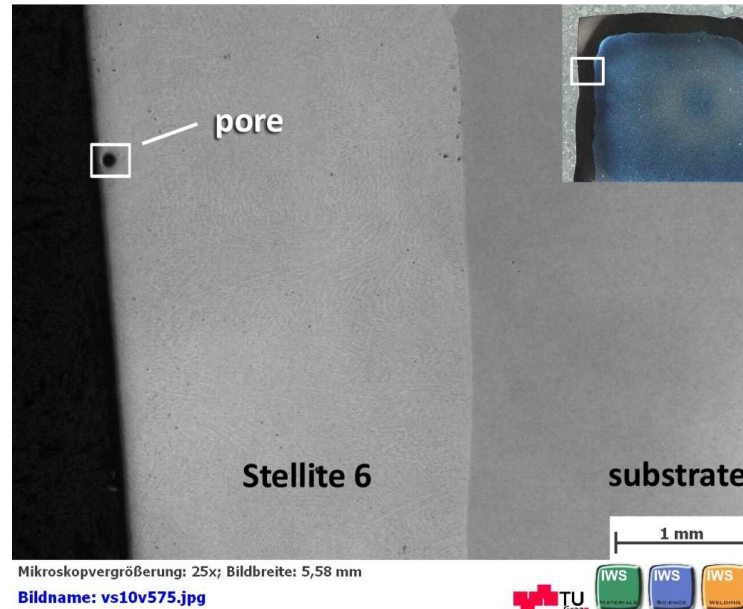


Figure 135: Specimen 27 – pore

5.10.2.3 Cracks

The same applies to LOF. The only crack-like imperfection was a bond imperfection and is shown in Figure 136. The reason that no cracks appear is the lower hardness compared to the other protective layers.

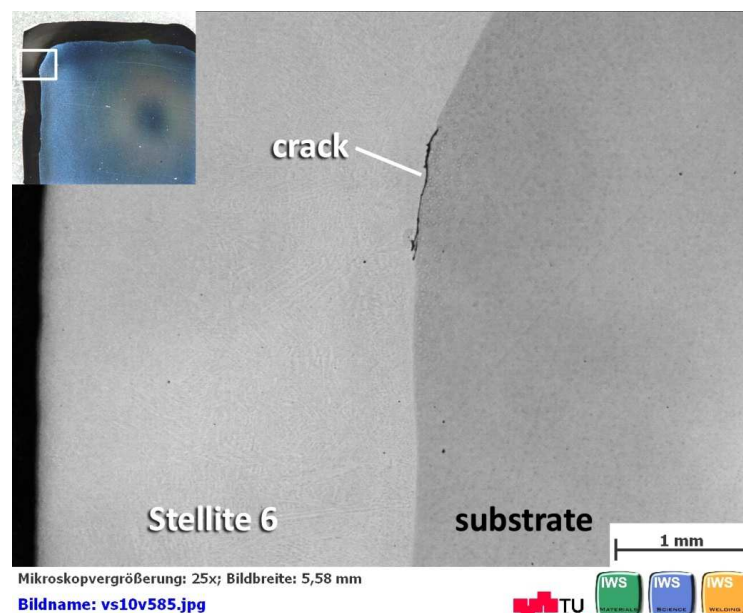


Figure 136: Specimen 28 – crack

5.10.2.4 Binding & Dilution

The next picture, Figure 137 shows a perfect binding on the substrate.

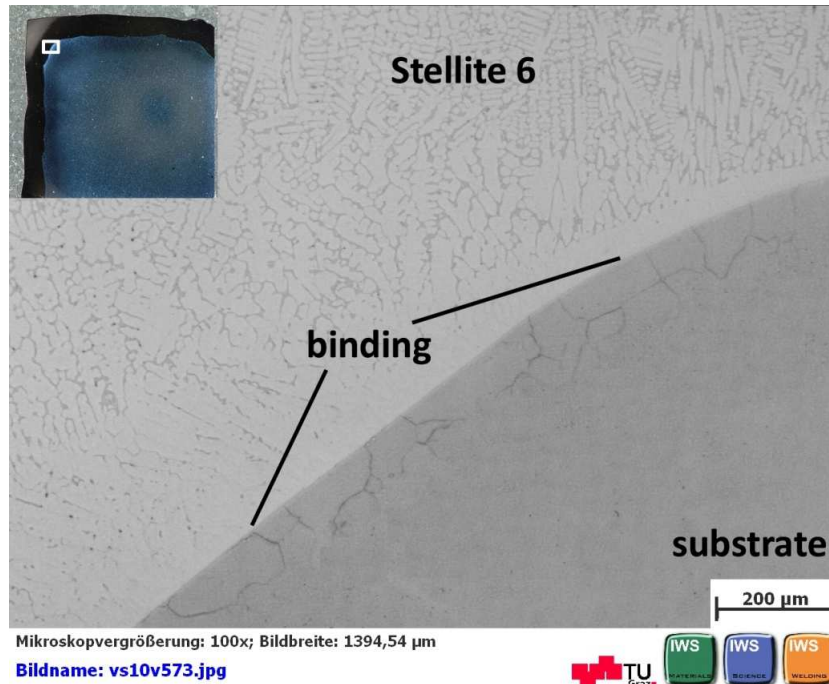


Figure 137: Specimen 27 – binding of Stellite 6

The dilution is quite high due to the deep weld penetration shown in Figure 138.

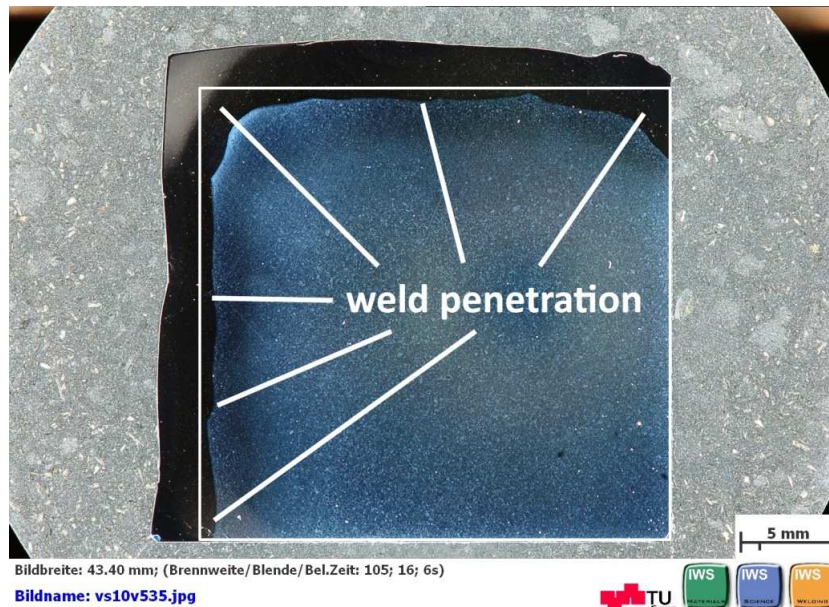


Figure 138: Specimen 27 – weld penetration

5.10.3 Sample VII – Keraloy

In Figure 139 specimen 29 and the buildup sequence is illustrated. The deposited welding consumables are Stellite 6 and Keraloy by PTA technique.

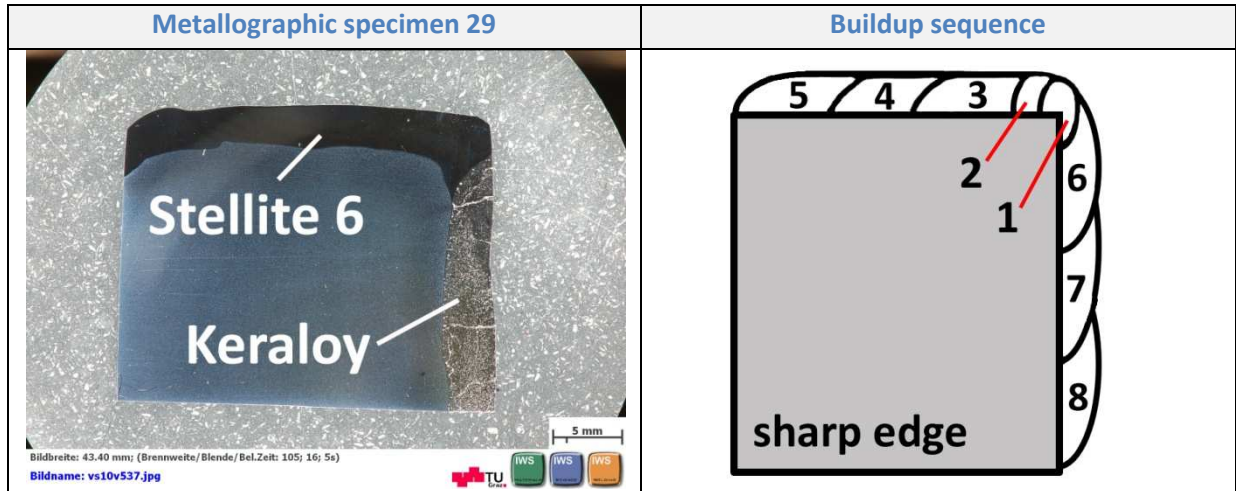


Figure 139: Specimen 29 – buildup sequence

5.10.3.1 Hardness

The hardness of Stellite 6 layer is very homogenous with about 450 HV1 what is shown in Figure 140. Also the Ni-matrix of Keraloy is homogenous and has an average hardness of about 600 HV1.

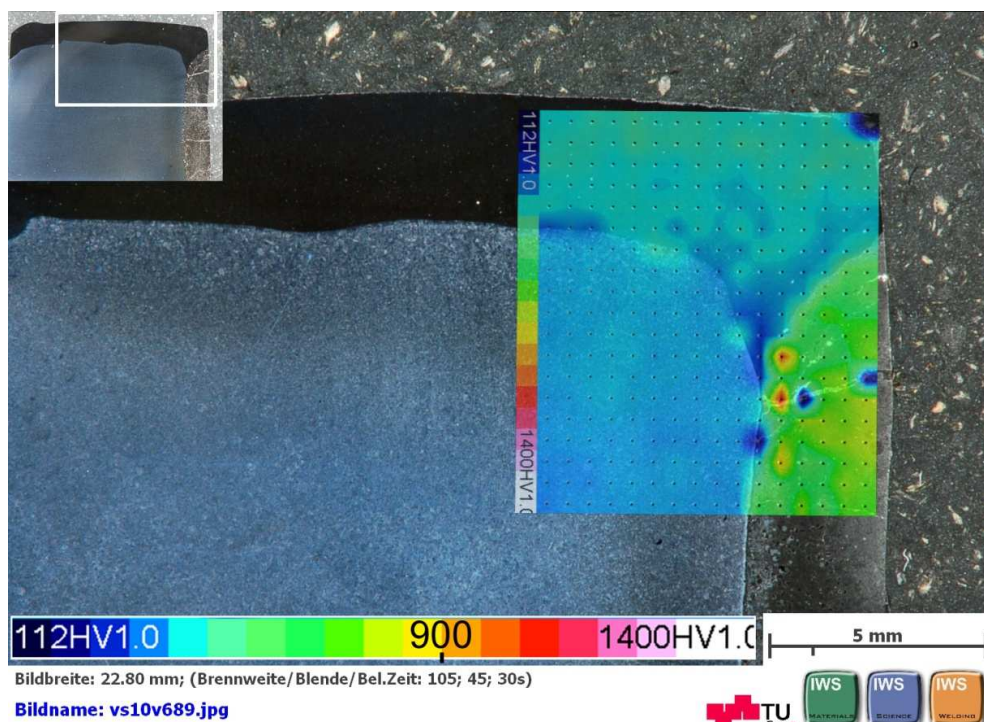


Figure 140: Specimen 29 – hardness mapping

5.10.3.2 EDX Keraloy

Figure 141 shows an EDX scan of Stellite 6 and Keraloy. The before mentioned high dilution of Stellite 6 with the substrate can be clearly seen because of the iron content in the Co-based Stellite coating. The dilution between Stellite 6 and Keraloy is lower. The tungsten carbide distribution is also illustrated as well as the molten tungsten carbides dissolved in the Ni-matrix. The amount of tungsten carbides should be about 60% in Keraloy coating. This amount is not reached by far.

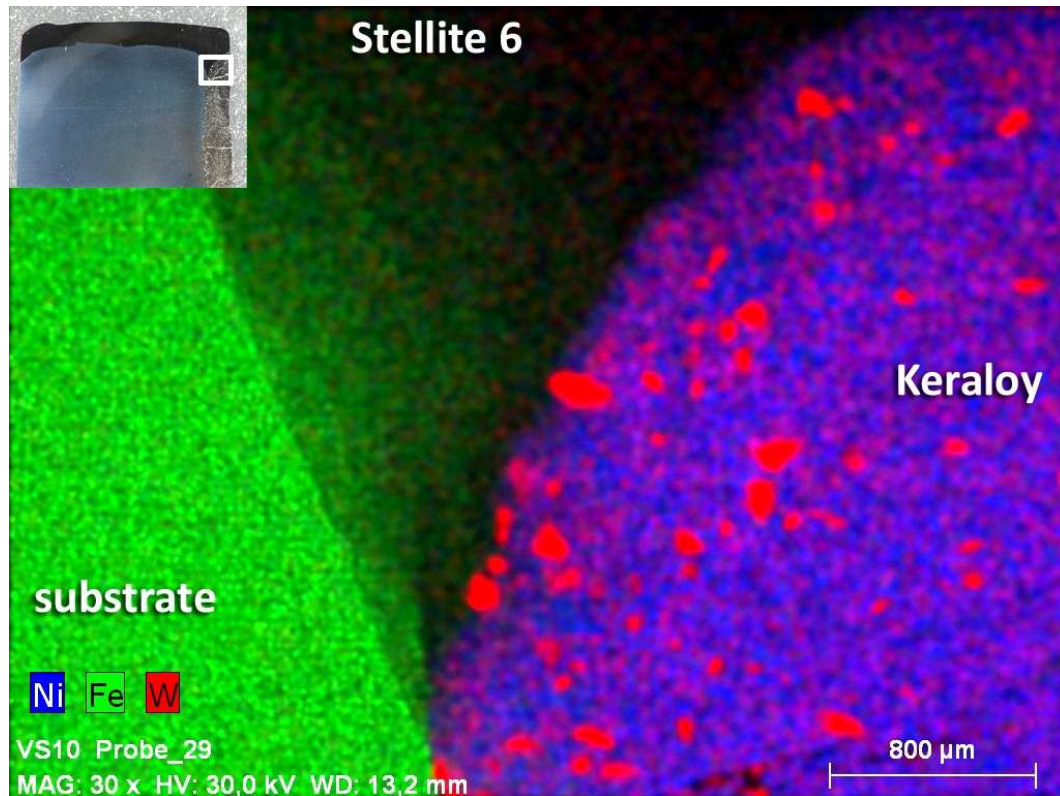


Figure 141: Specimen 29 – EDX scan Stellite 6 & Keraloy

5.10.3.3 Pores

The investigated area of Figure 142 shows one huge pore with a diameter of about 200 μm in Keraloy layer. The distribution of tungsten carbides is very inhomogeneous. Only in the area of the fusion zone, a certain amount of carbides can be detected. A reason can be the high density of the tungsten carbide which leads to segregation. Compare - Distribution of hard particles – page 44.

Some cracks can be seen. Especially along the fusion line cracks run through the Keraloy layer what enhances the risk of chipping and argues for a poor binding.

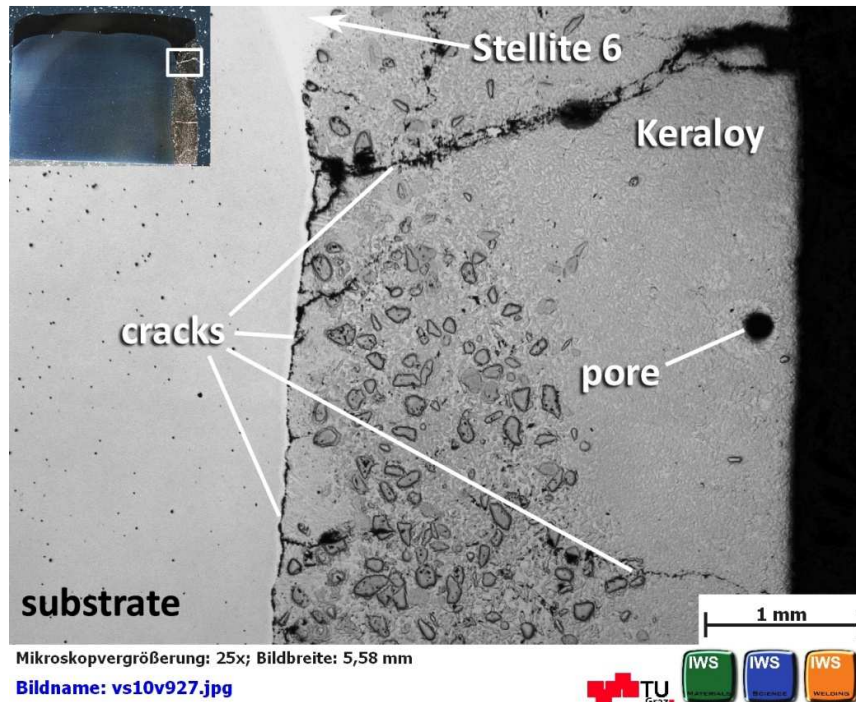


Figure 142: Specimen 29 – pore

5.10.3.4 Cracks

The same phenomenon is shown in Figure 143 where cracks propagate parallel to the fusion line as well as perpendicular to the surface. The amount of carbides is higher but their distribution is still inhomogeneous.

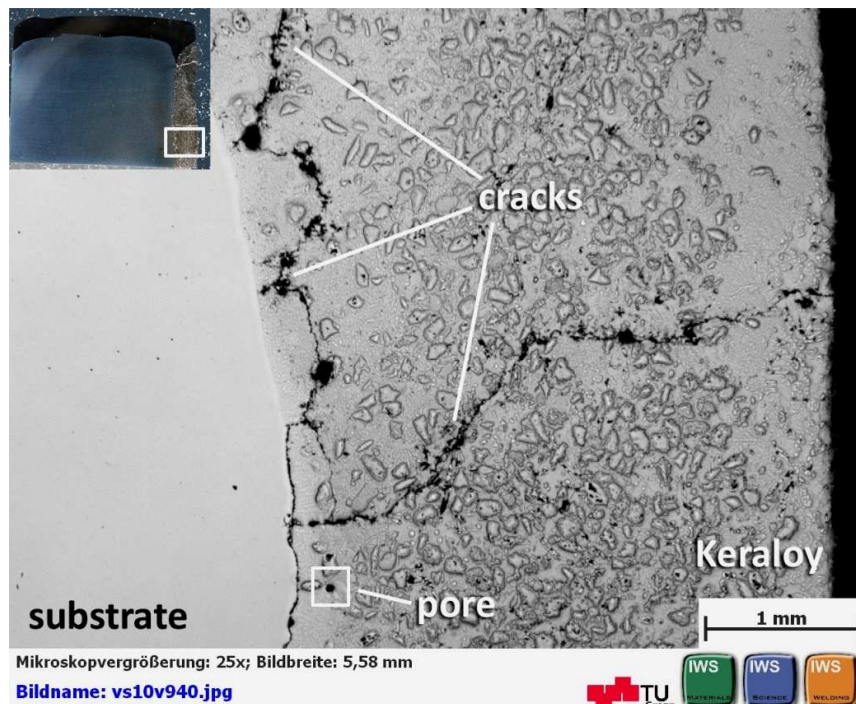


Figure 143: Specimen 29 – cracks in Keraloy

5.10.3.5 Binding & Chipping

The cracks in Figure 144 are quite similar to them shown in Figure 143. Only one crack propagates perpendicular to the fusion line. All the other are parallel to the fusion line or directly at the fusion zone. This fact makes the coating in this area susceptible for chipping. Due to the cracks in the fusion zone, the binding is also poor.

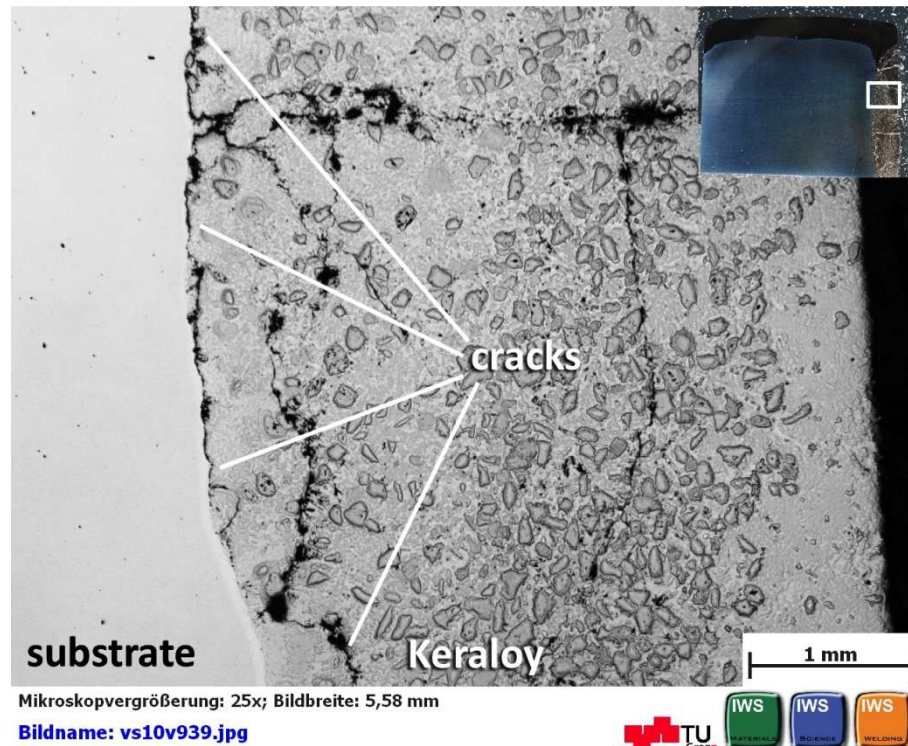


Figure 144: Specimen 29 – cracks along fusion line

5.10.4 Sample VII - Deloro 56

The next picture, Figure 145 shows specimen 31 and its buildup sequence. The deposited welding consumable is Ni-based Deloro 56 by PTA.

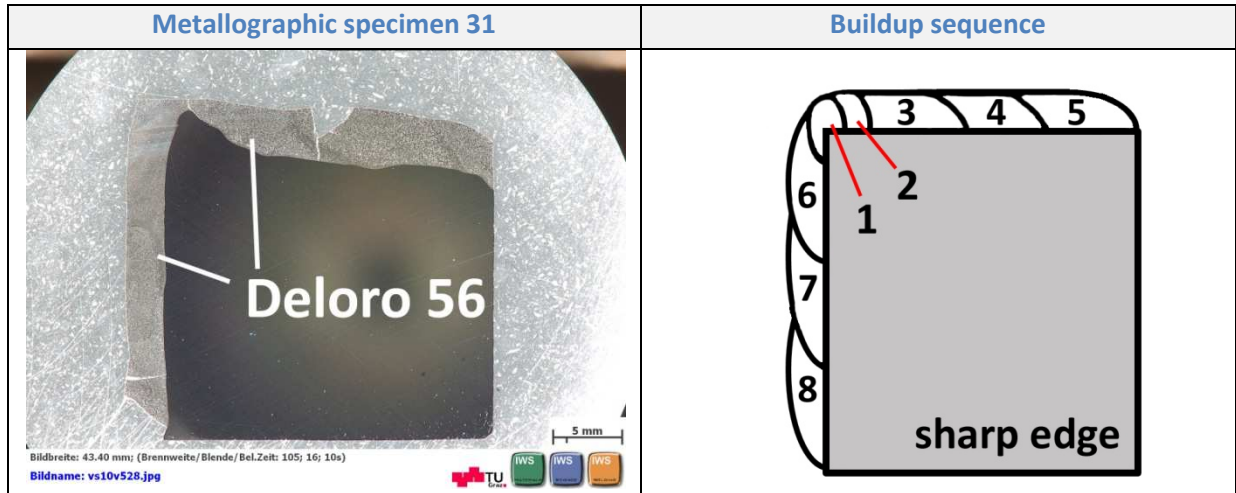


Figure 145: Specimen 31 – buildup sequence

5.10.4.1 Hardness

Figure 146 illustrates the hardness mapping of specimen 31. The hardness distribution of Deloro 56 is homogenous and the values are varying between about 450 HV1 and about 600 HV1.

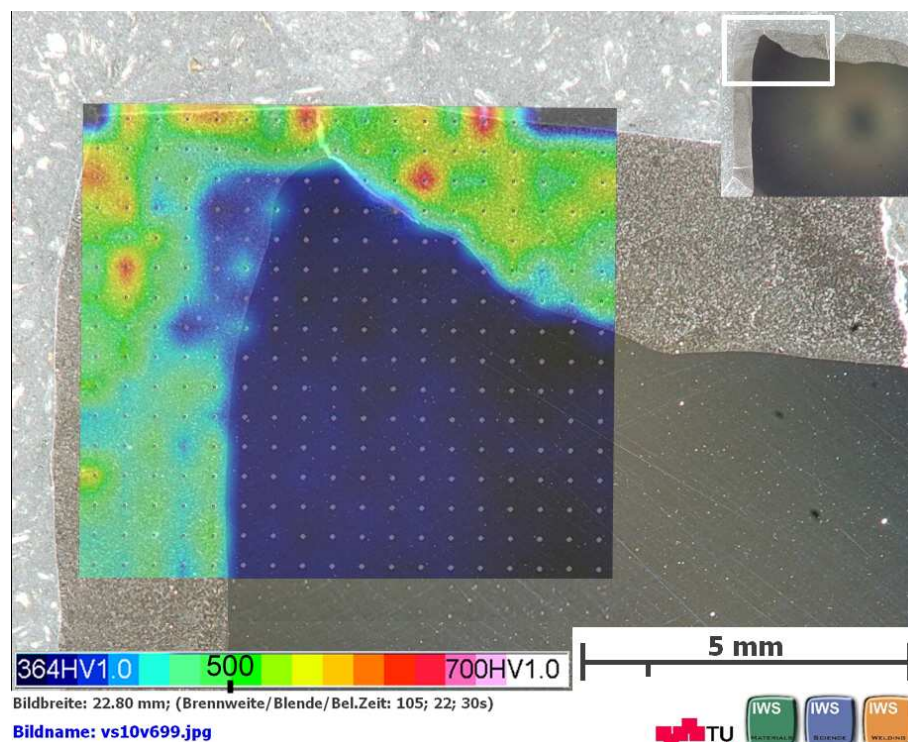


Figure 146: Specimen 31 – hardness mapping

5.10.4.2 EDX Deloro 56

The EDX scan in Figure 147 shows the hard phases – chromium borides of Deloro 56 in the Ni-matrix. The distribution of these precipitations is homogenous due to their small size compared to the synthetic tungsten carbides.

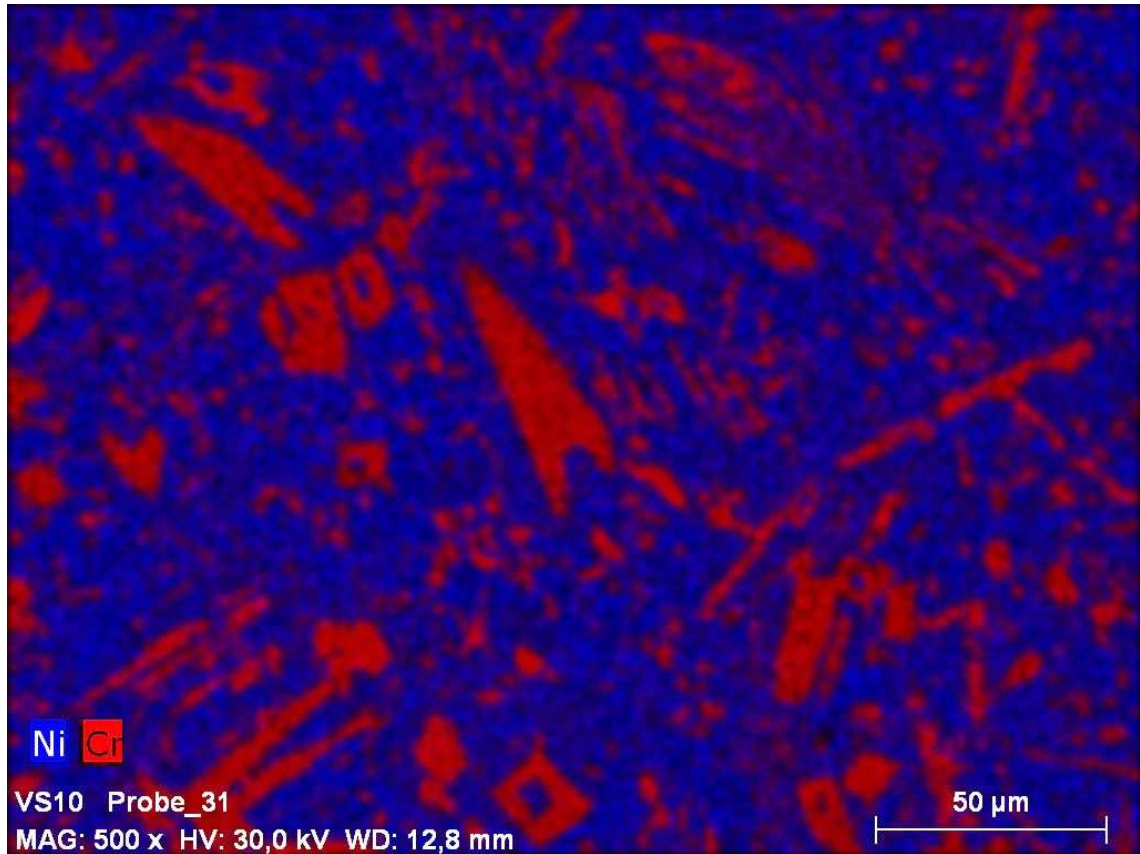


Figure 147: Specimen 31 – EDX scan of Deloro 56

5.10.4.3 Pores

The next picture, Figure 148 shows the only pore and one of the few cracks, which was found in two specimens. Similar to Stellite 6 coating, the layer is free of porosity and nearly free of cracks due to the lower hardness.

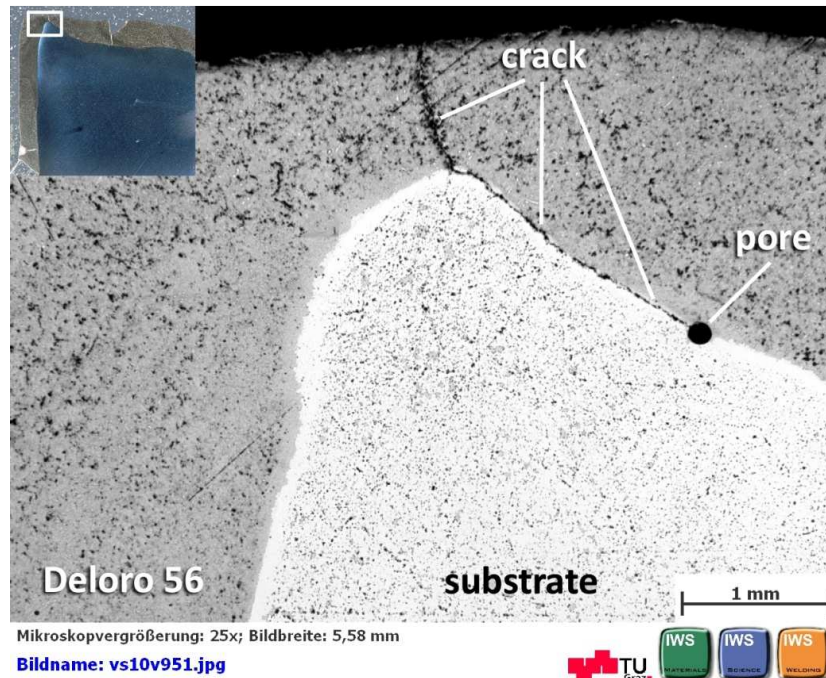


Figure 148: Specimen 31 – pore

5.10.4.4 Cracks

In Figure 148 a crack is exactly at the fusion line. A deep weld penetration can also be noticed and is indicated by the strange shape of the edge of the substrate, which implicates a high dilution at this area. In Figure 149 a crack propagates perpendicular to fusion line. The remaining Deloro 56 coating is free of cracks and shows a good binding to substrate.

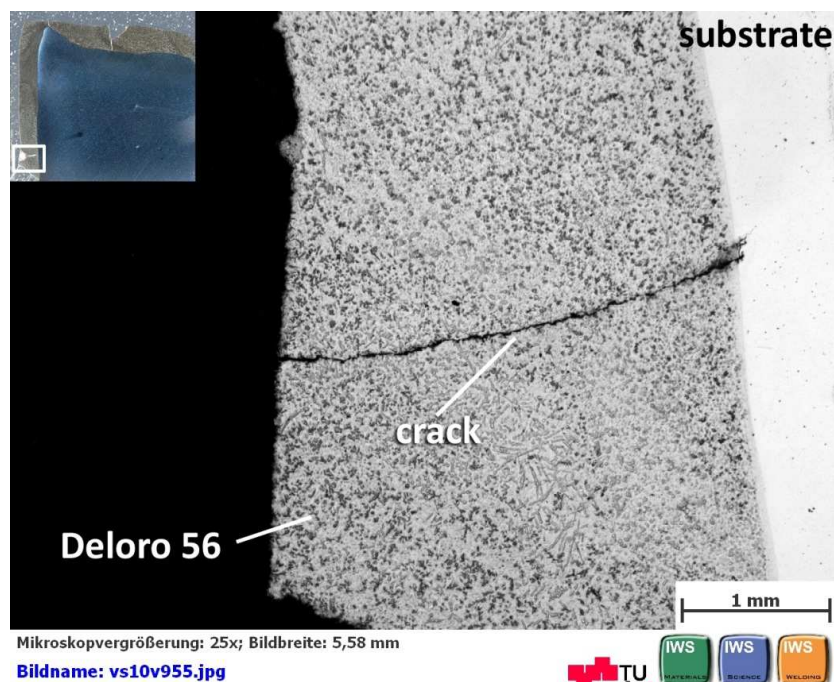


Figure 149: Specimen 31 – crack

5.10.4.5 Binding & Chipping

In the following picture, Figure 150 another crack appears in the coating and has probably led to chipping of Deloro 56 layer. The crack propagation direction is again perpendicular to the fusion line. The binding in this area of Deloro 56 looks good.

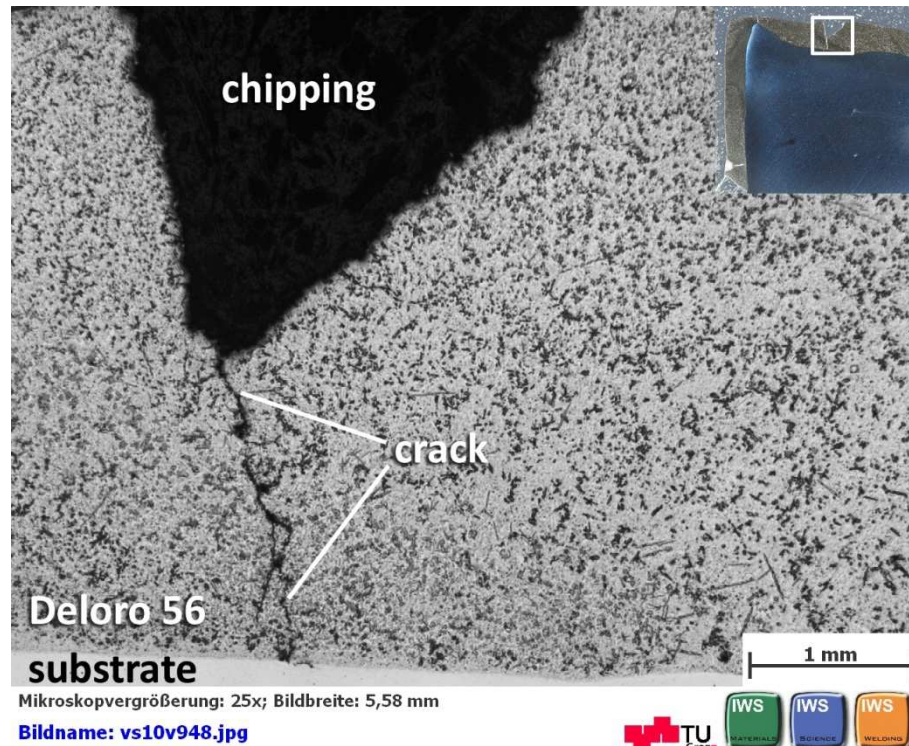


Figure 150: Specimen 31 – chipping of Deloro 56

6 Results

The following tables summarize the most important information of welding defects found on all investigated samples.

Each specimen has been investigated where the specific welding consumable had been deposited. Out of the data, average values (investigated area, pores and cracks per mm²) or maximum values (maximum diameter of pore) have been created to get an overview about each welding consumable.

Table 13 shows the data for the welding consumable 1302 A, applied by PTA technique.

In the upper part of the table, the most important information is briefly summarized with all according average and maximum values.

Underneath, the data from each specimen is illustrated which was used. In the case of 1302 A, 6 different specimens (1, 2, 3, 4, 5, & 26) have been investigated. Also the specific picture which was used for the investigation is listed.

welding consumable	technique	type of alloy	area	pores		cracks		
			φ size of area [mm ²]	#	average [# /mm ²]	size (max. ∅) [mm]	total length [mm]	average length [mm/mm ²]
1302A	PTA	Fe-alloy-matrix	13.33	24	1.84	0.35	6.1	0.46
specimen_1	picture, which was investigated	VS10V431	10.5	21	2.00	0.1	2.5	0.24
specimen_2		VS10V655	14	26	1.86	0.1	3	0.21
specimen_3		VS10V319	12.5	37	2.96	0.1	9	0.72
specimen_4		VS10V670	15	12	0.80	0.35	8.5	0.57
specimen_5		VS10V381	11	19	1.73	0.15	7	0.64
specimen_26		VS10V545	17	29	1.71	0.1	6.5	0.38

Table 13: Summary of investigation – PTA layer 1302 A

Like described for PTA powder 1302 A, the same investigations have been done for the other nine welding consumables as well. A problem which appeared was the different frequency of utilisation of each consumable. This means that for PTA powder 1302 A, six different specimens can be used for the investigation. In the cases of other consumables like TeroCote 7888T only two specimens are available.

6.1 Cracks

The following Table 14 summarizes the results of the investigation for each welding consumable considering cracks. Based on this information, tendencies can be noticed and evaluated from 1 – excellent to 5 - poor.

consumable	size of area [mm ²]	Σ length [mm]	φ length [mm/mm ²]	PTA	MAG	SMAW	EUTALLOY (Brazing)
1302 A	13,3	6,1	0,46	5			
DO 390N	14,2	5,7	0,45		5		
TeroCote 7888T	7,8	1,0	0,13				2
TungTec 10112	4,3	0,6	0,14				2
AbraTec 6088	10,9	2,9	0,27			3	
DO 321	7,8	2,1	0,27		3		
PG 6503	11,5	3	0,26	3			
Keraloy	15,8	5,3	0,34	3			
Deloro 56	12,3	0,8	0,06	1			
Stellite 6	12,8	0,3	0,02	1			

Table 14: Summary of investigation – cracks

The Fe-based consumables with the identical composition, 1302 A (PTA) & DO 390N (MAG), show the most cracks inside the coating. Although the technique is different, it seems that this issue does not have a real impact considering cracking.

The NiCrBSi-based welding consumables TeroCote 7888T & TungTec 10112 have much less cracks inside compared to the Fe-based ones. A reason can be the softer and more ductile Ni-matrix and lower heat input due to the coating technique. In the case of these two consumables the Eutalloy process (brazing) was used with maximum processing temperatures of about 1100 °C.

The NiBSi-based consumables PG 6503 (PTA), AbraTec 6088 (SMAW), DO 321(MAG) & Keraloy (PTA) show more cracks than NiCrBSi-based consumables mentioned above. A significant difference between the welding techniques (PTA, SMAW & MAG) used for NiBSi-based consumables cannot be seen.

Deloro 56 is also Ni-based consumable but has hard phases due to precipitation in opposite to the two other nickel groups with synthetic tungsten carbides. This layer can be seen as nearly ‘crack-free’.

Stellite 6 is the only exponent of Co-based consumables and has the lowest hardness. This is the main reason why no cracks can be found inside the layer.

6.2 Porosity

Table 15 summarizes the results of the investigation for each welding consumable considering porosity. The tendencies of porosity are not so significant and clear like for cracks.

Nevertheless an evaluation is done between 1 – excellent to 5 – poor as well as a differentiation between the average number of pores (#) and the maximum diameter of pores (\emptyset).

consumable	size of area [mm ²]	#	ϕ - # [# / mm ²]	Max \emptyset [mm]	PTA		MAG		SMAW		EUTALLOY (Brazing)	
					#	\emptyset	#	\emptyset	#	\emptyset	#	\emptyset
1302 A	13,3	24	1,8	0,3	2	3						
DO 390N	14,2	38	2,9	0,8			2	5				
TeroCote 7888T	7,8	25	3,2	0,05							3	1
TungTec 10112	4,3	23	5,6	0,1							5	1
AbraTec 6088	10,9	18	1,7	0,5					1	4		
DO 321	7,8	15	2	0,7			2	5				
PG 6503	11,5	33	2,9	0,2	2	2						
Keraloy	15,8	17	1,1	0,3	1	3						
Deloro 56	12,3	6	0,5	0,05	1	1						
Stellite 6	12,8	7	0,6	0,1	1	1						

Table 15: Summary of investigation – porosity

The Fe-based consumables 1302 A (PTA) & DO 390N (MAG), show both porosity inside the coating. It seems that MAG process enhance the tendency for porosity and the size of the pores as well.

The NiCrBSi-based welding consumables TeroCote 7888T & TungTec 10112 have more pores inside the coating compared to the Fe-based ones but they are much smaller. A reason for the higher amount of pores is the welding technique.

The other NiBSi-based consumables PG 6503 (PTA), AbraTec 6088 (SMAW), DO 321(MAG) & Keraloy (PTA) show less pores like the NiCrBSi-based consumables. A difference between the

welding techniques used for NiBSi-based consumables can be observed. The tendency for porosity is higher if MAG process or SMAW is used for hardfacing.

The pores in the Ni-based consumable Deloro 56 are few and they are very small. Porosity is definitely no problem of this layer.

Stellite 6 is the only exponent of Co-based consumables and has like Deloro 56 nearly no pores inside the coating.

6.3 Binding, Chipping & Dilution

Compared to cracks and pores the following presentation of results is qualitative due because of missing measurable criteria.

The evaluation is done by numbers; 1 – excellent & 5 – poor.

A distinction is made between:

Coating on substrate

consumable	Binding	Chipping	Dilution	PTA	MAG	SMAW	EUTALLOY (Brazing)
1302 A	1	2	1	1.3			
DO 390N	1	2	3		2		
DO 321	2	2	2		2		
PG 6503	2	2	1	1.7			
Keraloy	3	3	2	2.7			
Deloro 56	1	1	2	1.3			
Stellite 6	1	1	2	1.3			

Table 16: Summary of binding, chipping & dilution – on substrate

Refurbishment simulation

consumable	Binding	Chipping	Dilution	PTA	MAG	SMAW	EUTALLOY (Brazing)
DO 390N	3	5	4		4		
TeroCote 7888T	2	2	1				1.7
TungTec 10112							
AbraTec 6088	2	5	4			3.7	
DO 321	2	2	3		2.3		

Table 17: Summary of binding, chipping & dilution – refurbishment

7 Discussion

After the investigations, an assessment of the different welding consumables, welding techniques and their suitability for coating and refurbishment is done.

7.1 Welding consumables

- **1302A (PTA)**

This Fe-based coating type shows a huge amount of cracks and pores. Especially if a refurbishment simulation was done on it. That means that this welding consumable is only suitable for the first coating on a plug screw. On the other hand the coating is very homogenous and has high hardness. 1302 A PTA powder can be a new possibility for the coatings of plug screws at ANDRITZ, which should be tested systematically.

- **DO 390 N (MAG)**

DO 390N is also Fe-based and has the identical composition like 1302 A. The penetration and consequently the dilution are higher compared to 1302 A due the welding technique. The welding consumable DO 390N has only good properties if it is applied on substrate but for refurbishments on PTA layer 1302 A it seems to be not very promising. Further tests on other subjacent coating layers can be done.

- **TeroCote 7888 T (Eutalloy - brazing)**

TeroCote 7888T can be applied alone on substrate or like in this case, combined with TungTec 10112 powder in one layer by Eutalloy process. Therefore an assessment is only for the combination of both consumables possible. TeroCote 7888T is a self-fluxing consumable. Due to brazing (melting-in) no dilution occurs and the thermal effects of the coating process on the subjacent layer are relatively low compared to other welding techniques. The process temperature is about 1050 °C and the bonding looks quite good. The relative big size of TeroCote 7888T's tungsten carbides makes a homogenous distribution difficult. The combination of TungTec 10112 with smaller tungsten carbides is reasonable to reach a better carbide distribution within the coating.

- **Tungtec 10112 (Eutalloy – thermal spraying; spray & fuse)**

In the application of TungTec 10112 together with TeroCote 7888T, which serves a melt pool, the bonding is very good. The carbide distribution of TungTec 10112 is perfect because of the relative small size of hard particles and thermal spray technique. If TungTec 10112 is

applied alone, or no melt pool is provided by another welding consumable, the bonding on a hard subjacent layer is problematic.

- **PG 6503 (PTA)**

The coating of PG 6503 powder shows a relatively good bond and a good distribution of the hard particles. The PTA powder PG 6503 is very similar to Keraloy considering the composition and WC amount. But it seems to be more homogenous and optical pleasing. The different welding parameters can also be a reason. The welding consumable PG 6503 is another possibility which can be tried out on plug screws.

- **AbraTec 6088 (SMAW)**

The bonding of this layer type on the subjacent layer is good but the high heat input of the process causes problems. The high dilution mixes the different alloys and due to the heat input a lot of the tungsten carbides of the subjacent layer melt or cause huge cracks. Moreover the carbides of AbraTec 6088 melt as well and embrittle the matrix what reduces wear resistance.

- **DO 321 (MAG)**

This type shows good bonding on substrate and subjacent layer. The carbide distribution is homogenous but although the WC content is 60 %, few of them remain their shape. A lot of tungsten carbides are molten which leads to embrittlement of the matrix. A poor wear resistance is the consequence. DO 321 performs best in refurbishment simulation after Eutalloy process (TeroCote 7888T & TungTec 10112)

- **Keraloy (PTA)**

Keraloy is similar to PG 6503 and underperforms by optical evaluation. The carbide distribution is not so uniform and the cracks are slightly bigger. The different welding parameters can be the reason. Moreover, the dilution is higher compared to other PTA powders (1302 A & PG 6503). This phenomenon can only be noticed in Sample VII (Keraloy, Deloro 56 & Stellite 6) which was welded with rather different parameters.

- **Deloro 56 (PTA)**

Deloro 56 shows a very good bonding to substrate and nearly no pores can be noticed. Due to higher hardness compared to Stellite 6, Deloro 56 layer has a few cracks inside the coating. The dilution, as already mentioned, is relative high for PTA technique.

- **Stellite 6 (PTA)**

The coating type Stellite 6 shows perfect binding to substrate with 'no' pores and cracks. This good appearance of the coating result from the lowest hardness compared to all others.

7.2 Welding technique

Each welding technique has advantages and disadvantages which are described in chapter 3.12, Coating processes. In the following paragraphs the used techniques are briefly discussed.

- **Eutalloy process (brazing - spray & fuse)**

The Eutalloy process could be a good possibility for the refurbishment of worn plug screws. A better mixing of both consumables (TeroCote 7888T & TungTec 10112) should lead to a better distribution of tungsten carbides in the coating which is necessary to guarantee a good protective layer.

- **Shielded Metal arc welding (SMAW)**

The SMAW technique was only used for refurbishment simulation. Furthermore, AbraTec 6088 was the only welding consumable which was applied by this technique. The SMAW process combined with the consumable AbraTec 6088 is not very promising. The dilution is very high which leads to the melting of tungsten carbides and to embrittlement of the Ni-matrix of AbraTec 6088 and the subjacent coatings. A changing of parameters could help to prevent the enormous dilution.

- **Arc welding (MAG)**

The MAG process cannot be a real alternative to PTA technique. Compared to PTA process the dilution is higher and the surface quality underperforms as well. Relative good results can be noticed with DO 390N on substrate and DO 321 on substrate or for refurbishment on PTA coating 1302A.

- **Plasma Transferred arc welding (PTA)**

PTA technique is the best technique for the coating of plug screws. The weldings show relative low dilution with very precise surfaces. The deposition speed makes it a very economic coating technique for components of this size.

Table 18 shows a summary of the evaluation of the used welding consumables.

consumable	cracking	pores		binding		hardness		PTA	MAG		SMAW	EUTALLOY (Brazing)
		#	Ø	S	L	M	HP	1.C	1.C	Ref	Ref	Ref
1302 A	5	2	3	1	-	3		1				
DO 390N	5	2	5	2	4	3			2	5		
TeroCote 7888T	2	3	1	-	2	5	1					1
TungTec 10112		5	1	-		4	2					
AbraTec 6088	3	1	4	-	4	4	1				4	
DO 321	3	2	5	2	2	4	1		2	2		
PG 6503	3	2	2	2	-	4	2	2				
Keraloy	4	1	3	3	-	4	1	2				
Deloro 56	1	1	1	1	-	4		1				
Stellite 6	1	1	1	1	-	5		1				

Table 18: Assessment of welding consumables

Table 19 explains abbreviations of Table 18.

#	amount of pores
Ø	size of pores
S	substrate
L	layer (subjacent coating)
M	matrix
HP	hard particle
1.C	1 st coating
Ref	refurbishment

Table 19: Legend of Table 18

7.3 Recommendation & outlook

In the following lines some thought-provoking impulses are mentioned for further investigations and experiments.

- SMAW technique on substrate or with another welding consumable
- Optimization of inter pass temperatures & preheating temperatures
- To try the countermeasures like done at the sites in Canada. A slower cooling of the hardfaced parts in a sandbox could reduce the number of cracks.
 - To minimize thermal distortion the plug screw is placed in welding blankets and vermiculite insulation to slow the cooling of the part over a period of 24 hours or longer.
 - One important thing is to have slow cooling right after the welding process. So the vermiculite or a hot sand box must be ready to cover the screw after coating.
- Manual PTA torch can be used for new welding samples; perhaps it is an alternative refurbishment technique
- The use of a similar hardfacing alloy (D2PTA), which was investigated by RWTH Aachen University; mentioned in 3.11.1.3
- Modularity of plug screws; perhaps the construction can be changed to a modular construction which allows a faster service. Moreover, the different wear of the screw can be considered (extreme wear at front & less wear at the rear)
- The discussed welding consumable in 3.11.1.2, DO 48 & TeroCote 7888 LT should be tried out

8 Conclusion

Hardfacing plays a major role in applications exposed to wear and tear. Coating layers on new components protect and extend the durability or allow restoring dimensions of worn surfaces. Depending on the field of application, the protective layers must be adapted to the specific demands like abrasive, ambient medium, temperature and so on.

This thesis considers the demands in pulp and paper industry and gives a theoretical overview about wear in general and related topics like tribology and wear testing. Furthermore, a characterization of ten different welding consumables was worked out to handle influencing and determining factors. Several coating techniques were described and evaluated.

A theoretical elaboration of coating methods for screws using thermal spraying or polymer surfacing was not very promising. According to literature and the expertise of several interviewed engineers, thermal spraying is a coating technique for rather thin coatings. Besides, a field test of an HVOF – coating failed after a few weeks in use. Polymer surfacing is already applied as wear coating. According to two suppliers and literature, the coatings would not withstand the high demands of wear and impact load in the specific case of plug screws. Hardfacing is still the most promising deposition technique for these specific wear coatings.

Light microscopy provides a general idea of the different protective layers. The binding, dilution, porosity, cracks and carbide distribution can be evaluated. In addition, electron microscopy helped to test dilution of substrate in specific areas and dilution of hard particles. Hard phases, precipitations and elements can also be determined.

Hardness mappings show the hardness characteristics of the layer and hard phase distribution inside the coating. Furthermore, information about the HAZ due to welding process is given. Additional micro hardness and macro hardness measurements helped to determine and verify the hardness of specific coating areas and tungsten carbides.

The welding tests show that the PTA technique is the best technique for the coating of plug screws. The lower dilution and precise surface with the relative high deposition rate make it an economic coating technique. The MAG process can be an alternative to the PTA technique, whereas the EUTALLOY process could be a good possibility for the refurbishment of worn plug screws.

Considering the investigated welding consumables, the PTA powder 1302 A could be a new possibility for the first coating of plug screws at ANDRITZ. Similar potential was seen with flux cored wire DO 390N deposited by MAG, but this seems not very promising for refurbishments.

Another flux cored wire, DO 321 deposited by MAG, can be an alternative consumable. Although the WC content is 60 %, few of them remain in their original shape which is caused by the welding technique and parameters. DO 321 performs best in refurbishment simulation after EUTALLOY process.

The PTA powder PG 6503 is similar to Keraloy considering the composition and WC amount but seems to perform better. The different welding parameters can be the reason.

Consumables deposited on Sample VII, like Stellite 6, Keraloy and Deloro 56, are already standard coatings at ANDRITZ. These samples show higher dilution compared to other PTA powders (1302 A & PG 6503). Different welding parameters can be the reason for that.

To verify the assumptions and recommendations of this thesis, further systematically investigations of the most promising welding consumables should be done. Therefore a small number of promising welding consumables should be investigated with the same methods applied in this thesis and additional standardized wear tests (abrasive wear & impact) should be tried out. Due to the fact that wear tests only can give tendencies of the behaviour of protective layers, field tests must be done with the most promising ones.

Other thought-provoking impulses can be found in chapter 7.3 - Recommendation & outlook, which should be considered in further investigations and analysis.

9 Bibliography

- [1]. **Pohl, M.; Borst, K.; Feyer, M.; Husemann, R. U.; Klinger, Ch.** *Schadensanalyse - Schäden durch tribologische Beanspruchungen VDI 3822 Blatt1-5*. Düsseldorf : VDI - Verein Deutscher Ingenieure, 1999. 978-3-8348-0933-9.
- [2]. **Heimann, R. B.** *Plasma Spray Coating: Principles and Applications*. s.l. : Wiley-VCH Verlag GmbH & Co. KG, 2008. 978-3-527-32050-9.
- [3]. **Castolin Eutectic**. Castolin Eutectic - Wear. [Online] Castolin Eutectic, 2010. [Zitat vom: 18. Mai 2010.] http://www.castolin.com/wCastolin_com/solutions/wear.php?navid=18.
- [4]. **Blau, P. J.** *ASM Handbook Vol. 18*. Ohio : ASM International, 1992. 0871703807.
- [5]. **ANDRITZ AG**. Standard Refining Process. *Andritz AG*. [Online] Andritz AG, 2010. [Zitat vom: 22. Mai 2010.] <http://www.andritz.com/ANONID134FEA184382A183/ppp-panelboard/ppp-panelboard-mdf/ppp-panelboard-pr/ppp-panelboard-asrp.htm>.
- [6]. **ANDRITZ AG**. Pressurized Refining Process - Plug Screw Feeder. *Andritz AG*. [Online] Andritz AG, 2010. [Zitat vom: 26. Mai 2010.] <http://www.andritz.com/de/ANONID1994610D37643AEC/ppp-panelboard/ppp-panelboard-mdf/ppp-panelboard-pr/ppp-panelboard-plugscrewfeeder.htm>.
- [7]. **Hauck, E.** Sanierung von Stopfschnecken. *Interview*. Graz, 19. Jänner 2010.
- [8]. **Hölbling, M.** Panzerung von Stopfschnecken . *Bericht zur Besprechung Fa. Castolin*. Graz, 2010.
- [9]. **Bayer, R. G.** *Selection and use of wear tests for metals*. s.l. : ASTM American Society for Testing and Material, 1977. 0-8031-0563-0.
- [10]. **Stokes, J.** *Theory and Application of the High Velocity Oxy-Fuel (HVOF) Thermal Spray Process*. Dublin : Dublin City University, 2008. 1649-8232.
- [11]. **Mennig, G. und Lake, M.** *Verschleißminimierung in der Kunststoffverarbeitung: Phänomene und Schutzmaßnahmen*. München : Carl Hanser Verlag, 2008. 978-3-446-40776-3.
- [12]. **Gordon England**. Gordon England Thermal Spray Coating Consultant. [Online] [Zitat vom: 15. May 2010.] <http://www.gordonengland.co.uk/img/wear3.gif>.

- [13]. **Gates, J.D.** Two-body and three-body abrasion : A critical discussion. *Wear* . 1998, Bd. 214.
- [14]. *Wear mechanisms - New direction in Tribology*. **Kato, K.** s.l. : Mechanical Engineering Publications, 1997. 1 86058 099 8.
- [15]. **LUBRICANT CONSULT GMBH.** Lubricant Consult. [Online] [Zitat vom: 9. Juni 2010.] <http://www.lubcon.com/verschleiss.0.html?&L=1>.
- [16]. **Institute of Production Engineering.** University Duisburg-Essen. [Online] [Zitat vom: 14. June 2010.] http://www.uni-due.de/imperia/md/content/werkstofftechnik/sk_hwt_06_wearmechanisms_ss08.pdf.
- [17]. **Totten, G. E., Westbrook, S. R. und Shah, R. J.** *Fuels and Lubricants Handbook: Technology, Properties, Performance, and Testing*. s.l. : American Society for Testing & Materials (ASTM), 2003. 0803120966.
- [18]. **Bourithisa, L. und Papadimitriou, G.D.** The effect of microstructure and wear conditions on the wear resistance of steel metal matrix composites fabricated with PTA alloying technique. *Wear*. 2009, 266.
- [19]. **Czichos, H. und Habig, K.-H.** *Tribologie-Handbuch: Reibung und Verschleiß*. s.l. : Vieweg & Teubner, 2010. 3834800171.
- [20]. **Glaeser, W. A., et al.** *Tribology: the science of combatting wear*. Columbus, Ohio : Battelle Memorial Institute, 1982. TX0000839403.
- [21]. **Oerlikon Balzers Liechtenstein.** *Oerlikon Balzers*. [Online] [Zitat vom: 12. April 2010.] http://www.oerlikon.com/ecomaXL/index.php?site=BALZERS_EN_tribological_system.
- [22]. **Zietsch, Ch.** Institute of Production Engineering University Duisburg-Essen. [Online] [Zitat vom: 6. March 2010.] http://www.uni-due.de/imperia/md/content/werkstofftechnik/sk_ue_hwt_systemanalyse.pdf.
- [23]. **Blau, P. J. und Budinski, K. G.** Development and use of ASTM standards for wear testing. *Wear*. 1999, 225.
- [24]. **Van Acker, K., et al.** Influence of tungsten carbide particle size and distribution on the wear resistance of laser clad WC Ni coatings. *Wear*. 2005, 258.
- [25]. **Pauschitz, A.** AC²T research. [Online] AC²T research GmbH. [Zitat vom: 24. August 2010.] <http://www.ac2t.at/html/deutsch/d-tribolab.html>.

-
- [26]. **Services Solu-tex inc.** Solu-tex. [Online] Services Solu-tex inc. [Zitat vom: 28. August 2010.] <http://www.solu-tex.com/templates/design/file/trimay/hardness/Hardne5.jpg>.
- [27]. **Franek, F., Badisch, E. und Kirchgaßner, M.** Advanced Methods for Characterisation of Abrasion/Erosion Resistance of Wear Protection Materials. *FME (Faculty of Mechanical Engineering, Belgrade) Transactions* . 2009, 37.
- [28]. **Badisch, E. und Kirchgaßner, M.** Influence of welding parameters on microstructure and wear behaviour of a typical NiCrBSi hardfacing alloy reinforced with tungsten carbide. *Surface & Coatings Technology*. 2008, 202.
- [29]. **Dilthey, U.** *Schweißtechnische Fertigungsverfahren 1*. Berlin : Springer, 2006. 978-3-540-21673-5.
- [30]. **Deuis, R.L., Yellupb, J. M. und Subramanian, C.** METAL-MATRIX COMPOSITE COATINGS BY PTA SURFACING. *Composiws Science and Technology*. 1998, 58.
- [31]. **Davis, J.R.** *ASM Handbook Vol. 6*. Ohio : ASM International, 1993. 0871703823.
- [32]. **Welding Institute.** *Welding Metallurgy of Steels*. Cambridge : Abington Publishing, 1994. 185573172X.
- [33]. **Cerjak, H., Enzinger, N. und Pasic, O.** *Skriptum zur Vorlesung Schweißtechnik*. Graz : Institut für Werkstoffkunde, Schweißtechnik und Spanlose Formgebungsverfahren, 2005.
- [34]. **Dilthey, U.** *Schweißtechnische Fertigungsverfahren 2*. s.l. : Springer-Verlag GmbH, 2005. 354021674X.
- [35]. **Gesnouina, C., Hazarabediana, A. und Bruzzoni, P.** Effect of post-weld heat treatment on the microstructure and hydrogen permeation of 13CrNiMo steels. *Corrosion science*. 2004, 46.
- [36]. **Nisbett, E. G. und Melilli, A. S.** *Soft-martensitic stainless Cr-Ni-Mo steel for turbine rotors in geothermic power stations*. Philadelphia : ASTM International, 1986. 0803104650.
- [37]. **Berns, H. und Theisen, W.** *Eisenwerkstoffe - Stahl und Gusseisen*. s.l. : Springer-Verlag GmbH, 2006. 3540297928.
- [38]. **Canale, L. C. F., Mesquita, R. A. und Totten, G. E.** *Failure Analysis of Heat Treated Steel Components*. Ohio : ASM International, 2008. 087170868X.
-

- [39]. **Thibault, D., Bocherb, Ph. und Thomas, M.** Residual stress and microstructure in welds of 13%Cr-4%Ni martensitic stainless steel. *Journal of materials processing technology*. 2009, 209.
- [40]. **Vollertsen, F.** *Werkstoffeigenschaften und Mikrostruktur*. München : Hanser, 1989. 3446155848.
- [41]. **Wirth, B. D. und Olander, D.R.** *Diffusion in Solids*. Berkeley, California : University of Berkeley, 2009.
- [42]. **Million, A.** *Stand der Kenntnisse über die Kaltrissbildung und die Beurteilung der Kaltrissanfälligkeit*. Düsseldorf : DVS Bericht, 1980.
- [43]. **Schreiber, F.** *Wearing protection with fused tungsten carbides*. Willich : Durum-Verschleiß-Schutz GmbH, 6/2002.
- [44]. **Gebert, A., et al.** Neuentwicklungen für den Verschleiß- und Korrosionsschutz beim Plasma-Pulver-Auftragschweißen. *Materialwissenschaft und Werkstofftechnik*. 2008, Bd. 39, 1.
- [45]. **Reisgen, U., et al.** Investigation of wear resistance and microstructure of a newly developed chromium and vanadium containing iron-based hardfacing alloy. *Materialwissenschaft und Werkstofftechnik*. 2008, Bd. 39, 6.
- [46]. **Ebert, L., Thurner, S. und Neyka, S.** Beeinflussung der Hartstoffverteilung beim Plasma-Pulver-Auftragsschweißen. *Materialwissenschaften und Werkstofftechnik*. 2009, Bd. 40, 12.
- [47]. **Just, Ch., Badisch, E. und Wosik, J.** Influence of welding current on carbide/matrix interface properties in MMCs. *Journal of Materials Processing Technology*. 2010, Bd. II, 210.
- [48]. **Kirchgaßner, M.** *Castolin Eutectic*. 31. May 2010.
- [49]. **Castolin Eutectic.** Surfacing technology polymers for cold rapid repairs. [Online] [Zitat vom: 28. August 2010.]
http://www.castolin.de/wCastolin_com/pdf/products/coating/MeCaTec_Flyer_ENGLISH.pdf
.
- [50]. **Schreiber, F.** *Mobiles Plasma-Pulver-Handauftragschweißen: Erfahrungen aus der Praxis*. Willich : s.n., 2002.
- [51]. **Davis, J. R.** *Nickel, cobalt, and their alloys*. s.l. : ASM Specialty Handbook, 2000. 0871706857.

-
- [52]. **Dieter, G. E.** *ASM Handbook Vol. 20*. Ohio : ASM International, 1997. 0871703866.
- [53]. **Hou, Q.Y., Gao, J.S. und Zhou, F.** Microstructure and wear characteristics of cobalt-based alloy deposited by plasma transferred arc weld surfacing. *Surface & Coatings Technology*. 2005, 194.
- [54]. **Davis, J. R.** *Tool materials*. s.l. : ASM International, 1995. 0871705451.
- [55]. **Cuia, Chengyun, et al.** Characteristics of cobalt-based alloy coating on tool steel prepared by powder feeding laser cladding. *Optics & Laser Technology*. 2007, 39.
- [56]. **Schmucker, T.** *Deloro Stellite*. Graz, 15. January 2010.
- [57]. **Sidhu, T. S., Prakash, S. und Aerawal, R. D.** Hot corrosion and performance of nickel-based coatings. *Current Science Association; Indian Academy of Sciences*. 2006, 90.
- [58]. **Gedeon, M.** Nickel as a coating material. *Technical Tidbits*. 2002, 4.
- [59]. **Castolin Eutectic.** *TeroCote 7888LT*. [Online] [Zitat vom: 16. February 2010.] http://www.castolin.com/wCastolin_com/pdf/products/brazing/7888LT.pdf.
- [60]. **Klimpel, A. und Kik, T.** Erosion and abrasion wear resistance of GMA wire surfaced nanostructural deposits. *Archives of Materials Science and Engineering*. 2008, 30.
- [61]. **Pichler, K.-H.** *Sonnek Engineering Ges.m.b.H.* 3. February 2010.
- [62]. **Kavelius, W.** *Chesterton International*. 15. March 2010.
- [63]. **Pichler, K.-H.** *Sonnek Engineering Ges.m.b.H.* Wien, 3. February 2010.
- [64]. **Kavelius, W.** *Chesterton International*. München, 15. March 2010.
- [65]. **Durand, J. M., Vardavoulias, M. und Jeandin, M.** Role of reinforcing ceramic particles in the wear behaviour of polymer-based model composites . *Wear*. 1994, 181 - 183.
- [66]. **Hübner, A., Böbe, A. und Shirinow, E.** Einfluss unterschiedlicher Wolframkarbidarten auf das Verschleißverhalten von PPA. *Schweißen und Schneiden*. 2010, 62.
- [67]. **Bouaifi, Belkacem.** *Werkstoffsystem zum thermischen Beschichten zur Herstellung einer Schutzschicht auf metallischen Werkstücken*. DE102005020611A1 D, 16. November 2006. coating.
- [68]. **Technogenia Verschleißtechnik e. K.** Technogenia Broschüre SPHEROTENE. [Online] [Zitat vom: 19. march 2010.] http://www.technogenia.de/downloads/technogenia_broschuere_spherotene.pdf.
-

- [69]. **Castolin Eutectic**. Castolin Eutectic - TeroCote. [Online] [Zitat vom: 3. June 2010.] http://www.eutectic.com/wCastolin_com/products/brazing/TeroCote.php?navid=114.
- [70]. **Gebert, A. und Wocilka, D.** *Charakterisierung und Qualifizierung hochkarbidhaltiger Verschleißschutzbeschichtungen hinsichtlich des Einsatzes unter stark korrosiven Bedingungen*. Chemnitz : TU Chemnitz, Institut für Fertigungstechnik / Schweißtechnik, 2006.
- [71]. **Kirchgaßner, M., Badisch, E. und Franek, F.** Behaviour of iron-based hardfacing alloys under abrasion and impact. *Wear*. 2008, 265.
- [72]. **ESAB**. Handbuch für das Reparatur- und Instandhaltungsschweißen. [Online] [Zitat vom: 15. September 2010.] http://www.esab.de/de/de/support/upload/Rep-Handbuch-XA00086830_GE.pdf.
- [73]. **Austrian Standards Institute**. *Welding and allied processes - Classification of geometric imperfections - Part 1 - Fusion welding*. Vienna : s.n., 2007.
- [74]. **Zimmer, P.** Zur Bewertung der Kaltrissicherheit von Schweißverbindungen aus hochfesten Feinkornbaustählen. *BAM Dissertationsreihe*. 2007, 29.
- [75]. **Beckert, M.** *Kompendium der Schweißtechnik*. s.l. : DVS Verlag, 2002. 3871552070.
- [76]. **Hügel, H.** *Laser in der Materialbearbeitung*. Stuttgart : IFSW Stuttgart, 1996. 3-00-000532-3.
- [77]. **Fronius International GmbH**. Fronius International. *Glossary*. [Online] Fronius International. [Zitat vom: 23. June 2010.] http://www.fronius.com/cps/rde/xchg/SID-32840AFE-5884621E/fronius_international/hs.xsl/68_1185_ENG_HTML.htm?id=1415.
- [78]. **Probst, R. und Herold, H.** *Kompendium der Schweißtechnik - Band 2*. Düsseldorf : DVS Media, 1997. 3871551597.
- [79]. **ASM International**. *Weld Integrity and Performance*. Materials Park Ohio : ASM International, 1997. 0871706008.
- [80]. **DIN, Deutsche Institut für Normung und DVS, Deutscher Verband für Schweißen**. *Schweißtechnik 8*. s.l. : DVS Media, 2007. 3871559717.
- [81]. **Przyblyowicz, J. und Kusinski, J.** Structure of laser clad tungsten carbide composite coatings. *Journal of Materials Processing Technology*. 2001, Bde. I-II, 109.

-
- [82]. **Polak, R.; Kremser, F.** Thermal Spraying between erosion and corrosion challenges. 2005.
- [83]. **Fahrenwaldt, H. J., et al.** *Praxiswissen Schweißtechnik*. s.l. : Vieweg, 2006. 978-3-8348-0194-4.
- [84]. **Schneider, K. E., et al.** *Thermal Spraying for Power Generation Components*. Weinheim : Wiley, 2006. 978-3-527-31337-2.
- [85]. **Tucker, R. C.** Thermal Spray Coatings. *Uses of Thermal Spray Coatings*. 2002, Vol. 5.
- [86]. **Castolin Eutectic.** *SuperJet - Operation manual*. Lausanne : Castolin S.A., 2003. 716.18067-0053.
- [87]. GTS - Gemeinschaft Thermisches Spritzen e.V. [Online] 2009. [Zitat vom: 21. August 2010.] http://www.gts-ev.de/images/v_flp.gif.
- [88]. **Kou, S.** *Welding Metallurgy*. New York : John Wiley and Sons, 2003. 0471434914.
- [89]. **Castolin Eutectic.** Castolin Eutectic SuperJet. [Online] [Zitat vom: 13. June 2010.] http://www.castolin.de/wCastolin_com/images/products/coating/Super-Jet_3_.jpg.
- [90]. **Castolin Eutectic.** Brazing Technology CATALOGUE. [Online] 2008. [Zitat vom: 12. May 2010.] http://www.remoterm.com/catalogue/Brazing_Catalogue_English_09.05.08.pdf.
- [91]. **Shin, J.-C.I, et al.** Effect of molybdenum on the microstructure and wear resistance of cobalt-base Stellite hardfacing alloys. *Surface and Coatings Technology*. 2003, 166.
- [92]. **Liu, Yuan-Fu, et al.** Microstructure and wear behavior of (Cr,Fe)₇C₃ reinforced composite coating produced by plasma transferred arc weld-surfacing process. *Surface & Coatings Technology*. 2006, 201.
- [93]. **Reimer, L.** *Scanning electron microscopy: physics of image formation and microanalysis*. Berlin : Springer, 1998. 3540639764.
- [94]. **Egerton, R. F.** *Physical Principles of Electron Microscopy: An Introduction to TEM, SEM, and AEM*. Berlin : Springer, 2005. 0387258000.
- [95]. **Riviere, J. C.** *Handbook of Surface and Interface Analysis: Methods for Problem-Solving*. New York : Marcel Dekker Inc, 1998. 0824700805.
- [96]. **Chandler, H.** *Hardness Testing*. s.l. : ASM International, 1999. 0871706407.
-

[97]. **Dietmar Lober**. Metallograf. [Online] [Zitat vom: 10. November 2009.]
<http://www.metallograf.de/start-eng.htm?werkstoffkartei-eng/4313/4313.htm>.

10 List of figures

FIGURE 1: WORN PLUG SCREW [ANDRITZ]	3
FIGURE 2: PLUG SCREW FEEDER INSTALLATION IN PRODUCTION PROCESS [ANDRITZ].....	4
FIGURE 3: PLUG SCREW FEEDER – GENERAL ASSEMBLY [ANDRITZ].....	5
FIGURE 4: SCREW FEEDER – CROSS SECTION [ANDRITZ]	6
FIGURE 5: WORN COMPRESSION HOUSING BEFORE REFURBISHMENT [ANDRITZ]	6
FIGURE 6: PLUG SCREW WITH STELLITE 6 AT OUTER DIAMETER	8
FIGURE 7: PLUG SCREW WITH STELLITE 6 AT OUTER DIAMETER AND LEADING SIDE OF FLIGHT	8
FIGURE 8: PLUG SCREW WITH DELORO 56 / 60 COATING.....	9
FIGURE 9: PLUG SCREW WITH STELLITE 6 AT OUTER DIAMETER AND DELORO 56 AT THE REMAINING SURFACES.....	9
FIGURE 10: PLUG SCREW WITH ACTUAL COATING STANDARD (2009/2010)	9
FIGURE 11: CLASSIFICATION OF VARIOUS WEAR MECHANISMS [10]	12
FIGURE 12: TWO BODY ABRASION [12]	13
FIGURE 13: THREE BODY ABRASION [12]	13
FIGURE 14: FOUR TYPES OF WEAR [15]	16
FIGURE 15: EFFECT OF ABRASIVE HARDNESS, RELATIVE TO MATERIAL HARDNESS, ON ABRASIVE WEAR [4]	17
FIGURE 16: TRIBOLOGICAL SYSTEM [22]	19
FIGURE 17: SCHEMATIC OF PIN-ON-DISK TESTING MACHINE (ASTM G99) [23].....	21
FIGURE 18: SCHEMATIC OF ASTM G65 DRY-SAND RUBBER-WHEEL TESTER [26].....	22
FIGURE 19: IMPELLER-TUMBLER APPARATUS [25]	22
FIGURE 20: IMPELLER-TUMBLER SCHEMA [25]	23
FIGURE 21: SCHEMATIC DIAGRAM ILLUSTRATING THE CROSS-SECTIONAL AREAS FOR CALCULATION OF DILUTION CONTENT [30]	24
FIGURE 22: TEMPERATURE-TIME CYCLE DEPENDING ON THE DISTANCE TO WELD POOL [29].....	25
FIGURE 23: MICROSTRUCTURES IN HAZ OF LOW-ALLOYED STEELS [34]	26
FIGURE 24: SCHEMATIC OF STRUCTURE AND COMPOSITION OF COATING [49].....	31
FIGURE 25: NI-BASED MATRIX WITH EMBEDDED TUNGSTEN CARBIDES - SPECIMEN_29 (KERALOY).....	31
FIGURE 26: CO-BASED STELLITE 6 COATING ON 1.4313 STAINLESS STEEL – SPECIMEN_27.....	33
FIGURE 27: LEFT: DELORO 56; RIGHT: TEROCOTE 7888T & TUNGTEC 10122	35
FIGURE 28: LEFT: ABRAtec 6088, RIGHT: PG 6503	35
FIGURE 29: LEFT: DO 321; RIGHT: KERALOY	36
FIGURE 30: LEFT: DO 390N; RIGHT: 1302A.....	38
FIGURE 31: ABRASIVE WEAR BEHAVIOR AND HARDNESS FOR DIFFERENT ALLOYS A – F IN DRY SAND RUBBER WHEEL TEST [71]	45
FIGURE 32: WEAR RATE AT LOW LEVEL IMPACT TEST FOR DIFFERENT ALLOYS A – F TESTED BY IMPELLER-TUMBLER APPARATUS [71].	46
FIGURE 33: WEAR RATE AT UPPER IMPACT LEVEL FOR DIFFERENT ALLOYS A – F TESTED BY IMPELLER-TUMBLER APPARATUS [71]	46
FIGURE 34: DECOHESION OF CARBIDES AFTER IMPACT TEST [47]	48
FIGURE 35: CARBIDE CRACKING AFTER IMPACT TEST [47].....	49
FIGURE 36: METALLURGICAL AND MECHANICAL PORE FORMATION FOR MAG PROCESS [34]	50
FIGURE 37: DIFFERENT TYPES OF GAS POROSITY [79]	52
FIGURE 38: EXAMPLES FOR THE DETERMINATION OF IRREGULARITIES ACCORDING TO EN ISO 5817 [80]	53
FIGURE 39: DISPERSION AND MICROSTRUCTURE OF FUSED TUNGSTEN CARBIDES IN NICKEL-BASE ALLOY; “KERALOY” - SPECIMEN 29	55
FIGURE 40: EMBEDDED FUSED TUNGSTEN CARBIDE WITH RING OF SOLUTION; FRINGED DIFFUSION EDGE - SPECIMEN 29	55
FIGURE 41: OVERVIEW OF DIFFERENT THERMAL-SPRAY PROCESSES IN ANALOGY TO EN 657 [84]	57
FIGURE 42: THERMAL SPRAYING WITH POWDER [87]	58

FIGURE 43: SCHEMATIC OF AN HVOF POWDER SPRAY DEVICE [4]	59
FIGURE 44: CHIPPING OF HVOF COATED SCREW [ANDRITZ]	59
FIGURE 45: OXYACETYLENE WELDING (A) OVERALL PROCESS; (B) WELDING AREA [88]	60
FIGURE 46: CROSS SECTION OF SUPERJET-EUTALLOY TORCH [86].....	61
FIGURE 47: PRINCIPLE OF ‘ONE-STEP TECHNIQUE’ WITH SELF FLUXING CORD [90].....	62
FIGURE 48: COATING PROCESS WITH CASTOLIN SUPERJET-S EUTALLOY [89]	63
FIGURE 49: SHIELDED METAL ARC WELDING (A) OVERALL PROCESS; (B) WELDING AREA [88].....	64
FIGURE 50: FLUX-CORE ARC WELDING (A) OVERALL PROCESS; (B) WELDING AREA [88]	65
FIGURE 51: MANUAL PTA TORCH [50]	66
FIGURE 52: SCHEMATIC DIAGRAM OF THE PTA WELD-SURFACING SYSTEM [92]	67
FIGURE 53: THIN 1MM LAYER OF SURFACING POLYMER (MeCATec - CASTOLIN) ON SCREW [49]	69
FIGURE 54: LIGHT MICROSCOPE - ZEISS OBSERVER Z1M	71
FIGURE 55: SEM AT TU GRAZ - LEO 1450 VP (ZEISS).....	72
FIGURE 56: PRINCIPLE OF SEM [94]	73
FIGURE 57: DIAMOND PYRAMID INDENTER FOR VICKERS TESTING [96].....	75
FIGURE 58: MICROHARDNESS TESTING SPECIMEN_29 – KERALOY	76
FIGURE 59: MACRO HARDNESS TEST - EMCO TEST M4C.....	76
FIGURE 60: HARDNESS TESTER - EMCO TEST M1C	77
FIGURE 61: SPECIMEN 1 – HARDNESS MAPPING WITHOUT INTERPOLATION.....	78
FIGURE 62: SPECIMEN 1 – HARDNESS MAPPING WITH INTERPOLATION	78
FIGURE 63: UNSCALED HARDNESS MAPPING / SCALED HARDNESS MAPPING	79
FIGURE 64: SPECIMEN 19 – HARDNESS MAPPING WITH HAZ.....	80
FIGURE 65: DIMENSIONS OF SAMPLES AND INDICATED COATING.....	82
FIGURE 66: PREFABRICATION OF EDGES OF WELDING SAMPLES.....	82
FIGURE 67: SPECIMEN 1 – BUILDUP SEQUENCE	86
FIGURE 68: SPECIMEN 1 – HARDNESS MAPPING.....	86
FIGURE 69: SPECIMEN 1 – EDX SCAN	87
FIGURE 70: SPECIMEN 1 – PORES.....	88
FIGURE 71: SPECIMEN 1 – CRACKS IN 1302 LAYER	89
FIGURE 72: SPECIMEN 1 – BINDING OF EUTALLOY COATING.....	89
FIGURE 73: SPECIMEN 3 – BUILDUP SEQUENCE	90
FIGURE 74: SPECIMEN 3 – HARDNESS MAPPING	90
FIGURE 75: SPECIMEN 3 – PORES.....	91
FIGURE 76: SPECIMEN 3 – CRACKS IN LAYER 1302 A	92
FIGURE 77: SPECIMEN 3 – BINDING OF PTA LAYER 1302 A	92
FIGURE 78: PTA POWDER 1302 A INVESTIGATED BY EDX.....	93
FIGURE 79: SPECIMEN 1 – SEM - IMAGE OF PTA LAYER 1302 A AND DETAIL OF ANALYSIS	94
FIGURE 80: SPECIMEN 1 – FE-MATRIX	94
FIGURE 81: WDX – ANALYSIS: B, CR, W, V, MO, Nb.....	95
FIGURE 82: SPECIMEN 1 – WDX ANALYSIS OF 1302 A	96
FIGURE 83: SPECIMEN 4 – BUILDUP SEQUENCE	98
FIGURE 84: SPECIMEN 4 - HARDNESS MAPPING.....	98
FIGURE 85: SPECIMEN 4 – PORES.....	99
FIGURE 86: SPECIMEN 4 – CRACKS	100
FIGURE 87: SPECIMEN 4 – BINDING	100
FIGURE 88: SPECIMEN 13 – BUILDUP SEQUENCE	102

FIGURE 89: SPECIMEN 13 – PORE	102
FIGURE 90: SPECIMEN 13 - CRACK	103
FIGURE 91: SPECIMEN 13 – BINDING OF PG 6503.....	104
FIGURE 92: SPECIMEN 25 – BUILDUP SEQUENCE	104
FIGURE 93: SPECIMEN 25 – HARDNESS MAPPING	105
FIGURE 94: SPECIMEN 25 – EDX SCAN ABRATEC 6088 APPLIED ON PG 6503	106
FIGURE 95: SPECIMEN 25 – PORE	107
FIGURE 96: SPECIMEN 25 – CRACKS	108
FIGURE 97: SPECIMEN 25 – BINDING & DILUTION	108
FIGURE 98: SPECIMEN 15 – BUILDUP SEQUENCE	110
FIGURE 99: SPECIMEN 15 – HARDNESS MAPPING	110
FIGURE 100: SPECIMEN 15 – PORES.....	111
FIGURE 101: SPECIMEN 15 – CRACKS	112
FIGURE 102: SPECIMEN 15 – BOND OF DO 390N LAYER	112
FIGURE 103: SPECIMEN 17 – BUILDUP SEQUENCE	113
FIGURE 104: SPECIMEN 17 – HARDNESS MAPPING	113
FIGURE 105: SPECIMEN 16 – PORES.....	114
FIGURE 106: SPECIMEN 17 – CRACKS	114
FIGURE 107: SPECIMEN 17 – BOND OF DO 390N LAYER	115
FIGURE 108: SPECIMEN 19 – BUILDUP SEQUENCE	117
FIGURE 109: SPECIMEN 19 – HARDNESS MAPPING	117
FIGURE 110: SPECIMEN 19 – EDX SCAN DO 390N	118
FIGURE 111: SPECIMEN 19 – EDX SCAN DO 321.....	119
FIGURE 112: SPECIMEN 19 – PORE	119
FIGURE 113: SPECIMEN 19 – CRACK.....	120
FIGURE 114: SPECIMEN 19 – BINDING AND DILUTION OF DO 321	120
FIGURE 115: SAMPLE VI – ‘HAMMER FALL TEST’	122
FIGURE 116: SPECIMEN 6 – BUILDUP SEQUENCE	123
FIGURE 117: SPECIMEN 6 – HARDNESS MAPPING	123
FIGURE 118: SPECIMEN 6 – PORE IN ABRATEC 6088.....	124
FIGURE 119: SPECIMEN 6 – NO PORES IN ABRATEC 6088	125
FIGURE 120: SPECIMEN 6 – CRACKS INSIDE OF ABRATEC 6088 LAYER.....	125
FIGURE 121: SPECIMEN 6 – BINDING	126
FIGURE 122: SPECIMEN 9 – BUILDUP SEQUENCE	126
FIGURE 123: SPECIMEN 9 – HARDNESS MAPPING	127
FIGURE 124: SPECIMEN 9 – PORES.....	128
FIGURE 125: SPECIMEN 9 – CRACKS	129
FIGURE 126: SPECIMEN 9 – BINDING OF DO 390N ON PTA LAYER 1302 A	129
FIGURE 127: SPECIMEN 10 – BUILDUP SEQUENCE	130
FIGURE 128: SPECIMEN 10 – HARDNESS MAPPING	130
FIGURE 129: SPECIMEN 10 – PORES.....	131
FIGURE 130: SPECIMEN 10 – CRACKS IN DO 321 LAYER	132
FIGURE 131: SPECIMEN 10 – BINDING IN DO 321 LAYER	132
FIGURE 132: SAMPLE VII - PENETRATION TESTING	134
FIGURE 133: SPECIMEN 27 – BUILDUP SEQUENCE	135
FIGURE 134: SPECIMEN 27 – HARDNESS MAPPING.....	135

FIGURE 135: SPECIMEN 27 – PORE	136
FIGURE 136: SPECIMEN 28 – CRACK.....	136
FIGURE 137: SPECIMEN 27 – BINDING OF STELLITE 6.....	137
FIGURE 138: SPECIMEN 27 – WELD PENETRATION.....	137
FIGURE 139: SPECIMEN 29 – BUILDUP SEQUENCE	138
FIGURE 140: SPECIMEN 29 – HARDNESS MAPPING	138
FIGURE 141: SPECIMEN 29 – EDX SCAN STELLITE 6 & KERALOY.....	139
FIGURE 142: SPECIMEN 29 – PORE	140
FIGURE 143: SPECIMEN 29 – CRACKS IN KERALOY.....	140
FIGURE 144: SPECIMEN 29 – CRACKS ALONG FUSION LINE	141
FIGURE 145: SPECIMEN 31 – BUILDUP SEQUENCE	142
FIGURE 146: SPECIMEN 31 – HARDNESS MAPPING.....	142
FIGURE 147: SPECIMEN 31 – EDX SCAN OF DELORO 56	143
FIGURE 148: SPECIMEN 31 – PORE	144
FIGURE 149: SPECIMEN 31 – CRACK.....	144
FIGURE 150: SPECIMEN 31 – CHIPPING OF DELORO 56.....	145

11 List of equations

EQUATION 3-1: COEFFICIENT OF FRICTION [10] 11

EQUATION 3-2: WEAR RATE ARACHAND [16] 17

EQUATION 3-3: WEAR FACTOR K OF UNLUBRICATED SURFACE IN SLIDING WEAR [4] 18

EQUATION 3-4: DILUTION [29] 24

EQUATION 3-5: FICK'S FIRST LAW [42] 28

EQUATION 3-6: DIFFUSION COEFFICIENT [41] 29

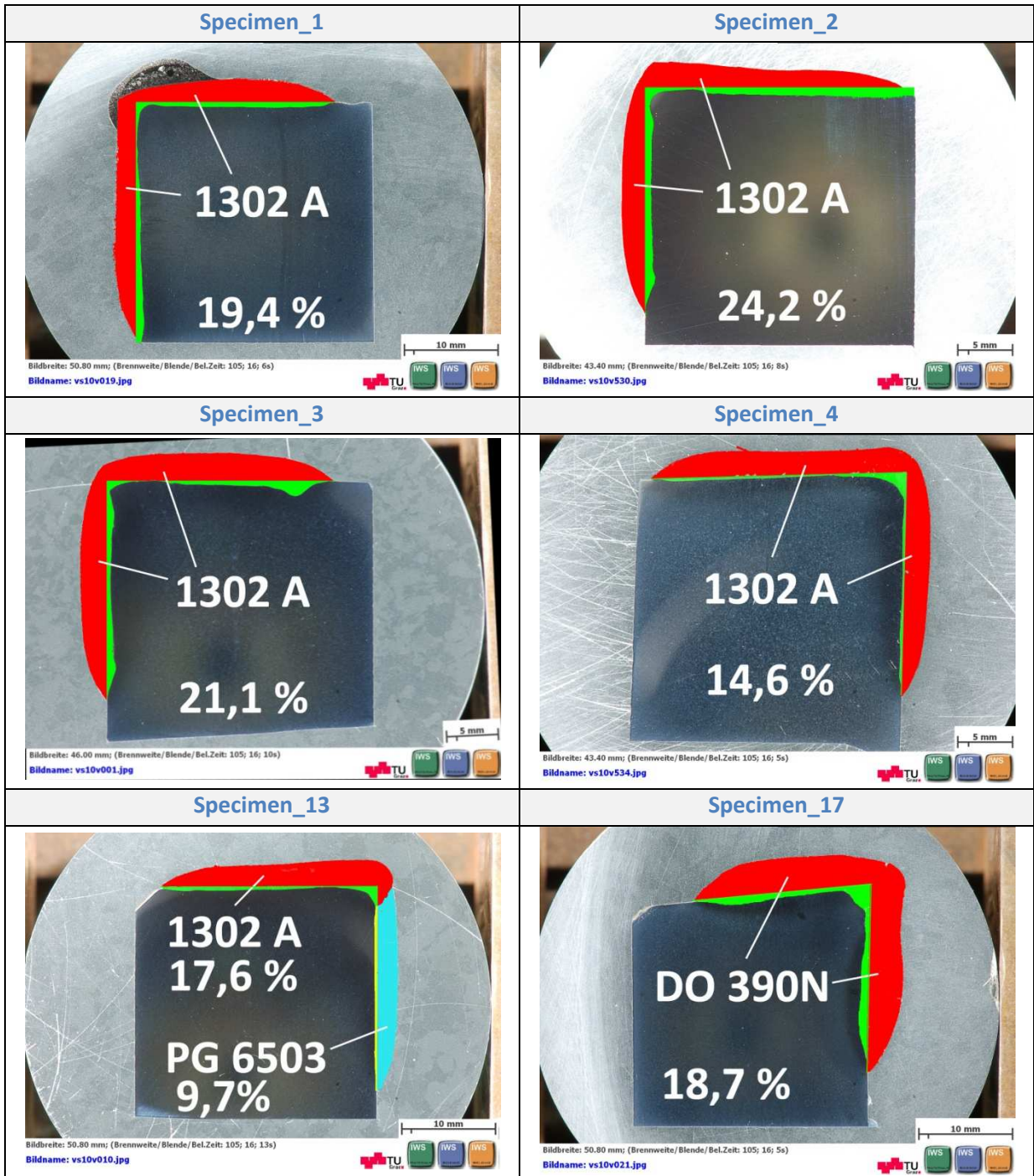
EQUATION 3-7: FICK'S SECOND LAW [42] 29

12 List of tables

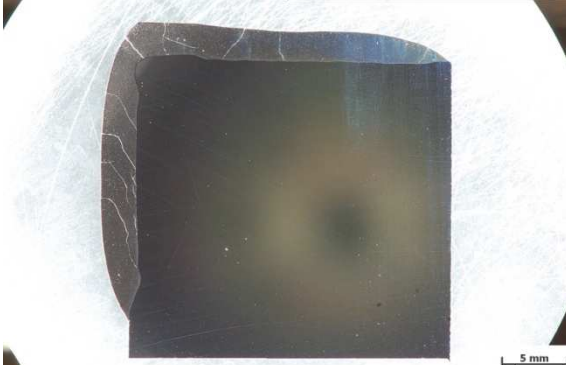

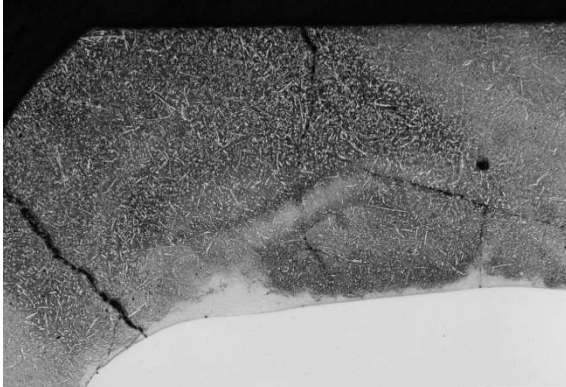
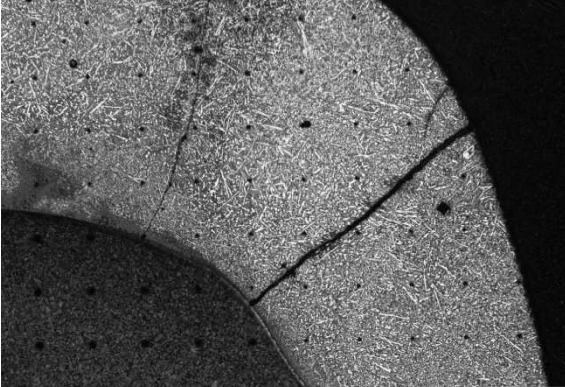
TABLE 1: COMPARISON OF CARBIDE TYPES [4] [44]	42
TABLE 2: COMPARISON OF COATING PROCESSES	70
TABLE 3: COMPOSITION OF 1.4313 MARTENSITIC STAINLESS STEEL [WT%] [97]	81
TABLE 4: SUMMARY OF ALL 10 DEPOSITED WELDING CONSUMABLES	83
TABLE 5: APPLIED WELDING CONSUMABLES ON EACH SAMPLE	84
TABLE 6: WELDING PARAMETERS - SAMPLE I	85
TABLE 7: WELDING PARAMETERS – SAMPLE II	97
TABLE 8: WELDING PARAMETERS – SAMPLE III	101
TABLE 9: WELDING PARAMETERS – SAMPLE IV	109
TABLE 10: WELDING PARAMETERS – SAMPLE V	116
TABLE 11: WELDING PARAMETERS – SAMPLE VI	121
TABLE 12: WELDING PARAMETERS – SAMPLE VII	133
TABLE 13: SUMMARY OF INVESTIGATION – PTA LAYER 1302 A	146
TABLE 14: SUMMARY OF INVESTIGATION – CRACKS.....	147
TABLE 15: SUMMARY OF INVESTIGATION – POROSITY	148
TABLE 16: SUMMARY OF BINDING, CHIPPING & DILUTION – ON SUBSTRATE	150
TABLE 17: SUMMARY OF BINDING, CHIPPING & DILUTION – REFURBISHMENT	150
TABLE 18: ASSESSMENT OF WELDING CONSUMABLES	154
TABLE 19: LEGEND OF TABLE 18	154

13 Appendix

13.1 Dilution



13.2 Comparison sharp edge - beveled edge

Sharp edge	Beveled edge
<p data-bbox="443 376 596 407">Specimen_2</p>  <p data-bbox="236 788 539 824">Bildbreite: 43.40 mm) (Brennweite/Blende/Bel.Zeit: 105; 16; 8s) Bildname: vs10v530.jpg</p>	<p data-bbox="1062 376 1216 407">Specimen_4</p>  <p data-bbox="855 788 1158 824">Bildbreite: 43.40 mm) (Brennweite/Blende/Bel.Zeit: 105; 16; 8s) Bildname: vs10v531.jpg</p>
 <p data-bbox="236 1258 507 1294">Mikroskopvergrößerung: 25x; Bildbreite: 5,58 mm Bildname: vs10v658.jpg</p>	 <p data-bbox="855 1258 1126 1294">Mikroskopvergrößerung: 25x; Bildbreite: 5,58 mm Bildname: vs10v979.jpg</p>

